

**INSTANTANEOUS MODAL PARAMETERS AND
THEIR APPLICATIONS TO STRUCTURAL HEALTH MONITORING**

by

Hera Adriana

Adriana Hera

A Dissertation

Submitted to the Faculty

of the

WORCESTER POLYTECHNIC INSTITUTE

in partial fulfillment of the requirements for the

Degree of Doctor of Philosophy

in

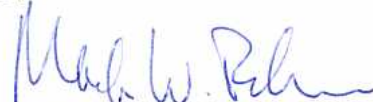
Mechanical Engineering

December 2005

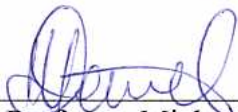
APPROVED:



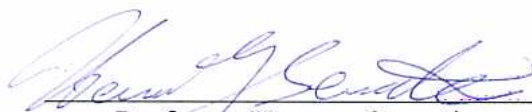
Professor Zhikun Hou
Advisor



Professor Mark W. Richman
Committee Member



Professor Michael A. Demetriou
Committee Member



Professor Herman Servatius
Committee Member



Professor Grétar Tryggvason
Representative for the Graduate Committee

Copyright © 2005 by Adriana Hera
ALL RIGHTS RESERVED

Abstract

This dissertation proposes a vibration-based approach to detect and monitor structural damage by tracking the instantaneous modal parameters. A change in the instantaneous modal parameters indicates change in the structural health condition. In contrast to many existing structural health monitoring schemes, the proposed approach is less model dependent and works well for both sudden and evolving damage, general loading conditions and complex structures.

The instantaneous modal parameters, including modal frequency, mode shape vector and modal damping ratio, are introduced as a bridge between the system properties and time varying vibration modes. The theoretical background of the time-varying vibration modes is developed. It has been shown that for slowly time-varying systems such modes exist and the instantaneous modal parameters have a clear physical interpretation and can be identified from free and forced vibration responses.

A set of known techniques are used in an innovative way to identify the instantaneous modal parameters. Applicability of the identification techniques depends on the nature and availability of measurement data. Wavelet ridge method is used to identify the instantaneous modal frequencies and normalized instantaneous mode shape vectors from free vibration data. Wavelet packet sifting technique in conjunction with Hilbert transform and confidence index is proposed to identify the normalized instantaneous mode shape from both free and forced vibration data. Time-varying Kalman filter is integrated with the wavelet packet sifting technique to identify the instantaneous modal frequencies and the instantaneous modal damping ratios from free and forced vibration data.

The proposed approach has been validated using both simulation and experimental data. The simulation data is obtained from a multi-degree-of-freedom system with time varying stiffness under different loading conditions. Experimental data include both impact testing data from the ASCE benchmark study and shaking-table test data of a full-size two-story wooden building structure, conducted at DPRI, Kyoto University, Japan. It has been shown that the proposed approach can successfully detect and monitor damage and, therefore, has great potential for real applications.

*In the memory of
Professor Dumitru Tudor*

Acknowledgments

I would like to express my sincere thanks and appreciation to my advisor, Professor Zhikun Hou, for his time, guidance, and support over the past several years. Also, I would like to thank him for introducing me to the research community and giving me the opportunity to attend conferences.

I am very grateful to the members of my dissertation Committee, Professor Grétar Tryggvason, Professor Michael A. Demetriou, Professor Herman Servatius, Professor Mark W. Richman and Professor John M. Sullivan, for their time and assistance in this work, and for guiding me through various courses at WPI. I would also like to extend my thanks to Professor Mikhail F. Dimentberg for shaping my understanding of the random and nonlinear phenomena.

I thank Prof. Suzuki and his team at Kyoto University, Japan, for providing part of the experimental data I used to validate the approach presented in this dissertation.

Professor Dumitru Tudor, my undergraduate Diploma Thesis advisor, foresaw me through this Ph.D. journey long before it even began. My accomplishments under his supervision are a milestone in my academic career and motivated me to continue my education. So, as my belated thanks and recognition of all he has done for me, I would like to dedicate this dissertation to his memory.

I thank the WPI Mechanical Engineering Department and Graduate Committee for supporting me with a teaching assistant position during my studies at WPI.

My special thanks go to Mr. Sia Najafi for choosing me as his TA for the last three years, and for generously helping me by providing computer facilities and with a temporary position on his team. I would also like to thank him for his continuous encouragement.

My thanks go to Barbara Furhman, Barbara Edilberti, Pam St Louis and Janice Dresser from ME Dept. office for all their kindness and cooperation.

I owe a great deal to my former colleagues. I thank Catalin Picu and Dan Frusescu, who started this same journey many years before me and convinced me to pursue the same road. I thank Abhijeet Shinde and Wei Liu for our very interesting and enlightening discussions on various research topics, and for their valuable input to my work.

I would like to thank my friends Edyta Soltan, Majeda Shabo, Oana Aldea, and Diana Lados for their friendship and support while I was working on this dissertation. Thanks also go to my friends and colleagues Elham Ghaem Maghami and Vasin Paradon for all their help, and Appu Thomas and Shilpa Jacobie for reading parts of this dissertation.

Many thanks to my cousin Mr. Gorgan, his family, and to Dr. Balaci and his family for their support, which gave me the confidence I needed to complete this work.

I am very grateful to my parents, brother, sisters, and in-laws for their unconditional love and support. I would also like to mention my nephews and my niece who are a source of joy in my life.

Finally, I would like to acknowledge a very dear friend, Catalin Picu, who deserves my deepest thanks and respect. A source of personal and professional inspiration, he was my mentor through this entire process. He nurtured my drive to explore the internal and external worlds in several different ways. I am indebted to him for the most enjoyable and rewarding period of my life, which includes this life-changing journey.

Adriana Hera

TABLE OF CONTENTS

List of Figures	vi
List of Tables	x
Nomenclature	xi
1 Introduction	
1.1 Concept of Structural Health Monitoring and Damage Identification	1
1.2 Wavelet Analysis in Damage Detection	5
1.3 Motivation and Objective	7
1.4 Dissertation Overview	10
2 Mathematical Background	
2.1 Linear Time Varying Systems	13
2.1.1 System Response Using the State Transition Matrix	14
2.1.2 Modal Decomposition	15
2.1.2.1 Modal Decomposition of Linear Time Invariant Systems	16
2.1.2.2 Dynamic Eigenvalue Problem	17
2.1.2.3 Modal Decomposition of Linear Time Varying Systems	18
2.1.3 System Response by Modal Decomposition Approach	19
2.1.4 Algorithms for Solving the Dynamic Eigenvalue Problem	21
2.2 Modal Analysis	23
2.3 Wavelet Analysis	25
2.3.1 Wavelet Function	25
2.3.2 Continuous Wavelet Transform	28
2.3.3 Multiresolution Analysis and Discrete Wavelet Transform	31
2.3.4 Wavelet Packet Decomposition	32
2.4 Hilbert Transform	35

3	Theoretical Basis of Time-Varying Vibration Modes and Instantaneous Modal Parameters	
3.1	Introduction	37
3.2	State Space Formulation of Damaged Structures	39
3.3	Real Modal Responses	39
3.4	Slowly Time-Varying Systems	42
3.4.1	Slowly Time-Varying Assumption	42
3.4.2	Definition of Instantaneous Modal Parameters	43
3.4.3	Instantaneous Modal Parameters in Velocity Response	44
3.4.4	Instantaneous Modal Parameters in Acceleration Response	45
3.4.5	Instantaneous Modal Parameters in Forced Vibration Response	46
3.5	Instantaneous Modal Parameters of a SDOF system	48
3.5.1	System Dynamics	48
3.5.2	Dynamic Eigenvalue Problem	49
3.5.3	Modal Equations and System Response	50
3.5.4	Free Vibration Response	50
3.5.5	Slowness Index	51
3.6	Second Order Formulation for Vibration Modes	51
3.7	Numerical Examples: Linear SDOF and 3DOF Systems with Time-varying Stiffness	54
3.7.1	Case Study I: SDOF System	55
3.7.2	Case Study II: 3DOF system	60
3.7.3	Remarks	62
3.8	Summary	66
4	Identification of Instantaneous Modal Parameters from Free Vibration Data	
4.1	Introduction	68
4.2	Theoretical Background	68
4.2.1	Free Vibration Modal Responses	68
4.2.2	Continuous Wavelet Transform – Ridge Method	70
4.2.3	Wavelet Packet Sifting Process	72
4.3	Methodology: Identification of Instantaneous Modal Frequency and Instantaneous Normalized Mode Shape	73
4.3.1	Identification by CWT-ridge Method	74

4.3.2 Identification by Wavelet Packet Sifting Technique and Hilbert Transform	74
4.4 Applications: A 3DOF Mass-spring-dashpot System with Time-varying Stiffness	75
4.4.1 Simulation Setup	75
4.4.2 Methodology and Results	76
4.5 Summary	77
5 Identification of Instantaneous Normalized Mode Shape from Forced Vibration Data and Applications to SHM	
5.1 Introduction	81
5.2 Methodology	82
5.2.1 Instantaneous Modal Parameters in Forced Vibration Responses	82
5.2.2 Identification of the Normalized Instantaneous Mode Shape	84
5.2.3 Practical Issues in Identification of Instantaneous Modal Parameters	84
5.2.4 Confidence Index	89
5.3 Applications: A 3DOF Mass-spring-dashpot System with Time-varying Stiffness	90
5.3.1 Simulation Set-up	90
5.3.2 Normalized Instantaneous Mode Shape and Confidence Index	92
5.3.3 Effect of Measurement Noise	95
5.3.4 Effect of Damage Severity	95
5.3.5 Monitoring Gradually Developed Damage	96
5.3.6 Effect of Excitation Frequency	96
5.4 Summary	104
6 Wavelet packet and Kalman Filter for Identification of Instantaneous Natural Frequency and Instantaneous Damping Ratio	
6.1 Introduction	106
6.2 Theoretical Background	107
6.3 Methodology	108
6.3.1 Instantaneous Natural Frequency and Modal Damping Ratio	108
6.3.2 Extraction of Modal Responses by Wavelet Packet Sifting Technique. New Sifting Criterion	110
6.3.3 Implementation Issues	111

6.3.4	Identification of Modal Parameters	112
6.4	Applications: A 2DOF Mass-spring-dashpot System with Time-varying Stiffness	114
6.4.1	Simulation Setup	114
6.4.2	Results and Discussion	115
6.5	Summary	118
7	Instantaneous Modal Parameters for Structural Health Monitoring of Nonlinear systems	
7.1	Introduction	121
7.2	Theoretical Background	122
7.2.1	Linear Slowly Time-varying Systems	122
7.2.2	Bilinear Systems	122
7.3	Methodology	124
7.4	Applications: A 2DOF Mass-spring-dashpot System	126
7.4.1	Simulation Set-up	126
7.4.2	Results - Impulse Excitation	127
7.4.3	Results - Harmonic Excitation	128
7.5	Summary	129
8	Applications to Experimental Data	
8.1	Introduction	133
8.2	ASCE SHM Benchmark Study	134
8.2.1	Description of the Structure	134
8.2.2	Simulation Data Results	134
8.2.3	Experimental Data Results	137
8.3	Shaking Table Test of a Wooden Building Structure	146
8.3.1	Experimental Setup	146
8.3.2	Simulation results	148
8.3.3	Experimental Data Results	150
8.3.3.1	Identification of Normalized Instantaneous Mode Shape and Instantaneous Frequency	150
8.3.3.2	Damage Detection in the Structure	153
8.4	Summary	169
9	Concluding Remarks	

9.1 Summary and Main Contributions	171
9.2 Future Work	172
Appendix	176
References	181

List of Figures

2.3.1	Examples of the representative wavelets	29
2.3.2	Wavelet packet decomposition tree at level 3	33
2.3.3	Discrete Meyer wavelet packet library (w_0, w_1, \dots, w_7)	34
3.1	a) Sketch of the system; Stiffness history; b) Scenario I, II, III; c) Scenario IV	57
3.2	Complex modulus of the 1 st dynamic eigenvector	57
3.3	The 1 st dynamic eigenvalue (real and imaginary part)	58
3.4	Results for Scenario II ($\alpha = 0.4$)	58
3.5	Results for Scenario I ($\alpha = 0.2$)	59
3.6	Results for Scenario III ($\alpha = 0.8$)	59
3.7	Results for Scenario IV	60
3.8	(a) Sketch of the system; (b) Stiffness history (K_2)	61
3.9	The first dynamic eigenvalue	63
3.10	The first dynamic eigenvector (the first three components corresponding to the displacement at M1, M2 and M3)	63
3.11	Instantaneous frequency: defined by dynamic eigenvalue problem and obtained from free vibration modal responses	64
3.12	(a) Instantaneous mode shapes; (b) Normalized instantaneous mode shape	65
4.1	CWT spectrum of the acceleration response of M3	78
4.2	Instantaneous frequencies estimated by the CWT-ridge method and the theoretical values	78
4.3	Normalized instantaneous modal vectors identified by the CWT-ridge method and the theoretical values	79
5.1	A sketch of the 3DOF mass-spring-damper system	86
5.2	CWT map of the El Centro earthquake signal	86
5.3	CWT map of the acceleration response measured at M1	88
5.4	CWT map of the simulated first modal response, $x_1^{(1)}(t)$	88
5.5	The excitation signals used in the study	98
5.6	NI mode shape and confidence index for the first vibration mode, in the case of Kobe earthquake excitation	99

5.7	NI mode shape and confidence index for the second vibration mode, in the case of Kobe earthquake excitation	99
5.8	NI mode shape and confidence index for the first vibration mode, in the case of Hachinohe earthquake excitation	100
5.9	NI mode shape and confidence index for the first vibration mode, in the case of El-Centro earthquake excitation	100
5.10	NI mode shape and confidence index for the first vibration mode, in the case of random earthquake excitation	101
5.11	NI mode shape and confidence index for the first vibration mode, in the case of Hachinohe earthquake excitation, 5% measurement noise	101
5.12	NI mode shape and confidence index for the first vibration mode, in the case of Hachinohe earthquake excitation, for different damage levels	102
5.13	NI mode shape and confidence index for the first vibration mode, in the case of Hachinohe earthquake excitation, gradual damage	102
5.14	NI mode shape components and confidence indices for the first vibration mode, in case of a harmonic excitation, no damage ;(cyan = $X_{3,1}^{(1)}$, green = $X_{2,1}^{(1)}$)	103
5.15	(a) NI mode shape components; (b) confidence indices; (c) instantaneous frequency of the sifted signals	104
6.1	(a) Sketch of system; (b) Stiffness history in case of progressive damage	115
6.2	Instantaneous frequency and frequency index of the decomposed acceleration responses	116
6.3	Estimated values for instantaneous modal parameters in the case of healthy system, the first vibration mode	117
6.4	Estimated values for instantaneous modal parameters in case of a system with progressive stiffness degradation after t=15s, subjected to a base excitation: (a) filtered Gaussian white noise, (b) El Centro earthquake signal	119
6.5	Estimated values for instantaneous modal parameters in the case of a system with progressive stiffness degradation after t=15s	120
7.1	Bilinear restoring force	123
7.2	Sketch of system	
7.3	(a) Restoring force; (b) Stiffness history in the case of progressive damage	127
7.4	CWT map of the displacement response measured at M1, zero damping, impulse excitation; (a) linear system (S1); (b) linear system with damage (S2); (c) bilinear system (S3); (d) bilinear system with damage (S4)	130

7.5	(a) Instantaneous mode shape and (b) instantaneous frequency, for systems of different nature in case of impulse excitation.	131
7.6	CWT map of the displacement response measured at M1, for a bilinear system with damping, subjected to impulse excitation	131
7.7	Normalized Instantaneous mode shape and instantaneous frequency for the first vibration mode in the case of a bilinear system with damping, subjected to impulse excitation	132
7.8	CWT map of the displacement response measured at M1, harmonic excitation, linear system (S1), (b) bilinear system (S3);	132
7.7	(a) Instantaneous mode shape and (b) instantaneous frequency for a system with damping subjected to a harmonic excitation	132
8.2.1	The prototype structure of ASCE health monitoring benchmark studies	139
8.2.2	Map of CWT coefficient modulus of the acceleration response measured at the 4th floor	140
8.2.3	Instantaneous modal frequency for the first three vibration modes	140
8.2.4	The normalized instantaneous mode shape	141
8.2.5	Map of the modulus of the CWT transform coefficients of the response measured at the 3rd floor	142
8.2.6	Map of the modulus of the CWT transform coefficients of the response measured at the 2nd floor	142
8.2.7	CWT of the response measured at the first story in North direction	143
8.2.8	Instantaneous modal frequency by analyzing the response at each floor of undamaged structure	144
8.2.9	Instantaneous mode shapes of undamaged structure	144
8.2.10	Instantaneous modal frequency (a) configuration no.1, undamaged structure; (b) configuration no.2 – damaged structure	145
8.2.11	Normalized instantaneous mode shape (a) configuration no1, undamaged structure; (b) configuration no.2 – damaged structure	145
8.3.1	An overview of the test site and the wooden frame specimen on the shaking table	156
8.3.2	A damaged wooden brace occurred during the test run at the load level 3.50m/s^2	156
8.3.3	First vibration mode. (a) Change in the natural frequency and (b) mode shape component $X_{2,1}^{(1)}$ with the change in system stiffness	157

8.3.4	Second vibration mode. (a) Change in the natural frequency and (b) mode shape component $X_{2,1}^{(1)}$ with the change in system stiffness	158
8.3.5	Plots of absolute displacements, interstory-drift, absolute acceleration	159
8.3.6	(a) Fourier spectrum of the relative of: (0) ground acceleration; (1) relative acceleration of the 1st floor (2) relative acceleration of the 2nd floor; (b) zoom in plots for frequency range of 0.5 – 2 Hz	160
8.3.7	CWT maps of: (a) the ground acceleration, (b) the relative acceleration of the first floor and, (c) the relative acceleration of the second floor	161
8.3.8	Plots of the absolute velocity obtained by integration	162
8.3.9	Comparison between the measured displacement signals and those obtained by time integration of the measured acceleration responses	162
8.3.10	Decomposition tree	163
8.3.11	Confidence index for different decomposition levels	163
8.3.12	(a) Instantaneous frequency of the reconstructed signals at node (7,3); (b) Confidence index; (c) normalized mode shape component	
8.3.13	(a) Confidence index; (b) Analytic amplitudes of $\ddot{u}_{1,(7,3)}$ and $\ddot{u}_{2,(7,3)}$; (c) calculated NI mode shape ; estimated NI mode shape by Kalman smoother	164
8.3.14	(a) Estimated instantaneous natural frequency; (b) Estimated instantaneous modal damping ratio	165
8.3.15	(a) Relative accelerations obtained from actual measurements; (b) innovation	165
8.3.16	CWT of the relative acceleration response	166
8.3.17	Identified instantaneous natural frequency of the wooden house	167
8.3.18	Identified instantaneous natural frequency for different excitation levels	167
8.3.19	Identified instantaneous modal damping ratio for different excitation levels	167
8.3.20	Identified normalized instantaneous mode shape for different excitation levels	168
8.3.21	CWT of \ddot{u}_1 (excitation level =100)	168
8.3.22	Fourier spectrum of \ddot{u}_1 normalized by its maximum value	168
8.3.23	Fourier spectrum of \ddot{u}_1 normalized by its maximum value, for different excitation levels	169

List of Tables

4.1	Comparison of the modal frequencies obtained by CWT and solving the dynamic eigenvalue problem at specified time instants	77
8.2.1	Comparison of the modal frequency results obtained by CWT and modal analysis	136
8.2.2	Comparison of the normalized instantaneous mode shapes results obtained by CWT and modal analysis	137
8.3.1	Estimates of the natural frequencies and the modal damping ratio of the wooden frame using ambient vibration and step-loading test	147

Nomenclature

ASCE	American Society of Civil Engineers
$A(t)$	amplitude of a signal
$\tilde{A}(t)$	analytic amplitude (Hilbert transform)
$A_J(t)$	the approximation signal at level J (<i>wavelets</i>)
$\mathbf{A}(t)$	system matrix of the 1 st order system in state space formulation
$A_{a,j}^{(n)}$	the amplitude of the j^{th} component of the n^{th} modal acceleration response
$A_{v,j}^{(n)}$	the amplitude of the j^{th} component of the n^{th} modal velocity response
$A_{x,j}^{(n)}$	the amplitude of the j^{th} component of the n^{th} modal displacement response
a	the scaling parameters (wavelets)
$a_j^{(n)}(t)$	the j^{th} component of the n^{th} modal acceleration response
$\mathbf{B}(t)$	input matrix
b	shifting parameters (wavelets)
CWT	Continuous Wavelet Transform
\mathbf{C}_d	damping matrix of second order system
$c_{d,n}(t)$	instantaneous modal damping coefficient
C_ψ	admissibility coefficient (wavelets)
$CI_{j,p}^{(n)}$	confidence index (analytic frequency of content of $\tilde{s}_j^{(n)}(t)$ divided by analytic frequency $\tilde{s}_p^{(n)}(t)$)
DOF	degree-of-freedom
$D_j(t)$	detail signal at level j (<i>wavelets</i>)
dt	time step
$E < >$	mean value of the variable in the parentheses.
FE	Finite element
F_c	center frequency (complex Morlet wavelet)
F_b	bandwidth parameter (complex Morlet wavelet)
$\mathbf{f}(t)$	input/force/excitation vector
HT	Hilbert Transform
$\text{Im}(\lambda)$	imaginary part of the complex number/function λ
\mathbf{K}	stiffness matrix of second order system
$[k]$	refers to the discrete values at time step $t[k]$.
LANL	Los Alamos National Laboratory
LTI	linear time invariant
LTV	linear time varying

L(t)	Lyapunov transformation
MRA	multiresolution analysis (wavelets)
M	mass matrix of second order system
NDE	Non-Destructive Evaluation
$\text{Re}(\lambda)$	real part of the complex number/function λ
rms	root mean square
$\mathbf{q}(t)$	elementary modal coordinate vector (1 st order system)
$q_k(t)$	the k^{th} elementary modal coordinate
$q_{kh}(t)$	the k^{th} homogeneous modal coordinate
$q_{fk}(t)$	the k^{th} forced modal coordinate
SHM	Structural Health Monitoring
$S_{STV}(t)$	slowness index
T	transpose
t	time
t_0	initial time
U	eigenvector matrix
$\mathbf{U}(t)$	dynamic eigenvector matrix
u	eigenvector
$\mathbf{u}(t)$	dynamic eigenvector
$\mathbf{u}^{(n)}$	the n^{th} eigenvector
$\mathbf{u}(t)^{(n)}$	the n^{th} dynamic eigenvector
$\mathbf{u}_{qs}(t)$	quasistatic eigen vector (calculated by the eigenvalue problem at frozen time)
$u_{k j}(t)$	the k^{th} component of the dynamic eigenvector $\mathbf{u}(t)$ normalized in respect to its j^{th} component.
$\mathbf{v}(t)$	velocity vector
$v_j^{(n)}(t)$	the j^{th} component of the n^{th} modal velocity vector
WP	Wavelet Packet
WPS	Wavelet Packet Sifting
$W_x(a,b)$	CWT coefficient of signal $x(t)$, at scale a and shifting parameter b
$\mathbf{X}^{(n)}$	the n^{th} instantaneous mode shape
$\mathbf{X}_{ j}^{(n)}(t)$	the n^{th} normalized mode shape vector in respect to its j^{th} component
$X_{j,p}^{(n)}(t)$	the j^{th} component of the n^{th} normalized mode shape vector in respect to its j^{th} component
$x(t)$	displacement vector
$x_j^{(n)}(t)$	the j^{th} component of the n^{th} modal displacement response
Y(t)	fundamental matrix
y	state space vector

\mathbf{y}_0	initial state
$\mathbf{y}^{(n)}(t)$	the n^{th} elementary modal response vector
$\mathbf{y}^{(2n-1),(2n)}(t)$	the n^{th} vibration modal response vector (real valued function of t)
$y_j^{(2n),(2n+1)}(t)$	the j^{th} component of the n^{th} real modal response vector
$z(t)$	analytic signal
$\gamma_{\lambda,k}(t)$	real part of $\lambda_{\lambda,k}(t)$
Δt	effective duration (wavelets)
Δf	effective frequency width (wavelets)
$\eta_i(t)$	the i^{th} modal coordinate (vibration modes)
$\Phi(t, t_0)$	state transition matrix
$\Phi_{ij}(t, t_0)$	component (i,j) of the matrix $\Phi(t, t_0)$
Λ	eigenvalue matrix
$\Lambda(t)$	dynamic eigenvalue matrix
λ	eigenvalue
$\lambda(t)$	dynamic eigenvalue
$\xi(t)$	instantaneous damping ratio of a SDOF system
$\xi_n(t)$	the n^{th} instantaneous nodal damping ratio
σ_t	temporal variance (wavelets)
σ_f	frequency variance (wavelets)
$\phi_{a,j}^n(t)$	the phase angle of the j^{th} component of the n^{th} modal acceleration response
$\phi_{v,j}^n(t)$	the phase angle of the j^{th} component of the n^{th} modal velocity response
$\phi_{x,j}^n(t)$	the phase angle of the j^{th} component of the n^{th} modal displacement response
$\phi(t)$	scaling function (wavelets)
$\psi(t)$	wavelet function
$\psi_{a,b}(t)$	shifted and scaled wavelet
$\hat{\psi}(\omega)$	Fourier transform of the wavelet function $\psi(t)$
$\Omega(t)$	instantaneous natural frequency of a SDOF system
$\Omega_n(t)$	the n^{th} instantaneous modal frequency of a SDOF system
$\omega_{\lambda,k}(t)$	imaginary part of $\lambda_k(t)$
$\omega_n(t)$	the n^{th} instantaneous modal frequency
$\omega_{x,nj}(t)$	instantaneous frequency of the n^{th} modal response of the j^{th} component of the displacement vector
ω	frequency (rad/sec)

- $\omega_{v,nj}(t)$ instantaneous frequency of the n th modal response of the j^{th} component of the velocity vector
- ω_{di} the i^{th} damped natural frequency
- \cong specify that left hand side of is equal to the right hand side up to the order of ε , where $\varepsilon \ll 1$, i.e. $x \cong y$ means: $x = y + O(\varepsilon)$
- multiplication element by element; $\mathbf{A} \bullet \mathbf{B}$ denotes multiplication of \mathbf{A} and \mathbf{B} , element by element

Chapter 1

INTRODUCTION

1.1 Concept of Structural Health Monitoring and Damage Identification

Damage is often observed in many engineering systems during their service life. It may be caused by factors such as material defects, cumulative crack growth, wear-and-tear of working parts, impact by a foreign object or excessive load. To ensure high system performance, structural safety and integrity, and low maintenance cost, structural health monitoring (SHM) has emerged as a reliable, efficient and economical approach to monitor the system performance, detect damage, asses/diagnose the structural health condition, and make corresponding maintenance decisions. An effective SHM process may detect structural damage in its early stage, well before a catastrophic structural failure, provide valuable information for the post-event damage assessment, and help to develop a condition based maintenance procedure. As results, the structural performance and safety is significantly improved. Recent advances and research activities in SHM can be found in the conference proceedings edited by Chang (1999, 2001, 2003, 2005).

A typical SHM system consists of two major components: a network of sensors for measurement of response data, and data analysis algorithms for interpretation of the measurements in terms of the structural physical condition. The algorithms and techniques used for information processing to provide useful and simple measures of the structure health condition are seen as one of the main problems in SHM, as mentioned in the motivation of ASCE SHM benchmark study (Johnson et al., 2004).

The key part of SHM is damage identification. Damage can be defined as changes in the structure that adversely affect its performance. Rytter (1993) introduced four levels of damage identification, as follows:

- Level 1: Determine if damage is present in the structure
- Level 2: Locate damage
- Level 3: Quantify the severity of damage
- Level 4: Predict the remaining service life of the structure

Damage identification includes *local* and *global* methods. *Local methods*, often known under the name of Non-Destructive Evaluation (NDE), include visual inspection, thermography, stress waves, magnetic field analysis, ultrasonic inspection, radiography and eddy-current methods (Hellier, 2001). Recently, a new trend in NDE has emerged. It consists in utilization of structurally integrated sensors to monitor the structural health condition in real time. A few examples of such systems are: ultrasonic transducers permanently attached to the structures (Giurgiutiu and Cuc, 2005), fiber optic sensor arrays embedded in composite structures (Zhou et al., 2002), sensing and actuation piezoelectric patches attached to the structure (Park et al, 2003.) or hybrid monitoring systems such as piezoelectric actuators together with fiber optic sensors (Qing et al., 2005). Although local methods can localize damage with a high precision, they require to know in advance the vicinity of the damage and to have access to the part of the structure to be inspected.

Global damage identification methods can overcome the shortcomings mentioned above. They are developed on the premise that commonly measured dynamic quantities such as displacement/velocity/acceleration time-histories and global vibration characteristics derived from these measurements are functions of the physical properties of the structure. However, the global nature of these methods may introduce drawbacks such as insensitivity to small local damage and poor damage localization and quantification. It is assumed that changes in the physical properties, such as reductions in stiffness resulting from the onset of cracks or loosening of a connection, will cause *detectable* changes in the vibration response of the structures. A comprehensive literature review of global damage identification methods based on vibration measurements can be found in Doebling et al. (1996)

Global damage identification can be seen either as an inverse problem or a pattern recognition problem. In the first approach, damage is regarded as a change of system parameters which are identified from measurement data. The second approach is based on the idea that there are damage sensitive features in measurement data which can be associated to different structural health conditions. *The inverse problem approach* encompasses modal based techniques, model updating techniques, and tracking methods

Modal-based techniques employ the modal information identified from vibration data. Using two sets of measurements recorded before and after damage, the modal parameters of the system, considered linear time-invariant over each record period, can be thus identified by well established techniques, such as experimental modal analysis (Allemang and Brown, 2002). A change in physical parameters of a structure results in change of its modal parameters; therefore, any change in the modal parameters (natural frequency, damping ratio, mode shape vector) or related measures (mode shape curvature or identified flexibility matrix) may indicate damage development in the structure, and the structural health condition. They address, mainly, damage identification level 1. When a finite element model is available, using the sensitivity of modal parameters to the change in the structural parameters, damage identification levels 2 and 3 can also be addressed. For a comprehensive survey of modal-based techniques the reader is referred to Doebling et al., (1998).

The *model updating techniques* consist in choosing the parameters of an analytical model to minimize an objective function based on the error between measurement data and those values predicted by the analytical model. A review of the literature published before 1993 can be found in Mottershead and Friswell (1993) and the more recent advances are presented in the special issue on model updating of the journal “Mechanical Systems and Signal Processing” (Mottershead and Friswell, 1998). When detailed physical models, such as finite element (FE) models are used, the damage location and quantification can be done with a high accuracy. The technique is applied off line as a batch process and the system is considered time-invariant during data recording.

Tracking methods, which employ simplified models and a reduced number of parameters to be updated, have better chances for on line implementation. They include techniques such as Kalman filter (Hoshiya and Saito, 1984; Shinozuka and Ghanem, 1995; Maruyama and Hoshiya, 2001), Bayesian model updating algorithms (Ching et al., 2004), particle filter (Yoshida and Sato, 2002; Masuda et al., 2002), or techniques based on adaptive tracking (Yang and Lin, 2005; Demetriou 2000, 2005). Since simplified physical models are used, their performance in damage localization and quantification would be moderate.

The *pattern recognition approach* associates different health conditions of the structure with damage features extracted from measurement data. The algorithms which extract the damage feature can work either in supervised or unsupervised learning models. Supervised learning applies to level 2 and 3 in damage identification. It deals with data from both damaged and undamaged structure and includes classification techniques (Lynch, 2004; Trendafilova and Hetlen, 2003) and regression analysis (Mahmoud and Abu Kiefa, 1999). Unsupervised learning is used when data from structure with different damage conditions is not available for comparison. It uses tools such as novelty detection (Worden, 1997, Masri et al. 1996), multivariate probability density function estimation, statistical process control (Fugate et al., 2000; Worden et. al, 2002) and addresses level 1 in damage identification. The SHM research group at the Los Alamos National Laboratory (LANL) (Farrar et al., 2000; Farrar and Sohn, 2005), describes SHM process as a problem in statistical pattern recognition, with four stages: (i) operational evaluation; (ii) data acquisition and cleansing; (iii) feature selection and data compression; and (iv) statistical model development for feature discrimination.

While a significant amount of research has been conducted during the last 30 years in the area of SHM and damage detection, applying in practice of SHM algorithms is still a challenging task due to measurement noise, nonstationarity of data, uncertainties in the parameters, modeling errors, time-varying nature of a system, non-linearities in the system, or inexistence of a detailed physical model. In order to address issues of implementation, a benchmark problem was proposed by the ASCE Task Group on Health Monitoring.

Different methods, as mentioned, are investigated in this context and the results are presented in a special issue of *J. Eng. Mech.* 2004 (Bernal, D., Beck, J., 2004).

As can be seen various damage detection schemes have been developed to extract information of structural health condition from appropriate vibration measurement data. However, the problem of health monitoring remains challenging when damage state evolves during the period when the data are recorded and a detailed physical model is not available. The aim of this study is to propose global vibration-based damage identification techniques, for structures with evolving damage, using time-varying (instantaneous) modal parameters.

1.2 Wavelet Analysis in Damage Detection

All SHM approaches require signal processing (SP) techniques to extract the relevant information from measurement data. The SP techniques span from the well-known Fourier Transform to newly developed wavelet transform (WT) or Hilbert-Huang transform. During the last decade, given its capabilities for analyzing the non-stationary response of a damaged system, time-frequency localization and sensitivity to abrupt changes in a signal, WT with its different forms: discrete wavelet transform (DWT), continuous wavelet transform (CWT) and wavelet packet (WP) decomposition, has been employed in many of damage identification methods mentioned above. In modal-based methods, CWT was used to separate the vibration modes and enhance the quality of the modal information obtained from response signals. Many pattern recognition-based techniques employ wavelet transform to define damage sensitive features. Sensitivity of wavelet transform to abrupt changes in the signal is exploited by unsupervised damage detection based on anomaly/novelty detection.

In order to give a flavor of the effervescent research going on in this field a brief overview of the applications of wavelet theory to damage detection and SHM is given. A comprehensive literature survey of the earlier applications is referred to Staszewski (1998).

First applications were mainly for rotating machinery where wavelet analysis of the response data showed certain patterns when a machine runs at a constant operation speed and a change in the wavelet pattern may indicate structural damage (Staszewski and

Tomlinson, 1994; Wang and McFadden, 1995). Wavelet transform was proposed as preprocessing tool to supply the input vectors in a neural network to identify the fault in rotating machinery (Paya, et al., 1997) and gearboxes (Staszewski and Worden, 1997).

Sensitivity of the energy of wavelet packet transform components to damage was proposed to locate damage in a structure (Law et al., 2005) . The method was validated on experimental data from a steel beam. The energy of wavelet packet transform of the response is used as input into a neural network for damage assessment, including identifying damage occurrence, location, and severity (Sun and Chang, 2002). The network is trained on data from healthy and damaged structure under impact load. The same authors proposed a damage detection method based on unsupervised learning, where damage indicators, calculated using the energy of the wavelet packet transform of the response covariance, are used in conjunction with statistical process control techniques. The method has been illustrated for simulation data of ASCE benchmark study.

Sensitivity of the wavelet transform to the singularities in the response data of a structure with damage has been exploited by different researchers. Spikes in DWT details of the response signals were utilized to identify and locate sudden damage in mechanical systems and civil structures (Corbin et al, 2000; Hera and Hou, 2001, 2004). The sudden change in the spatial variation of the wavelet coefficients was proposed to identify and locate damage in a beam with a crack under static and dynamic loading conditions (Wang et Deng, 1999). Lipschitz exponent estimated from the CWT of the fundamental mode shape of a beam was used to localize and asses the damage extend by Hong et al. (2002). Singularity analysis through the CWT is applied to bearing defect diagnosis in Sun and Tang (2002). A drop in Holder (Lipschitz) exponent calculated by CWT is proposed as damage feature for those types of damage which introduces discontinuity in the signals (Robertson et al., 2003).

Wavelet-based system identification techniques were also developed to identify modal parameters such as natural frequencies, damping ratios and mode shape vectors. Damping identification by wavelet modulus cross section and ridge methods was proposed by Staszewski (1997). Damping identification and its application to civil engineering

building were investigated by Lamarque et al. (2000) and Hans et al. (2000) using a method similar to the conventional logarithmic decrement technique. The cross section method was used by Ruzzene et al. (1997) to identify the natural frequencies and damping ratios using acceleration measurement data of a real bridge. Later, the method was also extended to the mode shape estimation (Piombo et al., 2000). The impulse response of a time invariant system is identified by a DWT deconvolution in (Robertson et al., 1998). The nonlinear system identification by WT has been addressed by Staszewski (1997), applying the ridge method to the impulse response to identify the backbone curve.

Although promising results were obtained, most the above-mentioned wavelet-based system identification methods have a few drawbacks: first, most of them are applied only to a time invariant system; secondly, those techniques applied to nonlinear systems require the impulse responses. These facts limit the application of wavelet theory for detection of cumulative damage for systems in use or subjected to environmental excitation. An attempt to solve this problem was made by Ghanem and Romeo (2000), who proposed to identify the physical parameters of a linear time varying dynamic systems by a wavelet-Galerkin approach. The method has been applied successfully to SDOF and 2DOF systems subjected to a harmonic excitation and it requires the knowledge of system dynamics equation. However, for a large-scale system with a big number of physical parameters prone to damage, or the case when a dynamical model is not available, the method may not be applicable. As an innovative approach in the application of wavelet theory to system identification, this dissertation proposes wavelet-based identification techniques for instantaneous modal parameters of systems with progressive or sudden damage and subjected to stationary and non-stationary excitations.

Practical aspects related to the applications of WT for analysis of civil engineering structures are discussed in (Kijewski and Kareem, 2002, 2003). A comparative study of wavelet packet sifting process, CWT and empirical mode decomposition on their application for structural health monitoring using the impulse responses, has been conducted by Hera et al. (2004).

1.3 Motivation and Objective

There are many situations in the engineering practice when damage occurs and evolves while the structure is in use or is subjected to environmental excitations, for example newly manufactured mechanical systems at the beginning part of their service life when the failure rate is high, or civil structures subjected to severe earthquake events. In addition, in many cases only limited structural information is available and building a physical model of the structure is a very challenging task.

Current global damage identification techniques based on vibration measurements have their limitations due to the assumption of time invariance while data is collected, the availability of the impulse responses, or the requirement for a physical model of the structure. For example, the modal-based approach is constrained to a time-invariant system; therefore damage should not occur when data is collected. The damage detection methods based on parameter updating require the existence of a physical model, but in many cases such a model is not available. The tracking methods, also, require a physical model of the structures and a limited number of parameters to be estimated. The unavailability of a detailed physical model and/or dynamic equations, combined with the lack of data from the same or similar structure with the same damage condition and subjected to the same excitation, excludes the use of pattern recognition algorithms which are based on supervised learning. The techniques based on regression analysis, neural network and novelty/anomaly detection can be still applied; however, since they are used in unsupervised learning mode, the obtained results may lack a physical meaning.

All of these given, the objective of this study is to develop global health monitoring techniques which use the vibration response data and are less model dependant, for structures with evolving damage while they are in use.

To achieve this goal, the damage identification problem is placed in the following framework. Starting from the known fact that change in physical parameters of a structure causes change in the values of modal parameters, damage identification is seen as an inverse problem, where change in the instantaneous modal parameters is an indication of change in the structural health condition. The instantaneous modal parameters are extracted from

vibration responses and should coincide with classical modal parameters in the case of a time-invariant structure. It is assumed that:

1. a structure with gradual stiffness deterioration can be approximately treated as a linear slowly time-varying system and a structure with sudden damage is treated as a linear system before and after the damage.
2. the structure considered is lightly damped and has well separated vibration modes

In addressing this problem, first we need to develop the theoretical basis for time-varying vibration modes. The concept of instantaneous frequency has been introduced before as a characteristic of a signal (Boashash, 1992). It has also been used for identification of nonlinear systems (Staszewski, 1997) and damage detection (Hera et al., 2004), but the connection between the system physical parameters and instantaneous frequency of the impulse response was only intuitive. Questions such as: what are the time-varying vibration modes, when these modes exist, how to define mathematically the instantaneous modal parameters and how to identify them from forced vibration responses, have not found an answer till date. In this dissertation, theoretical basis of time-varying vibration modes and their parameters is developed to address these concerns.

Secondly, we propose identification techniques of instantaneous modal parameters for real applications where the excitation may be nonstationary and problems related to observability and measurement noise may arise. The robustness of these techniques in the presence of measurement noise, incomplete measurements and system nonlinearities will be addressed. The effectiveness of the SHM based on instantaneous modal parameters is illustrated via both simulation and experimental data.

Although, some of the examples in the present study originate from the interest in the health monitoring of civil structures subjected to earthquake excitation, the time varying modal analysis and most of the discussion and results presented apply for the general field of structural dynamics.

1.4 Dissertation Overview

The remainder of the dissertation is organized as follows:

Chapter 2 provides the relevant mathematical background for this study. It includes concepts as time-varying system and dynamic eigenvalue problem, modal analysis, wavelet theory, and Hilbert Transform.

Chapter 3 develops the theoretical basis for time-varying vibration modes and instantaneous modal parameters. Concretely, it is shown that a modal decomposition for the 2nd order linear time-varying systems is possible by solving the dynamic eigenvalue problem associated to the corresponding 1st-order system. Then, the discussion focused on a subclass of time varying systems, which are called slowly-time varying systems. These systems have real time-varying vibration mode characterized by modal parameters with physical significance, i.e. positive instantaneous frequency and real instantaneous mode shapes. The chapter ends with an example which illustrates some of the concepts introduced in this chapter.

Chapter 4 presents identification methods for instantaneous modal frequency and normalized instantaneous mode shape from free vibration data. Two approaches are proposed for identification: the CWT–ridge method and wavelet packet sifting technique in conjunction with Hilbert transform. First, modal responses are extracted from the measured response, and then the instantaneous parameters are identified. The approach is tested on simulation data from a 3DOF with progressive stiffness degradation and nonzero initial velocity. The identified results are compared to those from solving the dynamic eigen-value problem, and they are in good agreement.

In *Chapter 5*, the normalized instantaneous mode shape is identified from the forced vibration response by using a wavelet packet sifting process. A confidence index, calculated using the instantaneous frequency of the sifted signals, is introduced to validate the identified results. It is demonstrated that the identified normalized instantaneous mode shapes in conjunction with the corresponding confidence indices can be effectively used to monitor damage development in a structure. The effectiveness of the proposed approach is illustrated for a three-degree-of-freedom structure subjected to a base excitation. Two

damage scenarios, sudden stiffness loss and progressive stiffness degradation, and different base excitations including three real earthquake signals, a random signal and few harmonic signals are considered. Issues related to robustness of the method in the presence of measurement noise and sensitivity to damage severity are discussed.

In *Chapter 6*, a time-varying Kalman filter technique is integrated with the wavelet approach to identify the instantaneous natural frequencies and the instantaneous modal damping ratios. The physical significance of the sifted components by wavelet packet sifting technique is assured by introducing a new sifting criterion based on the confidence index. The potential of the proposed approach for SHM is demonstrated by a simulation study for a two-degree-of-freedom system with progressive damage and subjected to two sets of excitation: one is a sample generated from a filtered Gaussian discrete process and the other is a true ground acceleration measurement. The effectiveness of the method in the presence of measurement noise is also addressed.

Chapter 7 presents a preliminary study on the meaning of instantaneous modal parameters and their use for SHM of systems with nonlinear dynamic behavior. A two-degree-of-freedom system with bilinear restoring forces, subjected to both impulse and harmonic excitation, is considered. The instantaneous modal parameters are identified from the simulated vibration responses by CWT in conjunction with the Hilbert Transform. It is illustrated that change in the identified instantaneous modal parameters may have different patterns for the linear system, the system with slow stiffness degradation, and the system with bilinear restoring forces. The results may help to distinguish change in the instantaneous modal parameters caused by structural damage or by structural nonlinear behavior and therefore to improve the accuracy of structural health monitoring.

Chapter 8 evaluates the performance of the proposed approaches for instantaneous modal parameter identification and SHM using the data from two sets of experiments. The first set refers to ASCE- SHM benchmark studies, Phase2 of the experiments. The response data of a hammer test before and after damage is used in analysis. The structure, which is time invariant during tests, is considered a particular case of a time varying system. Another experimental data are from a shaking table test of a full-size two-story Japanese wooden

building structure. The structure was excited by an earthquake ground motion scaled at several target intensity levels. Damages to various extents were observed during the tests. The integrated approach consisting in Kalman filter and wavelet packet sifting process is used to estimate the instantaneous natural frequencies; wavelet packet decomposition in conjunction with the confidence index is employed to identify the normalized instantaneous mode shape.

Chapter 9 summarizes the conclusions and contributions made in the dissertation and suggests some topics for the further research.

Chapter 2

MATHEMATICAL BACKGROUND

In this dissertation, we intend to develop the theoretical basis for time varying vibration modes and to propose a SHM approach based on instantaneous modal parameters. The required mathematical background includes concepts such as time-varying system, modal analysis, wavelet analysis, and Hilbert Transform. The concept of time varying system is used to describe mathematically a system with damage. Concepts from traditional modal analysis, such as vibration mode, modal frequency and mode shape, are extended to describe the time varying nature of a system with damage. Wavelet analysis is used for graphical illustration of time-frequency nature of the response data and identification of instantaneous modal parameters. Hilbert Transform is employed for explanation of the concept and identification of instantaneous modal frequency. All those relevant mathematical aspects are presented in this Chapter.

2.1 Linear Time Varying Systems

In this dissertation, the dynamics of a structure with damage is described by a set of second order differential equations with time varying coefficients. In the state space formulation such a system of equations is transformed into a first-order differential system whose state space vector is built by concatenation of the displacement and velocity vectors. Motivated by this formulation, the theoretical background of the first-order linear time varying systems is presented.

2.1.1 System Response Using the State Transition Matrix¹

A linear time varying (LTV) system is described by the following state space equation:

$$\dot{\mathbf{y}}(t) = \mathbf{A}(t)\mathbf{y}(t) + \mathbf{B}(t)\mathbf{f}(t) \quad (2.1.1)$$

where $\mathbf{y}(t)$ is the $n \times 1$ state space vector, $\mathbf{A}(t)$ is the $n \times n$ system matrix, $\mathbf{B}(t)$ is the $n \times p$ input matrix and $\mathbf{f}(t)$ is the $p \times 1$ input/force vector. It is assumed that the solution of this system is unique for a given initial condition $\mathbf{y}(t_0)$ and any input $\mathbf{f}(t)$. A sufficient condition which entitles this assumption is that $\mathbf{A}(t)$ is a continuous function of time. To solve the system (2.1.1) the definitions of the fundamental matrix and the state transition matrix are first introduced.

The *fundamental matrix* $\mathbf{Y}(t)$ of the system is a $n \times n$ matrix whose columns are a set of n linearly independent solutions of the homogeneous system (2.1.2). It satisfies the homogeneous system equation, i.e. $\dot{\mathbf{Y}}(t) = \mathbf{A}(t)\mathbf{Y}(t)$ and has the form in eq. (2.1.3).

$$\dot{\mathbf{y}}(t) = \mathbf{A}(t)\mathbf{y}(t) \quad (2.1.2)$$

$$\mathbf{Y}(t) = [\mathbf{y}_1(t), \mathbf{y}_2(t), \dots, \mathbf{y}_n(t)] \quad (2.1.3)$$

The *state transition matrix* of the system, $\Phi(t, t_0)$, is a matrix-valued function of t and t_0 , which is the solution of the eq. (2.1.4) and is connected with any fundamental matrix by expression (2.1.5).

$$\frac{\partial}{\partial t} \Phi(t, t_0) = \mathbf{A}(t)\Phi(t, t_0), \quad \Phi(t_0, t_0) = \mathbf{I}; \quad (2.1.4)$$

$$\Phi(t, t_0) = \mathbf{Y}(t)\mathbf{Y}^{-1}(t_0) \quad (2.1.5)$$

A few important properties of the state transition matrix, satisfied for any t, t_1, τ , are as follows:

$$\begin{aligned} \Phi(t, t) &= \mathbf{I}; \\ \Phi(t, \tau) &= \Phi(t, t_1)\Phi(t_1, \tau) \\ \Phi^{-1}(t, \tau) &= [\mathbf{Y}(t)\mathbf{Y}^{-1}(\tau)]^{-1} = \mathbf{Y}(\tau)\mathbf{Y}^{-1}(t) = \Phi(\tau, t) \end{aligned} \quad (2.1.6)$$

¹ The material presented in sections 2.1.1 and 2.1.2.1 is a well established theory which can be found in textbook on Linear Systems such as Zadeh and Desoer (1963) or Chen (1999).

Given the transition matrix $\Phi(t, \tau)$, the initial state \mathbf{x}_0 at t_0 and the input $\mathbf{f}(t)$ applied for $t \geq t_0$, the general solution of system (2.1. 1) can be expressed as shown in (2.1. 7):

$$\begin{aligned} \mathbf{y}(t) &= \Phi(t, t_0)\mathbf{y}(t_0) + \int_{t_0}^t \Phi(t, \tau)\mathbf{B}(\tau)\mathbf{f}(\tau)d\tau = \\ &= \Phi(t, t_0) \left[\mathbf{y}(t_0) + \int_{t_0}^t \Phi(t_0, \tau)\mathbf{B}(\tau)\mathbf{f}(\tau)d\tau \right], \quad t > t_0 \end{aligned} \quad (2.1. 7)$$

The response of the system has two components: the first term is the free response for zero input and the second term is the forced response. The zero-input response is caused by the nonzero initial values of the states. The second term is the solution for an input force vector $\mathbf{f}(t)$ and zero initial conditions. The state transition matrix $\Phi(t, t_0)$ can be seen as a linear transformation which maps the state \mathbf{y}_0 at t_0 into the state $\mathbf{y}(t)$ at t . Each component $\Phi_{ij}(t, t_0)$ of the state transition matrix, can be interpreted as the response of state i , at time t , due to a unity value of state j and zero value of all other states at time t_0 when no input/excitation is applied to the system.

2.1.2 Modal Decomposition

In the previous section, the system response has been formulated in terms of state transition matrix. It is well known that in the case of time invariant systems, the response can be expressed as a sum of elementary modal responses, which are obtained by solving the algebraic eigenvalue problem for the system matrix \mathbf{A} . Such a formulation is very useful for a vibration system, where the eigenvectors and eigenvalues are associated with physical properties of the system. Modal decomposition for time varying systems has been proposed before; however, according to the author knowledge, it has not yet found a place in the textbooks. Since it can be seen as an extension of the modal decomposition of linear time invariant (LTI) systems, for a better understanding, a summary of modal decomposition for the time invariant case is first presented.

2.1.2.1 Modal Decomposition of Linear Time Invariant Systems

For a time invariant system, with homogeneous equation (2.1. 8), the state transition matrix is given by expression in eq. (2.1. 9).

$$\dot{\mathbf{y}}(t) = \mathbf{A}\mathbf{y}(t) \quad (2.1. 8)$$

$$\Phi(t, t_0) = \Phi(t - t_0) = \exp(\mathbf{A}(t - t_0)) \quad (2.1. 9)$$

If there exists an algebraic transformation $\mathbf{U} = [\mathbf{u}^{(1)} \quad \mathbf{u}^{(2)} \quad \dots \quad \mathbf{u}^{(n)}]$ which diagonalizes matrix \mathbf{A} , i.e. $\mathbf{U}^{-1}\mathbf{A}\mathbf{U} = \mathbf{\Lambda}$ where $\mathbf{\Lambda} = \text{diag}(\lambda_i)$, the state transition matrix can be expressed as in eq. (2.1. 10) and the homogeneous response can be written as a weighted sum of system modes as shown in eq. (2.1. 11).

$$\Phi(t - t_0) = \mathbf{U} \exp(\mathbf{\Lambda}(t - t_0))\mathbf{U}^{-1} \quad (2.1. 10)$$

$$\mathbf{y}(t) = \Phi(t - t_0)\mathbf{y}(t_0) = \mathbf{U} \exp(\mathbf{\Lambda}(t - t_0))\mathbf{U}^{-1}\mathbf{y}_0 = \sum_{i=1}^n \exp(\lambda_i(t - t_0))\mathbf{u}^{(i)}\mathbf{v}^{(i)T}\mathbf{y}_0 \quad (2.1. 11)$$

In eq. (2.1. 11), the notation $[\mathbf{v}^{(1)}, \mathbf{v}^{(2)}, \dots, \mathbf{v}^{(n)}]^T = \mathbf{U}^{-1}$ has been introduced.

λ_i and $\mathbf{u}^{(i)}$ are known as the i^{th} eigenvalue and the i^{th} eigenvector of the system matrix \mathbf{A} , and they can be found by solving algebraic eigenvalue problem defined as follows:

λ is said to be an eigenvalue of \mathbf{A} and \mathbf{u} is the associate eigenvector of the matrix \mathbf{A} , if for the $n \times n$ matrix \mathbf{A} , there exists a scalar λ and a nonzero vector \mathbf{u} such that they satisfy the following condition:

$$\mathbf{A}\mathbf{u} = \lambda\mathbf{u} \quad (2.1. 12)$$

The eigenvalues are calculated as the solution of the characteristic equation: $\det(\mathbf{A} - \lambda\mathbf{I}) = 0$. If the system matrix \mathbf{A} has real coefficients, as it is the case in the present study, its eigenvalues are either real or they appear in complex conjugate pairs. The eigenvalues are important in assessing the stability of a dynamic system. A linear system is asymptotically stable if and only if all of its eigenvalues have a negative real part. If the eigenvalues of a matrix are distinct, the corresponding eigenvectors are linear independent and the transformation matrix \mathbf{U} is nonsingular. A system with repeated eigenvalues may not

necessarily be reduced to a diagonal form; however, they can be represented as a Jordan canonical form, which has the eigenvalues of \mathbf{A} on the main diagonal and zero or one on the next diagonal. Each Jordan block represents a set of coupled modes/differential equations.

The eigenvectors and eigenvalues have a clear physical meaning. In the case of a mechanical/structural system they are closely related to the mode-shapes, natural frequencies and modal damping ratios of the system.

2.1.2.2 Dynamic Eigenvalue Problem

Modal decomposition of time-varying systems has been a topic of interest during the last 25 years. The stability of such systems has been of crucial interest for control community (Wu, 1974, 1980). Some other studies have been also motivated by analysis of electrical and electronic circuits (Kloet, 2002). Applications to mechanical/civil engineering systems are not known to the author.

In contrast to the linear time invariant system, whose stability can be determined by the placement of eigenvalues of system matrix on the complex plane, it has been shown that the stability or instability of a time varying system described by eq. (2.1. 1) cannot be determined from the algebraic eigenvalues of the matrix $\mathbf{A}(t)$ with frozen t (Wu, 1974).

In order to asses the stability of a time varying system by a straightforward criterion, a new concept of dynamic eigenvalue and eigenvector, called dynamic eigenpair², has been defined by (Wu, 1980) as follows:

For a given $n \times n$ matrix $\mathbf{A}(t)$, if there exists a scalar $\lambda(t)$ and a nonzero differentiable vector $\mathbf{u}(t)$ such that they satisfy the following condition:

$$\mathbf{A}(t)\mathbf{u}(t) = \lambda(t)\mathbf{u}(t) + \dot{\mathbf{u}}(t), \quad \forall t \quad (2.1. 13)$$

then $\lambda(t)$ is said to be a dynamic eigenvalue of $\mathbf{A}(t)$ associated to the eigenvector $\mathbf{u}(t)$.³

² In the literature the dynamic eigenvalues/eigenvectors as defined in eq. (2.1.13) have been cited as: “eigenvalues”/ “eigenvectors” (Wu, 1980), extended eigenvalues/ extended eigenvectors or x-eigenvalues/x-eigenvalues (Wu, 1984). The name of dynamic eigenvalues/dynamic eigenvectors can be found, predominantly, in the work of the researchers at Delft University of Technology (Kloet, 2000).

The dynamic eigenpair $(\lambda(t), \mathbf{u}(t))$ reduces to the algebraic one, calculated for frozen time, when the eigenvectors of $\mathbf{A}(t)$ are constant. A few properties specific to the algebraic eigenvalue problem are preserved: (1) dynamic eigenvalues are invariant under an algebraic transformation, (2) there exists an algebraic transformation which will transform $\mathbf{A}(t)$ into a diagonal matrix, and (3) the impulse response can be realized by the new transformed diagonal matrix. It was shown that the stability of a time varying system requires consideration of both, dynamic eigenvalues and dynamic eigenvectors of matrix $\mathbf{A}(t)$.

According to the definition (2.1. 13) the solution of the system $\dot{\mathbf{y}}(t) = \mathbf{A}(t)\mathbf{y}(t)$ can be considered as a dynamic eigenvector of $\mathbf{A}(t)$ associated with the dynamic eigenvalue zero, and unity state transition matrix at the initial time. In the same reference (Wu, 1980), it has been shown that there exists a time varying transformation matrix which diagonalizes matrix $\mathbf{A}(t)$ to any given diagonal matrix.

2.1.2.3 Modal Decomposition of Linear Time Varying Systems

In the following, it is shown that the response of a LTV system in the state space formulation, can be decomposed into elementary modes similar to the modes of a LTI system (Kloet,2000; Wu, 1980).

Let's consider the algebraic transformation (2.1. 14), where $\mathbf{L}(t)$ is a Lyapunov transformation⁴.

$$\mathbf{y}(t) = \mathbf{L}(t)\mathbf{q}(t) \quad (2.1. 14)$$

By this transformation, the system (2.1. 2) is transformed into a new linear time-varying system in eq. (2.1. 15), where matrix $\mathbf{R}(t)$ is given by equation (2.1. 16).

³ The dynamic eigen problem in eq. (2.1. 13) is obtained by making the assumption that the solution of the homogeneous system has the following form $\mathbf{y}(t) = \mathbf{u}(t)\exp(\nu(t))$, where $\lambda(t) = \frac{d}{dt}\nu(t)$, $\nu(t) = \int_{t_0}^t \lambda(t)dt$, and then substituting it in eq. (2.1. 2)

⁴ A matrix $\mathbf{L}(t)$ is called a Lyapunov transformation if $\mathbf{L}(t)$ is nonsingular, $\mathbf{L}(t)$ and $\dot{\mathbf{L}}(t)$ are continuous, and $\mathbf{L}(t)$ and $\mathbf{L}^{-1}(t)$ are bounded for all t. (Chen, 1999)

$$\dot{\mathbf{q}}(t) = \mathbf{R}(t)\mathbf{q}(t) \quad (2.1.15)$$

$$\mathbf{R}(t) = \mathbf{L}^{-1}(t)\mathbf{A}(t)\mathbf{L}(t) - \mathbf{L}^{-1}(t)\dot{\mathbf{L}}(t) \quad (2.1.16)$$

The dynamic eigenvalue problem for the transformed system (2.1.15) is defined in eq.(2.1.17), where the dynamic eigenpair is $\{\lambda, (\mathbf{L}^{-1}\mathbf{u})\}$.

$$(\mathbf{A}(t) - \lambda(t)\mathbf{I})(\mathbf{L}^{-1}(t)\mathbf{u}(t)) = d/dt(\mathbf{L}^{-1}(t)\mathbf{u}(t)) \quad (2.1.17)$$

If $\mathbf{L}(t)$ has columns the dynamic eigenvectors of $\mathbf{A}(t)$, i.e. $\mathbf{L}(t) = [\mathbf{u}^{(1)}(t) \quad \mathbf{u}^{(2)}(t) \quad \dots \quad \mathbf{u}^{(n)}(t)]$, the matrix $\mathbf{R}(t)$ is equal to the diagonal matrix $\mathbf{\Lambda}(t)$ whose diagonal elements are the dynamic eigenvalues of $\mathbf{A}(t)$, and equation (2.1.15) is uncoupled. Once the diagonal matrix $\mathbf{\Lambda}(t)$ and the transformation matrix $\mathbf{L}(t)$ are found, the modal form of the solution. i.e. $\mathbf{y}(t) = \sum_i \mathbf{u}^{(i)}(t) \exp\left(\int_{t_0}^t \lambda_i(t) dt\right)$ is obvious.

$\mathbf{y}^{(i)}(t) = \mathbf{u}^{(i)}(t) \exp\left(\int_{t_0}^t \lambda_i(t) dt\right)$ is called the i^{th} elementary mode. Algorithms to calculate $\mathbf{L}(t)$ and $\mathbf{\Lambda}(t)$ are presented in Section 2.1.2.4.

The state transition matrix can be expressed as shown in eq. (2.1.18) (Wu, 1984):

$$\Phi(t, t_0) = \mathbf{L}(t) \exp\left(-\int_0^t \mathbf{\Lambda}(\tau) d\tau\right) \mathbf{L}^{-1}(t_0) \quad (2.1.18)$$

From its expanded form in eq. (2.1.19), it can be observed that the state transition matrix is a weighted sum of elementary modes, where the weighting coefficients are constant and depend on initial conditions.

$$\Phi(t, t_0) = \sum_{i=1}^N \exp\left(-\int_{t_0}^t \lambda_i(\tau) d\tau\right) \mathbf{u}^{(i)}(t) \mathbf{v}^{(i)T}(t_0) = \sum_{i=1}^n \mathbf{y}^{(i)}(t) \mathbf{v}^{(i)T}(t_0) \quad (2.1.19)$$

2.1.3 System Response by Modal Decomposition Approach

With the transformation in eq. (2.1.14) and with the assumption that $\mathbf{L}(t)$ is a Lyapunov transformation whose columns are the dynamic eigenvectors of matrix $\mathbf{A}(t)$, the system (2.1.1) reduces to a set of uncoupled equation as shown in (2.1.20):

$$\begin{aligned}\dot{\mathbf{q}}(t) &= [\mathbf{L}^{-1}\mathbf{A}\mathbf{L} - \mathbf{L}^{-1}\dot{\mathbf{L}}]\mathbf{q}(t) + \mathbf{L}^{-1}\mathbf{B}\mathbf{f}(t) = \boldsymbol{\Lambda}\mathbf{q}(t) + \mathbf{L}^{-1}\mathbf{B}\mathbf{f}(t) \\ \mathbf{q}(t_0) &= \mathbf{L}^{-1}(t_0)\mathbf{y}_0\end{aligned}\quad (2.1.20)$$

By using the notation $\mathbf{Q}(t) = \mathbf{B}\mathbf{f}(t)$, and the already introduced $\mathbf{L}^{-1}(t) = [\mathbf{v}^{(1)}(t), \mathbf{v}^{(2)}(t), \dots, \mathbf{v}^{(n)}(t)]^T$, eq. (2.1.20) can be written in the scalar form as:

$$\begin{aligned}\dot{q}_k(t) &= \lambda_k(t)q_k(t) + \mathbf{v}^{(k)T}(t)\mathbf{Q}(t), \quad k = 1, 2, \dots, n \\ q_k(t_0) &= \mathbf{v}^{(k)T}(t_0)\mathbf{y}_0,\end{aligned}\quad (2.1.21)$$

The solution of eq. (2.1.21) is called modal coordinate and is given by:

$$q_k(t, t_0) = \mathbf{v}^{(k)T}(t_0)\mathbf{y}(t_0) \exp\left(\int_{t_0}^t \lambda_k(\tau) d\tau\right) + \int_{t_0}^t \mathbf{v}^{(k)T}(\tau)\mathbf{Q}(\tau) \exp\left(\int_{\tau}^t \lambda_k(\xi) d\xi\right) d\tau \quad (2.1.22)$$

The modal coordinate has two components. The first term is called homogeneous or zero input modal coordinate and is due to nonzero initial conditions. With the notation in eq. (2.1.23) it can be expressed as shown in eq. (2.1.24).

$$\lambda_k(t) = \gamma_{\lambda,k}(t) + i\omega_{\lambda,k}(t), \quad \gamma_{\lambda,k}(t) = \text{Re}(\lambda_{\lambda,k}(t)), \quad \omega_{\lambda,k}(t) = \text{Im}(\lambda_k(t)) \quad (2.1.23)$$

$$q_{h,k}(t, t_0) = \mathbf{v}^{(k)T}(t_0)\mathbf{y}(t_0) \exp\left(\int_{t_0}^t \gamma_{\lambda,k}(\tau) d\tau\right) \exp\left(i \int_{t_0}^t \omega_{\lambda,k}(\tau) d\tau\right) \quad (2.1.24)$$

The second term reflects the effect of the excitation/input on the response and is called the forced modal coordinate. It is given by the formula in eq. (2.1.25).

$$q_{f,k}(t) = \int_{t_0}^t \mathbf{v}^{(k)T}(\tau)\mathbf{Q}(\tau) \exp\left(\int_{\tau}^t \lambda_k(\xi) d\xi\right) d\tau \quad (2.1.25)$$

The response of a linear time varying system can be written as a superposition of modal responses as shown in eq. (2.1.26), and it has homogeneous and forced components.

$$\mathbf{y}(t) = \sum_{k=1}^n \mathbf{y}^{(k)}(t) = \sum_{k=1}^n \mathbf{u}^{(k)}(t)q_k(t, t_0) \quad (2.1.26)$$

The homogeneous and forced components of the k^{th} modal response vector are given in eqs. (2.1.27) and (2.1.28), where $C_k(t_0) = \mathbf{v}^{(k)T}(t_0)\mathbf{x}(t_0)$ is a real or complex constant, which depends on the initial state and the dynamic eigenvector matrix at t_0 .

$$\begin{aligned} \mathbf{y}_h^{(k)}(t) &= \mathbf{u}^{(k)}(t)q_{k,h}(t) = \\ &= \left| \mathbf{u}^{(k)}(t) \right| C_k(t_0) \exp\left(\int_{t_0}^t \gamma_{\lambda,k}(\tau) d\tau \right) \bullet \exp\left(i \arg(\mathbf{u}^{(k)}(t)) + i \int_{t_0}^t \omega_{\lambda,k}(\tau) d\tau + \mathbf{1} i \arg(C_k(t_0)) \right) \end{aligned} \quad (2.1.27)$$

$$\mathbf{y}_f^{(k)}(t) = \mathbf{u}^{(k)}(t)q_{f,k}(t) = \left| \mathbf{u}^{(k)}(t) \right| q_{f,k}(t) \bullet \exp\left(i \arg(\mathbf{u}^{(k)}(t)) + \mathbf{1} i \arg(q_{f,k}(t)) \right) \quad (2.1.28)$$

2.1.4 Algorithms for Solving the Dynamic Eigenvalue Problem

It has been shown in Wu (1980), that there exists a time varying transformation matrix which diagonalizes matrix $\mathbf{A}(t)$ to any given diagonal matrix. However, for some systems, an arbitrary decomposition may not be physically meaningful. Two algorithms to solve the dynamic eigenvalue problem are presented in the following.

1. Iterative algorithm (Wu, 1984)

An iterative algorithm which gives a unique decomposition and meaningful modes for assessing the system stability has been proposed by Wu (1984). Later Kloet (2000) came with a complete convergence proof for this algorithm. Wu's algorithm used the algebraic eigenvalues and eigenvectors as starting point in the iteration process. This selection is based on the fact that if $\mathbf{A}(t)$ has distinct eigenvalues, it always can be diagonalized by a nonsingular matrix formed by the eigenvectors of $\mathbf{A}(t)$. The iteration algorithm is described by:

$$\mathbf{\Lambda}_j = \mathbf{S}_j^{-1} (\mathbf{A} - \dot{\mathbf{S}}_{j-1} \mathbf{S}_{j-1}^{-1}) \mathbf{S}_j, \quad (j = 1, 2, \dots), \quad \mathbf{S}_0 = \mathbf{I}, \quad \dot{\mathbf{S}}_0 = \mathbf{0} \quad (2.1.29)$$

Van der Kloet proved that if the $(\dot{\mathbf{S}}_j, j = 1 \dots \infty)$ is uniform convergent, then the diagonal matrix $\mathbf{\Lambda}(t)$ and transformation matrix $\mathbf{L}(t)$ can be obtained as:

$$\mathbf{\Lambda}(t) = \lim_{j \rightarrow \infty} \mathbf{\Lambda}_j(t) \quad \text{and} \quad \mathbf{L}(t) = \lim_{j \rightarrow \infty} \mathbf{S}_j(t) \quad (2.1.30)$$

This algorithm is called by Kloet (2000) "explicit" because the matrix \mathbf{A} is presented in the formulation (2.1.29) at each step. In the same paper a variation of Wu's algorithm, called "implicit diagonalization" has also been proposed, where instead of matrix \mathbf{A} , one may use

the value $\Lambda_{j-1}(t)$ from the previous iteration, and as starting values: $\mathbf{S}_0 = \mathbf{I}$, $\Lambda_0 = \mathbf{A}$. When the convergence criteria is satisfied, both algorithms converge to the same results.

2. Algorithm based on quasistatic eigenvalues

The iterative algorithm proposed by Wu (1984) may fail on numerical implementation due to the difficulties in satisfying the convergence criterion. Each iteration step requires solving the algebraic eigenvalue problem keeping the derivative of the eigenvector matrix continuous. Finding a normalization procedure for the eigenvector matrix which ensures the continuity condition is a very challenging task.

In the following, we propose an algorithm, referred as “*quasistatic algorithm*”, which can be easily implemented and leads to physically meaningful modes in the case of slow time-varying systems, which will be discussed in Chapter 3. Starting with the fact that a linear time varying system can be diagonalized to any given diagonal matrix, we impose as dynamic eigenvalues the quasistatic eigenvalues of matrix $\mathbf{A}(t)$, which are calculated by solving the algebraic eigenvalue problem $\{\lambda(t), \mathbf{u}_{qs}(t)\}$ at each time instant.

$$\mathbf{A}(t)\mathbf{u}_{qs}(t) = \lambda(t)\mathbf{u}_{qs}(t), \quad \forall \text{ frozen } t \quad (2.1.31)$$

Then, given the dynamic eigenvalue, $\lambda(t)$, the dynamic eigenvector is obtained from eq. (2.1.13) as:

$$\mathbf{u}(t) = \mathbf{u}(t_0) \exp\left(\int_{t_0}^t (\mathbf{A}(\tau) - \lambda(\tau)\mathbf{I})d\tau\right), \quad \mathbf{u}(t_0) = \mathbf{u}_{qs}(t_0) \quad (2.1.32)$$

This algorithm can be applied for any matrix $\mathbf{A}(t)$ but a physical meaning of dynamic eigenpair is ensured only for the case of slowly time-varying systems. Since $\mathbf{A}(t)$ has real coefficients, the dynamic eigenvalues are either real or complex conjugates. The dynamic eigenvectors have the same nature as the corresponding dynamic eigenvalues.

2.2 Modal Analysis

In this section, we present a brief review of modal analysis for LTI systems. For simplicity, only the case of real distinct eigenvalues is presented. A complete discussion including duplicated eigenvalues, can be found in advanced vibration textbooks (Ginsberg, 2001).

The dynamics of a linear time-invariant multi-degree-of-freedom (MDOF) system is governed by the following equation:

$$\mathbf{M}\ddot{\mathbf{x}}(t) + \mathbf{C}_d\dot{\mathbf{x}}(t) + \mathbf{K}\mathbf{x}(t) = \mathbf{f}(t) \quad (2.2.1)$$

where \mathbf{x} is the $N \times 1$ displacement vector and $\mathbf{f}(t)$ is the $N \times 1$ excitation vector, \mathbf{M} , \mathbf{K} and \mathbf{C}_d are the $N \times N$ mass, stiffness and damping matrices of the system, respectively. By modal analysis, when damping matrix satisfies certain criteria, the system (2.2.1) can be transformed into an equivalent system with N uncoupled equations of motion.

Modal analysis involves calculation of eigenvalues and eigenvectors for the corresponding undamped system:

$$\mathbf{K}\mathbf{X} = \mathbf{M}\mathbf{X}\mathbf{\Lambda}, \quad \mathbf{X} \neq \mathbf{0} \quad (2.2.2)$$

where $\mathbf{X} = [\mathbf{X}^{(1)}, \mathbf{X}^{(2)}, \dots, \mathbf{X}^{(N)}]$ is a matrix $N \times N$ whose columns represent the eigenvectors or the mode shapes, and $\mathbf{\Lambda}$ is a diagonal matrix whose diagonal elements represent the eigenvalues or the squared natural frequencies, i.e. $\lambda_i = \omega_i^2$, $i = 1, 2, \dots, N$.

To obtain the system response, damping should be defined. Different models are used to represent the damping in a structure, but the most common are the modal damping and proportional damping. The modal damping model extends the concept of damping ratio from SDOF systems to MDOF systems, by introducing the assumption that each vibration mode has its own damping. The proportional damping model assumes that damping matrix \mathbf{C}_d is a linear combination of the mass and stiffness matrices, that is $\mathbf{C}_d = \alpha\mathbf{M} + \beta\mathbf{K}$, where α and β are dimensional constants.

With the assumption that \mathbf{X} is nonsingular and normalized in respect to the mass matrix, i.e. $\mathbf{X}^{-1}\mathbf{M}\mathbf{X} = \mathbf{I}$, and considering one of the damping models mentioned in the

previous paragraph, the system (2.2. 1) reduces to a set of N uncoupled second order differential equations, each of them describing the motion of a damped SDOF system as follows:

$$\begin{aligned} \ddot{\eta}_i(t) + 2\zeta_i\omega_i\dot{\eta}_i(t) + \omega_i^2\eta_i(t) &= f_{\eta_i}(t) \quad i = 1,2, \dots N \\ \eta_i(0) &= \mathbf{X}^{(i)T} \mathbf{x}(0), \quad \dot{\eta}_i(0) = \mathbf{X}^{(i)T} \dot{\mathbf{x}}(0) \end{aligned} \quad (2.2. 3)$$

where $\eta_i(t)$ represents the modal coordinate, ω_i is the i^{th} natural frequency, ζ_i is the i^{th} modal damping ratio, and f_{η_i} stands for the i^{th} modal force.

$$f_{\eta_i}(t) = \mathbf{X}^{(i)T} \mathbf{f}(t) \quad (2.2. 4)$$

For a lightly damped system, when $0 \leq \zeta_i < 1$, the solution of eq. (2.2. 3) can be expressed as:

$$\begin{aligned} \eta_i(t) &= \exp(-\zeta_i\omega_i t) \left\{ \cos \omega_{di} t + \frac{\zeta_i}{\sqrt{1-\zeta_i^2}} \sin \omega_{di} t \right\} \eta_i(0) + \left\{ \frac{1}{\omega_{di}} \exp(-\zeta_i\omega_i t) \sin \omega_{di} t \right\} \dot{\eta}_i(0) \\ &+ \frac{1}{\omega_{di}} \int_0^t f_{\eta_i}(\tau) \exp(-\zeta_i\omega_i(t-\tau)) \sin(\omega_{di}(t-\tau)) d\tau \end{aligned} \quad (2.2. 5)$$

where $\omega_{di} = \omega_i \sqrt{1-\zeta_i^2}$ is the i^{th} damped natural frequency.

Moreover, the solution of system can be written as a weighted sum of modal coordinates as shown as:

$$\mathbf{x}(t) = \mathbf{X}\boldsymbol{\eta}(t) = \sum_{i=1}^N \mathbf{X}^{(i)} \eta_i(t) \quad (2.2. 6)$$

In Chapter 3, concepts as natural frequency, modal damping ratio and mode shape will be extended to the case of a linear time-varying system.

2.3 Wavelet Analysis

Applications of wavelet analysis cover many diverse areas, from quantum physics to signal and image processing. In this study, it is used as a tool to investigate nonstationary signals in the time-frequency domain. Mathematically, the process of wavelet analysis is represented by the Wavelet Transform. Major mathematical developments can be found in Chui (1992, 1997) and Daubechies (1992).

2.3.1 Wavelet Function

Wavelet analysis starts with an appropriately selected mother wavelet. A *wavelet* $\psi(t)$ is defined as a square-integrable waveform with an effectively finite support in time domain and zero time average. The wavelet function must satisfy the admissibility condition given in eq.(2.3.1) where $\hat{\psi}(\omega)$ is the Fourier transform of the wavelet function.

$$C_{\psi} = \int_{-\infty}^{+\infty} \frac{|\hat{\psi}(\omega)|^2}{|\omega|} d\omega < \infty \quad (2.3.1)$$

To guarantee this condition, $\hat{\psi}(0)$ should be zero. This explains the requirement of zero average over the time domain.

A *wavelet family* associated to the pre-selected mother wavelet $\psi(t)$ can be generated by two operations: *scaling* and *shifting*, as expressed in the following equation:

$$\psi_{a,b}(t) = \frac{1}{\sqrt{a}} \psi\left(\frac{t-b}{a}\right) \quad (2.3.2)$$

where a and b are the scaling and shifting parameters, respectively. Both are real numbers and a must be positive. The normalization factor $1/\sqrt{a}$ in eq. (2.3.2) introduced such that the whole wavelet family has the same L_2 norm for different scales, that is:

$$\int_{-\infty}^{+\infty} |\psi_{a,b}(t)|^2 dt = \int_{-\infty}^{+\infty} |\psi(t)|^2 dt \quad (2.3.3)$$

Expression (2.3.2) is the most common definition for the wavelet family. Another definition (ex. Carmona et al., 1998), is based on L_1 norm where $\psi_{a,b}(t) = \frac{1}{a} \psi\left(\frac{t-b}{a}\right)$.

The Fourier Transform of scaled and shifted wavelet $\psi_{a,b}(t)$ is given by:

$$\psi_{a,b}(\omega) = \sqrt{a} \hat{\psi}(a\omega) \exp(-i\omega b) \quad (2.3.4)$$

The wavelets may have an explicit formula as Haar, Mexican Hat and Morlet wavelets or can be generated by a recursion formula using a scaling function, such as Daubechies wavelets.

The scaling function $\phi(t)$ is obtained by means of a dilation equation and a sequence of constant coefficients $h_n \in L^2(Z)$, which has a form:

$$\phi(t) = \frac{2}{\sqrt{2}} \sum_{n \in Z}^1 h_n \phi(2t - n) \quad (2.3.5)$$

In most of the cases, eq. (2.3.5) is not possible to be solved directly to find out the function $\phi(t)$ and, as an alternative, an iterative algorithm is used. The wavelet function $\psi(t)$ is derived from the corresponding scaling function and another sequence of coefficients $g_n \in L^2(Z)$.

$$\psi(t) = \frac{2}{\sqrt{2}} \sum_{n \in Z}^1 g_n \phi(2t - n) \quad (2.3.6)$$

The coefficients $h_n \in L^2(Z)$ and $g_n \in L^2(Z)$ must satisfy certain conditions (Newland, 1993). A few wavelets used in this study are described in the following and plotted in Fig.2.3.1.

- **Complex Morlet wavelet** is a Gaussian complex modulated function, defined as:

$$\psi(t) = \frac{1}{\sqrt{\pi F_b}} \exp\left(-\frac{t^2}{F_b}\right) \exp(i2\pi F_c t) \quad (2.3.7)$$

where F_c and F_b are the center frequency and the bandwidth parameter of the wavelet, respectively, both being real and positive. In the frequency domain, the complex Morlet wavelet is given by:

$$\hat{\psi}(\omega) = \exp\left(-\frac{(\omega - 2\pi F_c)^2}{4/F_b}\right), \quad \omega > 0 \quad (2.3.8)$$

The complex Morlet wavelet has been preferred in this study due to its best time-frequency localization and simple mathematical formula. It does not have a finite support and does not satisfy exactly the admissibility condition. However, since its modulus decays to zero very quickly and $\hat{\psi}(\omega)$ is practically zero for $F_c > 0.8$ (i.e. $\hat{\psi}(\omega) = 0.00005$, if $F_c=0.8$ and $F_b=1$), it can be used successfully in wavelet analysis.

- **Daubechies Wavelets db_N** , $N=1,2, \dots$ (Daubechies,1992)

These wavelets have no explicit expression except for $db1$, which is also known as the *Haar* wavelet. They are determined recursively from their scaling function coefficients. Some properties of Daubechies wavelets are as follows:

- They have a finite support length of $2N - 1$. The number of vanishing moments of is N . Most db_N are not symmetrical.
- The regularity (smoothness) increases with the order.
- They display fractal geometry
- The wavelet analysis is orthogonal.

- **Meyer wavelet** is defined in the frequency domain, using an auxiliary function, ν , given in eq. (2.3. 9). The wavelet function is given by eq. (2.3. 10). For more details the reader is referred to Daubechies (1992). Plots of scaling and wavelet functions are shown in Fig. 2.3.1.

$$\nu(a) = \begin{cases} 0 & \text{if } a \leq 0 \\ 1 & \text{if } a \geq 1 \end{cases} \quad (2.3.9)$$

$$\nu(a) + \nu(1-a) = 1, \quad a \in (0, 1)$$

$$\psi(\omega) = \begin{cases} \frac{1}{2\pi} \exp(i\omega/2) \sin\left(\frac{\pi}{2} \nu\left(\frac{3}{2\pi}|\omega| - 1\right)\right) & \text{if } \frac{2\pi}{3} \leq |\omega| \leq \frac{4\pi}{3} \\ \frac{1}{2\pi} \exp(i\omega/2) \sin\left(\frac{\pi}{2} \nu\left(\frac{3}{4\pi}|\omega| - 1\right)\right) & \text{if } \frac{4\pi}{3} \leq |\omega| \leq \frac{8\pi}{3} \\ 0 & \text{otherwise} \end{cases} \quad (2.3.10)$$

This wavelet, although does not have finite support in time, has an asymptotic decay to zero when $t \rightarrow \infty$, and there exists a good approximation of the function which leads to finite impulse response (FIR) filters which make possible orthogonal analysis and discrete wavelet transform (DWT).

2.3.2 Continuous Wavelet Transform

Using a selected analyzing wavelet function $\psi(t)$, the continuous wavelet transform (CWT) of a signal $x(t) \in L^2(R)$ is defined as its inner product with the shifted and scaled versions of mother wavelet $\psi(t)$.

$$W_x(a, b) = \frac{1}{\sqrt{a}} \int_{-\infty}^{+\infty} x(t) \psi^*\left(\frac{t-b}{a}\right) dt \quad (2.3.11)$$

The inverse wavelet transform of $W_x(a, b)$ is given as follows:

$$x(t) = \frac{1}{C_\psi} \int_0^{+\infty} \int_{-\infty}^{+\infty} (W_x)(a, b) \psi\left(\frac{t-b}{a}\right) \frac{1}{a^2} da db \quad (2.3.12)$$

where C_ψ represents the admissibility coefficient defined in eq. (2.3.1).

Another method to calculate the CWT is based on the inverse Fourier transform as shown in eq.(2.3.13), where $\hat{x}(\omega)$ is the Fourier transform of the analyzed signal and $\hat{\psi}^*(a\omega)$ given by eq. (2.3.4).

$$W_x(a, b) = \frac{\sqrt{a}}{2\pi} \int_{-\infty}^{+\infty} \hat{x}(\omega) \hat{\psi}^*(a\omega) \exp(i\omega b) d\omega \quad (2.3.13)$$

The result of this process is a set of coefficients which depend on the time shift, b , and the scale, a . The absolute values of these coefficients show how the energy of the signal is distributed in the time and frequency domain.

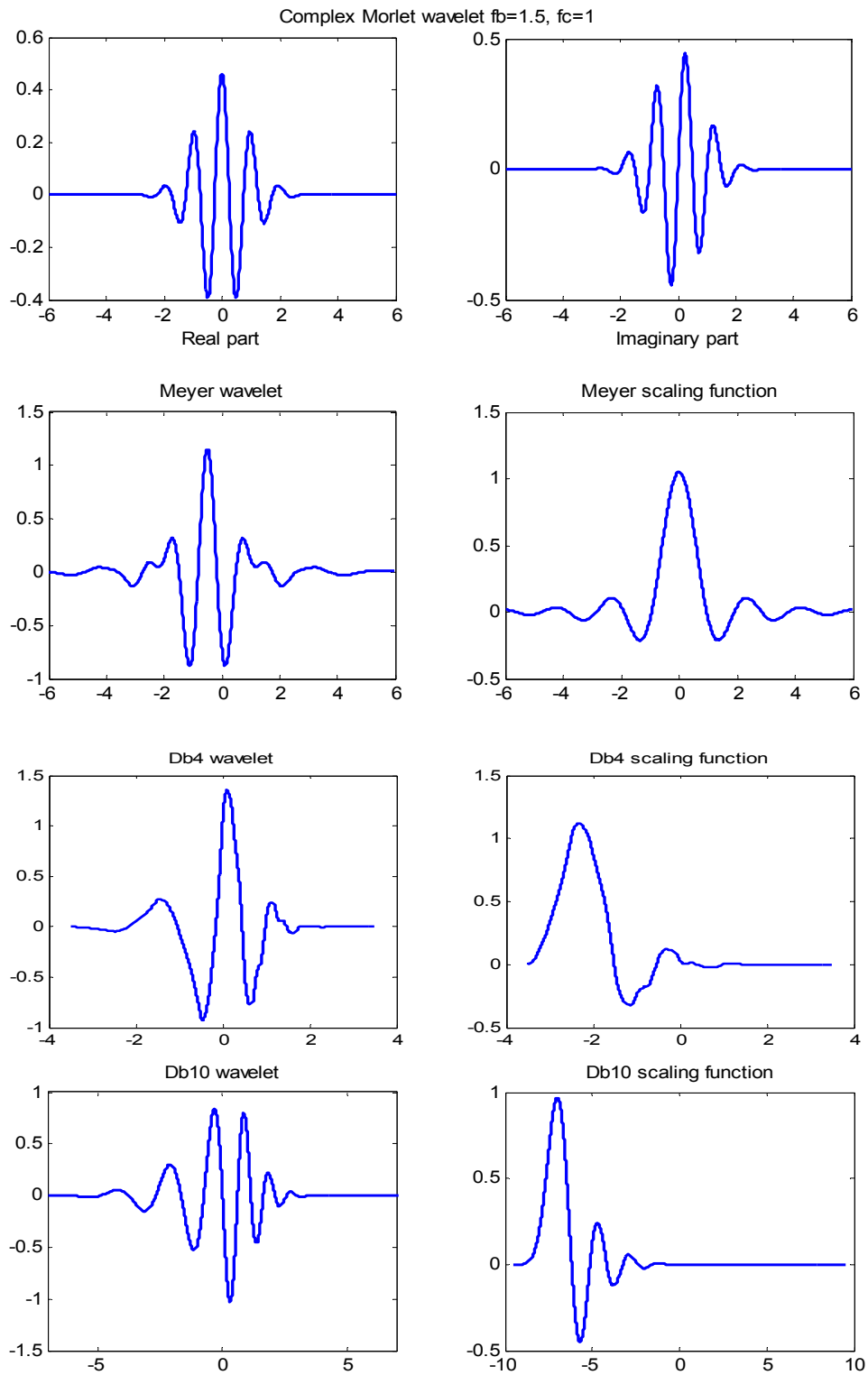


Figure 2.3.1. Examples of the representative wavelets

Since the wavelet function has effectively limited time duration, it acts like a window function in the time domain. Shifting the wavelet window along the time axis implies examining the signal in the neighborhood of the current window location. Therefore, the wavelet transform gives information about the local behavior of the signal. When the scaled wavelet has a similar frequency content with the truncated data, wavelet transform, in general, gives a higher value for its coefficients. Properties of the CWT as localization in time and frequency domains are important for damage detection using vibration measurements.

Time-Frequency Localization

The coefficients obtained by CWT are localized in a time-frequency window. The size of this window is determined by the temporal and frequency variances, σ_t and σ_f in eq. (2.3. 14), and its area is limited by the uncertainty principle (Gabor, 1940)

$$\sigma_t^2 = \frac{1}{\|\psi\|^2} \int_{-\infty}^{+\infty} (t - \bar{t})^2 \psi(t) \psi^*(t) dt, \quad (2.3. 14)$$

$$\sigma_f^2 = \frac{1}{\|\psi\|^2} \int_{-\infty}^{+\infty} (f - \bar{f})^2 \psi(f) \psi^*(f) df$$

where:

$$\|\psi\|^2 = \int_{-\infty}^{+\infty} \psi(t) \psi^*(t) dt = \int_{-\infty}^{+\infty} \psi(f) \psi^*(f) df \quad (2.3. 15)$$

$$\bar{t} = \frac{1}{\|\psi\|^2} \int_{-\infty}^{+\infty} t \psi(t) \psi^*(t) dt, \quad \bar{f} = \frac{1}{\|\psi\|^2} \int_{-\infty}^{+\infty} f \psi(f) \psi^*(f) df$$

The product between the temporal and the frequency variances is bounded by the uncertainty principle, i.e eq. (2.3. 15). In the literature, the rectangular box whose length and width are equal to σ_t and σ_f , respectively, is called the Heisenber box (Mallat, 99).

$$\sigma_t \sigma_f \geq \frac{1}{4\pi} \quad (2.3. 16)$$

The effective duration Δt and effective frequency width Δf of the window function $\psi(t)$ are defined as (Gabor, 1940).

$$\Delta t = \sqrt{2\pi}\sigma_t, \quad \Delta f = \sqrt{2\pi}\sigma_f \quad (2.3.17)$$

Alternatively, the same measures are defined as: $\Delta t = 2\sigma_t$, $\Delta f = 2\sigma_f$ in (Chui, 1992).

2.3.3 Multiresolution Analysis and Discrete Wavelet Transform

The multiresolution analysis (MRA) decomposes a signal in multiple levels of approximation and detail, which may reveal valuable signal information not clearly seen in the original data or in the results from other approaches. Each level of detail corresponds to a signal component in a certain frequency band.

In DWT the scaling parameter a and the shifting parameter b are discretized by using the dyadic scale, i.e.

$$a = 2^j, \quad b = 2^j k \quad j, k \in Z \quad (2.3.18)$$

Thus, by MRA, the signal $x(t) \in L^2(R)$ can be decomposed into a tree structure with wavelet details and approximations at various levels as shown in eq. (2.3.19).

$$x(t) = \sum_{j=1}^J D_j(t) + A_J(t), \quad A_J(t) = \sum_{k>J} D_k(t) \quad (2.3.19)$$

where $D_j(t)$ denotes the detail signal at level j and $A_J(t)$ stands for the approximation signal at level J .

Formula (2.3.19) sets the basis for a multiresolution analysis. Defining the approximations $A_j(t)$ as an orthogonal projection on a subspace $V_j \subset L^2(R)$, the mathematical properties of multiresolution analysis are as follows (Mallat, 1999):

1. $\forall (j, k) \in Z^2, \quad f(t) \in V_j \Rightarrow f(t - 2^j k) \in V_j$
2. $\forall j \in Z, \quad f(t) \in V_j \Leftrightarrow f(t/2) \in V_{j+1}$
3. $\forall j \in Z, \quad V_{j+1} \subset V_j$
4. $\lim_{j \rightarrow \infty} V_j = \bigcap_{j=-\infty}^{+\infty} V_j = \{0\}, \quad \lim_{j \rightarrow -\infty} V_j = \bigcup_{j=-\infty}^{+\infty} V_j = L^2(R)$

5. It can be shown that there exists a function $\phi \in V_0$ (called scale function) such that the set $\phi_{0,k}(t) = \phi(t - k), k \in Z$ constitutes an orthonormal basis for V_0 . The scaled

versions of function ϕ constitute orthonormal bases for all subspaces V_j . It has been proved that any scaling function is completely determined by a discrete filter called conjugate mirror filter.

Property 3, shows that V_{j+1} is included in V_j . Let W_{j+1} be the orthogonal complement of V_{j+1} in V_j , that is: $V_j = V_{j+1} \oplus W_{j+1}$. Therefore the orthogonal projection of signal $x(t)$ on space V_j is decomposed in approximation which is the orthogonal projection of the signal on V_{j+1} and details given by orthogonal projection on W_{j+1} . The wavelet function $\psi_{j,k}$, which is derived from the scale function, constitutes an orthonormal base for space W_j .

A relatively fast, recursive algorithm for computing DWT, by using a filter bank has been discovered by Mallat (1989). It uses a two channel filter bank coupled with a downsampling technique.

2.3.4 Wavelet Packet Decomposition

The wavelet packet (WP) transform is an extension of discrete wavelet transform in the sense that the wavelet detail component at each level is also further decomposed into its own approximation and detail components. Therefore, not only the approximation space is split into new spaces of approximation and detail, but also the detail space. As result, the signal components will have a better frequency resolution. Each component is identified by the level of decomposition and node number in the decomposition tree. As an example, Fig.2.3.2 shows a wavelet packet decomposition tree at level 3 .

For a given orthogonal wavelet, the wavelet packet library can be generated by the following formula, where $h(k)$ and $g(k)$ are the reversed versions of the low-pass and high-pass decomposition filter coefficients divided by $\sqrt{2}$.

$$\begin{aligned} w_{2n}(t) &= 2 \sum_{k=0}^{2N-1} h(k) w_n(2t-k), w_0(t) = \phi(t) \\ w_{2n+1}(t) &= 2 \sum_{k=0}^{2N-1} g(k) w_n(2t-k), w_1(t) = \psi(t) \end{aligned} \tag{2.3. 20}$$

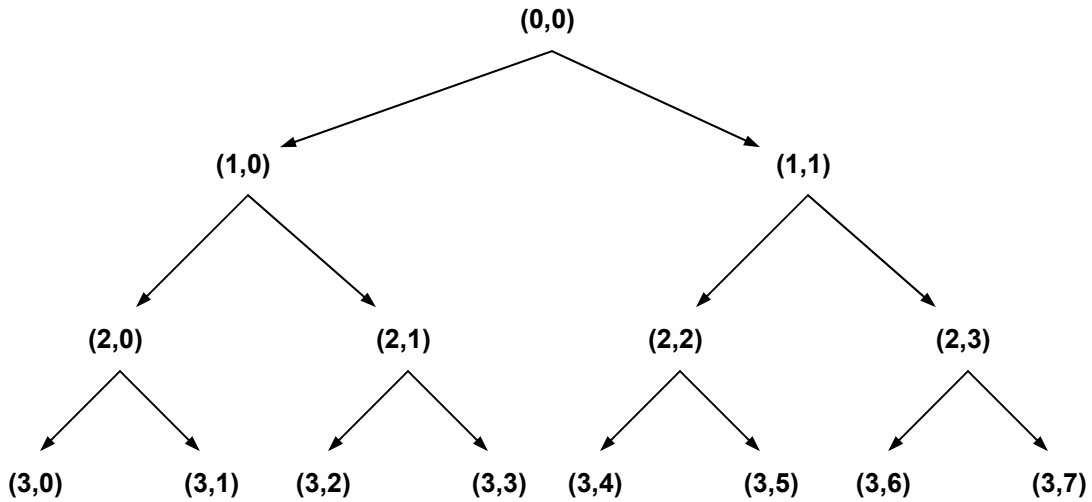


Figure 2.3.2. Wavelet packet decomposition tree at level 3

The wavelet packet function (eq. (2.3.21)) has three indices, j, k, n and analyzes a signal around time k , scale 2^j and a frequency related to the index n .

$$w_{j,k,n}(t) = 2^{-j/2} w_n(2^{-j}t - k), n \in N, j \in Z, k \in Z \quad (2.3.21)$$

The decomposition of a given signal in multiple components is not unique and there are more than $2^{2^{m-1}}$ possibilities of decomposition. In order to select the relevant decomposition different stopping criteria have been proposed, most of them based on definition of the entropy indices (Misiti, et al., 1996).

In this dissertation, discrete Meyer wavelet (Misiti et al, 1996) is chosen for wavelet packet decomposition. The first eight components of the wavelet packet library are plotted in Fig. 2.3.3.

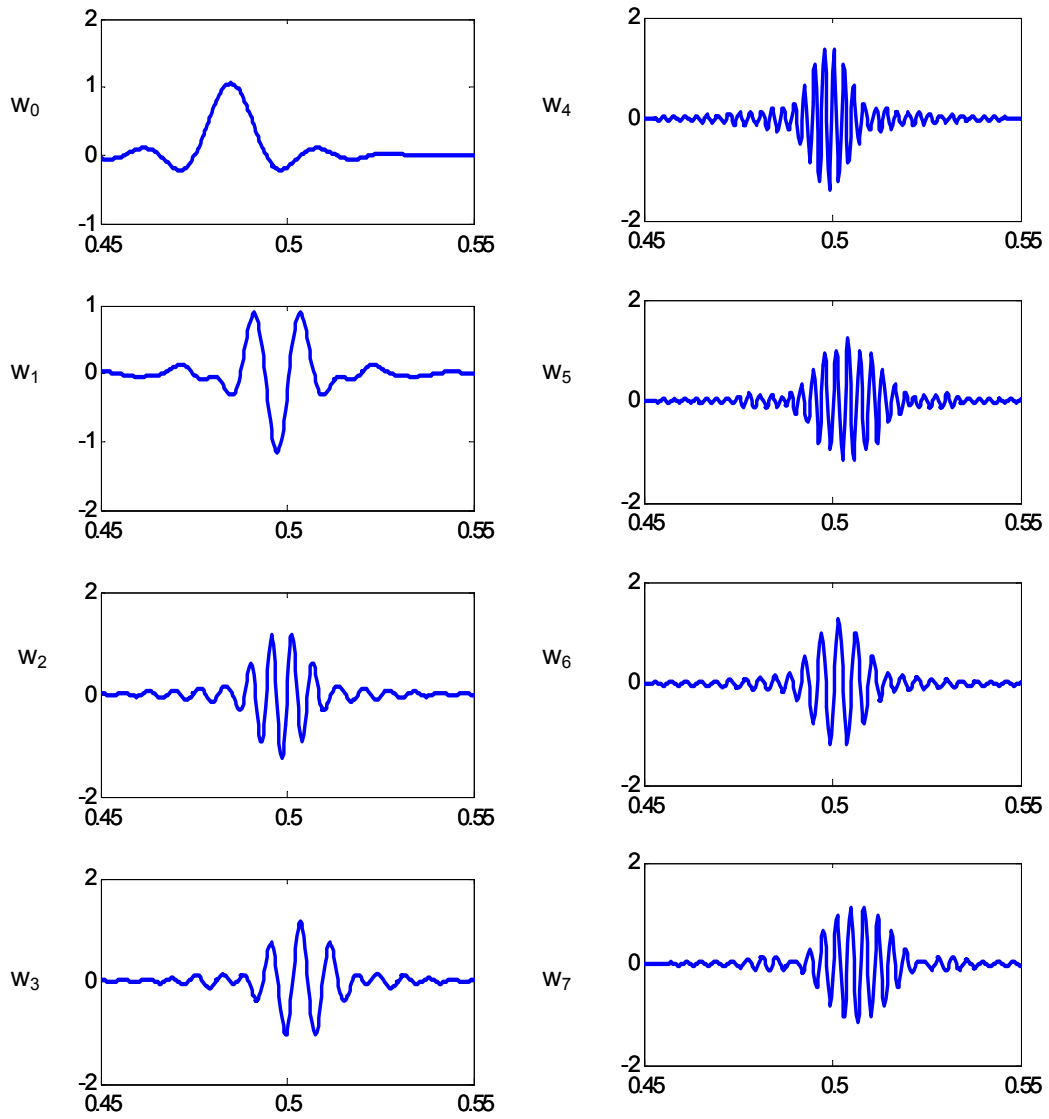


Figure 2.3.3. Discrete Meyer wavelet packet library (w_0, w_1, \dots, w_7)

2.4 Hilbert Transform

In the present study, the modal vibration responses are to be decomposed in the form $x(t) = A(t)\cos(\Phi(t))$. This decomposition can be uniquely determined by means of the analytic signal, which is a complex signal having the original signal, $x(t)$, as its real part and Hilbert transform (Hahn, 1996) of the original signal as its imaginary part. In this subsection we denote by $y(t)$ the HT of signal $x(t)$.

Hilbert transform (HT) of a real signal $x(t)$, and its inverse (IHT) are defined as:

$$y(t) = HT(x(t)) = \frac{1}{\pi} P \int_{-\infty}^{+\infty} \frac{x(\eta)}{t-\eta} d\eta, \quad x(t) = IHT(y(t)) = -\frac{1}{\pi} P \int_{-\infty}^{+\infty} \frac{y(\eta)}{t-\eta} d\eta \quad (2.4.1)$$

where P stands for the Cauchy principal value of the integral.

If the Fourier transforms of $x(t)$ and $y(t)$ are denoted by $\hat{X}(\omega)$ and $\hat{Y}(\omega)$, respectively, the relationship between $\hat{X}(\omega)$ and $\hat{Y}(\omega)$ is shown in eq. (2.4.4), where $\text{sgn}(\omega)$ stands for the *sign* function.

$$\hat{Y}(\omega) = -i \text{sgn}(\omega) \hat{X}(\omega) \quad (2.4.2)$$

The complex signal $z(t)$ which has $x(t)$ as its real part and $y(t)$ as its imaginary part is called analytic¹ signal:

$$z(t) = x(t) + iy(t) = x(t) + iHT(x(t)) \quad (2.4.3)$$

If the analytic signal is expressed in polar representation as $z(t) = A_z(t)\exp(i\phi_z(t))$, the amplitude of an analytic signal expressed in polar coordinates, $A_z(t)$ and $\phi_z(t)$ are called *analytic amplitude* and *analytic phase*, respectively, and the instantaneous frequency is defined as the time derivative of the analytic phase angle, as shown in eq. (2.4.4).

¹ The name of “analytic” comes from complex analysis where a function of complex variables $z = t + i\tau$, $w = f(z) = u(t, \tau) + iv(t, \tau)$ is called analytic in a domain D , if and only if the first partial derivatives of $u(t, \tau)$ and $v(t, \tau)$ exist and satisfy the Cauchy-Riemann conditions: $\frac{\partial u}{\partial t} = \frac{\partial v}{\partial \tau}$, $\frac{\partial u}{\partial \tau} = -\frac{\partial v}{\partial t}$. It can be

proved that a Hilbert pair $x(t)$ and $y(t)$ satisfy the Cauchy-Riemann conditions, therefore the signal $z(t)$ is an analytic function.

$$\omega(t) = \frac{d}{dt} \phi_z(t) \quad (2.4.4)$$

The Fourier spectrum of an analytic signal is twice the spectrum of its real part for positive values of frequency and zero for negative frequencies. It comes from :

$$\begin{aligned} FT(z(t)) &= FT(x(t)) + iFT(y(t)) = X(\omega) + i(-i \operatorname{sgn}(\omega)X(\omega)) = (1 + \operatorname{sgn}(\omega))X(\omega) = \\ &= \begin{cases} 2X(\omega) & \omega > 0 \\ X(\omega) & \omega = 0 \\ 0 & \omega < 0 \end{cases} \end{aligned} \quad (2.4.5)$$

From eq. (2.4.5), it can be observed that an analytic signal is a complex signal, which is completely characterized by its real part.

There is an important property of the analytic signal, which allows a meaningful decomposition of a real signal as $s(t) = A(t) \cos(\phi(t))$. This property can be expressed either in time or frequency domain as follows:

- *The analytic signal of an asymptotic real signal (Delprat et al, 1992)*

Assume that $s(t)$ is a real signal of finite energy, of the form $s(t) = A(t) \cos(\Phi(t))$, where $A(t) \geq 0$ and $\Phi(t) \in [0, 2\pi]$. Also, assume that $s(t)$ has a locally mono-frequency content

and is asymptotic, that is $\left| \frac{1}{A(t)} \frac{dA}{dt} \right| \ll \left| \frac{d\phi}{dt} \right|$. Then, its corresponding analytic signal is close to the exponential model, i.e. $z_s(t) \cong A(t) \exp(i\phi(t))$.

- *Bedrosian's Product Theorem*

Given a real signal of the form of a product $s(t) = f(t)g(t)$ where $f(t), g(t) \in L^2(\mathbb{R})$ and their Fourier Transform, $\hat{F}(\omega)$ and $\hat{G}(\omega)$ satisfy the following conditions:

$$\left| \hat{F}(\omega) \right| = 0, \text{ for } \omega > \omega_a, \text{ and } \left| \hat{G}(\omega) \right| = 0, \text{ for } \omega < \omega_a \quad (2.4.6)$$

then the Hilbert Transform of the product is given by:

$$HT(f(t)g(t)) = f(t)HT(g(t)). \quad (2.4.7)$$

If $A(t)$ and $\cos(\phi(t))$ satisfy the conditions imposed to $f(t)$ and $g(t)$, then the corresponding analytic signal is $z(t) = A(t) \exp(i\phi(t))$.

Chapter 3

THEORETICAL BASIS OF TIME-VARYING VIBRATION MODES AND INSTANTANEOUS MODAL PARAMETERS

3.1 Introduction

As shown in Chapter 1, identification of modal parameters has been a classical technique employed by damage identification based on vibration data. Any change in physical parameters of a structure results in change in its modal parameters, i.e. natural frequencies, modal damping ratios and mode shape vectors. Therefore, any change in the modal parameters may indicate damage development in the structure, and the structural health condition. While great successes of the modal based techniques were reported in the literature, there are some important and challenging issues which still need to be explored. One of them is related to the assumption of time invariance of the structure, therefore damage should not occur during the period when data is collected. This chapter addresses mainly this issue by developing the theoretical basis for time-varying vibration modes characterized by the instantaneous modal frequency, the instantaneous mode shape and the instantaneous modal damping ratio.

The concept of instantaneous frequency has been introduced before, as a characteristic of a signal (Boashash, 1992). It has also been used for identification of nonlinear systems (Staszewski, 1997) and damage detection (Hera et al., 2004), but the connection between the system parameters and instantaneous frequency of the impulse response was only intuitive. In the present study we show that if certain conditions are

satisfied the instantaneous frequency of free vibrations/impulse responses can be related by a mathematical relation to the system properties. Moreover, other concepts such as instantaneous mode shape and instantaneous damping ratio are defined for a time-varying system. Based on the theory to be developed here, we will be able to give answers to the questions as: what are the time-varying vibration modes, when these modes exist, how to identify them, or how to relate the system modal responses to the time-varying system parameters. The instantaneous modal parameters set the bridge between the free response characteristics and physical parameters of the system. By tracking the instantaneous modal parameters, useful information about the structural health condition in the case of evolving damage can be extracted.

This chapter is organized as follows. We start with the state space formulation of a system with damage and it is shown that a modal decomposition for the second order time-varying systems is possible by solving the dynamic eigenvalue problem associated to the corresponding first-order system in state space. Then, in the next sections, the discussion concentrates on a subclass of LTV systems, which are called slowly time-varying systems. These systems have real time-varying vibration modes characterized by modal parameters with meaningful physical interpretation, i.e. positive instantaneous frequency and real instantaneous mode shapes. This chapter ends with a numerical example which illustrates some of the concepts introduced here.

Note: Most of the notations and terminology have been already introduced in Chapter 2. In order to avoid confusion, part of the terminology is clarified in the following:

- *Elementary modes* are the time varying modes of the first order system. They can be either real or complex and are characterized by a real or complex dynamic eigenpair (eigenvector and eigenvalue).
- *Time-varying vibration modes* refer to the real vibration modes which can be obtained by a combination of two complex conjugate elementary modes. They are characterized by a positive instantaneous frequency and real mode shapes, which are related to dynamic eigenpair.

- A *normalized vector* is a new vector obtained from the original one divided by one of its nonzero component, say the j^{th} component, which has been chosen for normalization. For example, the normalized version of the vector $\mathbf{v}(t) = [v_1, v_2, v_3, \dots, v_j, \dots, v_N]^T$ is $\mathbf{v}_{N_j}(t) = [v_1/v_j, v_2/v_j, v_3/v_j, \dots, 1, \dots, v_N/v_j]$.
- As a convention, we will use the symbol $x \cong y$ to specify that the expression of x is approximated by y up the order ε , where $\varepsilon \ll 1$, i.e. $x = y + O(\varepsilon)$.

3.2 State Space Formulation of Damaged Structures

Damage in a system may cause a change in the structure parameters, mainly the stiffness and damping. In this study the dynamics of a NDOF structure with damage is described by a set of second order differential equations with time varying coefficients:

$$\mathbf{M}\ddot{\mathbf{x}}(t) + \mathbf{C}_d(t)\dot{\mathbf{x}}(t) + \mathbf{K}(t)\mathbf{x}(t) = \mathbf{f}(t) \quad (3.1)$$

where $\mathbf{x}(t)$ is the $N \times 1$ displacement vector and $\mathbf{f}(t)$ is the $N \times 1$ vector of external excitation. \mathbf{M} , \mathbf{K} , and \mathbf{C}_d are the $N \times N$ mass, stiffness and damping matrices of the system. In the state-space, eq (3.1) can be expressed as:

$$\dot{\mathbf{y}}(t) = \mathbf{A}(t)\mathbf{y}(t) + \mathbf{B}\mathbf{f}(t) \quad (3.2)$$

where the state space vector \mathbf{y} , the system matrix $\mathbf{A}(t)$, and input matrix \mathbf{B} are defined in eq. (3.3).

$$\mathbf{y} = \begin{bmatrix} \mathbf{x} \\ \dot{\mathbf{x}} \end{bmatrix}, \quad \mathbf{A}(t) = \begin{bmatrix} \mathbf{0} & \mathbf{I} \\ -\mathbf{M}(t)^{-1}\mathbf{K}(t) & -\mathbf{M}^{-1}\mathbf{C}_d(t) \end{bmatrix}, \quad \mathbf{B} = \begin{bmatrix} \mathbf{0} \\ \mathbf{M}^{-1} \end{bmatrix} \quad (3.3)$$

The state space formulation has the advantage of a modal decomposition similar to that of a time invariant system. This decomposition can reveal important physical properties of the system.

3.3 Real Modal Responses

Some important properties of the system can be assessed by analyzing the homogeneous part

of the system dynamics, expressed in eq. (3. 4).

$$\dot{\mathbf{y}}(t) = \mathbf{A}(t)\mathbf{y}(t) \quad (3. 4)$$

In Chapter 2, it has been shown that the system (3. 4) can be transformed into a set of $2N$ uncoupled equations, $\dot{\mathbf{q}}(t) = \mathbf{\Lambda}\mathbf{q}(t)$, by using the Lyapunov transformation $\mathbf{y}(t) = \mathbf{L}(t)\mathbf{q}(t)$. The columns of $\mathbf{L}(t)$ are the dynamic eigenvectors $\mathbf{u}^{(i)}(t)$ of matrix $\mathbf{A}(t)$, and the diagonal matrix $\mathbf{\Lambda}(t)$ is defined by the dynamic eigenvalues $\lambda_i(t)$, as shown in eq. (3.5).

$$\mathbf{L}(t) = [\mathbf{u}^{(1)}(t), \mathbf{u}^{(2)}(t), \dots, \mathbf{u}^{(2N)}(t)], \quad \mathbf{\Lambda}(t) = \text{diag}[\lambda_i(t)], \quad i = 1, 2, \dots, 2N \quad (3. 5)$$

The dynamic eigenpair $\{\lambda_i(t), \mathbf{u}^{(i)}(t)\}$ was found by solving the dynamic eigenvalues problem:

$$\mathbf{A}(t)\mathbf{u}(t) = \lambda(t)\mathbf{u}(t) + \dot{\mathbf{u}}(t), \quad \forall t \quad (3. 6)$$

At this point, we make the assumption that the algorithm which solve the dynamic eigenvalue problem, gives the complex eigenvalues and eigenvectors in conjugate pairs, which reduces to the classical eigenvalues and eigenvectors if the system is time invariant. If this assumption is satisfied, then:

1. the complex modal coordinates exist in complex conjugate pairs;
2. a real modal response is obtained by combining two complex conjugate elementary modal responses.

As example, the quasistatic algorithm introduced in Chapter 2.1 satisfies the above assumption. By this algorithm the dynamic eigenvalues are calculated by solving the algebraic eigenvalue problem at each time instant. Then, given the dynamic eigenvalue, $\lambda(t)$, the dynamic eigenvector is obtained by integrating the eq. (3. 6).

In the following, let's order the complex eigenvalues so that $|\text{Im}(\lambda_k)| \leq |\text{Im}(\lambda_{k+1})|$, $k = 1, \dots, 2N - 1$. Without loss of generality, we focus the discussion on the complex elementary modes $(2n - 1)$ and $(2n)$, characterized by the complex conjugate eigenvalues λ_{2n-1} and λ_{2n} . The corresponding modal equations have been presented in eq. (2.1.21), and for convenience are repeated here for modes $(2n - 1)$ and $(2n)$. All notations in eq. (3. 7) can be found in Chapter 2.

$$\begin{aligned}\dot{q}_{2n-1}(t) &= \lambda_{2n-1} q_{2n-1}(t), & q_{2n-1}(t_0) &= \mathbf{v}^{(2n-1)T}(t_0) \mathbf{y}_0, \\ \dot{q}_{2n}(t) &= \lambda_{2n} q_{2n}(t), & q_{2n}(t_0) &= \mathbf{v}^{(2n)T}(t_0) \mathbf{y}_0,\end{aligned}\quad (3.7)$$

By combining two complex conjugate elementary modal responses, a *real modal response* is obtained, as shown in eq. (3.8). The notation $\mathbf{y}^{(2n-1),(2n)}(t)$ is used for the modal response vector obtained by summing together the $(2n-1)$ and $(2n)$ elementary modal complex conjugate responses, characterized by: $\lambda_{2n} = \lambda_{2n-1}^*$, $\mathbf{u}^{(2n)} = \mathbf{u}^{(2n-1)*}$ and $q_{2n} = q_{2n-1}^*$. The symbol “ \bullet ” denotes the multiplication element by element, and $\mathbf{1}$ is a vector whose components are unity and has the same dimension as $\mathbf{u}(\mathbf{t})$.

$$\begin{aligned}\mathbf{y}^{(2n-1),(2n)}(t) &= \mathbf{y}^{(2n-1)}(t) + \mathbf{y}^{(2n)}(t) = \mathbf{u}^{(2n-1)}(t) q_{2n-1}(t) + \mathbf{u}^{(2n)}(t) q_{2n}(t) \\ &= \mathbf{u}^{(2n-1)}(t) q_{2n-1}(t) + \mathbf{u}^{(2n-1)*}(t) q_{2n-1}^*(t) = \\ &= 2 \operatorname{Re}\left\{ \mathbf{u}^{(2n-1)}(t) q_{2n-1}(t) \right\} = 2 \left| \mathbf{u}^{(2n-1)}(t) \right| \left| q_{2n-1}(t) \right| \bullet \cos\left(\arg\left(\mathbf{u}^{(2n-1)}(t) \right) + \mathbf{1} \arg\left(q_{2n-1}(t) \right) \right)\end{aligned}\quad (3.8)$$

The homogeneous part of the response (3.8) is of interest in this section, since it reflects the inherent properties of the system. Its scalar form is presented in eq. (3.9), where λ_{2n-1} and λ_{2n} were expanded in terms of their imaginary and real parts as $\lambda_{2n-1} = \gamma_{\lambda,n} + i\omega_{\lambda,n}$, $\lambda_{2n} = \gamma_{\lambda,n} - i\omega_{\lambda,n}$, $\omega_{\lambda,n} > 0$, $n < N$.

$$\begin{aligned}y_j^{(2n-1),(2n)}(t) &= 2 \operatorname{Re}\left\{ u_j^{(2n-1)}(t) q_{2n-1}(t) \right\} = \\ &= 2 \left| u_j^{(2n-1)}(t) \right| \left| C_{2n-1}(t_0) \right| \exp\left(\int_{t_0}^t \gamma_{\lambda,n}(\tau) d\tau \right) \cos\left(\arg\left(u_j^{(2n-1)}(t) \right) + \int_{t_0}^t \omega_{\lambda,n}(\tau) d\tau + \arg\left(C_{2n-1}(t_0) \right) \right) \\ &= 2 \left| u_j^{(2n-1)}(t) \right| \left| C_{2n-1}(t_0) \right| \exp\left(\int_{t_0}^t \gamma_{\lambda,n}(\tau) d\tau \right) \cos\left(\phi_j^{(n)}(t) \right)\end{aligned}\quad (3.9)$$

where $\phi_j^{(n)}(t)$ is defined as: $\phi_j^{(n)}(t) = \arg\left(u_j^{(2n-1)}(t) \right) + \int_{t_0}^t \omega_{\lambda,n}(\tau) d\tau + \arg\left(C_{2n-1}(t_0) \right)$.

It can be observed that the real modal response has time varying amplitude and a phase angle described by a general function of time. For $j = 1, \dots, N$, $y_j^{(2n),(2n+1)}(t)$ represents the displacement response, $x_j^{(n)}(t)$, and for $j = N+1, \dots, 2N$ it represents the

velocity response, $v_j^{(n)}(t) = \dot{x}_j^{(n)}(t)$. It will be shown that for a specific class of systems, defined as slowly time-varying systems, the instantaneous frequency of the modal responses is practically independent of location/DOF, here denoted by “ j ”.

3.4 Slowly Time-Varying Systems

In Chapter 2, the modal decomposition of a time varying system has been presented in the general terms, without specifying the algorithm for solving the dynamic eigenvalue problem. In Section 3.3, important properties of LTV systems have been revealed if the complex eigenvalues and eigenvectors are in conjugate pairs. Further, it will be shown that if an assumption of “slowly time-varying eigenvectors” is added to the system, the response can be decomposed in real time varying vibration modes, characterized by the same instantaneous frequency at different locations/DOFs.

3.4.1 Slowly Time-Varying Assumption

A linear system is said to be *slowly time varying* if its dynamic eigenvectors change slowly in respect to the corresponding dynamic eigenvalues as shown in eq. (3. 10), where u_k stands for the k^{th} component of dynamic eigenvector $\mathbf{u}(t)$.

$$\text{a) } \frac{|\dot{u}_k(t)|}{|u_k(t)|} \ll |\text{Im}(\lambda(t))|, \text{ b) } \frac{|\ddot{u}_k(t)|}{|\lambda(t)u_k(t)|} \ll |\text{Im}(\lambda(t))|, \text{ c) } \frac{|\dot{\lambda}(t)|}{|\lambda(t)|} \ll |\text{Im}(\lambda(t))|, \quad k = 1 \cdots 2N \quad (3. 10)$$

In Section 2.1.2.4, we proposed the quasistatic algorithm to solve the dynamic eigenvalue problem. The performance of this algorithm in finding the eigenpair which satisfies the condition in eq. (3. 10) is quantified by *the slowness index* defined in eq. (3. 11).

$$S_{STV}(t) = \max_{k=1,2N} \left| \frac{u_{k|j}(t) - u_{qs,k|j}(t)}{u_{k|j}(t)} \right|, u_{k|j}(t) \neq 0 \quad (3. 11)$$

where $u_{k|j}(t)$ is the k^{th} component of the dynamic eigenvector $\mathbf{u}(t)$ normalized in respect to its j^{th} component. $u_{qs,k|j}(t)$ refers to the normalized quasistatic eigenvector, calculated from the algebraic eigen-value problem with frozen time. The slowness index gives a measure of

the relative difference between the normalized dynamic eigenvector and normalized quasistatic eigenvector, and should be calculated for each mode of interest. If $S_{STV}(t) \ll 1$ for a certain time interval, the system can be considered slowly time-varying on that interval and the above decomposition leads to real vibration modes with a physical meaning, i.e. the same frequency at different locations/nodes, as it will be shown in the next sections.

3.4.2 Definition of Instantaneous Modal Parameters

Based on modal components of the free vibration displacement response in eq. (3.12) and the dynamic eigenpair, the following *system parameters* are defined:

1. Instantaneous modal frequency
2. Instantaneous mode shape and its normalized version
3. Instantaneous modal damping coefficient

$$x_j^{(n)}(t) = 2|u_j^{(2n-1)}(t)|C_{2n-1}(t_0) \exp\left(\int_{t_0}^t \gamma_n(\tau) d\tau\right) \cos(\phi_{x,j}^{(n)}(t)), \quad j = 1 \dots N \quad (3.12)$$

$$\phi_{x,j}^{(n)}(t) = \arg(u_j^{(2n-1)}(t)) + \int_{t_0}^t \omega_{\lambda,n}(\tau) d\tau + \arg(C_{2n-1}(t_0))$$

Instantaneous modal frequency

The n^{th} instantaneous modal frequency of the system is defined as the imaginary part of the dynamic eigenvalue $(2n-1)$.

$$\omega_n(t) = \omega_{\lambda,n}(t) = \text{Im}(\lambda_{2n-1}(t)), \quad j=1, \dots, N \quad (3.13)$$

This definition has its roots in the instantaneous frequency of the modal displacement component, which is defined as the time derivative of the phase angle of the free vibration modal displacement component of the response.

$$\omega_{x,nj}(t) = \frac{d(\phi_{x,j}^{(n)}(t))}{dt} = \frac{d(\arg(u_j^{(2n-1)}(t)))}{dt} + \omega_{\lambda,n}(t), \quad j=1, \dots, N \quad (3.14)$$

Employing the assumption of slowly time-varying eigenvector, it is proved in Appendix 1 that $d(\arg(u_j^{(2n-1)}(t)))/dt \ll \omega_{\lambda,n}(t)$ and, therefore, $\omega_{x,nj}(t) \cong \omega_{\lambda,n}(t)$. Consequently, the instantaneous frequency of the modal response is, practically, the same for all components

of the vibration modal response vector. In the case of a LTI systems, instantaneous modal frequency coincides with the damped natural frequency.

Instantaneous mode shape vector and its normalized version

The n^{th} instantaneous mode shape vector $\mathbf{X}^{(n)}$ is defined as the absolute value of the dynamic eigenvector $(2n-1)$ dynamic eigenvector:

$$\mathbf{X}^{(n)}(t) = \left[\left| u_1^{(2n-1)}(t) \right|, \left| u_2^{(2n-1)}(t) \right|, \dots, \left| u_N^{(2n-1)}(t) \right| \right]^T \quad (3.15)$$

Its normalized version represents the absolute value of the complex eigenvector normalized by the absolute value of one of its non-zero components; say the j^{th} component in eq.(3.16).

$$\mathbf{X}_j^{(n)}(t) = \frac{\left| \mathbf{u}^{(2n-1)}(t) \right|}{\left| u_j^{(2n-1)}(t) \right|}, \quad \left| u_j^{(2n-1)}(t) \right| \neq 0 \quad (3.16)$$

The presence of instantaneous mode shape is obvious in the amplitude of the modal displacement response vector in eq. (3.12). For a time invariant system the instantaneous mode shape vector reduces to the absolute value of the traditional mode shape vector.

Instantaneous modal damping coefficient

Instantaneous modal damping coefficient is defined as the real part of the dynamic eigenvalues with negative sign.

$$c_{d,n}(t) = -\text{Re}(\lambda_{2n-1}(t)) \quad (3.17)$$

Its time invariant correspondent is $c_{d,n} = \zeta_n \omega_n$, where ζ_n and ω_n are the modal damping ratio and natural frequency for the n^{th} vibration mode. A LTV system is lightly damped if $0 \leq c_{d,n}(t) \ll \omega_n(t)$.

3.4.3 Instantaneous Modal Parameters in Velocity Response

In real applications the recorded signals may not necessarily be the displacement responses. For the purpose of damage detection other responses such as velocity or acceleration may also be measured. Therefore, a legitimate question arises: How the instantaneous modal parameters are related to these response signals?

First, the case of velocity response is investigated. The expression of the j^{th} component of the n^{th} modal response is given in eq. (3. 18) and has its origin in eq. (3. 9).

$$v_j^{(n)}(t) = 2|u_{2j}^{(2n-1)}(t)| |C_{2n-1}(t_0)| \exp\left(\int_{t_0}^t \gamma_{\lambda,n}(\tau) d\tau\right) \cos(\phi_{v,j}^{(n)}(t)), \quad j = 1 \dots N \quad (3. 18)$$

$$\phi_{v,j}^{(n)}(t) = \arg(u_{2j}^{(2n-1)}(t)) + \int_{t_0}^t \omega_{\lambda,n}(\tau) d\tau + \arg(C_{2n-1}(t_0))$$

The instantaneous frequency of $v_j^{(n)}(t)$ is calculated in eq. (3. 19).

$$\omega_{v,nj}(t) = \frac{d(\phi_{v,j}^{(n)}(t))}{dt} = \frac{d(\arg(u_j^{(2n-1)}(t)))}{dt} + \omega_{\lambda,n}(t), \quad j=1, \dots, N \quad (3. 19)$$

The amplitude of $v_j^{(n)}(t)$ can be divided in two components: $|u_{2j}^{(2n-1)}(t)|$ which depends on position and $|C_{2n-1}(t_0)| \exp\left(\int_{t_0}^t \gamma_{\lambda,n}(\tau) d\tau\right)$ which is independent of position.

In Appendix I, it is shown that if the assumption of slowly time-varying system holds, $d(\arg(u_{2j}^{(2n-1)}(t)))/dt$ is negligible in respect to $\omega_{\lambda,n}(t)$ and $u_{2j}^{(2n-1)} \cong u_j^{(2n-1)} \lambda_{2n-1}$. Based on these observations, the following two conclusions can be drawn for the slowly time-varying systems:

1. the instantaneous frequency of the velocity modal response is, practically, independent of the node position and has the same value as instantaneous modal frequency, i.e. $\omega_{v,nj}(t) \cong \omega_n(t)$.
2. the amplitude of the signal is proportional to $|u_j^{(2n-1)}|$ which is the j^{th} component of the mode shape vector.

3.4.4 Instantaneous Modal Parameters in Acceleration Response

Accelerometers are the most used vibration measurement devices; therefore, the analysis of the acceleration response from the perspective of its relationship with instantaneous modal parameters is necessary. The modal acceleration response can be calculated as the time derivative of the modal velocity response, as shown in eq. (3. 20)

$$\begin{aligned}
a_j^{(n)}(t) &= \dot{v}_j^{(n)}(t) = \frac{d(2 \operatorname{Re}\{u_{2j}^{(2n-1)} q_{2n-1}(t)\})}{dt} = 2 \operatorname{Re}\{u_{2j}^{(2n-1)} \dot{q}_{2n-1} + \dot{u}_{2j}^{(2n-1)} q_{2n-1}\} = \\
&= 2 \operatorname{Re}\{(\lambda_{2n-1} u_{2j}^{(2n-1)} + \dot{u}_{2j}^{(2n-1)}) q_{2n-1}\} = \\
&= 2 |\lambda_{2n-1} u_{2j}^{(2n-1)} + \dot{u}_{2j}^{(2n-1)}| |C_{2n}(t_0)| \exp\left(\int_{t_0}^t \gamma_{2n}(\tau) d\tau\right) \cos(\phi_{a,j}^{(n)}(t)) \tag{3.20} \\
\phi_{a,j}^{(n)}(t) &= \arg(\lambda_{2n-1} u_{2j}^{(2n-1)} + \dot{u}_{2j}^{(2n-1)}) + \int_{t_0}^t \omega_{\lambda,n}(\tau) d\tau + \arg(C_{2n-1}(t_0))
\end{aligned}$$

In a simplified notation, equation (3.20) can be written as $a_j^{(n)}(t) = A_{a,j}^{(n)}(t) \cos(\phi_{a,j}^{(n)}(t))$.

With the assumption of slowly time-varying system, the amplitude $A_{a,j}^{(n)}(t)$ and the instantaneous frequency of the response can be approximated as shown in eq.(3.21).

$$\begin{aligned}
A_{a,j}^{(n)}(t) &\cong 2 |u_j^{(2n-1)}(t)| |\lambda_{2n-1}(t)|^2 |C_{2n}(t_0)| \exp\left(\int_{t_0}^t \gamma_{2n}(\tau) d\tau\right), j=1, \dots, N \tag{3.21} \\
\omega_{a,nj}(t) &= d(\phi_{a,j}^{(n)}(t))/dt \cong \omega_{\lambda,n}(t)
\end{aligned}$$

From equation (3.21), it can be observed that the instantaneous frequency of the modal acceleration response, practically, does not depend on the node position - given by index j , and has the same value as the instantaneous modal frequency of the system (up to order of ε , where $\varepsilon \ll 1$). Also, the instantaneous mode shape component appears explicitly in the response. These are important findings, which make acceleration responses suitable for solving the inverse problem of the identification of instantaneous modal parameters.

3.4.5 Instantaneous Modal Parameters in Forced Vibration Response

Practical applications require extraction of the instantaneous modal parameters from forced vibration responses; therefore, in the following, we will investigate the relationship between the forced modal responses and the instantaneous modal parameters. Mainly, we are looking for a simplified form of the amplitude and frequency of the response which may be related to the instantaneous modal parameters.

Let's consider a system subjected to a given excitation and zero initial conditions. Calculation of the n^{th} forced vibration modal response starts by solving the first-order modal equation (3.22) whose solution is given in eq. (3.23).

$$\dot{q}_n(t) = \lambda_n q_n(t) + f_{q,n}, \quad q_n(t_0) = 0, \quad n = 1, 2, \dots, 2N \quad (3.22)$$

$$q_{j_n}(t) = \int_{t_0}^t f_{q,n} \exp\left(\int_{\tau}^t \lambda_n(\xi) d\xi\right) d\tau \quad (3.23)$$

For simplicity of the expressions the following notation has been introduced:

$$f_{q,n} = \mathbf{v}^{(n)T}(\tau) \begin{bmatrix} \mathbf{0} \\ \mathbf{M}^{-1} \end{bmatrix} \mathbf{f}(t) \quad (3.24)$$

The real vibration modal displacement, velocity, and acceleration responses are given in eqs., (3.25), (3.26), (3.27), where $j = 1 \dots N$.

$$\begin{aligned} x_j^{(n)}(t) &= y_j^{(2n-1), (2n)}(t) = \\ &= 2|u_j^{(2n-1)}(t)| |q_{2n-1}(t)| \cos(\arg(u_j^{(2n-1)}(t)) + \arg(q_{2n-1}(t))) \end{aligned} \quad (3.25)$$

$$\begin{aligned} v_j^{(n)}(t) &= y_{2j}^{(2n-1), (2n)}(t) = \\ &= 2|u_{2j}^{(2n-1)}(t)| |q_{2n-1}(t)| \cos(\arg(u_{2j}^{(2n-1)}(t)) + \arg(q_{2n-1}(t))) \end{aligned} \quad (3.26)$$

$$\begin{aligned} a_j^{(n)}(t) &= \dot{v}_j^{(n)} = 2 \operatorname{Re} \left\{ \frac{d(u_{2j}^{(2n-1)}(t) q_{2n-1}(t))}{dt} \right\} = 2 \operatorname{Re} (\dot{u}_{2j}^{(2n-1)}(t) q_{2n-1}(t) + u_{2j}^{(2n-1)}(t) \dot{q}_{2n-1}(t)) = \\ &= 2 \operatorname{Re} \left(u_{2j}^{(2n-1)} \left(\dot{q}_{2n-1}(t) + \frac{\dot{u}_{2j}^{(2n-1)}(t)}{u_{2j}^{(2n-1)}} q_{2n-1}(t) \right) \right) = \\ &= 2|u_{2j}^{(2n-1)}| \left| \dot{q}_{2n-1}(t) + \frac{\dot{u}_{2j}^{(2n-1)}(t)}{u_{2j}^{(2n-1)}} q_{2n-1}(t) \right| \cos \left(\arg(u_{2j}^{(2n-1)}) + \arg \left(\dot{q}_{2n-1}(t) + \frac{\dot{u}_{2j}^{(2n-1)}(t)}{u_{2j}^{(2n-1)}} q_{2n-1}(t) \right) \right) \end{aligned} \quad (3.27)$$

Equations (3.25), (3.26) and (3.27) can be written as amplitude multiplied by a cosine term, as shown in eq. (3.28).

$$\begin{aligned} x_j^{(n)}(t) &= A_{x,j}^{(n)} \cos(\phi_{x,j}^n) \\ v_j^{(n)}(t) &= A_{v,j}^{(n)} \cos(\phi_{v,j}^n) \\ a_j^{(n)}(t) &= A_{a,j}^{(n)} \cos(\phi_{a,j}^n) \end{aligned} \quad (3.28)$$

Employing the assumption of slowly time-varying system, the simplified expression for amplitudes are obtained (eqs. (3.29) and (3.30)).

$$\begin{aligned}
A_{x,j}^{(n)}(t) &= 2|u_j^{(2n-1)}(t)| |q_{2n-1}(t)| \\
A_{v,j}^{(n)}(t) &\cong 2|u_j^{(2n-1)}(t)| |\lambda_n| |q_{2n-1}(t)|
\end{aligned} \tag{3.29}$$

$$\begin{aligned}
A_{a,j}^{(n)}(t) &= 2|u_{2j}^{(2n-1)}(t)| \left| \dot{q}_{2n-1}(t) + \frac{\dot{u}_{2j}^{(2n-1)}(t)}{u_{2j}^{(2n-1)}} q_{2n-1}(t) \right| = \\
&= 2|u_{2j}^{(2n-1)}(t)| \left| q_{2n-1}(t) \lambda_{2n-1}(t) + f_{q,2n-1}(t) + \frac{\dot{u}_{2j}^{(2n-1)}(t)}{u_{2j}^{(2n-1)}} q_{2n-1}(t) \right| \cong \\
&\cong 2|u_{2j}^{(2n-1)}(t)| |q_{2n-1}(t) \lambda_{2n-1}(t) + f_{q,2n-1}| \cong \\
&\cong 2|u_j^{(2n-1)}(t)| |\lambda_{2n-1}(t)| |q_{2n-1}(t) \lambda_{2n-1}(t) + f_{q,2n-1}|
\end{aligned} \tag{3.30}$$

From these equations, it can be observed that the amplitudes of the modal displacement, velocity, and acceleration are proportional to the mode shape component, $|u_j^{(2n-1)}(t)|$.

In respect to the phase angle, if the frequency content of the excitation is in a range defined by the instantaneous modal frequency, then the instantaneous frequency of the modal components of the displacement, velocity and acceleration are, practically, insensitive to the position, here defined by j . Therefore, all components of the modal response vector have approximately the same instantaneous frequency, which is not the same as the instantaneous modal frequency of the system, in most of the cases. Note the distinction between the instantaneous frequency, which is a property of a signal, and instantaneous modal frequency, which is a property of the system.

3.5 Instantaneous Modal Parameters of a SDOF system

In this section, some of the concepts discussed in this chapter are illustrated for a simple mass-spring dashpot SDOF system with time varying parameters.

3.5.1 System Dynamics

The dynamics of a SDOF system is described by the following second-order differential equation with time-varying coefficients:

$$M_1(t)\ddot{x}(t) + C_1(t)\dot{x}(t) + K_1(t)x(t) = f_1(t), \quad x(t_0) = x_0, \dot{x}(t_0) = \dot{x}_0 \quad (3.31)$$

For simplicity of the formulation, the equation is normalized by M_1 , and the following notations are introduced:

$$\Omega(t) = \sqrt{K_1(t)/M_1(t)}, \xi(t) = C_1(t)/\sqrt{M_1(t)K_1(t)}/2, \quad f(t) = f_1(t)/M_1(t) \quad (3.32)$$

With these notations, the system dynamic equation and its state space formulation can be expressed as shown in eqs. (3.33) and (3.34).

$$\ddot{x}(t) + 2\xi(t)\Omega(t)\dot{x}(t) + \Omega^2(t)x(t) = f(t) \quad (3.33)$$

$$\frac{d}{dt} \begin{pmatrix} x \\ \dot{x} \end{pmatrix} = \begin{pmatrix} 0 & 1 \\ -\Omega^2(t) & -2\xi(t)\Omega(t) \end{pmatrix} \begin{pmatrix} x \\ \dot{x} \end{pmatrix} + \begin{pmatrix} 0 \\ f(t) \end{pmatrix} \quad (3.34)$$

Consistent with the previous notations, let's denote the state space system matrix by $\mathbf{A}(t)$.

$$\mathbf{A}(t) = \begin{pmatrix} 0 & 1 \\ -\Omega^2(t) & -2\xi(t)\Omega(t) \end{pmatrix} \quad (3.35)$$

3.5.2 Dynamic Eigenvalue Problem

In order to perform the modal decomposition, first, the dynamic eigenvalue problem, expressed in eq. (3.36) has to be solved.

$$(\mathbf{A}(t) - \lambda(t)\mathbf{I})\mathbf{u} = \dot{\mathbf{u}} \quad (3.36)$$

Using the quasistatic algorithm in Chapter 2.1, the dynamic eigenvalues of the system are calculated from the algebraic eigenvalue problem with frozen time, as shown in eq. (3.37). Given the dynamic eigenvalues, the dynamic eigenvectors are calculated by integrating eq.(3.36), with initial values equal to the quasistatic eigenvectors at $t = t_0$. The result is presented in eq. (3.39). Details can be found in Chapter 2.1.2.4.

$$\lambda_{1,2}(t) = -\xi(t)\Omega(t) \pm i\Omega(t)\sqrt{1 - \xi(t)^2}, \quad 0 \leq \xi(t) < 1 \quad (3.37)$$

$$\mathbf{u}^{(i)}(t) = \mathbf{u}^{(i)}(t_0) \exp \int_{t_0}^t (\mathbf{A}(\tau) - \lambda_i(\tau)\mathbf{I}) d\tau, \quad i = 1, 2, \quad \mathbf{u}^{(i)}(t_0) = \mathbf{u}^{(i)qs}(t_0) \quad (3.38)$$

Note that $\lambda_2(t) = \lambda_1^*(t)$, $\mathbf{u}^{(2)}(t) = \mathbf{u}^{(1)*}(t)$ where $\mathbf{u}^{(i)} = \begin{bmatrix} \mathbf{u}_1^{(i)} \\ \mathbf{u}_2^{(i)} \end{bmatrix}, i = 1, 2$.

3.5.3 Modal Equations and System Response

The system has two first-order modal equations which are shown in eq. (3. 39). Their solutions, called modal coordinates, are complex conjugated, i.e. , $q_1(t) = q_2^*(t)$.

$$\begin{aligned} \dot{q}_1(t) &= \lambda_1 q_1(t) + \mathbf{v}^{(1)T}(t) \begin{bmatrix} 0 \\ f(t) \end{bmatrix}, \quad q_1(t_0) = \mathbf{v}^{(1)T}(t_0) [x_0, \dot{x}_0]^T, \\ \dot{q}_2(t) &= \lambda_2 q_2(t) + \mathbf{v}^{(2)T}(t) \begin{bmatrix} 0 \\ f(t) \end{bmatrix}, \quad q_2(t_0) = \mathbf{v}^{(2)T}(t_0) [x_0, \dot{x}_0]^T, \end{aligned} \quad (3. 39)$$

where:

$$\begin{bmatrix} \mathbf{v}^{(1)T}(t) \\ \mathbf{v}^{(2)T}(t) \end{bmatrix} = [\mathbf{u}^{(1)}(t) \quad \mathbf{u}^{(2)}(t)]^{-1} = \frac{1}{2i \operatorname{Im}(u_1 u_2^*)} \begin{bmatrix} u_2^{(2)} & -u_1^{(2)} \\ -u_2^{(1)} & u_1^{(1)} \end{bmatrix} \quad (3. 40)$$

The solution of system (3. 33) is a weighted superposition of the modal coordinates as expressed in eq. (3. 41) , where the notation $v(t) = \dot{x}(t)$ has been introduced for the velocity response.

$$\begin{bmatrix} x(t) \\ v(t) \end{bmatrix} = \begin{bmatrix} u_1^{(1)}(t) q_1(t) + u_1^{(1)*}(t) q_1^*(t) \\ u_2^{(1)}(t) q_1(t) + u_2^{(1)*}(t) q_1^*(t) \end{bmatrix} = \begin{bmatrix} 2|u_1^{(1)}(t)| |q_1(t)| \cos(\arg(u_1^{(1)}(t)) + \arg(q_1(t))) \\ 2|u_2^{(1)}(t)| |q_1(t)| \cos(\arg(u_2^{(1)}(t)) + \arg(q_1(t))) \end{bmatrix} \quad (3. 41)$$

3.5.4 Free Vibration Response

Of main interest is the free vibrations response in eq. (3. 42) because it directly reflects the inherent properties of the system.

$$\begin{aligned} x(t) &= 2|u_1^{(1)}(t)| \left| \mathbf{v}^{(1)T}(t_0) [x_0 \quad \dot{x}_0]^T \right| \exp\left(-\int_{t_0}^t \xi(\tau) \Omega(\tau) d\tau\right) \cos(\phi_x(t)) \\ v(t) &= 2|u_2^{(1)}(t)| \left| \mathbf{v}^{(1)T}(t_0) [x_0 \quad \dot{x}_0]^T \right| \exp\left(-\int_{t_0}^t \xi(\tau) \Omega(\tau) d\tau\right) \cos(\phi_v(t)) \\ \phi_x(t) &= \arg(u_1^{(1)}(t)) + \int_{t_0}^t \left(\Omega(\tau) \sqrt{1 - (\xi(\tau))^2} \right) d\tau + \arg\left(\left[\mathbf{v}^{(1)T}(t_0) \right] [x(t_0) \quad \dot{x}(t_0)]^T\right) \\ \phi_v(t) &= \arg(u_2^{(1)}(t)) + \int_{t_0}^t \left(\Omega(\tau) \sqrt{1 - (\xi(\tau))^2} \right) d\tau + \arg\left(\left[\mathbf{v}^{(2)T}(t_0) \right] [x(t_0) \quad \dot{x}(t_0)]^T\right) \end{aligned} \quad (3. 42)$$

If the system is slowly time-varying, the displacement and velocity have, practically, the same instantaneous frequency which coincides with the system instantaneous modal frequency (up to order of ε , where $\varepsilon \ll 1$), as shown in eq. (3. 43).

$$\frac{d\phi_x(t)}{dt} \cong \frac{d\phi_v(t)}{dt} \cong \Omega(t)\sqrt{1-(\xi(\tau))^2} \quad (3. 43)$$

3.5.5 Slowness Index

The normalized dynamic eigenvectors are defined as shown in (3.44):

$$\mathbf{u}_i^{(i)}(t) = [1 \quad u_2^{(i)}(t)/u_1^{(i)}(t)]^T, \quad u_1^{(i)}(t) \neq 0 \quad i = 1,2 \quad (3. 44)$$

To check if the system is indeed slowly time-varying, as it was assumed, the values of slowness index should be calculated. Since the dynamic and quasistatic eigenvalues/eigenvectors for the above system are in complex conjugate pairs, only the slowness index for $i=1$ is calculated in eq. (3. 45).

$$S_{STV}(t) = \left| \frac{u_2^{(1)}(t)/u_1^{(1)}(t) - u_{qs,2}^{(1)}(t)/u_{qs,1}^{(1)}(t)}{u_2^{(1)}(t)/u_1^{(1)}(t)} \right|, \quad (u_1^{(1)}, u_{qs,1}^{(1)}, u_2^{(1)}) \neq 0 \quad (3. 45)$$

3.6 Second Order Formulation for Vibration Modes

In the following we propose to find a second order differential equation to describe the real time-varying vibration modal responses of a system whose dynamics was given in eq. (3. 1) which, for the reader's convenience is repeated here.

$$\mathbf{M}\ddot{\mathbf{x}}(t) + \mathbf{C}_d(t)\dot{\mathbf{x}}(t) + \mathbf{K}(t)\mathbf{x}(t) = \mathbf{f}(t) \quad (3. 1)$$

Each modal component of the displacement and velocity free response vectors can be described by eq. (3. 46) and eq. (3. 47).

$$x_j^{(n)}(t) = 2|u_j^{(2n-1)}(t)| |C_{2n-1}(t_0)| \exp\left(\int_{t_0}^t \gamma_{\lambda,n}(\tau) d\tau\right) \cos(\phi_{x,j}^{(n)}(t)), \quad j = 1 \cdots N \quad (3. 46)$$

$$\phi_{x,j}^{(n)}(t) = \arg(u_j^{(2n-1)}(t)) + \int_{t_0}^t \omega_{\lambda,n}(\tau) d\tau + \arg(C_{2n-1}(t_0))$$

$$v_j^{(n)}(t) = 2|u_{2j}^{(2n-1)}(t)|C_{2n-1}(t_0)\exp\left(\int_{t_0}^t \gamma_{\lambda,n}(\tau)d\tau\right)\cos(\phi_{v,j}^{(n)}(t)), \quad j = 1 \dots N \quad (3.47)$$

$$\phi_{v,j}^{(n)}(t) = \arg(u_{2j}^{(2n-1)}(t)) + \int_{t_0}^t \omega_{\lambda,n}(\tau)d\tau + \arg(C_{2n-1}(t_0))$$

The parameters in this equations, such as: $u_j^{(2n-1)}(t)$, $u_{2j}^{(2n-1)}(t)$, $\gamma_{\lambda,n}(t)$, $\omega_{\lambda,n}(t)$, and $C_{2n-1}(t_0)$, are related to the system physical properties by the dynamic eigenvalue problem in eq. (3.6).

In the previous section, it has been shown that the response of a SDOF governed by eq. (3.33) can be expressed by eq. (3.48). The subscript ‘‘S’’ has been added to the notations in order to avoid the confusion.

$$\ddot{x}_S(t) + 2\xi(t)\Omega(t)\dot{x}_S(t) + \Omega^2(t)x_S(t) = 0, \quad x_S(t_0) = x_{S,0}, \dot{x}_S(t_0) = \dot{x}_{S,0} \quad (3.33)$$

$$x_S(t) = 2|u_{S,1}^{(1)}(t)|\mathbf{v}_S^{(1)T}(t_0)[x_{S,0} \quad \dot{x}_{S,0}]^T \exp\left(-\int_{t_0}^t \xi(\tau)\Omega(\tau)d\tau\right)\cos(\phi_{S,x}(t))$$

$$v_S(t) = 2|u_{S,2}^{(1)}(t)|\mathbf{v}_S^{(1)T}(t_0)[x_{S,0} \quad \dot{x}_{S,0}]^T \exp\left(-\int_{t_0}^t \xi(\tau)\Omega(\tau)d\tau\right)\cos(\phi_{S,v}(t)) \quad (3.48)$$

$$\phi_{S,x}(t) = \arg(u_{S,1}^{(1)}(t)) + \int_{t_0}^t \left(\Omega(\tau)\sqrt{1 - (\xi(\tau))^2}\right)d\tau + \arg([\mathbf{v}_S^{(1)T}(t_0)][x_S(t_0) \quad \dot{x}_S(t_0)]^T)$$

$$\phi_{S,v}(t) = \arg(u_{S,2}^{(1)}(t)) + \int_{t_0}^t \left(\Omega(\tau)\sqrt{1 - (\xi(\tau))^2}\right)d\tau + \arg([\mathbf{v}_S^{(2)T}(t_0)][x_S(t_0) \quad \dot{x}_S(t_0)]^T)$$

The similarities between eqs. (3.46), (3.47) and (3.48) suggest that each real vibration modal response can be described by a second order equation as shown in (3.33), with the following relationship between the parameters:

$$\omega_{\lambda,n}(t) = \Omega(t)\sqrt{1 - \xi(t)^2}, \gamma_{\lambda,n}(\tau) = -\Omega(\tau)\xi(\tau)$$

$$x_S(t_0) = 2 \operatorname{Re}\left(u_j^{(2n-1)}(t_0)\mathbf{v}^{(2n-1)T}(t_0)\right) \begin{bmatrix} \mathbf{x}_0 \\ \dot{\mathbf{x}}_0 \end{bmatrix}$$

$$\dot{x}_S(t_0) = 2 \operatorname{Re}\left(u_{2j}^{(2n-1)}(t_0)\mathbf{v}^{(2n-1)T}(t_0)\right) \begin{bmatrix} \mathbf{x}_0 \\ \dot{\mathbf{x}}_0 \end{bmatrix} \quad (3.49)$$

$$u_j^{(2n-1)}(t) = u_{S,1}^{(1)}(t), \quad u_{2j}^{(2n-1)}(t) = u_{S,2}^{(1)}(t)$$

Second order formulation in the presence of an excitation

In the following, we will try to find a second order formulation, for a vibration modal response obtained in the presence of an excitation. Specifically, we are looking for a second order SDOF system of form in eq. (3. 50) whose response is equal to the modal response at location $j. n$ (3. 48).

$$\ddot{x}_s(t) + 2C_d(t)\dot{x}_s(t) + \Omega^2(t)x_s(t) = f_s(t), \quad x_s(t_0) = x_{s,0}, \dot{x}_s(t_0) = \dot{x}_{s,0} \quad (3. 50)$$

In addition to the relationships already presented in eq. (3. 49), we are interested in a relationship between the force $f_s(t)$ and the system excitation $\mathbf{f}(t)$.

The first elementary modal coordinate of the SDOF system is described by eq. (3. 51).

$$\dot{q}_{s,1}(t) = \lambda_{s,1}q_{s,1}(t) + \mathbf{v}_s^{(1)T}(t) \begin{bmatrix} 0 \\ 1 \end{bmatrix} f_s(t), \quad q_{s,1}(t_0) = \mathbf{v}_s^{(1)T}(t_0) \begin{bmatrix} x_{s,0} \\ \dot{x}_{s,0} \end{bmatrix} \quad (3. 51)$$

The n^{th} real vibration modal response is a weighted sum of two complex conjugate elementary modal coordinates. The elementary modal coordinate (2n-1) is given in eq. (3.53).

$$\dot{q}_{2n-1}(t) = \lambda_{2n-1}q_{2n-1}(t) + \mathbf{v}^{(2n-1)T}(t) \begin{bmatrix} \mathbf{0} \\ \mathbf{M}^{-1} \end{bmatrix} \mathbf{f}(t), \quad q_{2n-1}(t_0) = \mathbf{v}^{(2n-1)T}(t_0) \begin{bmatrix} \mathbf{x}_0 \\ \dot{\mathbf{x}}_0 \end{bmatrix} \quad (3. 52)$$

The equality between the terms in eqs. (3. 51) and (3. 52) gives a relationship between $f_s(t)$ and $\mathbf{f}(t)$ as follows:

$$\mathbf{v}^{(2n-1)T}(t) \begin{bmatrix} \mathbf{0} \\ \mathbf{M}^{-1} \end{bmatrix} \mathbf{f}(t) = [v_{s,1}^{(1)}(t) \quad v_{s,2}^{(1)}(t)] \begin{bmatrix} 0 \\ f_s(t) \end{bmatrix} \quad (3. 53)$$

Replacing the vector $[v_{s,1}^{(1)}(t) \quad v_{s,2}^{(1)}(t)]$ by expression in eq. (3. 40) and (3. 49) the following formulation is obtained for the modal force $f_s(t)$:

$$f_s(t) = \frac{\mathbf{v}_{N+1, \dots, 2N}^{(n)T}(t) \mathbf{M}^{-1} \mathbf{f}(t)}{v_{s,2}^{(1)}(t)} = \frac{2i \operatorname{Im}(u_j^{(2n-1)}(t) u_{2j}^{(2n-1)*}(t))}{-u_j^{(2n-1)*}(t)} \mathbf{v}_{N+1, \dots, 2N}^{(n)T}(t) \mathbf{M}^{-1} \mathbf{f}(t) \quad (3. 54)$$

Note that $f_s(t)$ is a real function of time. The justification of this statement is as follows:

It is obvious that $u_j^{(2n-1)}(t) \mathbf{v}^{(2n-1)T}(t) + u_j^{(2n-1)*}(t) \mathbf{v}^{(2n-1)*T}(t) = \mathbf{0}, j = 1, 2, \dots, N$, then by simple

algebra it is shown that $\frac{\mathbf{v}^{(2n-1)T}(t)}{u_j^{(2n-1)*}(t)}$ has zero real part; therefore, the vector

$$\frac{2i \operatorname{Im}\left(u_j^{(2n-1)}(t)u_{2j}^{(2n-1)*}(t)\right)}{-u_j^{(2n-1)*}(t)} \mathbf{v}_{N+1, \dots, 2N}^{(n)T}(t) \text{ has real components.}$$

As conclusion, each real vibration modal response of a time-varying system can be described by a second-order equation (3. 55) whose parameters are related to the system by dynamic eigenpair as shown in eq. (3. 56).

$$\ddot{x}_j^{(n)}(t) + 2\xi_n(t)\Omega_n(t)\dot{x}_j^{(n)}(t) + \Omega_n^2(t)x_j^{(n)}(t) = f_n(t) \quad (3. 55)$$

$$x_j^{(n)}(t_0) = u_j^{(2n-1)}(t_0)\mathbf{v}^{(2n-1)T}(t_0) \begin{bmatrix} \mathbf{x}_0 \\ \dot{\mathbf{x}}_0 \end{bmatrix}, \dot{x}_j^{(n)}(t_0) = u_{2j}^{(2n-1)}(t_0)\mathbf{v}^{(2n-1)T}(t_0) \begin{bmatrix} \mathbf{x}_0 \\ \dot{\mathbf{x}}_0 \end{bmatrix}$$

$$\xi_n(t) = -\frac{\gamma_{\lambda,n}(t)}{\sqrt{\omega_{\lambda,n}^2 + \gamma_{\lambda,n}^2(t)}}, \Omega_n = \sqrt{\omega_{\lambda,n}^2 + \gamma_{\lambda,n}^2} \quad (3. 56)$$

$$f_n(t) = \frac{2i \operatorname{Im}\left(u_j^{(2n-1)}u_{2j}^{(2n-1)*}\right)}{-u_j^{(2n-1)*}} \mathbf{v}_{N+1, \dots, 2N}^{(n)T}(t)\mathbf{M}^{-1}\mathbf{f}(t),$$

where $\gamma_{\lambda,n}(t) = \operatorname{Re}(\lambda_{2n-1}(t))$, $\omega_{\lambda,n}(t) = \operatorname{Re}(\lambda_{2n-1}(t))$.

In this section (3.6) no assumption of slowly time-varying system has been made. However, to solve the inverse problem by, first, extracting the vibration modal components from the response, the assumption of slowly time-varying system is instrumental.

3.7 Numerical Examples: Linear SDOF and 3DOF Systems with Time-varying Stiffness

In Chapter 2, a quasistatic algorithm has been introduced to solve the dynamic eigenvalue problem. In Chapter 3.4 it has been explained that if the dynamic eigenvectors are slowly time-varying in comparison to the eigenvalues, the quasistatic algorithm gives a modal decomposition with physical meaning. In order to quantify the slowly time-varying condition, a slowness index has been introduced in Chapter 3.4.1. This index has zero value

for a time invariant system. , For a time-varying system it should be zero or in the vicinity of zero in order to have a modal decomposition with physical meaning. In this case the instantaneous frequency of the free vibration modal components is, practically, the same (up to the order of ε , where $\varepsilon \ll 1$) as the imaginary part of the dynamic eigenvalue, and modal displacement, velocity and acceleration responses measured at a given location have the same instantaneous frequency (up to the order of ε).

In this section, the above findings are verified numerically for a single degree-of-freedom (SDOF) system and a three degree-of-freedom (3DOF) system, with time varying stiffness. The system response is obtained by two methods: time varying modal decomposition and direct numerical integration and the results are compared. The dynamic eigenvalues and eigenvectors, and the associated slowness index are calculated. A sensitivity study which compares the slowness indices and instantaneous modal frequencies for different stiffness evolution is performed. It is found that the slowly time-varying assumption can be used for systems with significant change in system physical parameters, if the change is gradual with a slower rate than the system fundamental frequency. In the case of a 3DOF system the instantaneous frequency of the free modal responses at different positions are compared to the calculated modal frequencies.

3.7.1. Case Study I: SDOF System

Simulation setup:

In the present study, first, a SDOF system with time-varying stiffness is considered. The parameters of the reference system are: $M_1=1\text{kg}$, $K_1= 39.4784 \text{ N/m}$, $C_1= 0.1257 \text{ Ns/m}$. These parameters have been chosen so that the natural frequency and damping ratio of the reference system are: $f_n = \Omega/(2\pi) = 1\text{Hz}$ and $\zeta = 0.01$. A sketch of the system is presented in Fig. 3.1a.

Four scenarios for stiffness variation are proposed. In the first three scenarios, stiffness reduces linearly with a rate proportional to the parameter α , as shown in Fig. 3.1b, where α has the following values: Scenario I: $\alpha = 0.2$; Scenario II: $\alpha = 0.4$; Scenario III: $\alpha = 0.8$. In the Scenario IV a sinusoidal stiffness evolution, $K = K_0(1 + 0.2\sin(\pi t))$ (Fig.

3.1.c) is proposed. by:. This is considered as a fast evolution of the stiffness, being of the same order of magnitude as the natural frequency of the reference system.

Results

First, a system subjected to damage Scenario II ($\alpha = 0.4$) is considered. The dynamic eigenvalues and eigenvectors are calculated by eqs. (3. 37) and (3. 38). The results are plotted in Figs. 3.2 and 3.3. As expected the values are constant during the first 10 seconds, when no damage occurs. The dynamic eigenvalue is a complex function of time and in this example its real part is constant because the damping factor C_I was not time dependant. The values of the second eigenpair are the complex conjugate of the first one and, therefore, only plots of the first eigenpair are sufficient in this study.

The free response of the system is calculated in two ways: by direct integration of system (3. 31) and by using the time varying modal decomposition described above. The results are practically the same, the root mean square (rms) error between the results being of order 10^{-8} , as compared to the rms value of the response of 0.317.

Figure 3.4(a) shows plots of the system modal frequency (green), displacement instantaneous frequency (magenta) and velocity instantaneous frequency (blue). A zoom-in plot of the same data is presented in Fig. 3.4(b). It can be observed that all three frequencies are very close, which is a good indication that the assumption of slowly time-varying system holds. A quantitative measure of the slowly time varying nature is given in Fig. 3.4(d), where it can be seen that the slowness index is smaller than 0.001. Figure 3.4(c) shows the contribution of the eigenvector to the instantaneous frequency of displacement. Results similar to those in Fig. 3.4(c) can be seen for the slowness index in Fig. 3.4(d). In this case, the explanation is based on the fact that the normalized eigenvector component is approximately equal to the imaginary part of the dynamic eigenvalue due to the insignificant contribution of the eigenvalue real part which reflects the damping into the system.

For practical purpose, it is useful to know when the condition of slowly time-varying system is satisfied. Due to the complexity of the dynamic eigenvalue problem, an analytic answer may not be feasible for the general case; therefore, a sensitivity analysis may be useful. Figures 3.4-3.7 show the results of this study where figures denoted by (b) show

zoom-in plots for figures (a), figures (c) show the contribution of the phase angle to the instantaneous frequency of the modal response, and figures (d) present the slowness index. From the results in Fig.3.6, we can conclude that the slowly time-varying assumption still holds when the stiffness change its value linearly by 80% during a time interval of 30s.

Figures 3.7(a) and 3.7 (b) show plots of the instantaneous frequency of the free vibration responses for a stiffness evolution according to Scenario IV. We can see from zoom-in plot in Fig. 3.7(b) that there is a significant difference between the system modal frequency calculated as imaginary part of the dynamic eigenvalue, and the instantaneous frequency of the displacement and velocity. This difference is quantified in Fig. 3.7(c) which shows the contribution of the dynamic eigenvector to the instantaneous frequency (aprox. 10%).

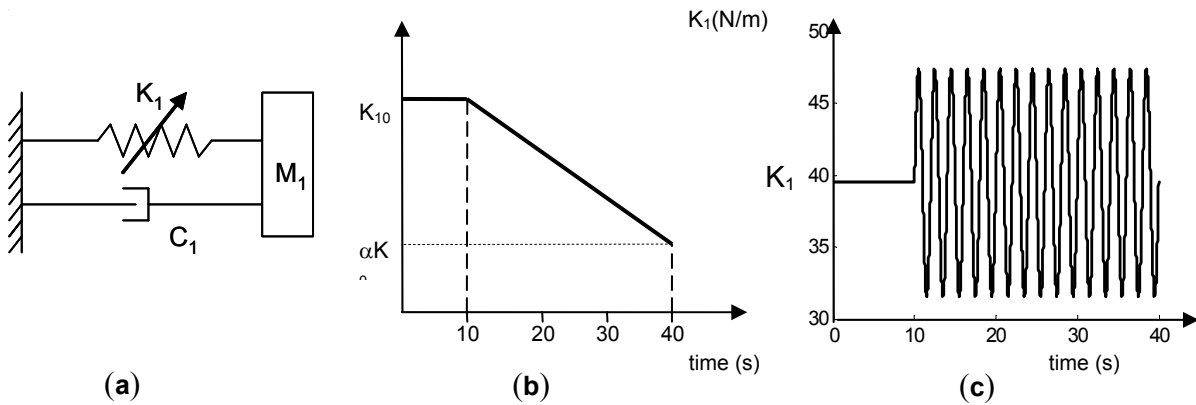


Figure 3.1 (a) Sketch of the system; Stiffness history: (b) Scenario I, II, III; (c) Scenario IV

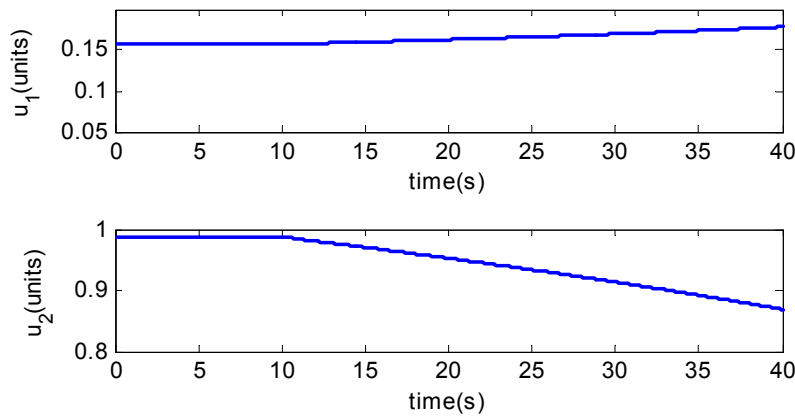


Figure 3.2 Complex modulus of the 1st dynamic eigenvector.

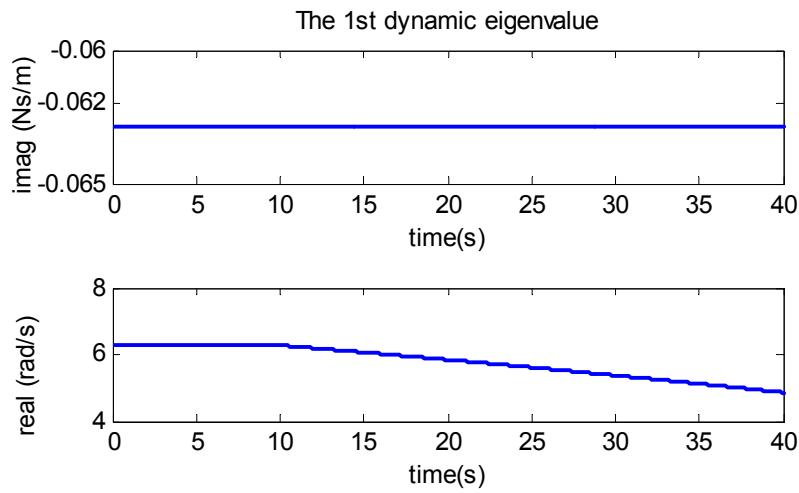


Figure 3.3 The 1st dynamic eigenvalue (real and imaginary part)

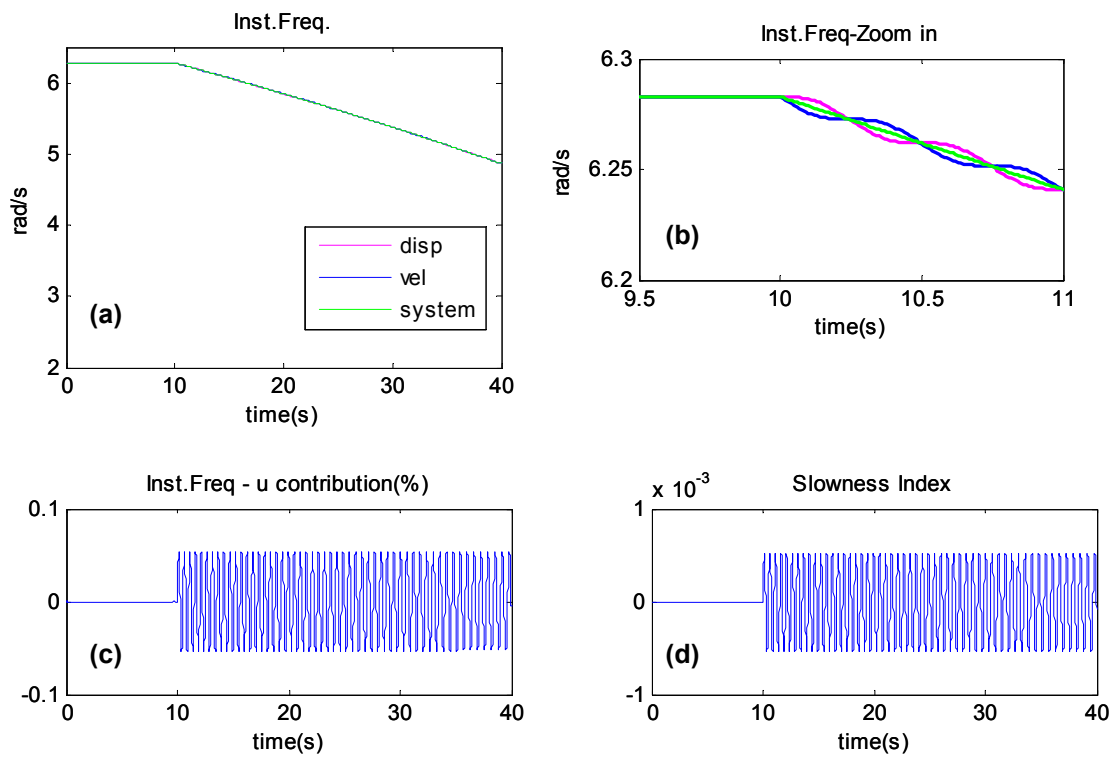


Figure 3.4. Results for Scenario II ($\alpha = 0.4$)

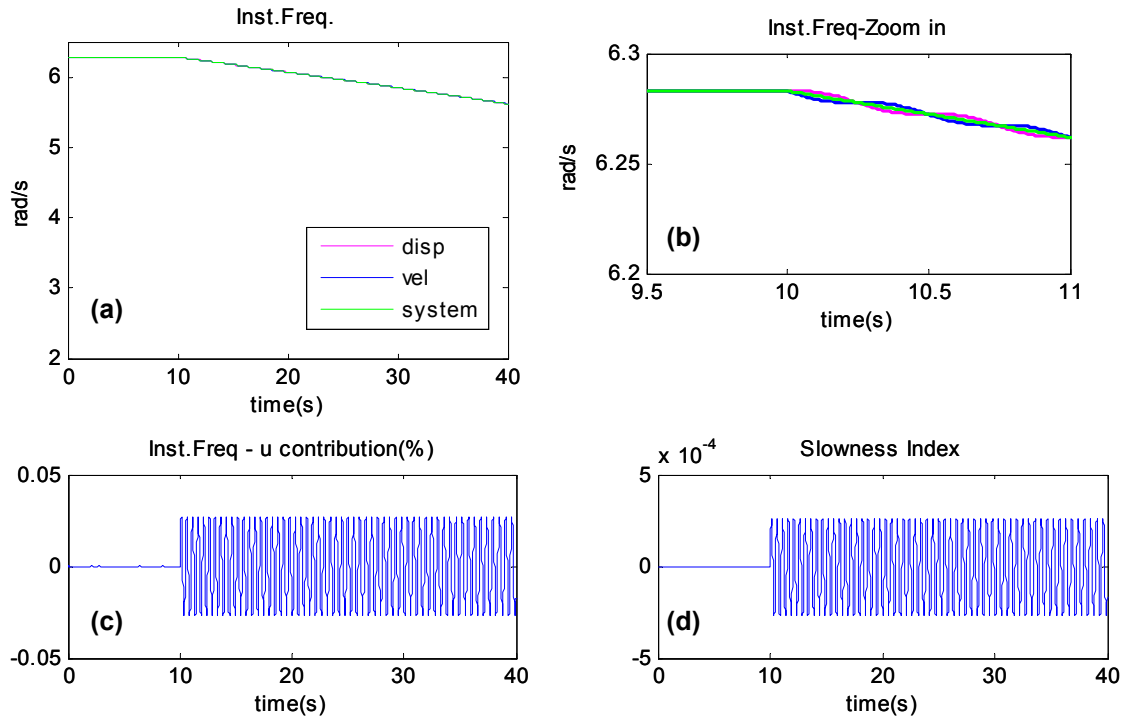


Figure 3.5 Results for Scenario I ($\alpha = 0.2$)

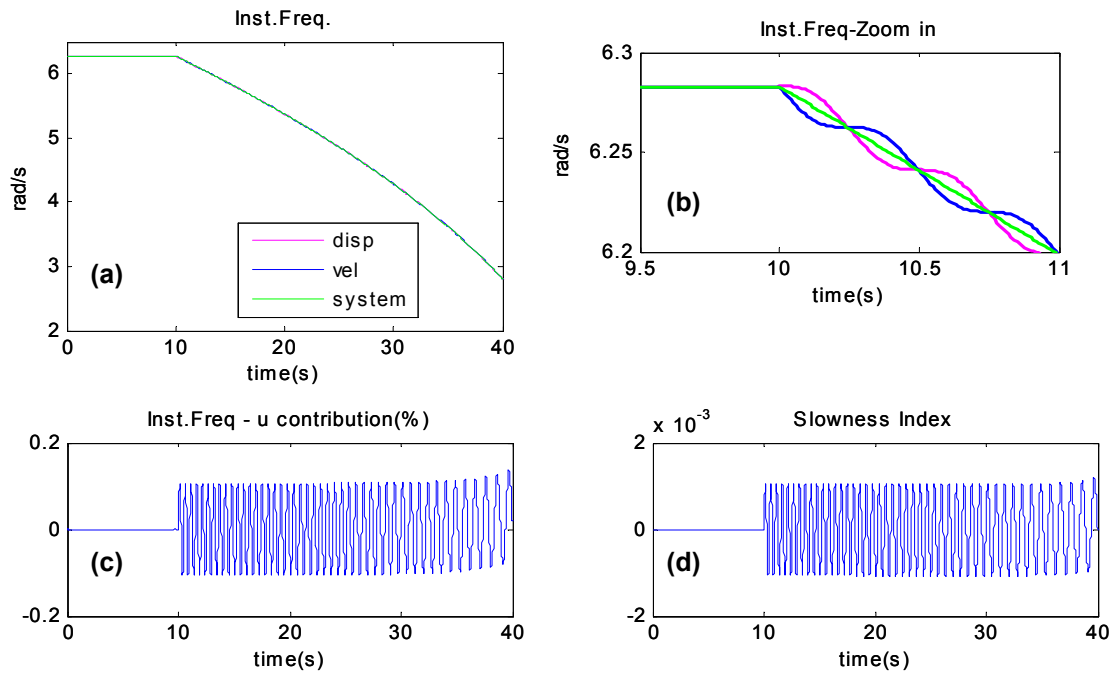


Figure 3.6. Results for Scenario III ($\alpha = 0.8$)

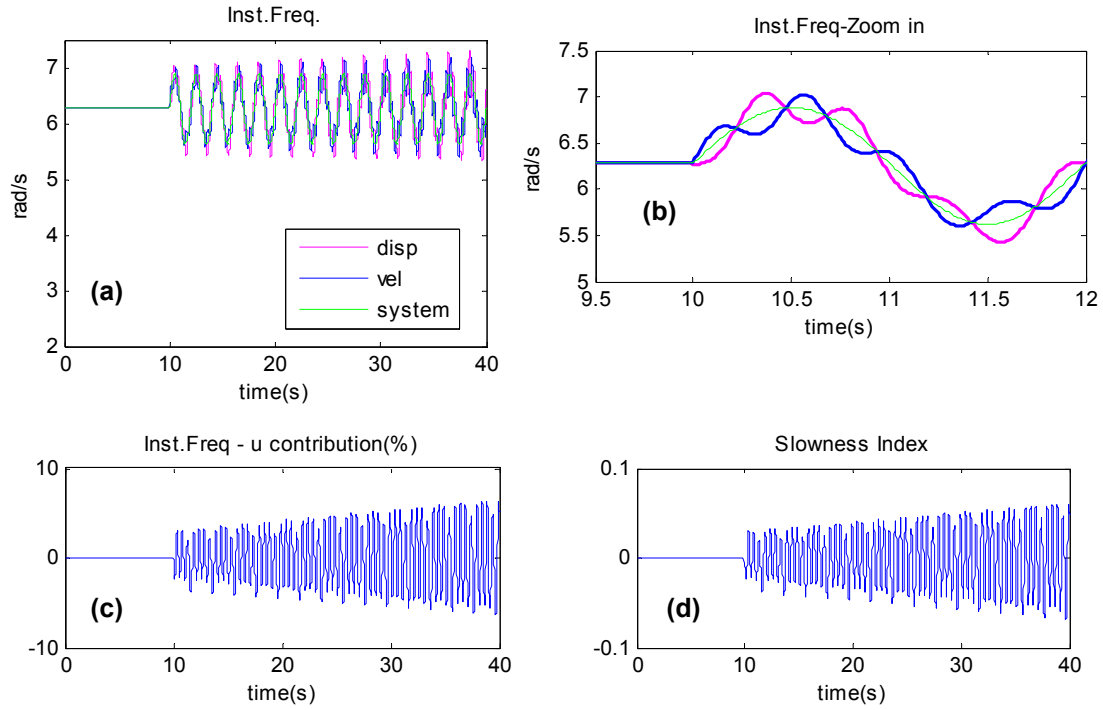


Figure 3.7. Results for Scenario IV

3.7.2. Case Study II: 3DOF system

Simulation setup:

The 3DOF system employed in this simulation study is sketched in Fig. 3.9. The reference system has the following parameters: $M_1=M_2=M_3=300\text{kg}$, $K_1=K_2=K_3=100000\text{N/m}$ and the damping matrix is proportional to the stiffness matrix by a factor $\beta = 0.0002\text{ s}$. Its natural frequencies are: 8.1253, 22.7666, 32.8987 rad/s and the modal damping ratios are 0.0008, 0.0023, 0.0033. A progressive degradation of K_2 after the first 12 seconds, as shown in Fig. 3.9(b), is proposed for the damaged system. The system dynamics is given in eq. (3.58) and the free response is simulated using a nonzero velocity for M_3 ($\dot{x}_3 = 0.5\text{m/s}$).

$$\mathbf{M}\ddot{\mathbf{x}} + \mathbf{C}\dot{\mathbf{x}} + \mathbf{K}\mathbf{x} = \mathbf{f}(t) \quad (3.58)$$

where

$$\mathbf{x} = \begin{bmatrix} x_1 \\ x_2 \\ x_3 \end{bmatrix}, \quad \mathbf{M} = \begin{bmatrix} M_1 & 0 & 0 \\ 0 & M_2 & 0 \\ 0 & 0 & M_3 \end{bmatrix}, \quad \mathbf{K} = \begin{bmatrix} K_1 + K_2 & -K_2 & 0 \\ -K_2 & K_2 + K_3 & -K_3 \\ 0 & -K_3 & K_3 \end{bmatrix},$$

$$\mathbf{C} = \begin{bmatrix} C_1 + C_2 & -C_2 & 0 \\ -C_2 & C_2 + C_3 & -C_3 \\ 0 & -C_3 & C_3 \end{bmatrix}, \quad \mathbf{f} = \begin{bmatrix} 0 \\ 0 \\ 0 \end{bmatrix}, \quad (3.59)$$

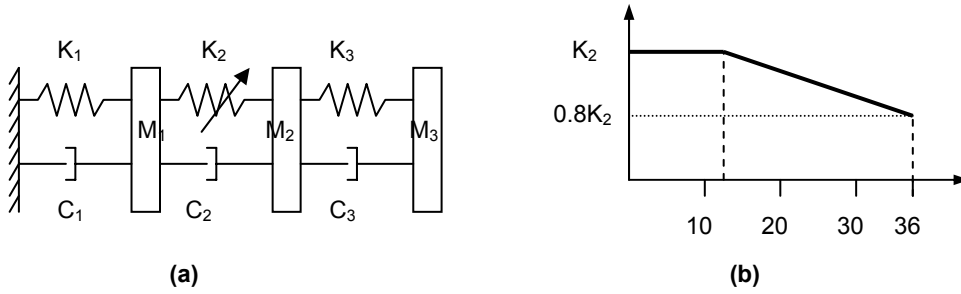


Figure 3.8. (a) Sketch of the system; (b) Stiffness history (K_2)

Results

The quasistatic algorithm is used to solve the dynamic eigenvalue problem for the corresponding first-order system in state space. The responses obtained by numerical integration of the governing equation in state space and by using the modal decomposition are compared. The maximum root mean square (rms) of the error between the responses calculated by two methods is less than 0.1% of the rms of the response over the time interval of 0-36 s.

Plots of the first dynamic eigenvalue are presented in Fig. 3.9. The real and imaginary parts are constant over the time interval of 0-12 seconds when the system is time invariant, than a gradual change in their values can be observed. The imaginary parts gives the first instantaneous modal frequency of the system, and the real part is related to the instantaneous modal damping. Plots of the first three components of the first eigenvector are shown in Fig. 3.10. These components correspond to the displacements of \$M_1\$, \$M_2\$ and

M3. The other three components, not plotted here, correspond to the velocities at the same locations. Since the mode shape is a complex function, the complex modulus and the phase angle are plotted in the figure.

Figure 3.11 shows a comparison of the instantaneous modal frequencies defined as imaginary part of the eigen-values and instantaneous frequencies of the free vibration responses (displacements and accelerations). Figure 3.11 (b) shows “zoom in” plots for the case of displacement at different locations, i.e. M1, M2, M3. Figure 3.11(c) shows zoom in plots for the case of velocities. Ideally, all the values should be the same. The small differences between the instantaneous modal frequencies and the instantaneous frequency of the impulse responses are due to the influence of the time varying and complex nature of the eigenvector. For the 3DOF system investigated, the contribution of the eigenvector to the instantaneous frequency of the responses is less than 0.12% . The maximum values of the slowness index are less than 0.005.

3.7.3 Remarks

A few aspects of time varying modal decomposition have been investigated numerically in section 3.7.

- It has been observed that the slowly time-varying condition is still satisfied for a linear degradation of stiffness of 80% during a time interval of 30s. In this case, the instantaneous frequency of the response is affected less 0.1% by the time varying nature of the eigenvector.
- In the case of the 3DOF system, the instantaneous frequency of the free vibration modal components is practically the same (up to the order of ε , where $\varepsilon \ll 1$) as the modal frequency of the system given by the imaginary part of the dynamic eigenvalue. Free modal displacement, velocity and acceleration responses measured at different locations have the same instantaneous frequency up to the order of ε . These important observations allow the development of the damage detection techniques proposed in the next chapters.

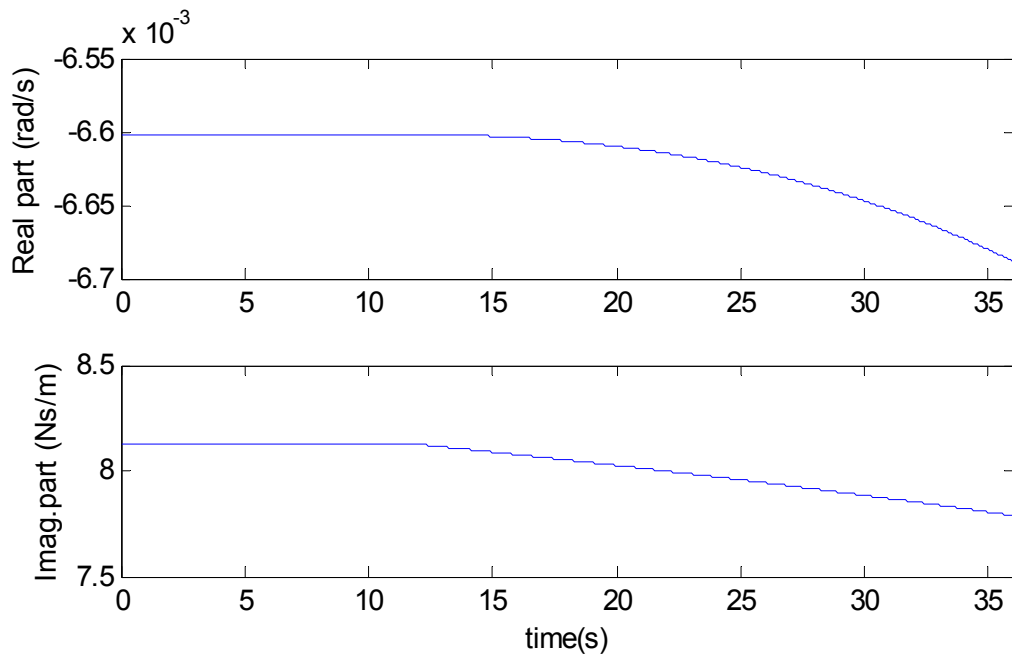


Figure 3.9. The first dynamic eigenvalue

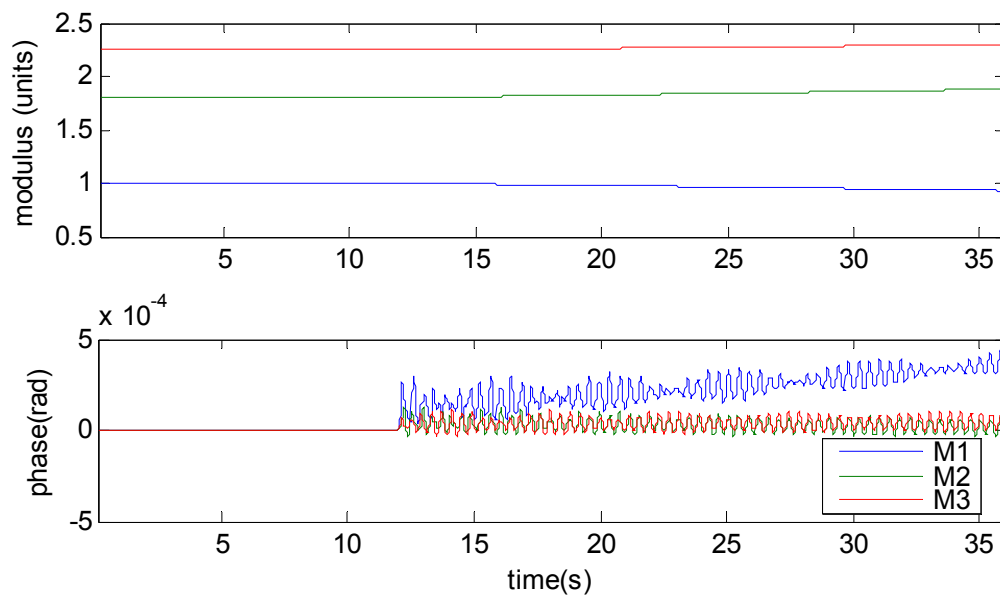
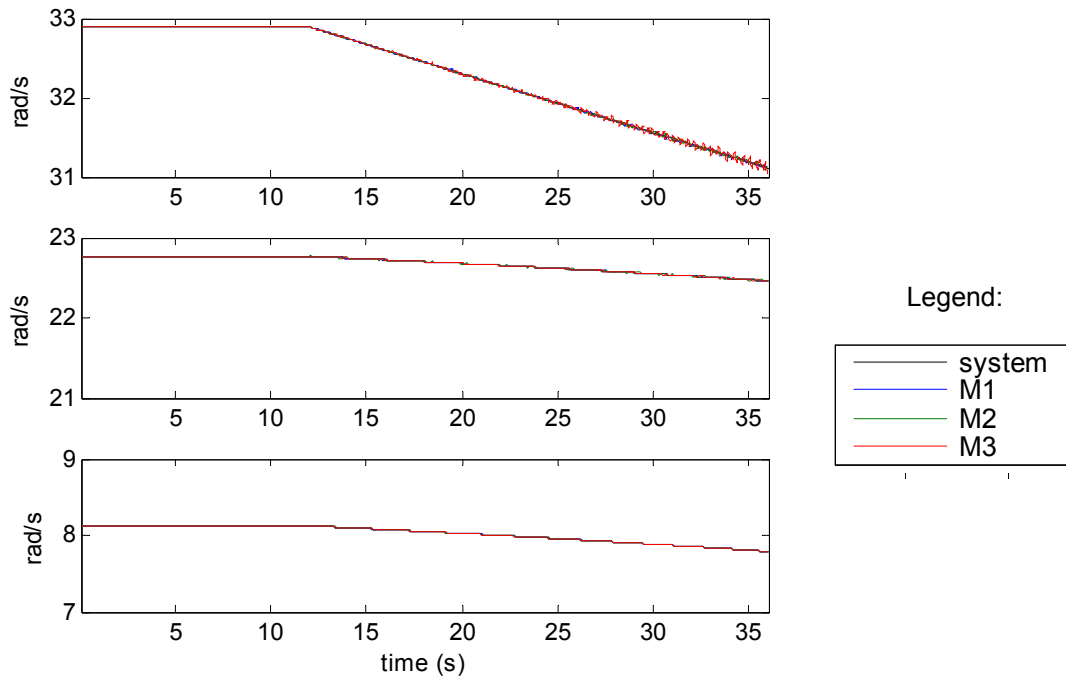
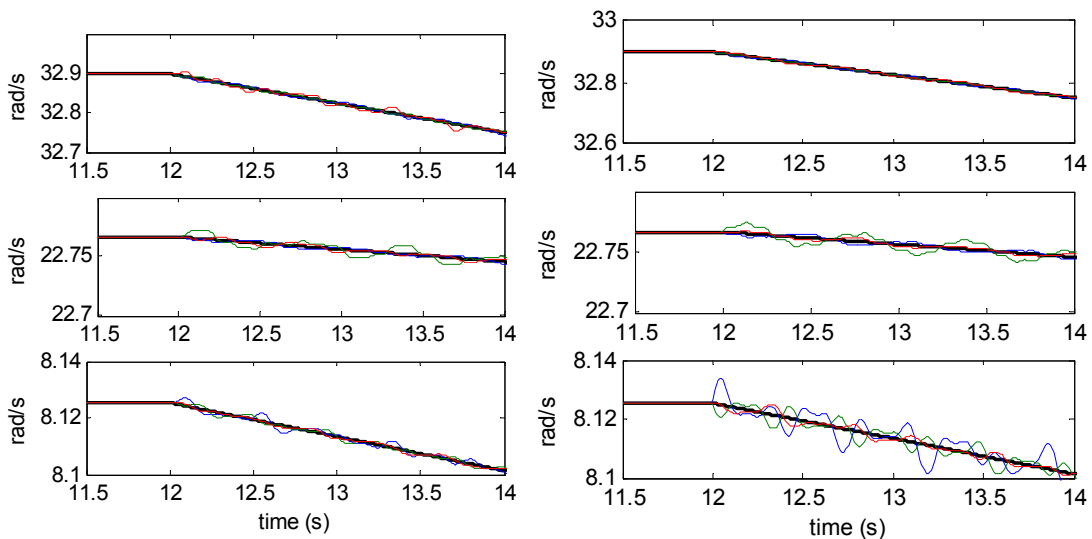


Figure 3.10. The first dynamic eigenvector (the first three components corresponding to the displacement at M1, M2 and M3)



(a)



(b)

(c)

Figure 3.11. Instantaneous frequency: defined by dynamic eigenvalue problem and obtained from free vibration modal responses at M1 (blue), M2 (red) and M3 (green). Results from displacement responses and zoom in plots for the case of (a) displacement responses and (c) velocity responses.

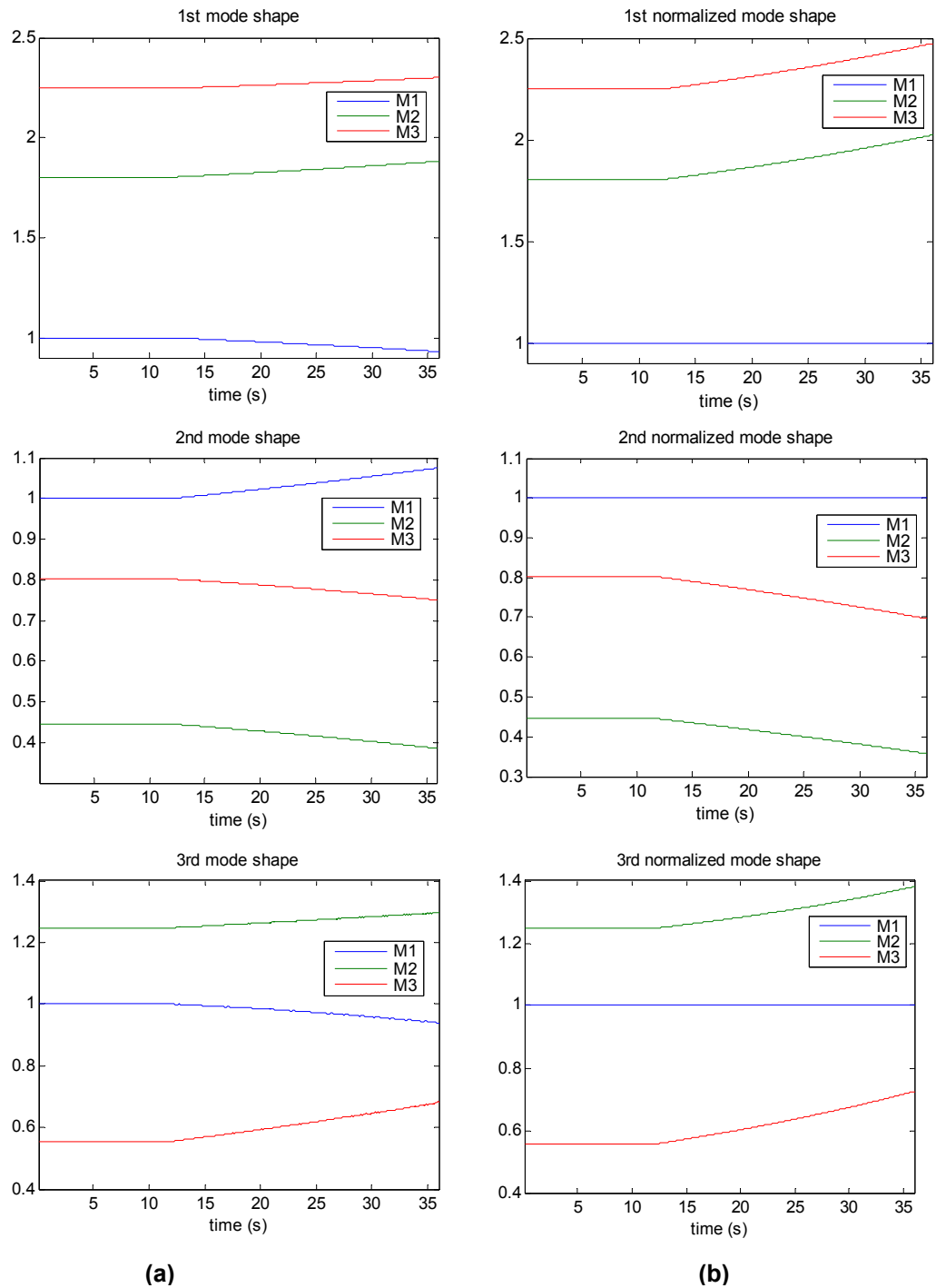


Figure 3.12. (a) Instantaneous mode shapes; (b) Normalized instantaneous mode shape

3. 8 Summary

In this chapter, it has been proved that the vibration response of a linear slowly time-varying system can be written as a sum of real modal responses characterized by instantaneous measures such as: the instantaneous mode shape, the instantaneous modal frequency and the instantaneous damping. A second-order formulation for each modal response has been also proposed. The instantaneous modal parameters are related to the system physical parameters by the dynamic eigenvalues/eigenvectors of the associated state space first-order system. The slowly time-varying condition was introduced as a relationship between dynamic eigenvectors and dynamic eigenvalues of the first-order system.

The instantaneous modal frequency was defined as the imaginary part of the eigenvalue. The instantaneous mode shape was defined by the complex modulus of the dynamic eigenvector. For the purpose of identification its normalized version, instantaneous normalized mode shape, was introduced. The modal damping was defined as the imaginary part of the eigenvalue with a negative sign.

It was also shown that the instantaneous modal frequency can be approximated by the frequency of the modal components of the free responses which is practically independent (up to the order of ε , where $\varepsilon \ll 1$) of the measurement location/DOF and is the same for displacement, acceleration and velocity response data (also up to the order of ε).

In case of the forced vibration, if the frequency content of the excitation is in a range defined by the instantaneous modal frequency, the instantaneous frequency of the modal components of the displacement, velocity and acceleration are, practically, insensitive to the position, j . Therefore, all components of the modal response vector have approximately the same instantaneous frequency, which is not the same as the instantaneous modal frequency of the system, in most of the cases.

The instantaneous normalized mode-shape can be calculated from the amplitude of the displacement or velocity or acceleration modal responses. This applies to the case of free vibrations and the forced vibrations.

Although for the numerical example the quasistatic algorithm was used to solve the dynamic eigenvalue problem, the theory developed in this chapter is valid for any other algorithm which gives complex conjugate eigenvalue and eigenvectors, and ensure the slowly time-varying condition.

If a linear time varying system is not slowly time-varying, as defined in the present chapter, one cannot guaranty that real vibration modes with the same instantaneous frequency can be identified in the responses at different DOFs.

The instantaneous modal parameters, defined in this chapter, set the bridge between the free response characteristics and physical parameters of the system. By tracking the instantaneous modal parameters, useful information about the structural health condition in case of evolving damage can be extracted.

Chapter 4

IDENTIFICATION OF INSTANTANEOUS MODAL PARAMETERS FROM FREE VIBRATION DATA

4.1 Introduction

In Chapter 3, it has been proved that the vibration response of a linear slowly time-varying system can be decomposed, by using the dynamic eigenvalue problem, in real vibration modes characterized by instantaneous modal parameters such as modal frequency, mode shape and modal damping. In this section, we propose to solve the inverse problem of identification of instantaneous modal frequency and normalized instantaneous mode shape from free vibration data by using two approaches: CWT–ridge method and wavelet packet sifting in conjunction with Hilbert transform. The CWT approach is illustrated using the simulated free vibration responses of a 3DOF with progressive stiffness degradation and subjected to nonzero initial conditions. The identified results are compared to those obtained by solving the dynamic eigen-value problem.

4.2 Theoretical Background

4.2.1 Free Vibration Modal Responses

It has been shown in the previous chapter that the response of a linear slowly time-varying system can be written as a sum of modal responses, i.e. $x_j(t) = \sum_n x_j^{(n)}(t)$. The free vibration modal components of displacement, velocity and acceleration responses were

presented in Chapter 3, in eqs. (3.12), (3.18) and (3.20). They are rewritten in a simplified form in eqs. (4. 1) and (4. 2), with the notations in eq. (4.3).

$$x_j^{(n)}(t) = A_{x,j}^{(n)}(t) \cos(\phi_{x,j}^{(n)}), \quad v_j^{(n)}(t) = A_{v,j}^{(n)}(t) \cos(\phi_{v,j}^{(n)}), \quad a_j^{(n)}(t) = A_{a,j}^{(n)}(t) \cos(\phi_{a,j}^{(n)}) \quad (4. 1)$$

$$\begin{aligned} A_{x,j}^{(n)}(t) &\cong X_j^{(n)}(t) B_n(t_0) \exp\left(\int_{t_0}^t \gamma_n(\tau) d\tau\right) & \phi_{x,j}^{(n)}(t) &= \phi_{ux,j}^{(n)}(t) + \phi_0^{(n)} + \int_{t_0}^t \omega_n(\tau) d\tau \\ A_{v,j}^{(n)}(t) &\cong X_j^{(n)}(t) B_n(t_0) |\lambda_n(t)| \exp\left(\int_{t_0}^t \gamma_n(\tau) d\tau\right) & \phi_{v,j}^{(n)}(t) &= \phi_{uv,j}^{(n)}(t) + \phi_0^{(n)} + \int_{t_0}^t \omega_n(\tau) d\tau \\ A_j^{(n)}(t) &\cong X_j^{(n)}(t) B_n(t_0) |\lambda_n(t)|^2 \exp\left(\int_{t_0}^t \gamma_n(\tau) d\tau\right) & \phi_{a,j}^{(n)}(t) &= \phi_{ua,j}^{(n)}(t) + \phi_0^{(n)} + \int_{t_0}^t \omega_n(\tau) d\tau \end{aligned} \quad (4. 2)$$

$$\begin{aligned} X_j^{(n)}(t) &= |u_j^{(2n-1)}(t)|; \quad B_n(t_0) = 2|C_{2n-1}(t_0)|; \\ \phi_{ux,j}^{(n)}(t) &= \arg(u_j^{(2n-1)}(t)); \quad \phi_{uv,j}^{(n)}(t) = \arg(u_{2j}^{(2n-1)}(t)); \\ \phi_{ua,j}^{(n)}(t) &= \arg(\lambda_{2n-1} u_{2j}^{(2n-1)}(t) + \dot{u}_{2j}^{(2n-1)}(t)); \quad \phi_0^{(n)} = \arg(C_{2n-1}(t_0)); \end{aligned} \quad (4. 3)$$

It can be observed that modal components in eq. (4.1), can be uniquely described by a signal $s(t)$ of the form $s(t) = A_s(t) \cos(\Phi_s(t))$, where “s” stands for the modal displacement $x_j^{(n)}$, velocity $v_j^{(n)}(t)$, or acceleration $a_j^{(n)}(t)$. The amplitude and phase angle of $s(t)$ are as follows:

$$\begin{aligned} A_s(t) &\cong X_j^{(n)}(t) B_n(t_0) |\lambda_n|^k \exp\left(\int_{t_0}^t \gamma_n(\tau) d\tau\right) \\ \text{where } k &= 0 \text{ if } s = x_j^{(n)}; \quad k = 1 \text{ if } s = v_j^{(n)}; \quad k = 2 \text{ if } s = a_j^{(n)}; \\ \Phi_s(t) &= \left(\phi_{us,j}^{(n)}(t) + \phi_0^{(n)} + \int_{t_0}^t \omega_n(\tau) d\tau \right) \end{aligned} \quad (4. 4)$$

With the assumption of a slowly time-varying system, it has been shown in Chapter 3 that $\dot{\phi}_{us}^{(n)}(t) \ll \omega_n(t)$, therefore the instantaneous frequency of each response in eq. (4. 1), practically, does not depend on position “j” and is equal to $\omega_n(t)$ up to the order of epsilon, where epsilon $\ll 1$. On the same ground, the amplitude changes slowly in respect to the

instantaneous modal frequency $\omega_n(t)$, i.e. $\left| \frac{1}{A_s(t)} \frac{dA_s(t)}{dt} \right| \ll \omega_n(t)$. Therefore each modal component has mono-frequency content and is asymptotic (see Section 2.4).

The normalized instantaneous (NI) mode shape was introduced in Chapter 3. Its expression is repeated in eq. (4.5), where the p^{th} mode shape component has been chosen for normalization.

$$\mathbf{X}_{|p}^{(n)}(t) = \left[\frac{\mathbf{X}^{(n)}}{X_p^{(n)}} \right] = \left[\frac{X_1^{(n)}}{X_p^{(n)}} \quad \frac{X_2^{(n)}}{X_p^{(n)}} \quad \dots \quad \frac{X_p^{(n)}}{X_p^{(n)}} \quad \frac{X_N^{(n)}}{X_p^{(n)}} \right]^T \quad (4.5)$$

The separation of the modal responses and identification of NI mode shape and frequency of each modal response can be done by wavelet analysis, either by CWT-ridge method or WP decomposition in conjunction with Hilbert Transform. The theoretical background of these two procedures is presented in the following.

4.2.2 Continuous Wavelet Transform – Ridge Method

CWT has the capability to separate mono-frequency components of a signal, each mono-frequency component being represented on wavelet transform map as a band of high energy. In the case of free vibration data, if the modes are well separated, each ridge on the CWT map corresponds to a time varying vibration mode.

In the following, let us assume that the harmonic components of the response are asymptotic and they do not interact, that means that the vibration modes are well separated. Then, let us restrict the CWT to the time-scale domain Ω_n , where the wavelet coefficients of all but the n^{th} response component are negligible. We denote this n^{th} component by $s(t)$. On the above assumptions $s(t)$ is a narrow band asymptotic signal, which can be written in the following form:

$$s(t) = A(t) \cos(\Phi(t)) \quad (4.6)$$

where $A(t)$ and $\Phi(t)$ are the time-varying amplitude and phase, respectively, which satisfies

the condition $\left| \frac{1}{A(t)} \frac{dA(t)}{dt} \right| \ll \frac{d}{dt}(\phi(t))$.

CWT ridge can be defined in two ways:

1. A ridge is defined as the set of points in domain Ω_n characterized by a stationary phase of CWT coefficients. An estimation procedure based on this definition was proposed by (Delprat et al., 1992).

2. Alternatively, the ridge can be defined as those points in Ω_n where the modulus of the wavelet transform is maximum (Carmona et al, 1997; Mallat, 1999). The estimation algorithm based on this definition is more robust to noise and it is preferred in the present study.

To calculate the CWT, the complex Morlet wavelet, defined in eq. (4.7) has been chosen as mother wavelet.

$$\psi(t) = \frac{1}{\sqrt{\pi F_b}} \exp\left(-\frac{t^2}{F_b}\right) \exp(i2\pi F_c t) \quad (4.7)$$

This selection was based on the best time-frequency resolution and the simple analytic formula which allows a better interpretation of the results. The wavelet transform of the signal $s(t)$ is given by eq. (4.8) (Mallat, 1999):

$$W_f(a, b) = \frac{1}{2} \sqrt{a} A(b) \exp(i\Phi(b)) \left[\exp\left(-\frac{F_b(2\pi F_c - a\Phi'(b))^2}{4}\right) - \varepsilon\left(b, \frac{2\pi F_c}{a}\right) \right] \quad (4.8)$$

It has been proven that the term $\varepsilon\left(b, \frac{\omega_c}{a}\right)$ in the above equation becomes negligible if $A(t)$ and $\phi'(t)$ have small variations over the support of the wavelet function $\psi_{a,b}(t)$ and the amplitude $A(t)$ is slower varying as compared to the rate of change of $\Phi(t)$. As a result, the wavelet transform coefficients can be approximated as:

$$W_f(a, b) \cong \frac{1}{2} \sqrt{a} A(b) \exp(i\Phi(b)) \exp\left(-\frac{F_b(2\pi F_c - a\Phi'(b))^2}{4}\right) \quad (4.9)$$

The coefficients are complex numbers, with the phase and modulus given by eqs. (4.10) and (4.11), respectively.

$$\angle W_f(a, b) = \Phi(b) \quad (4.10)$$

$$|W_f(a, b)| = \frac{1}{2} \sqrt{a} A(b) \exp\left(-\frac{f_b (2\pi F_c - a\Phi'(b))^2}{4}\right) \quad (4.11)$$

The ridge is the curve $a_{ridge}(b)$ representing the modulus maxima of the CWT coefficients. It can be observed that the instantaneous frequency of the signal, can be found by, first, identifying the ridge $a_{ridge}(b)$ and, then, using the formula (4.12).

$$\Phi'(b) = 2\pi F_c / a_{ridge}(b) \quad (4.12)$$

The signal amplitude, $A(b)$, can be found by a similar procedure. First, identify the ridge and then use the formula in eq.(4.13).

$$A(b) = 2 |W(a_{ridge}(b), b)| / \sqrt{a_{ridge}(b)} \quad (4.13)$$

If the corrective term $\varepsilon\left(b, \frac{\omega_c}{a}\right)$ is negligible, by equations (4.12) and (4.13) we can uniquely decompose the signal $s(t)$ as $A(t) \cos(\Phi(t))$. It should be noted that $A(t)$ and $\Phi'(t)$ are the analytic amplitude and instantaneous frequency of $s(t)$, as obtained from the corresponding complex analytic signal.

The results summarized in eqs. (4.12) and (4.13) are used in the Section 4.3 for identifying the instantaneous modal frequencies and normalized instantaneous mode shapes of a time varying dynamic system. It should be mentioned that the accuracy of the results depends on the wavelet transform resolution. A discussion on time-frequency wavelet transform resolution was given in Chapter 2.3.

4.2.3 Wavelet Packet Sifting Process

The wavelet packet sifting process may be used to identify the dominant vibration modes in the response signal (Shinde and Hou, 2005). The binary wavelet packet decomposition is performed on data, and a sifting criterion based on entropy index is used to select the signal modal components. So, the signal can be expressed as a sum of sifted components $s^{(i)}(t)$ and a residual signal $r_k(t)$.

$$s(t) = \sum_{i=1}^k s^{(i)}(t) + r_k(t) \quad (4.14)$$

Different sifting criteria can be used (Shinde, 2005), for example:

1. the entropy index defined as the difference between the number of zero crossings and the number of extrema in a signal component corresponding to a particular node of the wavelet packet tree. Those components which have an entropy index smaller than or equal to unity are selected as the relevant components of the signal, $s^{(i)}(t)$.

2. the energy-entropy which is defined as sum of the square values of the wavelet packet decomposition coefficients for a given node. Each wavelet packet tree node is split into two child-nodes if the splitting makes the energy-entropy decrease. If the criterion is not satisfied anymore, the reconstructed signal corresponding to the given node is sifted as a relevant component.

Among all wavelet packet components at a level, only those with more than a given percentage contribution to the total signal energy are viewed as significant components that are needed to be considered for sifting. Ideally, for the purpose of the present study, each signal component, $s^{(i)}(t)$, should represent a vibration mode. However, contamination from other modes is possible. The new sifting/stopping criterion introduced in Chapter 6, guarantees that only those components which have a minimum contamination are selected for identification procedure.

4.3 Methodology: Identification of Instantaneous Modal Frequency and Instantaneous Normalized Mode Shape

Given a set of response measurements $\mathbf{s}(t) = [s_1(t), s_2(t), \dots, s_j(t), \dots, s_{nS}(t)]^T$, where $s_j(t)$ is the j^{th} component of the response vector $\mathbf{s}(t)$ and nS is the number of measurements, we are interested in identifying the instantaneous modal parameters of the system. The assumption of slowly time-varying system is imposed.

4.3.1 Identification by CWT-ridge Method

First, the CWT of the signal $s_j(t)$ is performed. Let us denote the transform coefficients by W_{s_j} . Since the wavelet parameters are chosen such that the harmonics to be well separated

on the CWT coefficient map, the n^{th} ridge corresponds, predominantly, to the n^{th} modal component. Each ridge is analyzed separately and instantaneous modal frequency and normalized instantaneous mode shapes are estimated. The procedure is summarized as follows:

1. Start the analysis with a rough estimation of the frequency range of interest, say, from f_1 (Hz) to f_2 (Hz). Choose the scale range (from a_1 to a_2) according to the following relationships:

$$a_1 = \frac{F_c}{f_2}, \quad a_2 = \frac{F_c}{f_1} \quad (4.15)$$

2. Perform the CWT for the response signal and identify the bands of the higher coefficient value on the coefficient map. To improve the accuracy and reduce the computational effort, a zoom-in analysis can be performed with the scale range corresponding to each band.
3. Identify the ridge $a_{ridge}(t)$ which corresponds to the n^{th} time-varying vibration mode and then, by using the eq. (4.12), calculate the instantaneous frequency $\Phi'(t)$. The function $\omega_n(t) = \Phi'(t)$ represents the n^{th} instantaneous modal frequency of the response signal. It should be noted that the ridge $a_{ridge}(t)$ is the same if the other components of vector $s(t)$ are analyzed, provided the vibration modes are well separated and the system is slowly varying.
4. Calculate the normalized instantaneous mode shape by taking the ratio of modulus of the CWT for signal $s_j(t)$ and signal $s_p(t)$ (which has been choose for normalization) for the scales corresponding to the ridge $a_{ridge}(t)$, as shown in eq. (4.16).

$$X_{j,p}^{(n)}(t) = \frac{|W_{s_j}(a_{ridge}(t), t)|}{|W_{s_p}(a_{ridge}(t), t)|} \quad (4.16)$$

4.3.2 Identification by Wavelet Packet Sifting Technique and Hilbert Transform

When HT is used to find the instantaneous frequency and normalized mode shape from sifted narrow band signals obtained from wavelet packet decomposing, the identification procedure is as follows:

1. Perform wavelet packet decomposition and sift out the dominant vibration modes. Let us

concentrate on the n^{th} modal component, extracted from the response measured at location j.

2. Construct the analytic signal

$$\tilde{s}_j^{(n)}(t) = s_j^{(n)}(t) + HT(s_j^{(n)}(t)) = \tilde{A}_j^{(n)}(t) \exp(i\tilde{\phi}_j^{(n)}(t)) \quad (4.17)$$

3. Calculate the modal instantaneous frequency as the time derivative of the analytic phase angle $\tilde{\phi}_j^{(n)}(t)$, as shown in eq. (4.12).

4. Calculate the NI mode shape as the ratio of the analytic amplitude of the signal $s_j^{(n)}(t)$ and the analytic amplitude of signal $s_p^{(n)}(t)$.

$$X_{j,p}^{(n)}(t) = \frac{\tilde{A}_j^{(n)}(t)}{\tilde{A}_p^{(n)}(t)} \quad (4.18)$$

4.4 Applications: A 3DOF Mass-spring-dashpot System with Time-varying Stiffness

In the following, the identification procedure of instantaneous modal frequencies and NI mode shapes is illustrated for the case of a 3DOF mass-spring-dashpot system with progressive stiffness degradation. The CWT-ridge method is applied to free vibration responses. For applications of WPS technique in conjunction with HT, the reader is referred to Shinde (2005). A study of the sensitivity of the methods to measurement noise and damage severity can be found in the author's previous work (Hera et al, 2004) and in Chapter 8.2 of this dissertation.

4.4.1 Simulation Setup

In order to validate the methodology, a linear three-degree-of-freedom system in Fig. 3.8, is employed. All masses, M_1 , M_2 and M_3 , have the same value of 300 kg and all three springs have an identical initial stiffness of 100,000 N/m. The system-damping matrix is proportional to the stiffness matrix of the healthy system by a factor of 0.0002s. Damage is modeled as a time-varying stiffness. It is supposed that it occurs during an impact test,

simulated by a nonzero velocity at M_3 , after 12 seconds from impact time. During damage, the stiffness K_2 of the spring connecting M_1 and M_2 decreases linearly as shown in Fig. 3.8(b). The simulation was run for 36 seconds, with a time increment (dt) of 0.01 seconds.

4.4.2 Methodology and Results

The wavelet ridge approach applied to the acceleration responses is used in this example. As a first step, the complex Morlet function with $F_c = 5/dt = 500s^{-1}$ and $F_b = dt^2 = 0.0001s^2$ is chosen as the mother wavelet. The CWT is performed on the acceleration response. Other measurements can also be used. A scale range from 10 to 500 which corresponds to a frequency from 10Hz to 1Hz is used in analysis.

Figure 4.1 plots the absolute value of the wavelet coefficients of the acceleration response measured at M_1 . Three bands of high-value coefficients can be identified, which indicates that in this scale range there are three wavelet ridges. The first band corresponds to the scales from 350 to 450, the second band is from 125 to 150 and the last band is from 85 to 115. In order to improve the accuracy of the results and, in the same time, to reduce the computational effort, the CWT will be performed separately, for each of the observed bands, with a smaller scale increment. The computational noise in the absolute value of the CWT coefficients is removed by a low-pass filtering technique applied first in the scale domain and, then, in the time domain. To avoid the edge effect in the wavelet analysis only the CWT coefficients for the time interval from 2.5seconds to 34seconds are considered in identification.

Each identified wavelet ridge corresponds to a vibration mode. The corresponding instantaneous modal frequency, calculated by eq.(4.12), is shown in Fig. 4.2(b). It is observed that the instantaneous modal frequencies are constant for the first 12 seconds – when no damage occurs, then slowly decrease as a result of the stiffness degradation. The observed frequencies are in good agreement with the time varying stiffness history specified in data generation. For verification, the instantaneous frequencies were also calculated by solving the associated dynamic eigenvalue problem. The relative error between the

calculated and identified results for each time instant is less than 1% and, as example, the results for $t=5, 15, 25, 30$ s are presented in Table 4.1.

Time (s)	Instantaneous modal frequency (rad/s)					
	1 st mode		2 nd mode		3 rd mode	
	CWT	Dynamic eig.value problem	CWT	Dynamic eig.value problem	CWT	Dynamic eig.value problem
5	8.12	8.12	22.73	22.77	32.86	32.90
15	8.07	8.08	22.71	22.74	32.65	32.68
25	7.95	7.96	22.60	22.62	31.90	31.93
30	7.87	7.88	22.53	22.55	31.53	31.56

Table 4.1. Comparison of the modal frequencies obtained by CWT and solving the dynamic eigenvalue problem at specified time instants.

The NI mode shape vectors can also be found from the identified wavelet ridges. The mode shape component at M1 is chosen for normalization. The results are plotted in Fig. 4.3. The relative error between the results from the wavelet approach and the dynamic eigen-solution is smaller than 1%.

Note that a positive or negative sign, can be associated to the NI mode shape, using the phase shift between the coefficients on the ridge corresponding to the analyzed and normalization signals. If the phase shift is in the range $[-\pi/2, \pi/2]$ the sign is positive, otherwise the sign is negative.

4.5 Summary

In this chapter we proposed two techniques, namely CWT-ridge method and WP sifting in conjunction with Hilbert Transform, for identification of instantaneous modal frequency and normalized mode shape from free vibration response data.

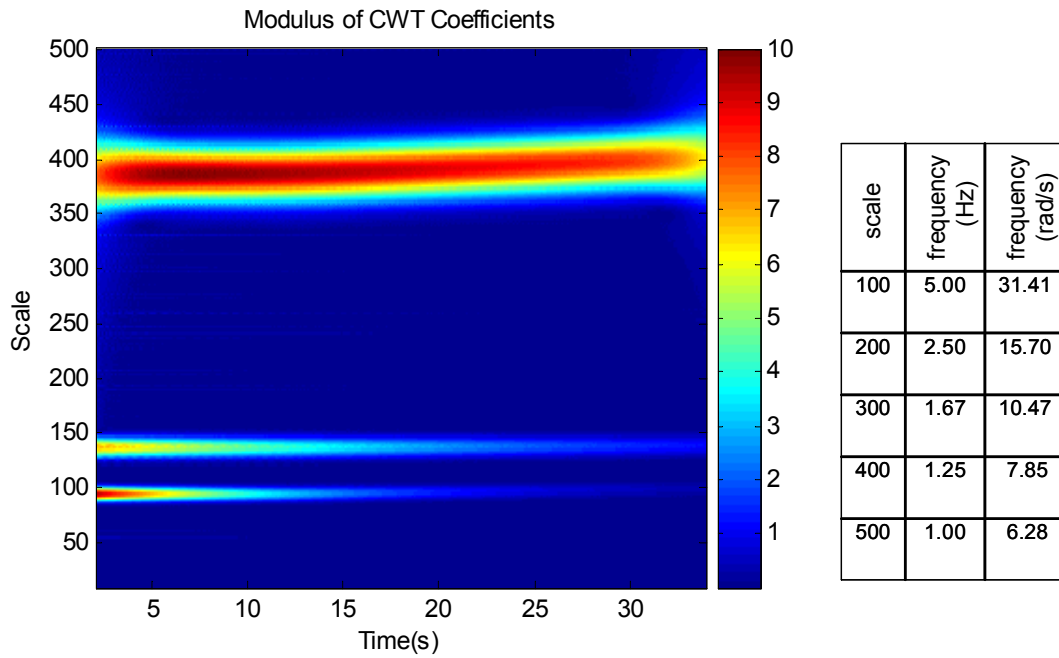


Figure 4.1. CWT spectrum of the acceleration response of M3

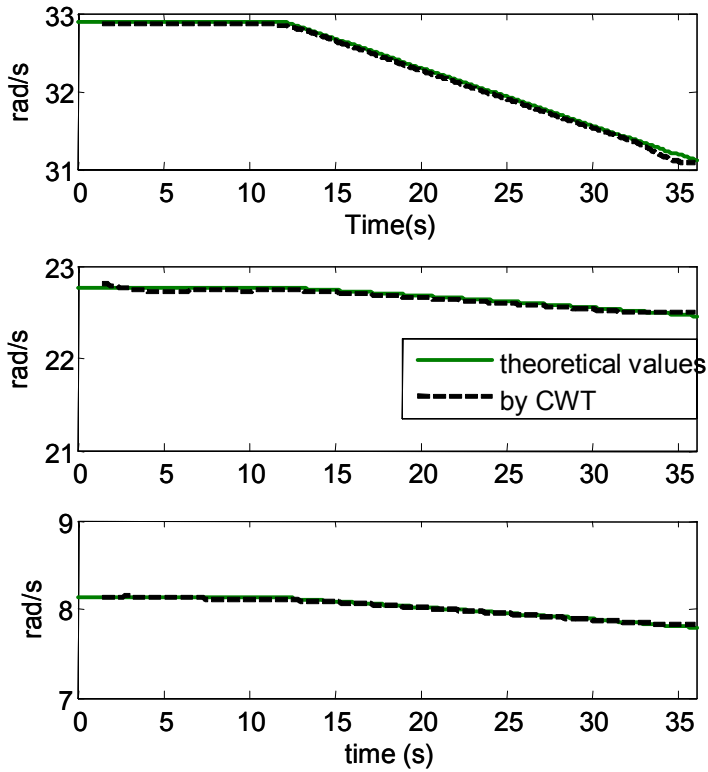


Figure 4.2. Instantaneous frequencies estimated by the CWT-ridge method (black) and the theoretical values (green)

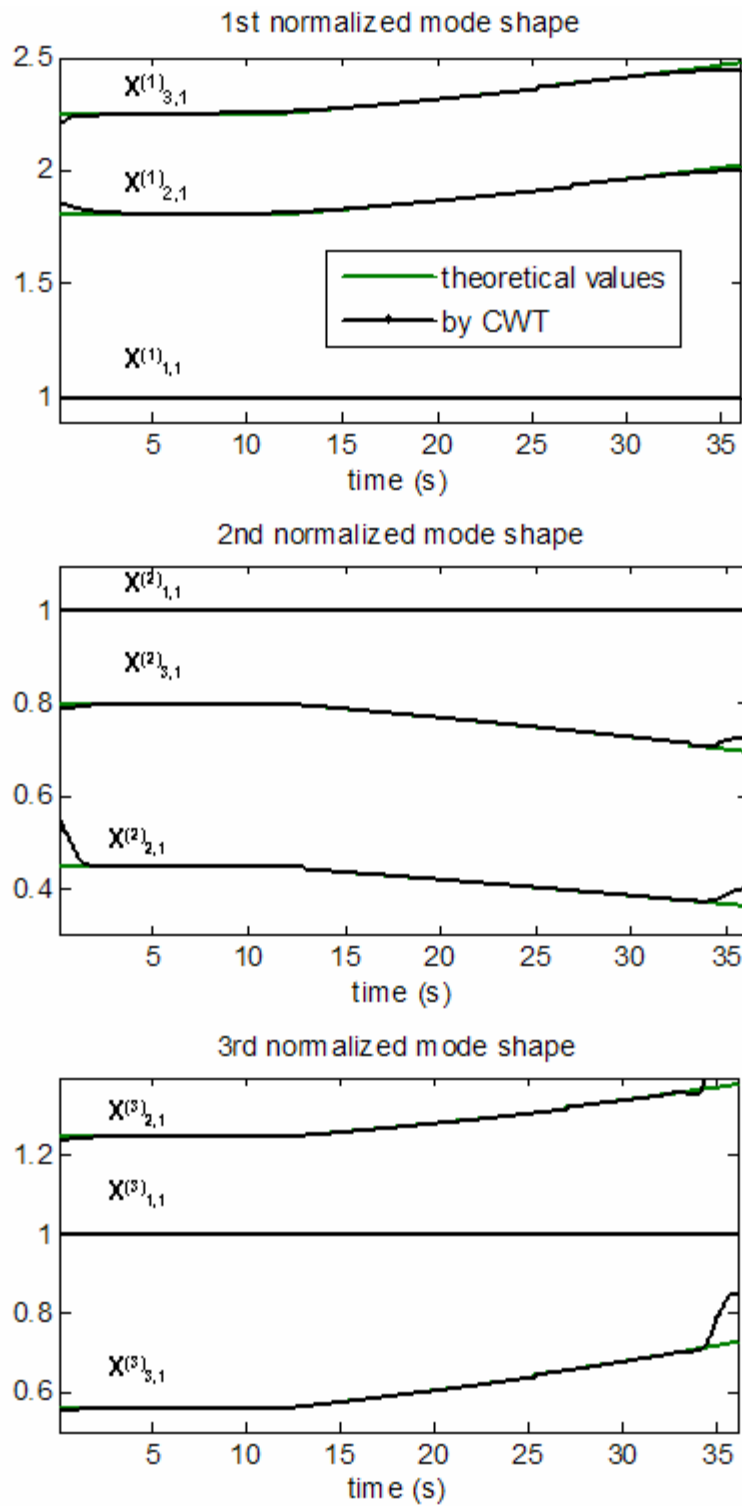


Figure 4.3. Normalized instantaneous modal vectors identified by the CWT-ridge method (black) and the theoretical values (green)

First, it is shown that the free vibration modal responses of a slowly time-varying system are asymptotic signals. Then, it is observed that the existing methods of identification of instantaneous frequency of a signal, such as CWT-ridge method and Hilbert transform, are based on the assumption that the analyzed signals are asymptotic. This assumption makes the CWT-ridge method and the Hilbert transform-based techniques the perfect candidates for the identification of instantaneous modal parameters. Both techniques first separate the vibration modes and then identify the instantaneous modal frequency and instantaneous normalized mode shape. The CWT-ridge method is illustrated for a 3DOF system with progressive stiffness degradation. The identified results are very close to the theoretical ones obtained by means of the dynamic eigen-value problem. For an illustration of the WP sifting technique in conjunction with Kalman filter the reader is referred to (Shinde and Hou, 2005; Shinde, 2005), where a similar numerical example was used. The sensitivity of the methods to damage severity and the robustness issues in the case of noisy data are presented in the author's previous work (Hera et. al., 2004) and in Chapter 8.2.

Chapter 5

IDENTIFICATION OF INSTANTANEOUS NORMALIZED MODE SHAPE FROM FORCED VIBRATION DATA AND APPLICATIONS TO SHM

5.1 Introduction

Using a wavelet based approach, instantaneous modal parameters can be extracted and their evolution may be monitored to assess the health condition of a structure. The approach has been successfully applied to the case of impulse response or free-vibration data (Chapter 4). However, the respective approach would be less accurate for the forced vibration data due to the interference between the system frequency characteristics and the dominant frequency content of the excitation. This section presents a health monitoring technique for structures subjected to stationary and non-stationary excitation using instantaneous mode shape information. The normalized instantaneous mode shape is estimated from the forced vibration response by using a wavelet packet sifting technique. In order to validate the results, a confidence index, calculated using the instantaneous frequency of the sifted signals, is defined. It is found that the identified normalized instantaneous mode shapes in conjunction with the corresponding confidence indices can be effectively used to monitor damage development in the structure. The effectiveness of the proposed approach is illustrated for an example from civil engineering. It is assumed that the structure is lightly damped and can be treated as a linear slow time-varying system in the case of progressive damage or linear before and after damage in the case of sudden damage. A three-degree-of-

freedom building structure subjected to a ground motion signal is used to simulate the response at different floors. Two damage scenarios, sudden stiffness loss and progressive stiffness degradation, and different base excitations including three real earthquake signals, a random signal and few harmonic signals are considered. Consistently good results were obtained in all cases. Issues related to robustness of the method in the presence of measurement noise and sensitivity to damage severity are discussed.

5.2 Methodology

5.2.1 Instantaneous Modal Parameters in Forced Vibration Responses

The concept of instantaneous modal parameters has been explained in Chapter 3. For completeness, the relevant information for this section is summarized here. It has been shown that if the following assumptions hold:

1. The system is linear and slowly time varying as defined in eq. (3.10), and a linear time invariant is considered a particular case. Also, the case of a piecewise linear system is included here.
2. The excitation does not have components of significant energy, whose frequency is in the vicinity of or less than $d(\varphi_{us,j}^{(n)}(t))/dt$ (where $s = x, v, a$).

the response of a structure with damage can be written as a weighted sum of modal responses, as expressed in eq. (5.1).

$$\begin{aligned}
 x_j &= \sum_{n=1}^N x_j^{(n)} = \sum_{n=1}^N A_{x,j}^{(n)}(t) \cos(\phi_{x,j}^{(n)}) \\
 v_j &= \sum_{n=1}^N v_j^{(n)} = \sum_{n=1}^N A_{v,j}^{(n)}(t) \cos(\phi_{v,j}^{(n)}) \\
 a_j &= \sum_{n=1}^N a_j^{(n)} = \sum_{n=1}^N A_{a,j}^{(n)}(t) \cos(\phi_{a,j}^{(n)})
 \end{aligned} \tag{5.1a}$$

$$\begin{aligned}
 \phi_{x,j}^{(n)}(t) &= \varphi_{ux,j}^{(n)}(t) + \arg(q_{2n-1}(t)) & \phi_{ux,j}^{(n)}(t) &= \arg(u_j^{(2n-1)}(t)) \\
 \phi_{v,j}^{(n)}(t) &= \varphi_{uv,j}^{(n)}(t) + \arg(q_{2n-1}(t)) & \phi_{uv,j}^{(n)}(t) &= \arg(u_{2j}^{(2n-1)}(t)) \\
 \phi_{a,j}^{(n)}(t) &= \varphi_{ua,j}^{(n)}(t) + \arg(\dot{q}_{2n-1}(t)) & \phi_{ua,j}^{(n)}(t) &= \arg(\lambda_{2n-1} u_{2j}^{(2n-1)} + \dot{u}_{2j}^{(2n-1)})
 \end{aligned} \tag{5.1b}$$

Moreover, the modal amplitudes are proportional to the mode shape components, as can be seen, in eq. (5. 2), and $\{d(\varphi_{s,j}^{(n)}(t))/dt, \text{ where } s = x, v, a\}$, practically, does not depend on measurement location/DOF, here specified by “ j ”.

$$\begin{aligned} A_{x,j}^{(n)}(t) &= 2X_j^{(n)}(t)|q_{2n-1}(t)| \\ A_{v,j}^{(n)}(t) &\cong 2X_j^{(n)}|\lambda_{2n-1}||q_{2n-1}(t)| \\ A_{a,j}^{(n)}(t) &\cong 2X_j^{(n)}|\lambda_{2n-1}||\dot{q}_{2n-1}(t)| \end{aligned} \quad (5. 2)$$

The notations in the above equations are as follows: (n) represents the vibration mode, x_j, v_j, a_j denote the displacement, velocity and acceleration, respectively, measured at “ j ” measurement position (DOF), λ_{2n-1} represents the dynamic eigenvalue $(2n-1)$ and $u_j^{(2n-1)}$ is the j^{th} component of the dynamic eigenvalue of the elementary mode $(2n-1)$, $q_{2n-1}(t)$ is the elementary modal coordinate $(2n-1)$. More details and other notations can be found in Chapter 3.

The instantaneous modal frequency and instantaneous mode shape have been defined based on the dynamic eigenvalue problem and the free vibration response, as shown in eqs. (5. 3) and (5. 4).

$$\omega_n(t) = \omega_{\lambda,n}(t) = \text{Im}(\lambda_{2n-1}(t)) \quad (5. 3)$$

$$\mathbf{X}^{(n)}(t) = \left[|u_1^{(2n-1)}(t)|, |u_2^{(2n-1)}(t)|, \dots, |u_N^{(2n-1)}(t)| \right]^T \quad (5. 4)$$

The normalized instantaneous (NI) mode shape was defined as the instantaneous mode shape vector normalized by one of its components which is different of zero, i.e. the p^{th} component in eq. (5.6). A new notation is introduced, $X_{j,p}^{(n)}$, which represents the j^{th} component of the n^{th} mode shape vector normalized by the p^{th} component.

$$\begin{aligned} \mathbf{X}_{|p}^{(n)}(t) &= \left[\frac{\mathbf{X}^{(n)}}{X_p^{(n)}} \right] = \left[\frac{X_1^{(n)}}{X_p^{(n)}} \quad \frac{X_2^{(n)}}{X_p^{(n)}} \quad \dots \quad \frac{X_p^{(n)}}{X_p^{(n)}} \quad \dots \quad \frac{X_N^{(n)}}{X_p^{(n)}} \right]^T = \\ &= \left[X_{1,p}^{(n)} \quad X_{2,p}^{(n)} \quad \dots \quad X_{p-1,p}^{(n)} \quad 1 \quad X_{p+1,p}^{(n)} \quad \dots \quad X_{N,p}^{(n)} \right]^T \end{aligned} \quad (5. 5)$$

5.2.2 Identification of the Normalized Instantaneous Mode Shape

In order to identify the instantaneous modal parameters, the modal response $\mathbf{x}^{(n)}(t)$ needs to be separated from the vibration data. If the above assumptions are satisfied the normalized instantaneous (NI) mode shape can be calculated using concepts specific of the analytic signal. The analytic signal $\tilde{\mathbf{x}}^{(n)}(t)$ is a complex signal having the original signal $\mathbf{x}^{(n)}(t)$ as its real part and Hilbert transform of the original signal as its imaginary part. The normalized instantaneous mode-shapes can be calculated as the ratio of the analytic amplitude of the modal response $x_j^{(n)}(t)$ and the analytic amplitude of the normalization signal $x_p^{(n)}(t)$:

$$X_{j|p}^{(n)}(t) = \frac{\tilde{A}_j^{(n)}(t)}{\tilde{A}_p^{(n)}(t)} \quad (5.6)$$

where $\tilde{A}_j^{(n)}(t)$ and $\tilde{A}_p^{(n)}(t)$ refer to the analytical amplitudes of the signals $x_j^{(n)}(t)$ and $x_p^{(n)}(t)$, respectively.

5.2.3 Practical Issues in Identification of Instantaneous Modal Parameters

There are two practical issues in calculating the instantaneous mode shape, the first one is related to the separation of the modal responses, while the second issue is related to the assumptions we made in the Subsection 5.1.

Modal Separation

As previously mentioned, in order to identify the mode shape, it is necessary to sift out, from the measured response data, the n^{th} vibration mode of interest, $\mathbf{x}^{(n)}(t)$. This can be accurately done in the case of a free vibration response, where each modal response can be described as a signal with mono-frequency content and slow time varying amplitude. Thus, the modal components can be sifted out and the instantaneous natural frequency and normalized mode shape can be accurately identified and use for SHM (Chapter 3).

When a structure is subjected to other excitations, the separation of each modal component in the vibration response is not as evident as in the case of the free vibration response. Moreover, if some damage happened in the system during this excitation period,

due to the time varying structural properties, the classical Fourier transform based deconvolution technique cannot be applied to deconvolve the impulse response from the vibration response. This fact rules out the possibility of obtaining impulse response of a structure to accurately calculate the instantaneous modal parameters. However, in the case of a structure subjected to a broadband excitation, the energy of the vibration response is concentrated in frequency bands corresponding to the instantaneous natural frequencies of the structure. This property is further used to sift out the signals of interest by a wavelet packet sifting (WPS) technique explained in details in (Shinde and Hou, 2005).

The methodology can be illustrated in a better way by representing the signal energy in time-scale (frequency) domain. The signal energy is graphically shown with help of the continuous wavelet transform (CWT) maps. Here, complex Morlet wavelet with center frequency of 500 Hz and bandwidth parameter of $0.0001s^2$ has been used as mother wavelet.

Without loss of generalization, the methodology is explained for a linear 3DOF system sketched in Fig. 5.1, subjected to a nonstationary base excitation, which is the El-Centro earthquake signal. The structural response is simulated for the case of no stiffness loss. The CWT map of the excitation is presented in Fig. 5.2, whereas Fig. 5.3 shows the CWT map of the acceleration response (with respect to ground) at location M1.

Three significant energy bands can be identified in the areas corresponding to the instantaneous natural frequencies of the structure (Fig. 5.3). Therefore, from point of view of the energy distribution in the time-frequency domain, the response at location/DOF "j" can be expressed as:

$$x_j(t) = s_j^{(1)}(t) + s_j^{(2)}(t) + s_j^{(3)}(t) + r_j(t) \quad (5.7)$$

where $s_j^{(n)}(t)$ is the signal component of the response measured at j DOF, whose energy is localized in a band corresponding to the n^{th} natural frequency, i.e. from $f_a^{(n)}$ to $f_b^{(n)}$, and $r_j(t)$ is a residual signal. The components $s_j^{(n)}(t)$ will be sifted out from the response by using a wavelet packet sifting process.

Combining eq. (5.7) with the modal decomposition of the response in eq. (5.1a), a decomposition of the response on frequency bands is obtained, as shown in eq. (5.8).

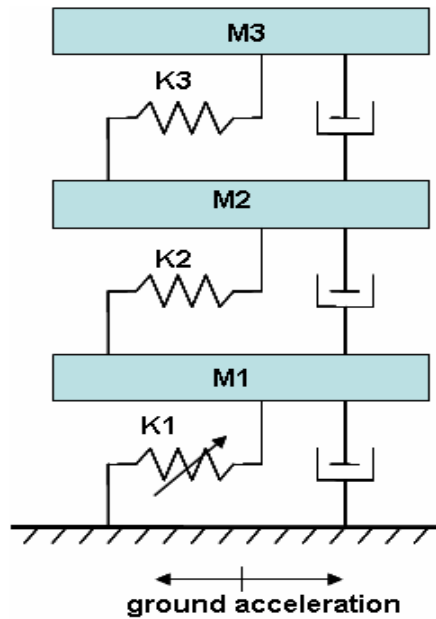


Figure 5.1. A sketch of the 3DOF mass-spring-damper system used in simulation study

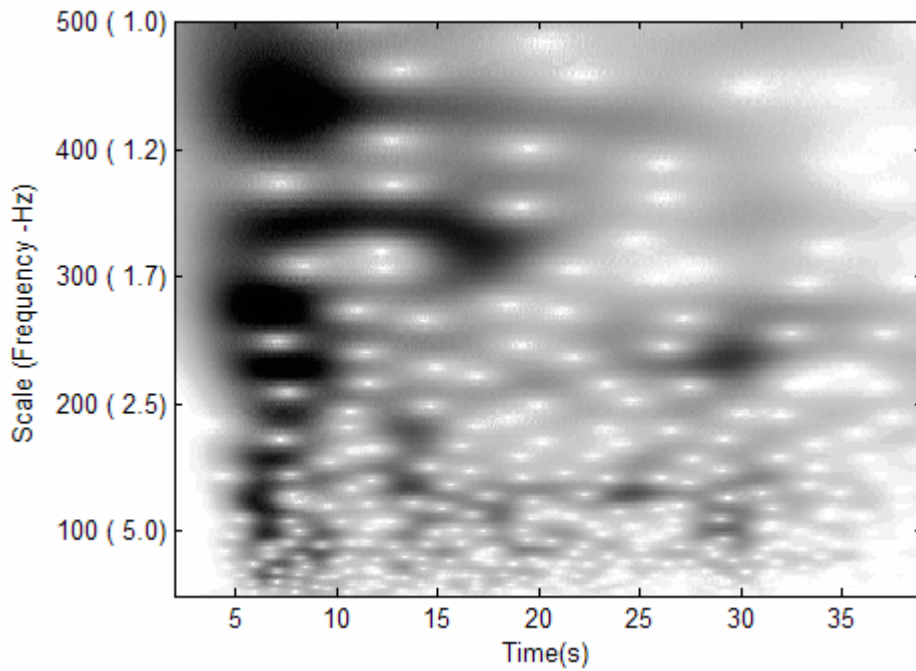


Figure 5.2. CWT map of the El Centro earthquake signal. NS component recorded at Imperial Valley Irrigation District substation in El Centro, California, during the Imperial Valley, California earthquake of May, 18, 1940

$$x_j(t) = \sum_{n=1}^3 x_j^{(n)}(t) = \sum_{n=1}^3 \left(\eta_j^{(n),1}(t) + \eta_j^{(n),2}(t) + \eta_j^{(n),3}(t) + \rho_j^{(n)}(t) \right) \quad (5.8)$$

where $\eta_j^{(n),k}(t)$ is that part of the modal response $x_j^{(n)}(t)$, whose energy lies in the frequency range from $f_a^{(k)}$ to $f_b^{(k)}$, where $k = 1, 2, 3$, and can be expressed as a product between $X_j^{(n)}(t)$, which is slow varying, and a fast varying term whose frequency is in the range from $f_a^{(k)}$ to $f_b^{(k)}$ and does not depend on position “ j ”, i.e. $\eta_j^{(n),k}(t) = X_j^{(n)}(t)\nu^{(n),k}(t)$. A significant part of the energy is concentrated in the component $\eta_n^{(n)}(t)$, and this is illustrated in Fig. 5.4 which shows the CWT map of the simulated first modal response, $x_1^{(1)}(t)$. Combining eqs. (5.7) and (5.8) it results that the sifted component $s_j^{(n)}(t)$ can be written as follows:

$$s_j^{(n)}(t) = \eta_j^{(1),n}(t) + \eta_j^{(2),n}(t) + \eta_j^{(3),n}(t) \quad (5.9)$$

Therefore, the sifted component $s_j^{(n)}(t)$ may not necessarily be the desired pure n^{th} modal response, but is a combination of the most significant part of n^{th} modal response and the less significant components corresponding to the modal responses due to other modes. This leads to small errors in the results for the n^{th} instantaneous mode shape vector. A confidence index, defined in the next section, can be used as a measure of these errors introduced by the interference of the modal response of interest with other modal responses in the sifted components. On the same token, the confidence index covers also the case when the vibration modes cannot be separated well due to the limited time-frequency resolution of the wavelet analysis.

Assumption of slowly time-varying system and frequency content of excitation

Another issue is related to the assumptions that the system is slow-time varying and the excitation does not have components of significant energy whose frequencies are in the vicinity of or less than $d(\varphi_{us,j}^{(n)}(t))/dt$ (where $s = x, v, a$). These two assumptions ensure that the modal responses at different DOFs have the same instantaneous frequency and the modal response amplitudes are proportional to the corresponding mode shape components. If these assumptions are not satisfied, the instantaneous frequency of the sifted modal components

will not be the same for all DOFs and errors will be introduced in the calculated mode shape. The deviation of the confidence index from the unity value includes also the departure from these assumptions.

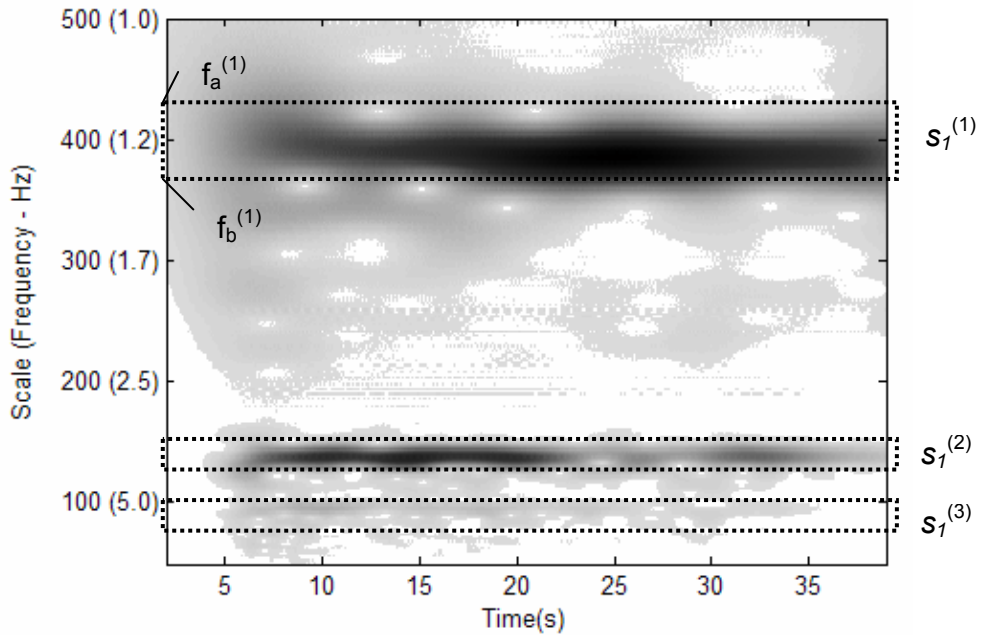


Figure 5.3. CWT map of the acceleration response measured at M1.

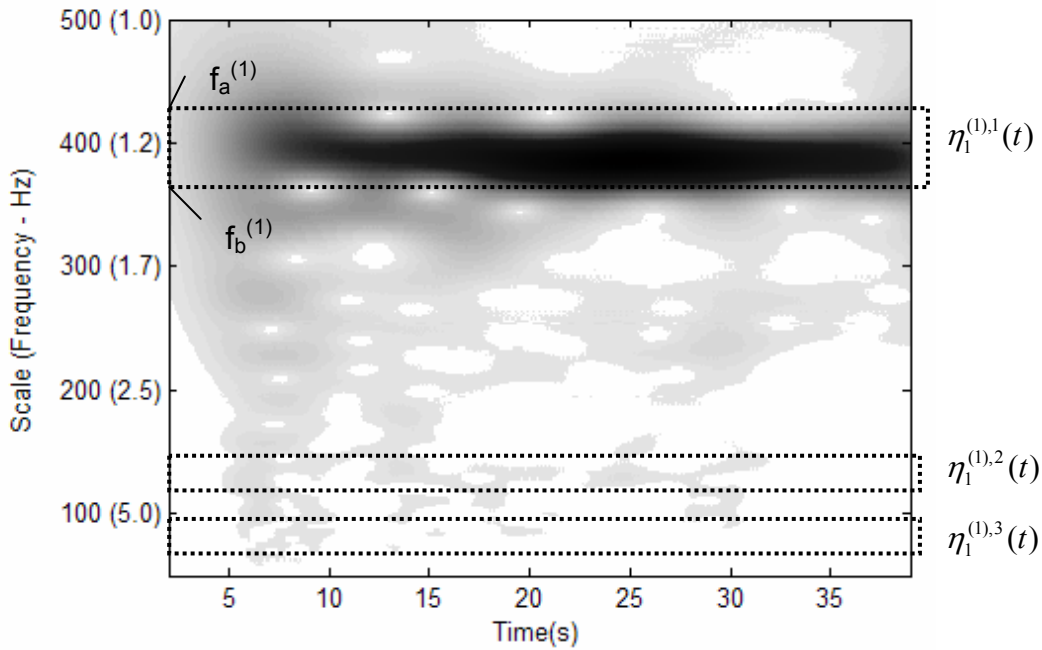


Figure 5.4. CWT map of the simulated first modal response, $x_1^{(1)}(t)$

5.2.4 Confidence Index (CI)

If the modal separation is perfect, i.e. $s_j^{(n)}(t) = X_j^{(n)}(t)v^{(n),1}(t)$, and the assumptions in Section 5.2.1 hold, the analytic signal corresponding to the sifted component from the vibration response measured at DOF j , $s_j^{(n)}(t)$, can be expressed as shown in eq. (5.10). It can be observed that there is an amplitude part which depends on measurement location and a complex exponential part independent of location.

$$\tilde{s}_j^{(n)}(t) = s_j^{(n)}(t) + iHT(s_j^{(n)}(t)) = X_j^{(n)}(t)A_v^{(n)}(t)\exp(i\phi_v^{(n)}(t)) \quad (5.10)$$

The instantaneous frequency of $s_j^{(n)}(t)$ is defined as:

$$\omega_j^{(n)}(t) = \frac{d(\phi_v^{(n)}(t))}{dt} \quad (5.11)$$

In practical applications there are interferences with other modes and the assumptions in Section 5.1 are not completely satisfied. All of these will be reflected in the instantaneous frequencies of the signal $s_j^{(n)}(t)$, which will lose its independency of location/DOF. Based on this observation we define a confidence index as the ratio of the instantaneous frequency of the analytic signals $\tilde{s}_j^{(n)}(t)$ and $\tilde{s}_p^{(n)}(t)$, as expressed in eq. (5.12)

$$CI_{j,p}^{(n)} = \frac{\omega_j^{(n)}(t)}{\omega_p^{(n)}(t)} \quad (5.12)$$

When there is an insignificant mode mixture and assumptions in Section 5.1 are practically satisfied, the frequency content of the two signals $\tilde{s}_j^{(n)}(t)$ and $\tilde{s}_p^{(n)}(t)$ remains the same and the ratio of amplitudes gives the correct instantaneous mode shape component, i.e.

$$X_{j,p}^{(n)} = \frac{\tilde{A}_j^{(n)}(t)}{\tilde{A}_p^{(n)}(t)} \quad (5.13)$$

In this case, the confidence index shows unit value. For a practical implementation, a confidence index which validates the corresponding instantaneous mode shape component needs to be in a range close to 1, generally 0.98 to 1.02, with an ideal value equal to one. The range [0.98 : 1.02] has been chosen based on a sensitivity study, using different types of

excitations. The deviation of the CI may also be caused by measurement noise, insignificant participation of the mode of interest, and nonlinear behavior of the structure. For those time intervals when the confidence index is beyond this range, the identified normalized mode shape component may show some deviation from exact values and may not be reliable for damage monitoring.

5.3 Applications: A 3DOF Mass-spring-dashpot System with Time-varying Stiffness

5.3.1 Simulation Set-up

In the present study, simulated vibration response of a three degree-of-freedom spring-mass-damper chain model shown in Fig. 5.1 is analyzed. The system can be considered as a scaled model of a three story building. All masses have the same value of 300 Kg, initial stiffness of each spring is 100 KN/m and the system damping is assumed to be a Rayleigh damping, the damping matrix being proportional to the stiffness matrix with a factor of 0.0005. The natural frequencies of the healthy structure are 1.29, 3.62 and 5.23 Hz. In order to evaluate the effectiveness of the proposed method, the structure is base excited with 5 different excitation signals, namely:

1. Kobe earthquake signal: NS component recorded at Kobe city, Japan during the Kobe earthquake of Jan 17, 1995.
2. Hachinohe earthquake signal: NS component recorded at Hachinohe City during the Takochi-oki earthquake of May, 16, 1968
3. El-Centro earthquake signal: NS component recorded at Imperial Valley Irrigation District substation in El Centro, California, during the Imperial Valley, California earthquake of May, 18, 1940
4. Random excitation signal modeled as a Gaussian white noise discrete process with zero mean and RMS value of 0.5 m/s^2
5. Harmonic signal of different frequencies and intensity of 5 m/s^2 .

The time history and the Fourier spectrum of the excitation signals 1-4, are shown in Fig. 5.5. The sampling frequency was 100 Hz and only the first 40 seconds of the records are considered in the present study in all cases except the case of Hachinohe earthquake, where the signal record has 36 s.

Damage in the structure is simulated by reducing stiffness of one of the springs by a certain amount. Two damage scenarios, namely sudden damage and gradual stiffness degradation, are considered here. A sudden damage is simulated by reducing stiffness of spring K1 at $t=12s$, whereas the gradual stiffness degradation is simulated by a linear stiffness reduction of spring K1 from $t = 12$ to 36s. A damage level of 20% is considered here. This relatively higher damage level is used for an illustration purpose and a damage sensitivity study of the method is also performed in the later part.

The performance of the proposed approach in presence of measurement noise is evaluated for one of the case of Hachinohe earthquake by adding noise to all vibration acceleration responses. . The measurement noise is simulated using a time step of 0.01s as a discrete Gaussian white noise process with zero mean and RMS value of 5% of the RMS value of third floor acceleration signal over a time interval of 36s . The 5% noise level is justified with the fact that in the case of an earthquake excitation, as the ground acceleration is very high and the measuring instrumentation is very sturdy, the measurement noise is of a fairly low level in comparison to the measured signal.

Discrete Meyer wavelet has been chosen as mother wavelet. The confidence index is used to improve the sifting results. After finding the node which satisfies the energy-entropy criterion, one more level of decomposition is performed and from these three nodes we select for the sifting process the node characterized by the best confidence index. Only the significant signal components, defined as those components whose energy contribution to the total signal energy is bigger than 5%, are sifted out.

In this study, the effectiveness of the proposed method, effect of measurement noise, and effect of damage severity is evaluated for a sudden damage scenario and discussed in detail in Sections 5.3.2, 5.3.3 and 5.3.4. The applicability of the approach for monitoring progressive damage is illustrated in Section 5.3.5.

5.3.2 Normalized Instantaneous (NI) Mode Shape and Confidence Index (CI)

In the case of a multi-story building, modal parameters calculated based on inter-story acceleration signals are more sensitive to damage as compared to those based on relative acceleration with respect to ground. Therefore in the present study the normalized instantaneous mode shape information and the corresponding confidence index is extracted from the inter-story acceleration data. The relationship between the mode shape components calculated in this way and those calculated using the relative acceleration with respect to the ground is as follows:

$$X_{|1}^{(n)} = \left[\frac{X_1^{(n)}}{X_1^{(n)}} \quad \frac{X_2^{(n)} - X_1^{(n)}}{X_1^{(n)}} \quad \frac{X_3^{(n)} - X_2^{(n)}}{X_1^{(n)}} \right]^T = [1 \quad X_{21,1}^{(n)} \quad X_{32,1}^{(n)}]^T \quad (5.14)$$

where $X_{jp,1}^{(n)}$ is the j^{th} component extracted from the relative acceleration between the j^{th} and the p^{th} floors, and normalized by the first component of the mode shape vector $X_1^{(n)}$. The NI mode shape components along with corresponding confidence indices are used to monitor the health condition of the structure.

Fig. 5.6 shows the identified NI mode shape components for the first vibration mode and the corresponding confidence index, when the structure was excited by Kobe earthquake signal. The theoretical values obtained by solving the system eigen-value problem at each time step are also plotted as a dotted line for comparison. The NI mode shape value is changed in the region of $t = 12s$ indicating damage in structure. The results for NI mode shape components are in quite good agreement with the theoretical results along the whole time interval except in certain regions where the confidence index is not in a validation range of 0.98 and 1.02.

The NI mode shape components for the second vibration mode and the corresponding confidence index plots are shown in Fig. 5.7. The values of the mode shape components are changed around $t=12s$. The results for mode shape fluctuate around the theoretical results when the confidence index is out of the validation range. The confidence index is very bad in initial region due to the interferences of the first mode components in the frequency range of interest.

The NI mode shape results for the third vibration mode are not shown as the contribution of this mode to the total signal is very low and the confidence index is out of validation range.

Figure 5.8 shows results obtained for NI mode shape components of the first vibration mode when the structure was excited by the Hachinohe earthquake signal. The NI mode shape shows change in the region of $t=12$ s and the results show deviation from the exact values when the confidence index deviates from the unity.

The results of the first NI mode shape when the structure was excited by the El-Centro earthquake signal are shown in Fig. 5.9. The change in value of the NI mode shape at $t=12$ sec indicates damage in structure. The confidence index is more fluctuating as compared to the respective results for Hachinohe earthquake signal. These fluctuations are also reflected in NI mode shape results.

In order to evaluate the effectiveness of the proposed approach for a random excitation, the structure was excited by a signal modeled as a Gaussian white noise process with zero mean and RMS value of 0.5 m/s^2 . NI mode shape varies exactly as theoretical values as shown in Fig. 5.10 and shows change in values when damage was introduced in the simulation of the response.

Comments

The results of NI mode shape for the first vibration mode have shown good agreement with the theoretical values for all of the four excitation signals as shown in Figs. 5.6 – 5.9. A permanent change in NI mode shape corresponding to the first mode clearly indicates stiffness loss of the structural member. One of the common observations in all these figures is that at the points where the confidence index values deviates from the ideal value of 1, the deviation in the NI mode shape value at the corresponding points can be observed. Moreover the deviation of the NI mode shape results is proportional to the deviation of the confidence index value at corresponding point. This is evident because the deviation of confidence index from unit value indicates that either the mode is not excited at that point or there is a contamination of other mode components. The larger the contamination, higher the

deviation in mode shape value. The confidence index value thus indicates the reliability of the results obtained.

It is also observed that the results obtained in case of Kobe earthquake excitation (Fig. 5.6) are the best among the results, whereas the ones obtained with El-Centro earthquake are more fluctuating when compared with respective theoretical values.

In case of Kobe earthquake, the excitation signal strength after $t = 12$ s is very low which results in insignificant contribution of the forced vibration response to the total acceleration response. Since the signal is a nearly free vibration response, the modal components lie only in the vicinity of the instantaneous natural frequencies of the system and the mode mixture in the sifted signal is insignificant. Because of very low possibility of mode interference, the NI mode shape values are accurately identified except at the point of damage where the values are slightly different from theoretical results. In contrast to the Kobe earthquake, in the case of the El-Centro signal, relatively higher contribution of forced vibration response increases the mode mixture, which in turn, affects the mode shape results. This observation is also supported by the confidence index values. Even if there are some fluctuations in NI mode shape results, these fluctuations are smaller and can be clearly distinguished from the permanent change of NI mode shape value due to structural damage.

In the case of Kobe earthquake, the excitation signal intensity after $t = 12$ sec is very low which results in insignificant contribution of the forced vibration response to the total acceleration response, or equivalently, the signal becomes a nearly free vibration response and, in turn, the mode interference due to the presence of excitation is greatly reduced. As a result, the NI mode shape values can be more accurately identified except at the point of damage where the values are slightly different from theoretical results. This observation is also supported by the confidence index values.

In contrast to the Kobe earthquake, the El-Centro earthquake signal is of relatively high magnitude over the whole time interval. The mode interference resulted from the strong presence of the excitation over the whole time interval would reduce the accuracy of the presented approach, as observed. This observation is also supported by the confidence index values.

It can be noticed that the change in the first NI mode shape due to damage in case of Hachinohe earthquake (Fig. 5.8) is smoother as compared to the corresponding results obtained for remaining excitation signals. This rate of NI mode shape value depends on the level of decomposition used in the WPS technique (Shinde and Hou, 2004).

5.3.3 Effect of Measurement Noise

The simulation data used in the study so far didn't consider measurement noise. In order to evaluate the robustness of this method in presence of a measurement noise, a '5%' random noise was added to the vibration response obtained for the structure excited by the Hachinohe earthquake signal. The results in Fig. 5.11 show that the damage can still be detected and the methodology is robust in presence of a measurement noise.

If the results are compared with corresponding results in the absence of noise (Fig. 5.8), it can be observed that the deviation of the NI mode shape results and corresponding confidence indices from the exact values in region of $t=25\text{sec}$ is further amplified by inclusion of noise. The significant large deviation of the confidence index indicates that the NI mode shape results obtained in this region are not reliable. The noise level is specified as 5% RMS value of the acceleration response of the third floor for the total time interval of 0-40 seconds. However, in the vicinity of $t=25\text{s}$ the amplitude of the signal is locally low, which leads to much severer noise contamination locally, as compared to the overall level of "5%". It has been checked for the simulation data that in the time interval of 23s – 28s, the RMS of the added noise represents approximately 25% of the RMS of the acceleration response signals in the same time interval.

5.3.4 Effect of Damage Severity

The damage level simulated in the study so far was 20% and was employed to illustrate the concept of this methodology. In a real life case, damage in structural member may not be so large. The sensitivity of this method to damage level is analyzed by comparing the NI mode shape results for first mode, in case of three different stiffness loss values i.e. 5%, 10% and 20%. The results are shown in Fig. 5.12. It can be observed that with the increase in damage

severity, the change in NI mode shape becomes more recognizable. The change in the NI mode shape for damage level of 5% is relatively smaller and in order to detect this much small damage, a very good confidence index is necessary to validate the results.

5.3.5 Monitoring Gradually Developed Damage

There are cases when damage evolves gradually during a seismic event. In order to study the effectiveness of the method in this situation, a gradual stiffness degradation case with Hachinohe earthquake signal as a base excitation is considered. Fig. 5.13 shows results obtained for NI mode shape and the corresponding confidence index. The NI mode shape components shows a gradual change in their values for the time interval when damage was introduced in the simulation. For a comparison purpose, the theoretical values are shown by dotted line on the same plots. Good agreement between the results is observed. The confidence index is in the validation range for the whole time interval except the end regions, where due to the end effect the results are unreliable.

5.3.6 Effect of Excitation Frequency

Excitation signals 1-4 can be described, from frequency content point of view, as broad-band signals. In the following, we will focused on identification of NI mode-shape when the system is subjected to a harmonic signal with constant frequency, which is considered an extreme case of a narrow band signal. In order to isolate the effect of a harmonic excitation on identification results, we change the simulation setup by analyzing, first, the healthy (time invariant) system. Also, the mode shape is defined using the acceleration responses in respect to the ground as shown in eq. (5.15), and not the inter-story accelerations, as previously used.

$$X_{||}^{(n)} = \begin{bmatrix} \frac{X_1^{(n)}}{X_1^{(n)}} & \frac{X_2^{(n)}}{X_1^{(n)}} & \frac{X_3^{(n)}}{X_1^{(n)}} \end{bmatrix}^T = [1 \quad X_{2,1}^{(n)} \quad X_{3,1}^{(n)}]^T, n = 1,2,3 \quad (5.15)$$

In this discussion, we will consider only the first vibration mode; however, the conclusions can be extended to for the other vibration modes. Figure 5.14, shows the identified mode shape components and confidence indices for different force excitations.

A brief description of the plots is given in the following. Each figure, identified by its title, contains the results obtained from the response of the system excited by a sinusoidal excitation of constant frequency of value written in the figure title. The upper window shows the second (green color) and the third (cyan color) components of the identified NI mode shape. Due to the normalization procedure the first component of the NI mode shape is unity. The exact values of the mode shape components are plotted on the same window, by a blue dot line. The confidence indices are plotted in the lower window, by the same color as the corresponding IN mode shape components, i.e. green and magenta. The validation range (0.98-1.02) is marked by black dot lines.

Good results are obtained if the excitation frequency is not very close to the natural frequency of the vibration mode of interest (here, if excitation frequency is bigger than 1.8 Hz and smaller than 1.1 Hz.). If the excitation is close to the natural frequency, due to the limited time-frequency resolution of wavelet analysis, the forced and free vibration modal responses cannot be separated completely. In this case the mode shape components and confidence index show big oscillations (as can be observed in Fig. 5.14 (d,f)). However, for an excitation of 1.30 Hz, which is about the same as the natural frequency of the first vibration mode, that is 1.29 Hz, the results are in agreement with the theoretical values. The explanation is based on the fact the first vibration mode is exceedingly excited, and the forced response due to other vibration modes is insignificant. If the excitation frequency is not known in advance, the results can be misleading, since the forced component of the response can be interpreted as another vibration mode, which may appear due to damage in the structure, since it is known that damage can introduce additional DOFs.

The results for a system with progressive damage, after the scenario specified in Simulation Setup, and an excitation frequency of 1Hz, are presented in Fig. 5.15. Fig. 5.15(a) shows the mode shape components, Fig. 5.15(b) presents the confidence index, and Fig. 5.15(c) plots the instantaneous frequency of the sifted component from the response at the first floor. The waving shape of the instantaneous frequency of the sifted signal is an indication that the sifted signal has some traces of the forced component. Good results for the confidence indices and mode shape components are obtained. The quality of the results

will be affected if the excitation frequency is close to the natural instantaneous frequency of the system and the sifting process cannot separate the free modal response from forced response. This separation can be possible if we go to higher decomposition level, but in that case the time localization will be very poor.

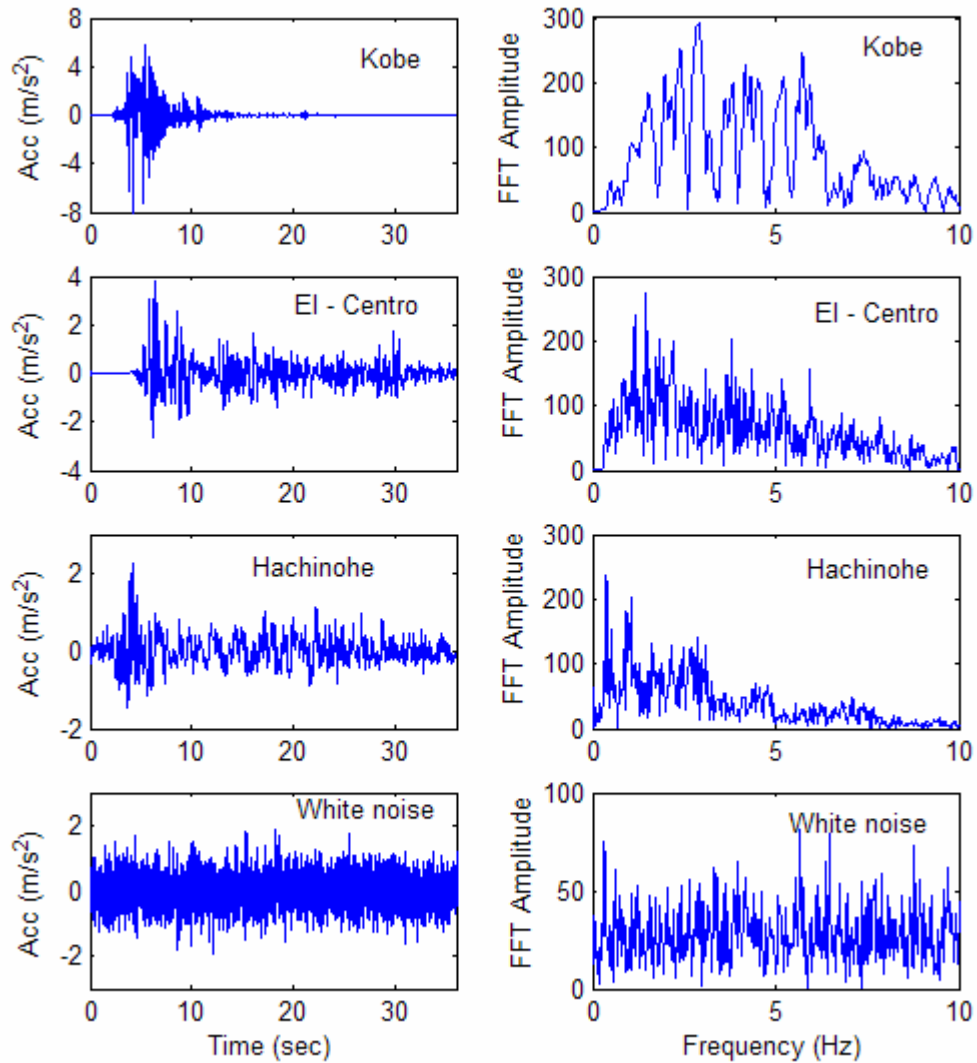


Figure 5.5. The excitation signals used in the study

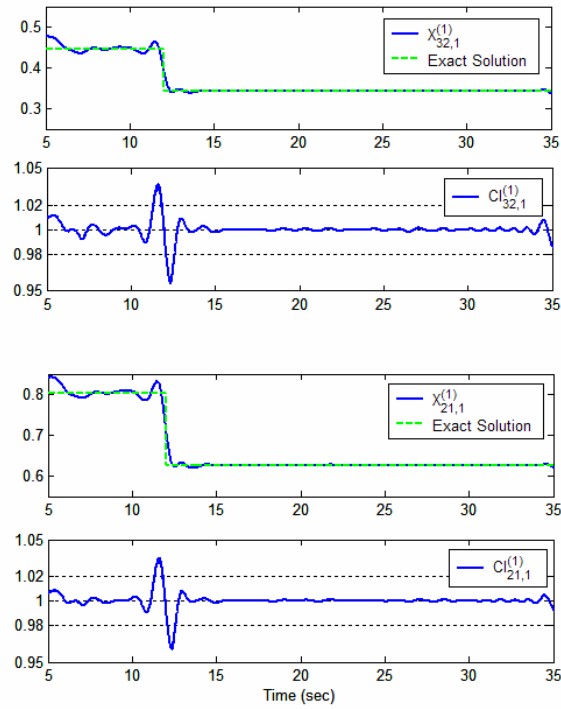


Figure 5.6. NI mode shape and confidence index for the first vibration mode, in case of Kobe earthquake excitation

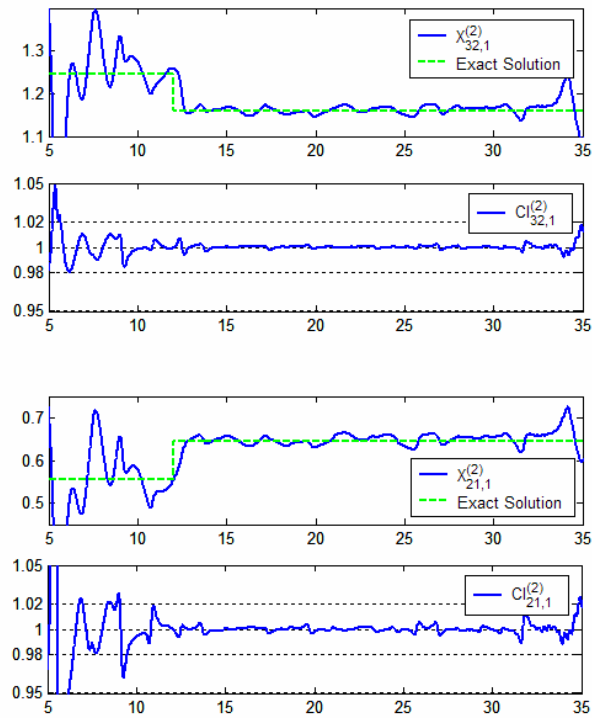


Figure 5.7. NI mode shape and confidence index for the second vibration mode, in case of Kobe earthquake excitation

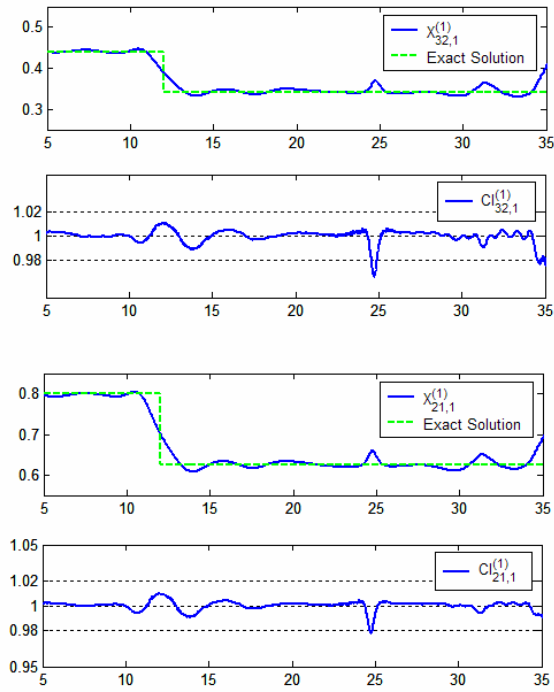


Figure 5.8. NI mode shape and confidence index for the first vibration mode, in case of Hachinohe earthquake excitation

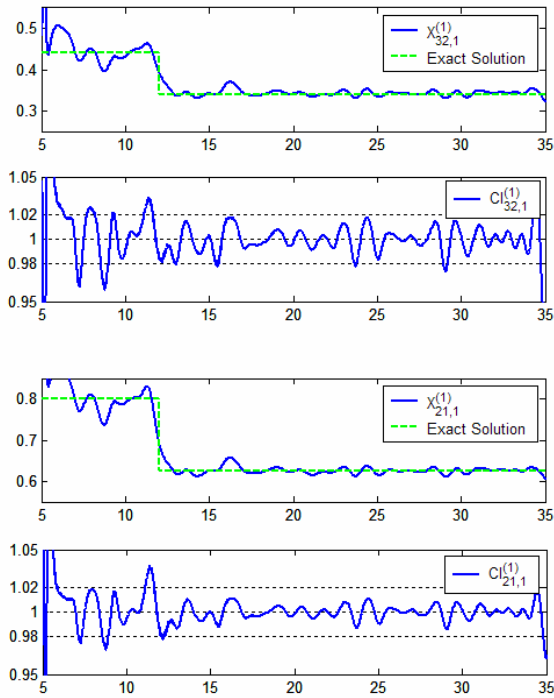


Figure 5.9. NI mode shape and confidence index for the first vibration mode, in case of El-Centro earthquake excitation

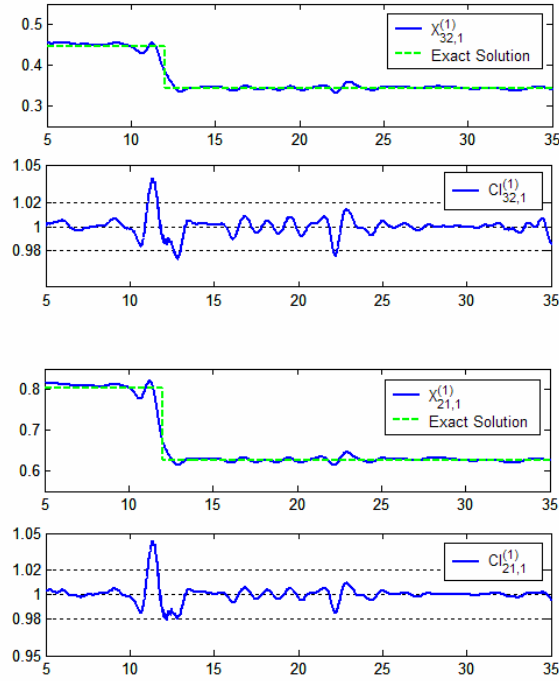


Figure 5.10. NI mode shape and confidence index for the first vibration mode, in case of random earthquake excitation

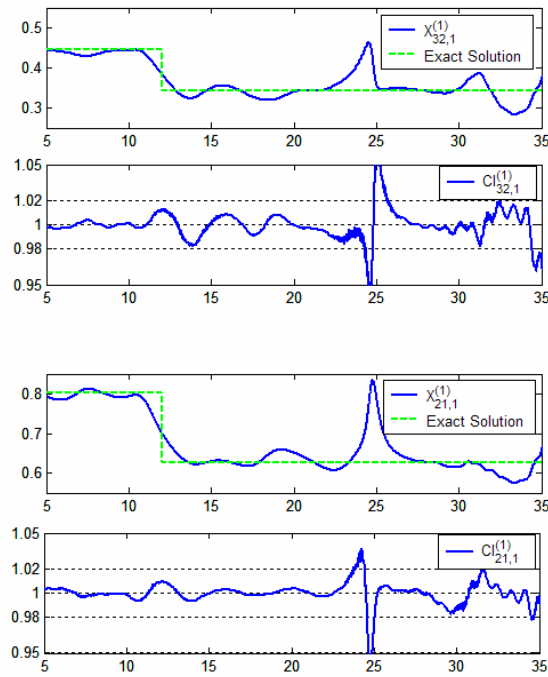


Figure 5.11. NI mode shape and confidence index for the first vibration mode, in case of Hachinohe earthquake excitation, 5% measurement noise

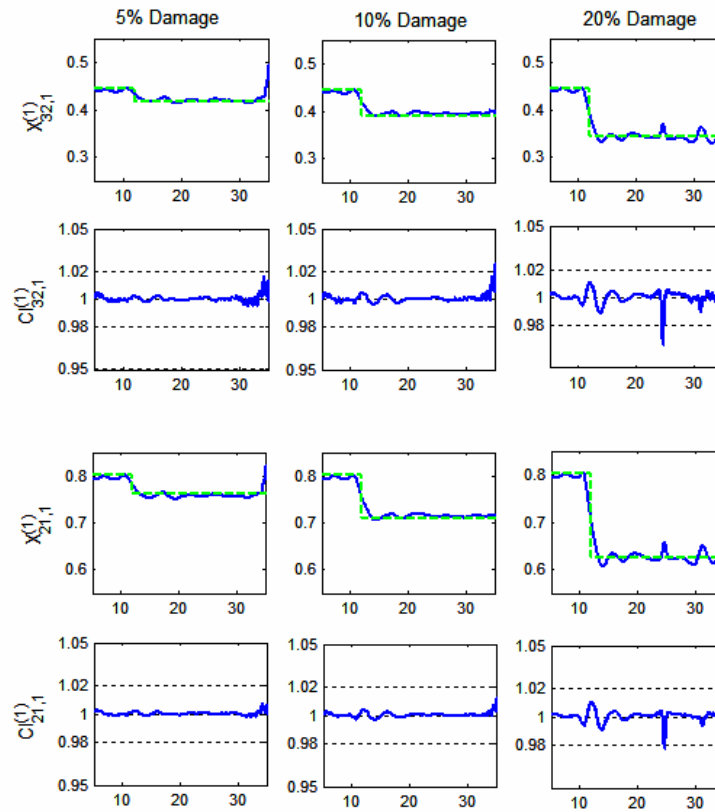


Figure 5.12. NI mode shape and confidence index for the first vibration mode, in case of Hachinohe earthquake excitation, for different damage levels

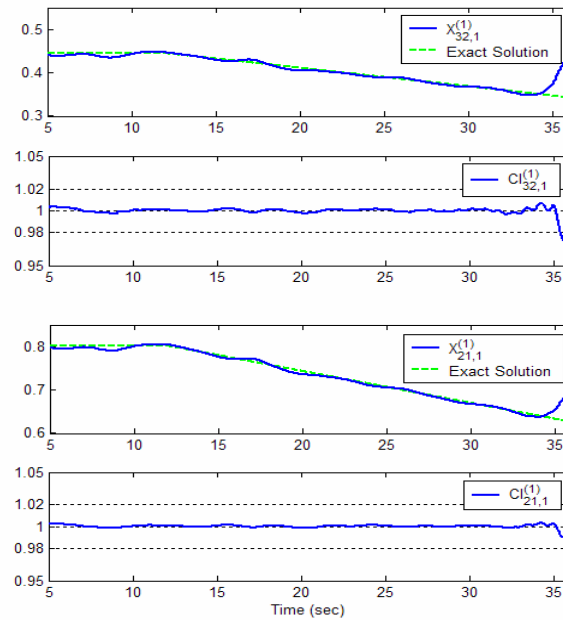


Figure 5.13. NI mode shape and confidence index for the first vibration mode, in case of Hachinohe earthquake excitation, gradual damage

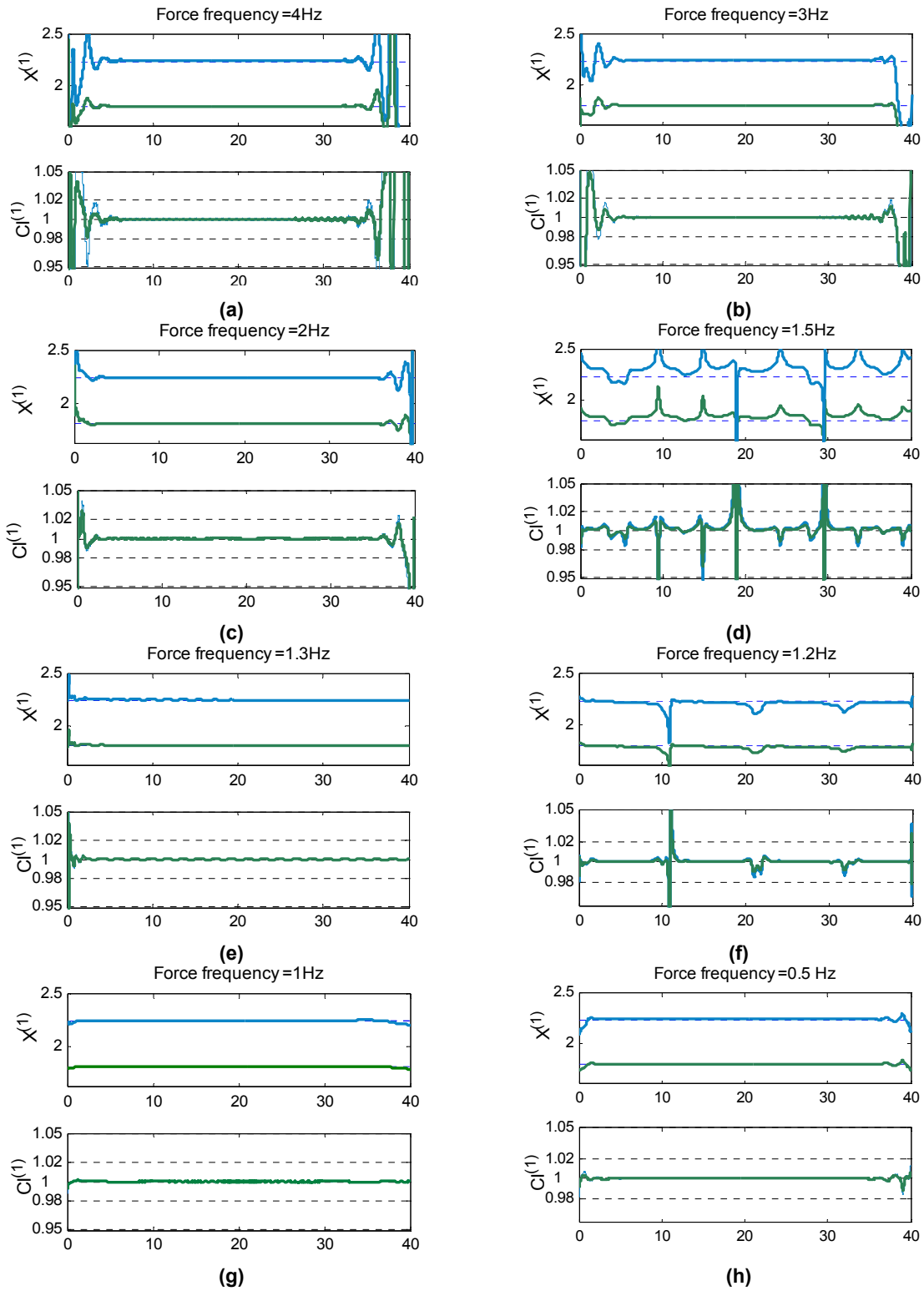


Figure 5.14. NI mode shape components and confidence indices for the first vibration mode, in case of a harmonic excitation, no damage ; (cyan = $X_{3,1}^{(1)}$, green = $X_{2,1}^{(1)}$)

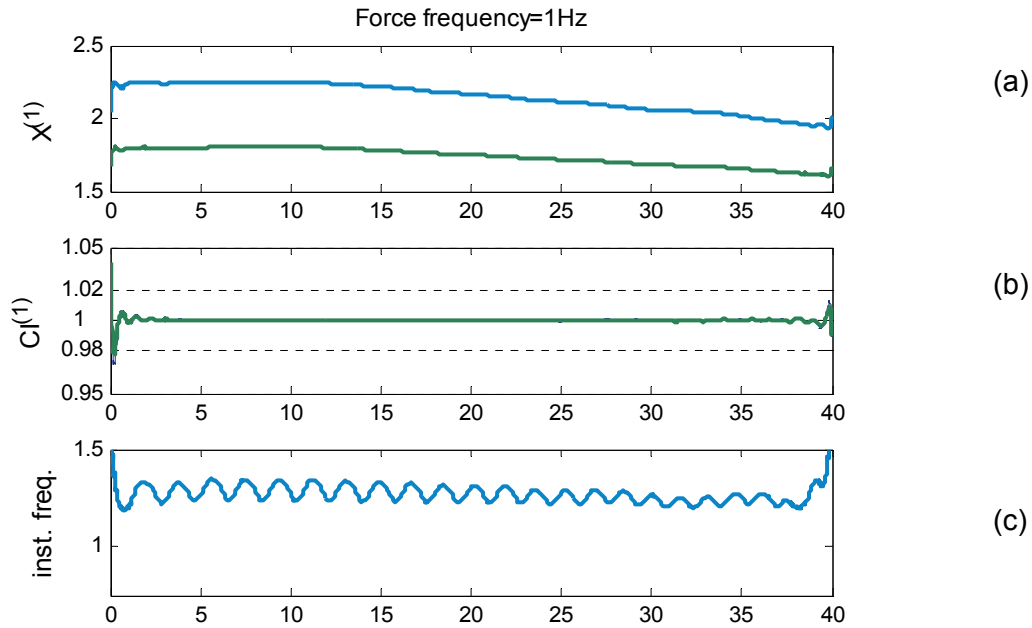


Figure 5.15. (a) NI mode shape components; (b) confidence indices; (c) instantaneous frequency of the sifted signals; in the case of progressive damage (cyan = $X_{3,1}^{(1)}$ and corresponding confidence index, green = $X_{2,1}^{(1)}$ and corresponding confidence index)

5.4 Summary

The normalized instantaneous (NI) mode shape vectors in conjunction with respective confidence indices can be effectively used to monitor health condition of structures subjected to earthquake excitation. Irrespective of base excitation signal, the NI mode shape value changes with subsequent structural stiffness loss and the change is in proportion with damage severity. Both damage types, i.e. sudden as well as progressive stiffness degradation, can be monitored and the trend of NI mode shape values can be used to identify the nature of damage in structure. The measurement noise does not significantly affect the results. The identified NI mode shapes are reliable for SHM when the corresponding confidence index lies between 0.98 and 1.02. The acceptable range of the confidence index was selected mainly by a sensitivity study. A further investigation on guidelines for selection of an appropriate CI range for a given application is needed in the future.

The method is proposed to be used as a preliminary structural damage identification technique in the aftermath of an earthquake event, when a quick decision regarding structural safety and management of the inspection resources has to be taken. In case of an observed change in the NI mode shape, further investigations are recommended in order to quantify and localize damage.

Few assumptions are made in this section. The structure considered is lightly and classically damped and has well separated vibration modes. It is assumed that a system with slow stiffness deterioration is approximately treated as a linear slow time-varying system and a system with a sudden damage is treated as linear before and after the damage and the excitation is broadband in comparison to the system natural frequencies. The approach works also for a narrow-banded excitation provided that the dominant frequency content of the excitation is either in the range of resonance or well separated from the system frequencies. In this case, knowledge of the excitation frequency is important in order to differentiate between forced and modal components of the response.

Several issues need to be further investigated. For example, the proposed approach needs to be tested for real vibration measurements from either experiments or true seismic events. In contrast to the stationary case, a time misalignment of the measurement records may introduce significant errors in identification of the instantaneous mode shape vectors. A change in the instantaneous modal parameters reflects structural nonlinearity that may not only be associated with structural damage and certain criteria need to be developed to identify the changes associated with damage. A preliminary study addressing the presence of a bilinear component in a 2DOF system can be found in Chapter 7. Further studies for other types of nonlinearities and complex systems are required.

Chapter 6

WAVELET PACKET AND KALMAN FILTER FOR IDENTIFICATION OF INSTANTANEOUS NATURAL FREQUENCY AND DAMPING RATIO

6.1 Introduction

Since change in structural health condition has as effect change in the natural frequency and mode shape, the instantaneous values of these parameters are of great importance in SHM. In Chapter 5, the normalized instantaneous mode shape was identified by the WPS technique and HT. A confidence index, defined as the ratio of the instantaneous frequency of the sifted signals from two different measurement locations, was proposed to ensure quality of the results. While the identified instantaneous frequencies of the sifted components of the measured responses may be used for SHM, in most of the cases they are not the instantaneous *natural* frequencies, and they may be related to the frequency content of the excitation.

In this section, a time-varying Kalman filter technique is integrated with the wavelet approach to identify the instantaneous natural frequencies and, also, the instantaneous modal damping ratios. The physical significance of the sifted components is assured by introducing a new sifting criterion based on the confidence index.

The potential of the proposed approach is demonstrated by a simulation study for a two-degree-of-freedom system with progressive damage and subjected to two sets of excitation: one is a sample generated from a filtered Gaussian discrete process and the other

is a true ground acceleration measurement. Good estimates for instantaneous modal parameters are obtained. The effectiveness of the method in the presence of measurement noise is also addressed.

6.2 Theoretical Background

In order to identify the instantaneous modal parameters the following concepts are employed: time varying modal decomposition and the second order system formulation for time varying vibration modes, instantaneous frequency, wavelet packet decomposition and Kalman filter. Since most of these concepts have been already presented in the previous chapters, this section will only briefly describe the discrete Kalman filter; more details can be found in (Brown, 1983).

Discrete Kalman filter is employed to estimate the instantaneous modal parameters of time varying vibration modes identified by the sifting process. The discrete Kalman filter is a well established algorithm for estimation of the state vector $\mathbf{x} \in R^n$ of a discrete-time process that is governed by the linear stochastic difference eq. (6.1)

$$\mathbf{x}[k+1] = \mathbf{A}[k]\mathbf{x}[k] + \mathbf{w}[k], \quad (k = 1, 2, \dots) \quad (6.1)$$

with a measurement $\mathbf{y}[k]$ described by:

$$\mathbf{y}[k] = \mathbf{C}[k]\mathbf{x}[k] + \mathbf{v}[k] \quad (6.2)$$

where $[k]$ refers to the discrete values at time step $t[k]$.

The random variables $\mathbf{w}[k]$ and $\mathbf{v}[k]$ represent the process and measurement noise, respectively. They are assumed to be independent, zero mean Gaussian white processes, with the variances as:

$$\begin{aligned} \mathbf{Q}[k] &= E \langle \mathbf{w}[k]\mathbf{w}[k]^T \rangle \\ \mathbf{R}[k] &= E \langle \mathbf{v}[k]\mathbf{v}[k]^T \rangle \end{aligned} \quad (6.3)$$

where $E \langle \rangle$ stands for the mean value of the variable in the parentheses.

Adding the assumption that the prior state has a Gaussian distribution, Kalman filter gives the best state estimate in the sense that the square norm of the estimation error is minimum.

Kalman filter works in a predictor-corrector manner by first predicting the values of

the state variables using the dynamic model, and then correcting them based on the new measurement and the measurement equation. With following notations:

- $\hat{\mathbf{x}}[k | k - 1]$ - the estimate of $\mathbf{x}[k]$ given the past measurements up to $\mathbf{y}[k]$;
- $\hat{\mathbf{x}}[k | k]$ - the updated estimate of $\mathbf{x}[k]$ given the last measurement $\mathbf{y}[k]$;
- $\mathbf{P}[k | k] = E < [\mathbf{x}[k] - \hat{\mathbf{x}}[k | k]][\mathbf{x}[k] - \hat{\mathbf{x}}[k | k]]^T >$ - the error covariance matrix
- $\mathbf{P}[k | k - 1] = E < [\mathbf{x}[k] - \hat{\mathbf{x}}[k | k - 1]][\mathbf{x}[k] - \hat{\mathbf{x}}[k | k - 1]]^T >$

the two stages of the Kalman filter algorithm can be summarized as shown in eqs. (6.4) and (6.5).

Prediction (time update) equations:

$$\begin{aligned}\hat{\mathbf{x}}[k | k - 1] &= \mathbf{A}[k - 1]\hat{\mathbf{x}}[k - 1 | k - 1] \\ \mathbf{P}[k | k - 1] &= \mathbf{A}[k - 1]\mathbf{P}[k - 1 | k - 1]\mathbf{A}[k - 1]^T + \mathbf{Q}[k - 1]\end{aligned}\quad (6.4)$$

Correction (measurement update) equations:

$$\begin{aligned}\mathbf{K}[k] &= \mathbf{P}[k | k - 1]\mathbf{C}[k]^T (\mathbf{C}[k]\mathbf{P}[k | k - 1]\mathbf{C}[k]^T + \mathbf{R}[k])^{-1} \\ \hat{\mathbf{x}}[k | k] &= \hat{\mathbf{x}}[k | k - 1] + \mathbf{K}[k](\mathbf{y}[k] - \mathbf{C}[k]\hat{\mathbf{x}}[k | k - 1]) \\ \mathbf{P}[k | k] &= (\mathbf{I} - \mathbf{K}[k]\mathbf{C}[k])\mathbf{P}[k | k - 1]\end{aligned}\quad (6.5)$$

The Kalman gain, $\mathbf{K}[k]$, in eq. (6.5) was obtained by minimizing the square norm of the

estimation error, that is: $\frac{\partial \text{trace}(\mathbf{P}[k | k])}{\partial \mathbf{K}[k | k]} = 0$.

6.3 Methodology

6.3.1 Instantaneous Natural Frequency and Modal Damping Ratio

In this chapter, we use the second order formulation for real time-varying vibration mode, since here the natural frequency of the system appears explicitly.

The dynamics of a system with damage can be described by a set of differential equation with time varying coefficients, as shown in eq. (6.6).

$$\mathbf{M}\ddot{\mathbf{x}}(t) + \mathbf{C}_d(t)\dot{\mathbf{x}}(t) + \mathbf{K}(t)\mathbf{x}(t) = \mathbf{f}(t)\quad (6.6)$$

If the slow varying criterion is satisfied, the response of the system, $\mathbf{x}(t)$, can be decomposed in a sum of vibration modal responses, $\mathbf{x}^{(n)}(t)$, characterized by the same instantaneous frequency for different measurement locations.

$$\mathbf{x}(t) = \sum_{n=1}^N \mathbf{x}^{(n)}(t) \quad (6.7)$$

It has been proved in Chapter 3, that each time-varying vibration mode can be described by a second order equation with time-varying coefficients, as shown in eq. (6.8).

$$\ddot{x}_j^{(n)}(t) + 2\xi_n(t)\Omega_n(t)\dot{x}_j^{(n)}(t) + \Omega_n^2(t)x_j^{(n)}(t) = f_j^{(n)}(t), x_j^{(n)}(t_0) = x_0^{(n)}, \dot{x}_j^{(n)}(t_0) = \dot{x}_0^{(n)} \quad (6.8)$$

where $f_j^{(n)}(t)$ represents the modal force and is given in eq. (3.54), and $x_j^{(n)}(t_0), \dot{x}_j^{(n)}(t_0)$ are the initial conditions expressed in eq. (3.49). $\Omega_n(t)$ and $\xi_n(t)$ are called the n^{th} instantaneous natural frequency and instantaneous modal damping ratio. $f_j^{(n)}(t)$ is a time varying weighted sum of forces which are applied to the structure. For example, in the case of a base excitation, i.e. ground acceleration denoted by $a_g(t)$, the modal force, $f_j^{(i)}(t)$, can be expressed as $f_j^{(i)}(t) = F_j^{(n)}(t)a_g$, where the load participation factor $F_j^{(n)}(t)$ is a function of time and location j, as shown in eq. (6.9).

$$F_j^{(n)}(t) = \frac{2i \operatorname{Im}(u_j^{(2n-1)} u_{2j}^{(2n-1)*})}{-u_j^{(2n-1)*}} \mathbf{v}_{N+1, \dots, 2N}^{(n)T}(t) \begin{bmatrix} -1 \\ \dots \\ -1 \end{bmatrix} \quad (6.9)$$

Without loss of generality and just for simplicity of the explanations, the base excitation is considered in the following.

Since Kalman filter which gives an optimal solution for linear systems, the time varying modal stiffness and modal damping are introduced as shown in eq. (6.10).

$$k_n = \Omega_n^2, c_n = 2\xi_n(t)\Omega_n(t) \quad (6.10)$$

With these notations, eq. (6.8) gets linear in the unknown c_n, k_n and $F_j^{(n)}(t)$. This equation can be written in vector form as:

$$\ddot{\mathbf{x}}^{(n)}(t) + c_n(t)\dot{\mathbf{x}}^{(n)}(t) + k_n(t)\mathbf{x}^{(n)}(t) = \mathbf{F}^{(n)}(t)a_g(t) \quad (6.11)$$

The identification of instantaneous modal parameters can be summarized as follows: first, the modal responses $\ddot{x}_j^{(n)}(t)$, $\dot{x}_j^{(n)}(t)$, $x_j^{(n)}(t)$ are extracted by a wavelet packet sifting technique and then k_n , c_n and $F_j^{(n)}(t)$ are estimated by a Kalman filter technique. In case multiple excitation forces are applied to the structure, the RHS of equation (6.11) should be reformulated and some other unknowns are added to the estimation set.

The instantaneous natural frequency and instantaneous modal damping ratio will be calculated using the following formula:

$$\Omega_n(t) = \sqrt{k_n(t)}, \zeta_n(t) = \frac{c_n(t)}{2\Omega_n(t)} \quad (6.12)$$

6.3.2 Extraction of Modal Responses by Wavelet Packet Sifting Technique.

New Sifting Criterion

A wavelet packet sifting technique is used to extract the relevant parts of the modal responses, $\ddot{x}_j^{(n)}(t)$, $\dot{x}_j^{(n)}(t)$, $x_j^{(n)}(t)$. The technique consisting in wavelet packet decomposition in conjunction with the entropy index as sifting criterion has been described in (Shinde et Hou, 2005). In this section, the confidence index, defined in Chapter 5, is proposed to be used as sifting criterion. So that, two response signals measured at two different locations/DOFs are simultaneously decomposed until their components at the same decomposition node have a close instantaneous frequency, which means a confidence index close to unity.

This sifting criterion guarantees the minimum contamination from other vibration modes and that the assumption of slowly time-varying system (Chapter 3) is satisfied. In the sifting process, an energy threshold is, also, imposed. Any signal component whose energy is smaller than 1% of the original signal energy is ignored, because it does not carry enough information to be used in identification. Using the above two criteria, signal components

relevant to the vibration modes are selected for identification of instantaneous modal parameters.

The sifting procedure can be summarized as follows:

Setup:

Let us consider the signals $x_j(t)$ and $x_p(t)$, which represent the system response at two measurement locations, and the node (m, q) in the wavelet packet tree. By WP decomposition the following detail signals are obtained: $D_{m,q}(x_j(t))$ and $D_{m,q}(x_p(t))$.

Sifting Procedure:

1. Verify if the energy of $D_{m,q}(x_j(t))$ and $D_{m,q}(x_p(t))$ is bigger than the threshold value. If not, stop the decomposition for this node here, without sifting any signal, and go to the next wavelet packet node.
2. Identify the instantaneous frequency, $\omega_{j,mq}(t)$ and $\omega_{p,mq}(t)$, of the signals $D_{m,q}(x_j(t))$ and $D_{m,q}(x_p(t))$ by using the analytic signal concept and HT, as explained in Chapter 3.
3. Calculate the confidence index by eq. (6.13).

$$CI_{j,p}(t) = \frac{\omega_{j,mq}(t)}{\omega_{p,mq}(t)} \quad (6.13)$$

4. If the confidence index is close to unity (i.e. range 0.98-1.02, but this range may depend also on application) over most of the time domain, select these two signals as relevant vibration modal responses for location “j” and “p”. If not, continue the decomposition and repeat this procedure.

6.3.3 Implementation Issues

One of the difficulties in extracting the modal responses from the vibration measurements is that the energy of a signal $x_j^{(n)}(t)$ can be distributed over a wide frequency range, as it is the case of a broadband excitation. However, a significant part of the energy is in the vicinity of the n^{th} instantaneous natural frequency, therefore from energy content point of view the signal $x_j^{(n)}(t)$ can be written as:

$$x_j^{(n)}(t) = x_j^{(n),n}(t) + x_j^{(n),r}(t) \quad (6.14)$$

where $x_j^{(n),n}(t)$ represents the signal component whose energy is in a band around the n^{th} instantaneous natural frequency and $x_j^{(n),r}(t)$ is the residual component equal to the rest of the n^{th} modal response.

If $x_j^{(n),n}(t)$ can be identified as the signal component at node (m,q) in the wavelet packet decomposition tree, i.e. $x_j^{(n),n}(t) = D_{m,q}(x_j^{(n)}(t))$. With the assumption that k_n , c_n , $F_j^{(n)}$ are slowly varying in comparison to the frequency content of the modal response and excitation, eq. (6.8) can be re-written as:

$$D_{m,q}(\ddot{x}_j^{(n)}(t)) + c_n(t)D_{m,q}(\dot{x}_j^{(n)}(t)) + k_n(t)D_{m,q}(x_j^{(n)}(t)) = F_j^{(n)}(t)D_{m,q}(a_g(t)) \quad (6.15)$$

Equation (6.15) shows that the parameters to be identified remain the same in case only the dominant part of the n^{th} modal response is considered.

There is, also, another difficulty due to the fact that in the frequency range of interest corresponding to the n^{th} mode there are some residual components of other vibration modes. By WPS technique with the sifting criterion based on the confidence index, we adequately select the decomposition level and node (m,q) to minimize the contamination with other vibration modes.

6.3.4 Identification of Modal Parameters

Once the signals $D_{m,q}(\ddot{x}_j^{(n)}(t))$, $D_{m,q}(\dot{x}_j^{(n)}(t))$, $D_{m,q}(x_j^{(n)}(t))$ are identified, a discrete time-varying Kalman filter technique is used to estimate the modal stiffness and modal damping for the n^{th} vibration mode, i.e. k_n and c_n in eq. (6.15). The unknown state vector is $[k_n, c_n, F_1^{(n)}, \dots, F_j^{(n)}, \dots, F_M^{(n)}]$, where M represents the number of measurements. In the present study, the unknown dynamics of state variables is modeled as a random walk process. In the discrete form, the state space dynamics can be formulated as:

$$\begin{bmatrix} k_n[k+1] \\ c_n[k+1] \\ F_1^{(n)}[k+1] \\ \vdots \\ F_M^{(n)}[k+1] \end{bmatrix} = \begin{bmatrix} 1 & 0 & 0 & \cdots & 0 \\ 0 & 1 & 0 & \cdots & 0 \\ 0 & 0 & 1 & \cdots & 0 \\ & & & \ddots & \\ 0 & 0 & 0 & \cdots & 1 \end{bmatrix} \begin{bmatrix} k_n[k] \\ c_n[k] \\ F_1^{(n)}[k] \\ \vdots \\ F_M^{(n)}[k] \end{bmatrix} + \begin{bmatrix} w_k[k] \\ w_c[k] \\ w_{F_1}[k] \\ \vdots \\ w_{F_M}[k] \end{bmatrix} \quad (6.16)$$

There are M measurement equations expressed in a discrete form as:

$$\begin{aligned} D_{m,q}(\ddot{x}_j^{(n)})[k] &= -c_n(k)D_{m,q}(\dot{x}_j^{(n)})[k] - k_n(k)D_{m,q}(x_j^{(n)})[k] + \\ &+ F_j^{(n)}(t)D_{m,q}(a_g)[k] + v_j[k], j = 1 \cdots M \end{aligned} \quad (6.17)$$

The components of the process and measurement noise vector $\mathbf{w}[k]$ and $\mathbf{v}[k]$, respectively, are assumed to be independent and Gaussian white noise discrete processes. The measurement noise vector $\mathbf{v}[k]$ represents, in a broad sense, the actual measurement noise and other errors due to the sifting process, as well as the modeling. After the estimation of the state space vector, the n^{th} instantaneous natural frequency and instantaneous modal damping ratio are calculated by eq. (6.12).

The variances of measurement and process noise vectors, can be identified using adaptive techniques, Monte Carlo simulations or by experience. In this study a Monte Carlo simulation is performed, and those values which ensure a minimum measurement innovation have been chosen. The measurement innovation reflects the discrepancy between predicted measurement and actual measurement.

The n^{th} normalized instantaneous mode shape vector is calculated from the corresponding sifted component of the acceleration responses, as the ratio of the analytic amplitude of the vector $D_{m,q}(\mathbf{x}^{(n)}(t))$ and the analytic amplitude of the component chosen for normalization, as explained in Chapter 5.

6.4 Applications: A 2DOF Mass-spring-dashpot System with Time-varying Stiffness

6.4.1 Simulation Setup

In the present study, the simulated vibration responses of a two degree-of-freedom spring-mass-damper system with a damageable spring, are analyzed. A sketch of the system is presented in Fig. 6.1. The mass M_1 is 2800kg and the mass M_2 is 3000kg. The initial value of the stiffness of each spring is 500 KN/m and the system damping is assumed to be a Rayleigh damping. The damping matrix is proportional to the initial stiffness matrix with a factor of 0.005. The natural frequencies of the healthy structure are 1.278 and 3.387 Hz. In order to test the effectiveness of the wavelet packet sifting technique in identification of instantaneous modal parameters, the structure is base excited by two different excitation signals, namely:

- the NS component of El-Centro earthquake signal, recorded at the Imperial Valley Irrigation District substation in El Centro, CA, on May 18, 1940.
- a random excitation signal, sampled by a Gaussian white noise discrete process with zero mean and RMS value of 2.5 m/s^2 and filtered by a low-pass filter with a cut-off frequency of 20 Hz. The sampling frequency is 100Hz.

The relative responses in respect to the ground are simulated with a sampling frequency of 100 Hz. The method is validated for a system without damage and then is applied to a system with progressive degradation of the stiffness K_1 as shown in Fig. 6.1(b). Discrete Meyer wavelet is chosen for the wavelet packet analysis. Since the system is subjected to a base excitation and the first vibration mode is excited predominantly, only the modal parameters for this mode are identified.

The variances of measurement and process noise vectors in the Kalman filter estimation are chosen after Monte Carlo simulation so that to ensure a minimum measurement innovation, which reflects the discrepancy between predicted measurement and actual measurement.

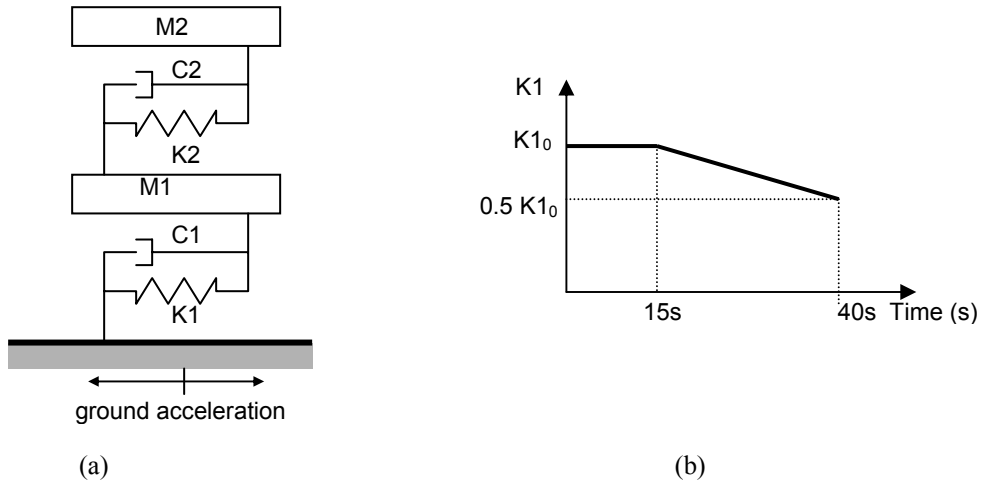


Figure 6.1. (a) Sketch of system; (b) Stiffness history in case of progressive damage

6.4.2 Results and Discussion

In order to validate the method, first a time invariant structure subjected to a filtered white noise excitation is considered. The wavelet packet sifting process is performed on acceleration responses measured at M_1 and M_2 , and the decomposed signals at node (6,1) are selected as relevant for the first vibration mode. Figure 6.2.(a) shows the instantaneous frequency and the confidence index for the acceleration components at this node. It can be seen that the confidence index is very close to the ideal value of unity. This indicates a minimum contamination with the second mode components. In contrast, a component in the previous levels of decomposition, say the component at node (4,0) demonstrates significant contamination, as observed in Fig. 6.2.(b).

Figure 6.3 shows the estimated values for the natural frequency, the modal damping ratio and the mode shape component of M_2 , for the first vibration mode. They are compared with the theoretical values obtained by modal analysis. It can be seen that the estimates for instantaneous natural frequency and the damping ratio are in good agreement with the theoretical values. The estimate for the normalized instantaneous mode shape component at mass M_2 is very close to the theoretical value. Since the mode shape values

are more sensitive to the contamination of extracted signals with the second vibration mode, the confidence index should be used for validation, as explained in details in Chapter 5. Note that the normalized instantaneous mode shape component at mass M1 is unity because the mode shape component at M1 has been used for normalization.

Figure 6.4 shows the estimates of modal parameters for the case of progressive damage scenario, as described in the simulation setup.

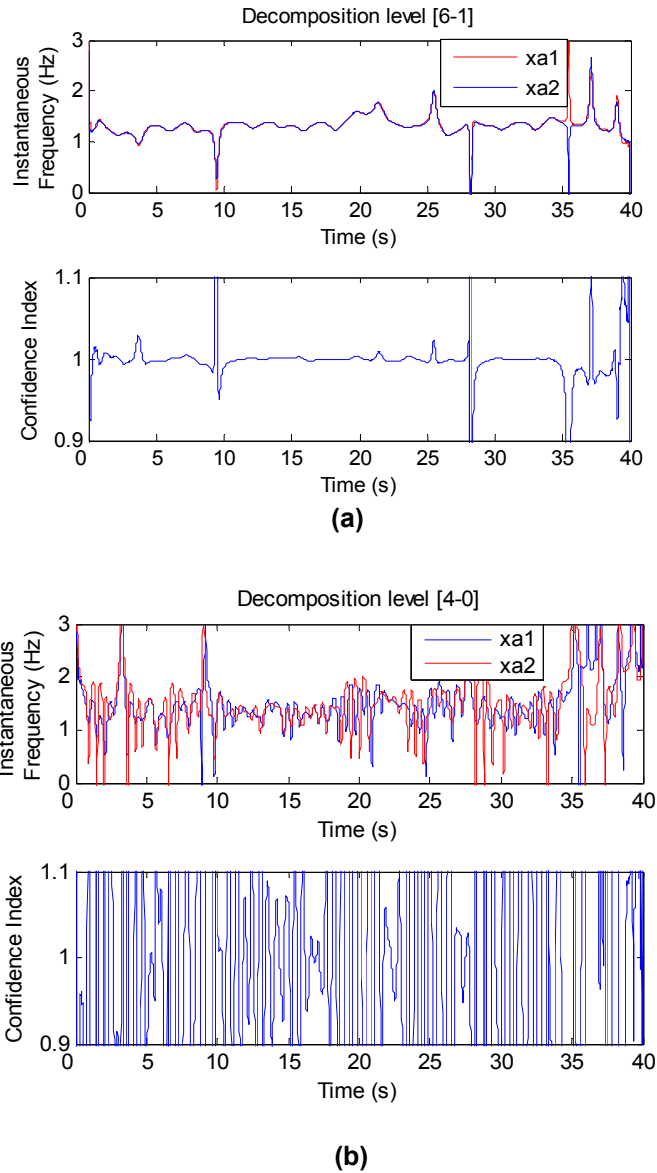


Figure 6.2. Instantaneous frequency and confidence index of the decomposed acceleration responses at: (a) level 6, node 1 and (b) and level 4, node 0.; xa1 and xa2 represents the acceleration responses in respect to the ground at M1 and M2, respectively.

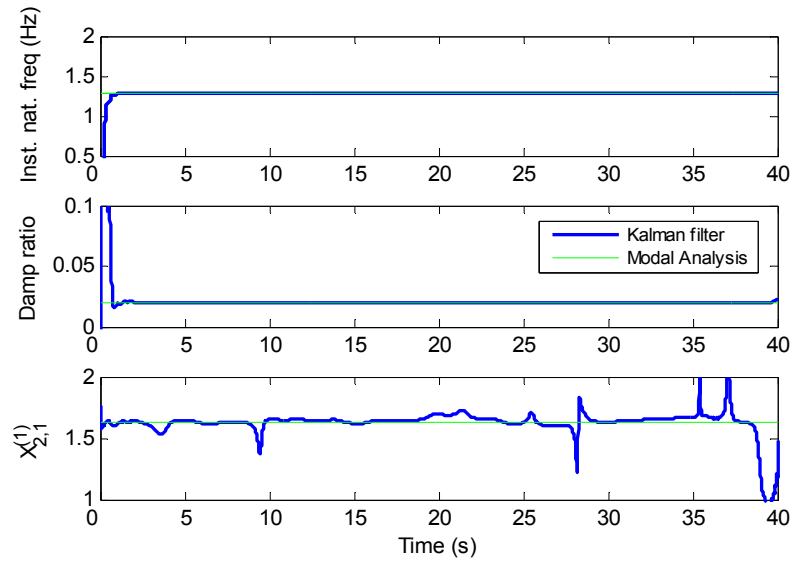


Figure 6.3. Estimated values for instantaneous modal parameters in case of healthy system, first vibration mode

Since the system stiffness changes slowly, the results from the dynamic eigenvalue problem can be used as a reference. Figure 6.4(a) shows the estimated results in the case of a filtered Gaussian white noise excitation, and Fig. 6.4(b) presents the results in the case of a real earthquake signal, i.e. the El Centro earthquake ground motion data. The estimated instantaneous frequency values are in very good agreement with the reference values. The instantaneous modal damping ratio shows small deviation from the reference. In the case of an earthquake excitation, the intensity of the signals during the first 5 seconds of the record is very small, i.e. at the level of measurement noise; therefore the estimated results on this time interval should be disregarded.

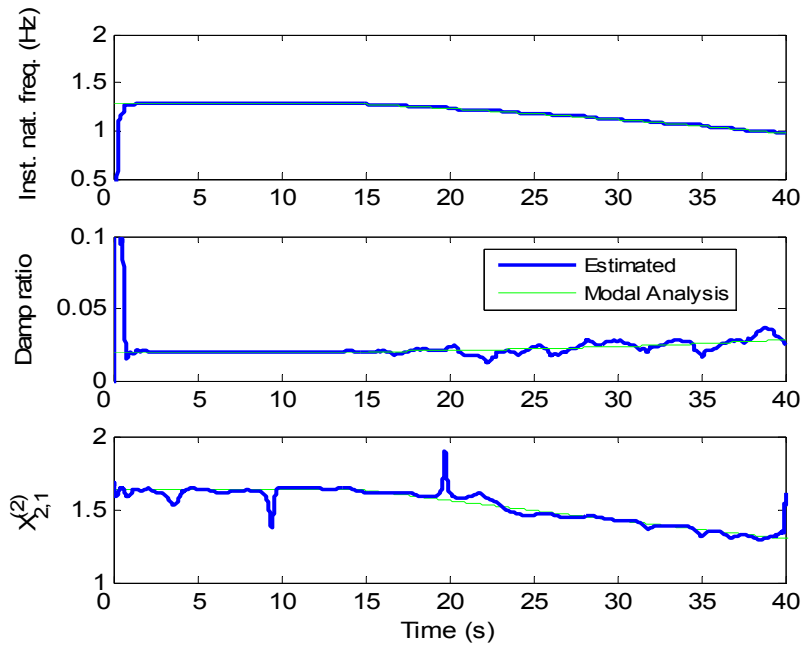
Figure 6.5 presents the effect of measurement noise and incomplete measurements on the estimated results. A complete measurement here is referred to the fact that all displacements, velocities, and accelerations are directly measured. In Fig. 6.5, only the acceleration responses are measured and the velocity and displacement responses are obtained by numerical integration of the signal $D_{m,q}(\dot{x}_j^{(n)}(t))$. To investigate the noise effects, the acceleration measurements are contaminated by noises, modeled as a Gaussian white noise discrete process with a RMS value being 10% of the RMS value of the acceleration response at M2. The first 40 seconds of the records are considered for RMS

calculation. It can be observed that the estimated natural frequency is less sensitivity to the measurement noise and incomplete measurements and the modal damping ratio and normalized mode shape component exhibit oscillations around the theoretical values.

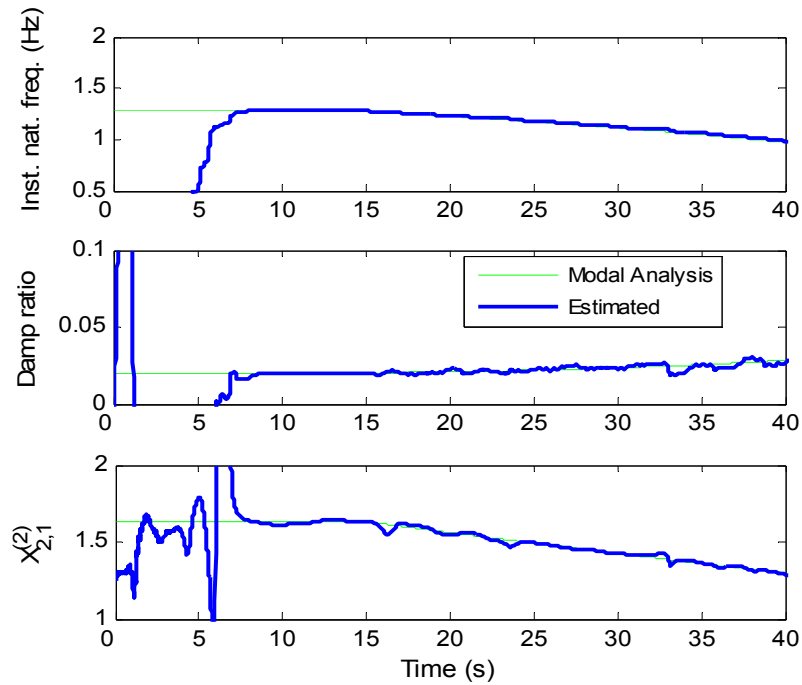
6.4 Summary

This Chapter presents an identification technique for instantaneous natural frequency, damping ratio from forced vibration data. In the proposed methodology, structural responses are first decomposed in relevant vibration modal components by wavelet packet sifting technique. Based on a new sifting criterion, two response signals, measured at two different locations/DOFs, are simultaneously decomposed until their components at the same WP decomposition node have a close instantaneous frequency. The instantaneous frequencies are identified by the Hilbert transform and their closeness can be measured by the confidence index. For each identified vibration mode, a time varying Kalman filter approach was utilized to estimate the instantaneous *natural* frequency and the modal damping ratio. The instantaneous mode shape is calculated using the amplitudes of analytical functions associated with the Hilbert transform of the modal responses.

The proposed approach was implemented for a two-degree-of-freedom mass-spring system with a damageable spring subjected to two sets of random excitation: one is a sample generated from a filtered Gaussian white noise process and the other is a true ground acceleration measurement. The estimated instantaneous frequency values are in very good agreement with the reference values, but instantaneous modal damping ratio shows small deviation from the reference. The estimated natural frequency is less sensitive to the measurement noise. In contrast, the estimated modal damping ratio and normalized mode shape component show oscillations around the theoretical values. Although the mathematical proof is presented for a system with slowly-time varying parameters in respect to the fundamental frequency of the healthy system, the method can be easily extended to linear systems with sudden damage.

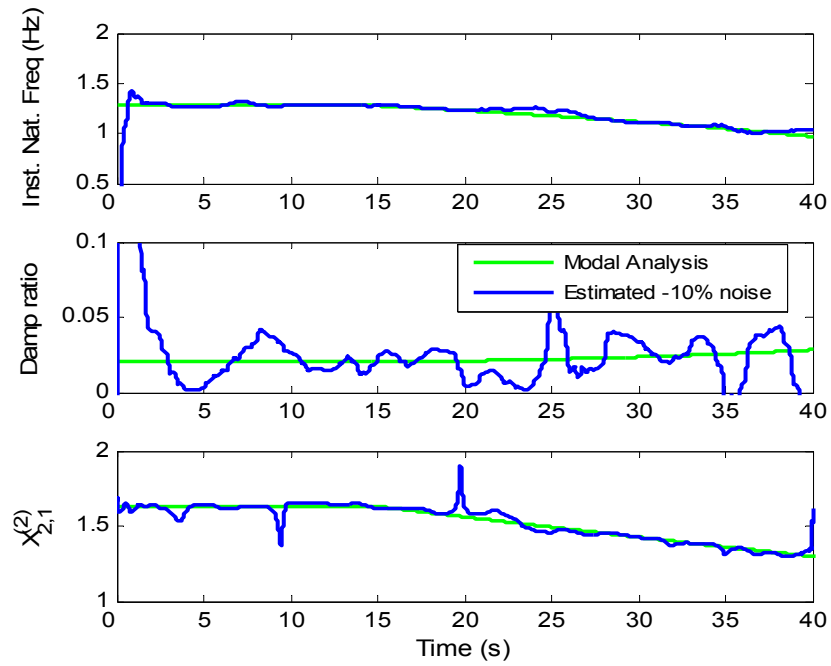


(a)

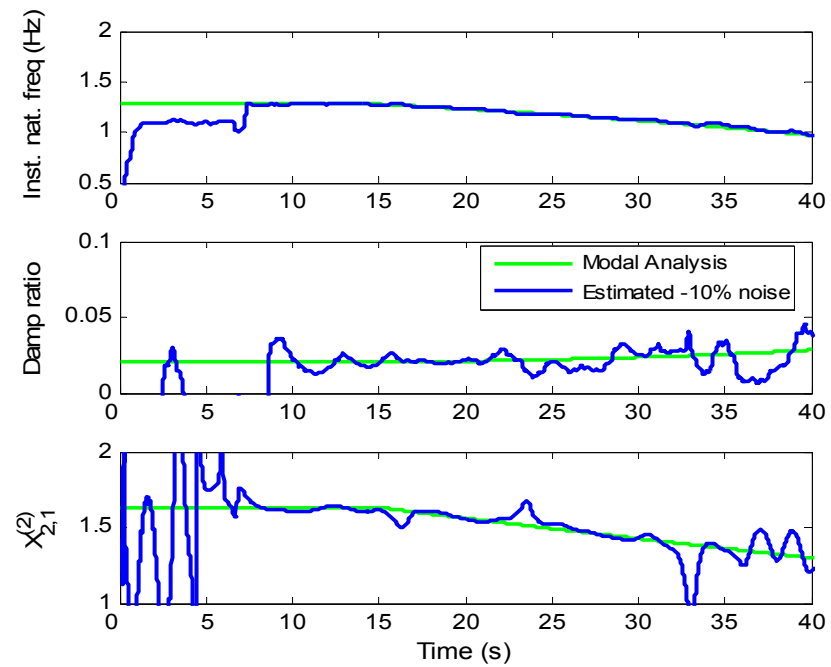


(b)

Figure 6.4. Estimated values for instantaneous modal parameters in case of a system with progressive stiffness degradation after $t=15s$, subjected to a base excitation: (a) filtered Gaussian white noise, (b) El Centro earthquake signal



(a)



(b)

Figure 6.5. Estimated values for instantaneous modal parameters in case of a system with progressive stiffness degradation after $t=15s$. The acceleration measurements are contaminated by “10%” measurement noise. The based excitation is: (a) filtered Gaussian white noise, (b) El Centro earthquake signal

Chapter 7

INSTANTANEOUS MODAL PARAMETERS FOR STRUCTURAL HEALTH MONITORING OF NONLINEAR SYSTEMS

7.1 Introduction

In the previous sections, a structure with damage was seen as a linear time varying system with instantaneous modal parameters which change their trend according to damage evolution.

However, due to a possible dynamic nonlinear behavior of the structure, change in the instantaneous modal parameters may not necessarily indicate structural damage. Ignoring the structural nonlinear behavior may lead to false-alarm of damage in structural health monitoring. This chapter presents a preliminary study on the meaning of instantaneous modal parameters and their use for SHM of systems with nonlinear dynamic behavior.

A two-degree-of-freedom system with bilinear components, subjected to both impulse and harmonic excitation, is considered. The instantaneous modal parameters are identified from the simulated vibration responses by continuous wavelet transform (CWT) in conjunction with the Hilbert Transform (HT). It is illustrated that change in the identified instantaneous modal parameters may have different patterns for the linear system, the system with slow stiffness degradation, and the system with bilinear restoring forces. The results may help to distinguish change in the instantaneous modal parameters caused by

structural damage or by structural nonlinear behavior and therefore to improve the accuracy of structural health monitoring.

7.1 Theoretical Background

7.2.1 Linear Slowly Time-varying Systems

Here, we present the instantaneous modal parameters from the inverse problem point of view. Therefore, given a signal, in the absence of any other information, we make the assumption of a linear slowly time-varying system. The correctness of this assumption can further be verified by using the confidence indices, previously introduced. It has been shown in Chapter 3 that the free vibration response of such a system can be written as a superposition of modal responses. Equation (7.1) shows the response measured at

position/DOF j ; the notation $C_{xn}(t) = 2|C_{2n-1}(t_0)| \exp\left(\int_{t_0}^t \gamma_n(\tau) d\tau\right)$ has been used.

$$x_j(t) = \sum_{n=1}^N x_j^{(n)} = \sum_{n=1}^N X_j^{(n)}(t) C_{xn}(t) \cos(\Phi_j^{(n)}(t)) \quad (7.1)$$

The component $x_j^{(n)} = X_j^{(n)}(t) C_{xn}(t) \cos(\Phi_j^{(n)}(t))$ was called as the n^{th} modal response.

It was shown that the instantaneous modal frequency does not depend, practically, on measurement location, here denoted by “ j ”, and can be calculated as:

$$\omega_n(t) = \frac{d}{dt} \Phi_j^{(n)}(t) \quad (7.2)$$

The normalized mode shape vector is given in eq.(7.3), where the p^{th} component has been chosen for normalization.

$$\mathbf{X}_{|p}^{(n)}(t) = \left(\frac{\mathbf{X}^{(n)}(t)}{X_p^{(n)}(t)} \right), \quad \text{where } \mathbf{X}^{(n)} = [X_1^{(n)}, X_2^{(n)}, \dots, X_N^{(n)}]^T \quad (7.3)$$

7.2.2 Bilinear Systems

In the case of a bilinear system, the instantaneous frequency and amplitude of the response

change very fast. However, a decomposition of the response similar to the modal decomposition is still possible. The meaning of the identified instantaneous modal frequency and normalized mode shape needs to be discussed here. Without loss of generality, this discussion will be focused on a bilinear single degree-of freedom (SDOF) system subjected to impulse excitation. The SDOF was selected because of its simple mathematical form of the response. The dynamics of such a system is given by:

$$M(t)\{\ddot{x}\} + C_d(t)\{\dot{x}\} + Rf(x,t) = F(t) \quad (7.4)$$

where $Rf(x,t)$ is the restoring force, shown in Fig. 7.1.

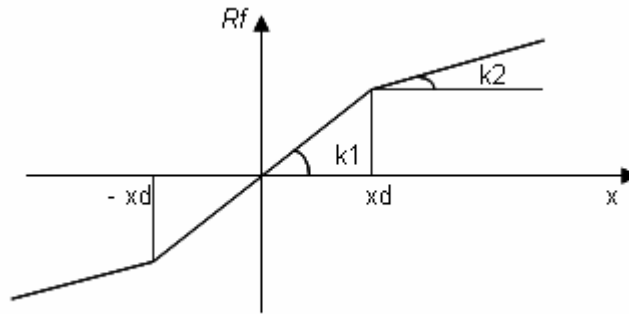


Figure 7.1. Bilinear restoring force

The bilinear system can be treated as a piecewise linear system with two natural frequencies in different ranges of the displacement response, as expressed in eq. (7.5).

$$f = \begin{cases} f_1 = 1/2\pi\sqrt{k_1/m} & |x| \leq x_d \\ f_2 = 1/2\pi\sqrt{k_2/m} & |x| > x_d \end{cases} \quad (7.5)$$

It is intuitive that the duration of the response with a constant frequency, f_i , could be less than a period, i.e. $1/(2f_i)$. Because each CWT coefficient reflects the energy of the signal in a window whose size is governed by uncertainty principle, the fast changes in the signal frequency are locally averaged on CWT map. By CWT, the response is mapped to few components of slower varying frequency and it can be represented as a sum of few vibration modes :

$$x(t) = \sum_n A^{(n)}(t) \cos(\phi^{(n)}(t)) \quad (7.6)$$

Note that for a bilinear system, the instantaneous modal frequency is not necessarily the same as instantaneous frequency of the response, but it reflects the time varying nature of the system in a time-frequency window. For a SDOF bilinear system, the instantaneous modal frequency of the highest energy component is a function of excitation and its value lies between f_1 and f_2 .

7.3 Methodology

The first step in identification of instantaneous modal parameters is to sift out the modal responses, procedure which has been explained in details in the previous chapters. Because we are interested in the nature of instantaneous modal parameters of a system with possible nonlinearities, instead of wavelet packet sifting technique we prefer CWT and its inverse, which give a better visual representation. Details regarding CWT have been given in Chapter 2; therefore, only the mathematical formula and the issues relevant for the study in this chapter are included herein.

The CWT of a signal $x(t)$ is given by:

$$W_x(a, b) = \int_{-\infty}^{+\infty} x(t) \psi_{a,b}^*(t) dt = \frac{1}{\sqrt{a}} \int_{-\infty}^{+\infty} x(t) \psi^*\left(\frac{t-b}{a}\right) dt, \quad x \in L^2 \quad (7.7)$$

The CWT coefficients, $W_x(a, b)$, are localized in a time-frequency window, whose size is characterized by the temporal variance σ_t and frequency variance σ_f . The complex Morlet wavelet, defined in eq. (7.8), is chosen as the mother wavelet in the present study, because it gives an optimal window for time and frequency localization, i.e. $\sigma_t \sigma_f = 1/4\pi$.

$$\psi(t) = \frac{1}{\sqrt{\pi F_b}} \exp\left(-\frac{t^2}{F_b}\right) \exp(2i\pi F_c t) \quad (7.8)$$

F_c and F_b are the center frequency and the bandwidth parameter, respectively, and are real and positive. The temporal and frequency variances of this wavelet function are given in eq. (7.9).

$$\sigma_t = \frac{\sqrt{Fb}}{2}, \quad \sigma_f = \frac{1}{2\pi\sqrt{Fb}} \quad (7.9)$$

The effective duration (Δt) and effective frequency width (Δf) are calculated by the expressions $\Delta t = \sqrt{2\pi}\sigma_t$ and $\Delta f = \sqrt{2\pi}\sigma_f$. With complex Morlet wavelet as mother wavelet, the CWT coefficients $W_x(a,b)$ reflects the energy of the signal $x(t)$ in a time frequency window defined by:

$$\left[b - a \frac{\Delta t}{2}, b + a \frac{\Delta t}{2} \right] \times \left[\frac{Fc}{a} - \frac{1}{a} \frac{\Delta f}{2}, \frac{Fc}{a} + \frac{1}{a} \frac{\Delta f}{2} \right] \quad (7.10)$$

In this study, the wavelet parameters, Fb and Fc , are chosen so that they guaranty a good time localization, as well as a clear separation of the vibration modes on the CWT map. $Fc=200\text{Hz}$ and $Fb= 0.0005\text{s}^2$ are considered. The time increment used in simulation is $dt=0.01\text{s}$.

The significant vibration modes are identified as high-energy bands on CWT map. The modal components of the vibration response are reconstructed by inverse continuous wavelet transform calculated for each selected scale range as:

$$x^{(n)}(t) = \frac{1}{C_\psi} \int_{a_1}^{a_2} \int_{-\infty}^{+\infty} (W_x)(a,b) \psi\left(\frac{t-b}{a}\right) \frac{1}{a^2} da db \quad (7.11)$$

where a_1 and a_2 are scales which delimit the n^{th} band of high energy on the CWT map of the signal $x(t)$.

The instantaneous frequency of the component $x^{(n)}(t)$, and its analytic amplitude are obtained from the polar representation of the corresponding analytic signal obtained by HT.

$$\tilde{x}_j^{(n)}(t) = x_j^{(n)}(t) + iHT(x_j^{(n)}(t)) = \tilde{A}_j^{(n)}(t) \text{Exp}(i\tilde{\phi}_j^{(n)}(t)) \quad (7.12)$$

The instantaneous frequency is defined as the rate of change of the phase angle $\tilde{\phi}_j^{(n)}(t)$. The instantaneous normalized mode shape is calculated as ratio of analytic amplitudes: $X_{j,p}^{(n)}(t) = \tilde{A}_j^{(n)}(t) / \tilde{A}_p^{(n)}(t)$.

7.4 Applications: A 2DOF Mass-spring-dashpot System

7.4.1 Simulation Set-up

A two degree-of-freedom spring-mass-dashpot system with spring elements of different nature is considered. The baseline (S1) is a time invariant linear system, sketched in Fig. 7.2(a), with $M_1=M_2=200\text{kg}$ and $K_1=K_2=100000\text{N/m}$. The system is assumed undamped or with Rayleigh damping. In the case of Rayleigh damping, the damping matrix is proportional to the stiffness matrix with a factor of 0.0005s . The natural frequencies of this system are 2.2 Hz and 5.7 Hz . By changing the evolution of the spring stiffness or restoring forces, three more study cases are developed as follows:

- (S2) a linear system with damage where the stiffness K_2 degrades progressively as illustrated in Fig. 7.3(b). Damage develops after 5 seconds from the initial time.
- (S3) a system with a bilinear restoring force for the spring K_1 , as illustrated in Fig. 7.3(a).
- (S4) a bilinear system with damage, composed by a bilinear spring K_1 , as shown in Fig. 7.3(a) and a spring K_2 with progressive stiffness degradation, as shown in Fig. 7.3(b).

Two types of excitations are considered: (1) impulse excitation, simulated by a nonzero initial velocity at M_2 and (2) a base harmonic excitation of frequency 1 Hz .

The responses are simulated using the Runge-Kutta method with an integration step of 0.01 seconds.

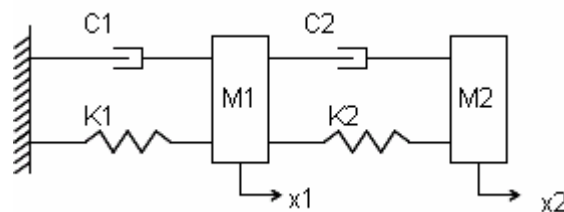


Figure 7.2. Sketch of the system

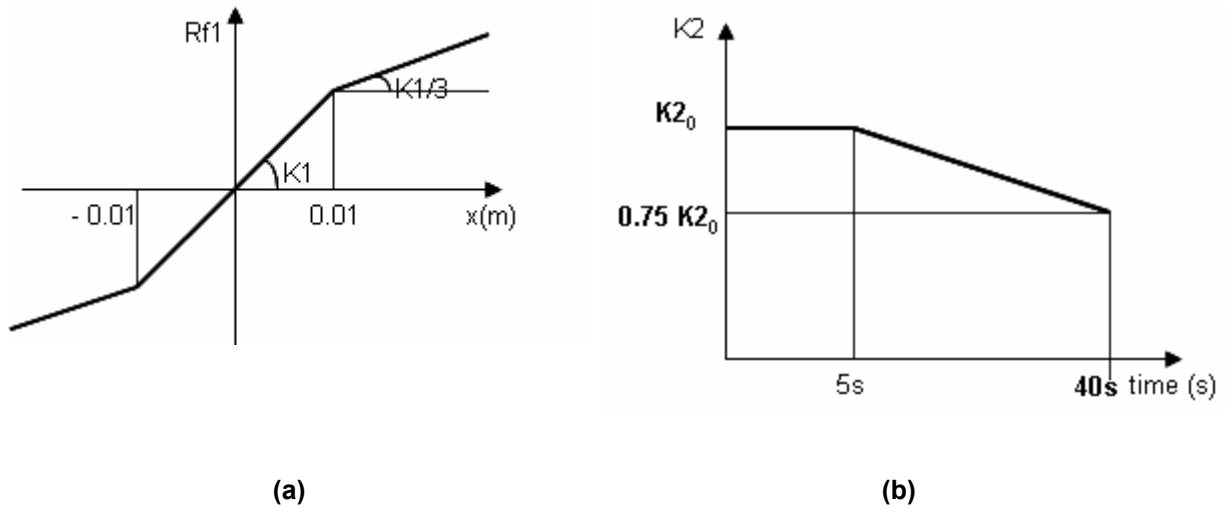


Figure 7.3. (a) Restoring force; (b) Stiffness history in the case of progressive damage

7.4.2 Results - Impulse Excitation

First, the response due to an impulse excitation is simulated for each type of system, considering the zero damping case. For the linear system and the system with progressive stiffness degradation, two bands of high energy can be identified on the CWT maps. For illustration, CWT maps of the displacement response measured at M1 are shown in Fig. 7.4(a) for the linear system (S1) and Fig. 7.4(b) for the system with progressive damage (S2). Each high-energy band corresponds to a vibration mode. The identified instantaneous modal frequency and normalized mode shape are plotted in Figs. 7.5(a) and 7.5(b). As expected, the instantaneous modal parameters are constant for the case of a linear healthy system. In the case of progressive damage, the frequency decays slowly starting at $t=5$ s, when damage has been introduced in the simulation. The normalized instantaneous mode shape at mass M2 increases for the first vibration mode and decreases for the second vibration mode. A continuous change in the normalized instantaneous mode shape is an indication of progressive change in the system parameters.

Figures 7.4(c) and 7.4(d) show the CWT map of a healthy bilinear system (S3) and of a bilinear system with damage (S4). Here, three bands of high energy can be observed. By examining only this CWT map, it is difficult to make a difference between a 2DOF bilinear system and a multi-degree of freedom linear system with a low excited first mode.

The wavy appearance of the band corresponding to scales around 35-40 is a result of interference between signal components with closely spaced modal frequencies. It can be observed that the bilinear healthy system (S3) presents an evolution of its instantaneous modal parameters similar to that of the healthy system (S1), as long as the instantaneous modal parameters of the bilinear damaged system (S4) is similar to that of damaged linear system (S2). The average effective duration and frequency width of the wavelet window is: 0.2Hz x 2.52s for the first vibration mode and 0.5Hz x 0.98s for the second vibration mode.

A damped bilinear system has a behavior similar to that of system with progressive increase of stiffness as illustrated in Figs. 7.6 and 7.7. The bilinear behavior can be observed over the first 15 seconds of the response. Then, due to the small amplitude of the response, the systems remains in the first linear regime and the instantaneous modal parameters are constant. The increase of instantaneous modal frequency is an indication of nonlinear elastic behavior, since damage consists, in most of the cases, in reducing of the instantaneous modal frequency. However, in the case of systems with other type of nonlinearities a conclusion based only on the evolution of modal parameters could be misleading.

7.4.3 Results - Harmonic Excitation

Another study case is when a harmonic excitation of frequency of 1Hz is applied as a base excitation. In this case, as can be seen from the CWT maps in Fig. 7.8, there are two bands of high energy. The band around scale of 200 corresponds to the forced response and that around scale of 100 corresponds to the first vibration mode, which is predominantly excited.

If the system has a bilinear spring (S3 and S4) some other harmonics of low energy can be observed on the CWT map, for example around scale of 70. Also, the second mode, placed around scale 35, is excited for the whole time period and it does not decay to zero due to damping as in the case of linear system. However, its energy is very low, which makes the identification difficult. Plots of identified modal parameters of the first vibration mode are shown in Fig. 7.9. It can be observed that, if damage is present, there is a clear

trend in their evolution for both, linear as well as bilinear systems; the instantaneous modal frequency decreases and the normalized instantaneous mode shape increases.

7.5 Summary

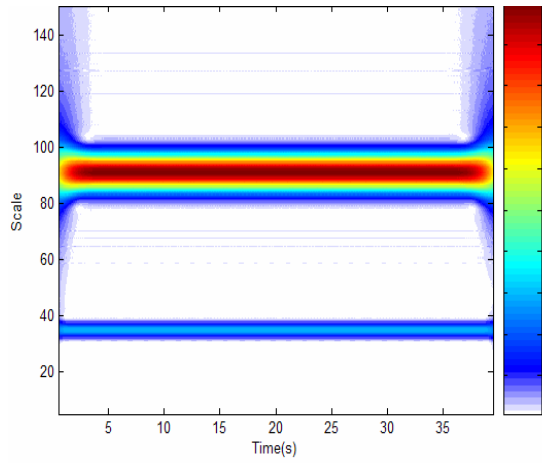
This chapter presents a preliminary study on the meaning of instantaneous modal parameters and their use for SHM of systems with nonlinear dynamic behavior.

Systems of different natures of the restoring forces are discussed, including linear invariant systems, a linear system with slow stiffness degradation and/or a bilinear restoring force. Both, the impulsive and harmonic loading is considered. In this study, the displacement responses are used for analysis, but the results remain the same for the acceleration data.

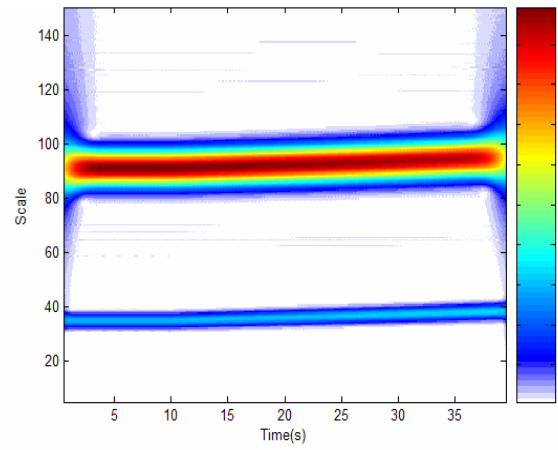
For a linear healthy structural system, the instantaneous modal parameters remain constant whereas, for a system with slowly varying stiffness degradation, they demonstrate an evolution from their healthy status. A bilinear healthy system under a harmonic excitation has an evolution of its instantaneous modal frequency and normalized instantaneous mode shape similar to that of the healthy system, as long as the instantaneous modal parameters of the bilinear damaged system behave similar to those of a linear damaged system. For a damped bilinear system subjected to an impulsive force, the modal instantaneous frequency might increase with time due to the decaying amplitude of the vibration, in contrast to the decreasing trend of the instantaneous modal frequency in the case of a damaged system.

Also, it should be reemphasized that the identified instantaneous modal frequency of a bilinear system is not necessary the same as instantaneous frequency of the response; however its trend reflects the permanent change in the system stiffness and therefore can be used for structural health monitoring. For a correct interpretation of the identified results, especially in case of bilinear systems, one should take into account the effective duration and effective frequency width of the analyzing wavelet.

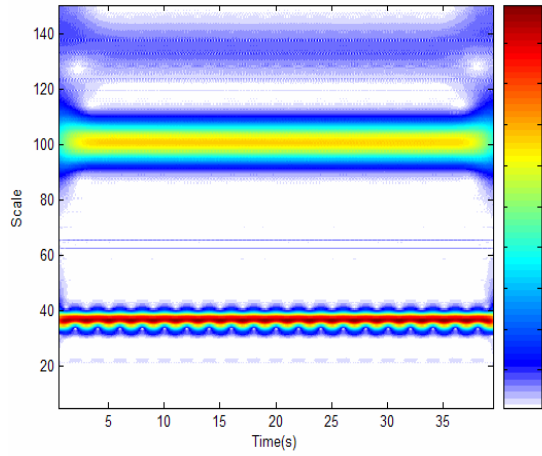
A more elaborated study which includes different types of nonlinearities in a real system and nonstationary excitations is proposed for the future work.



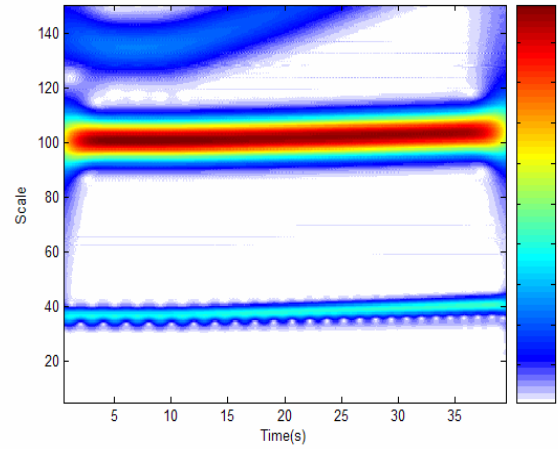
(a)



(b)



(c)



(d)

Figure 7.4. CWT map of the displacement response measured at M1, zero damping, impulse excitation; (a) linear system (S1); (b) linear system with damage (S2); (c) bilinear system (S3); (d) bilinear system with damage (S4)

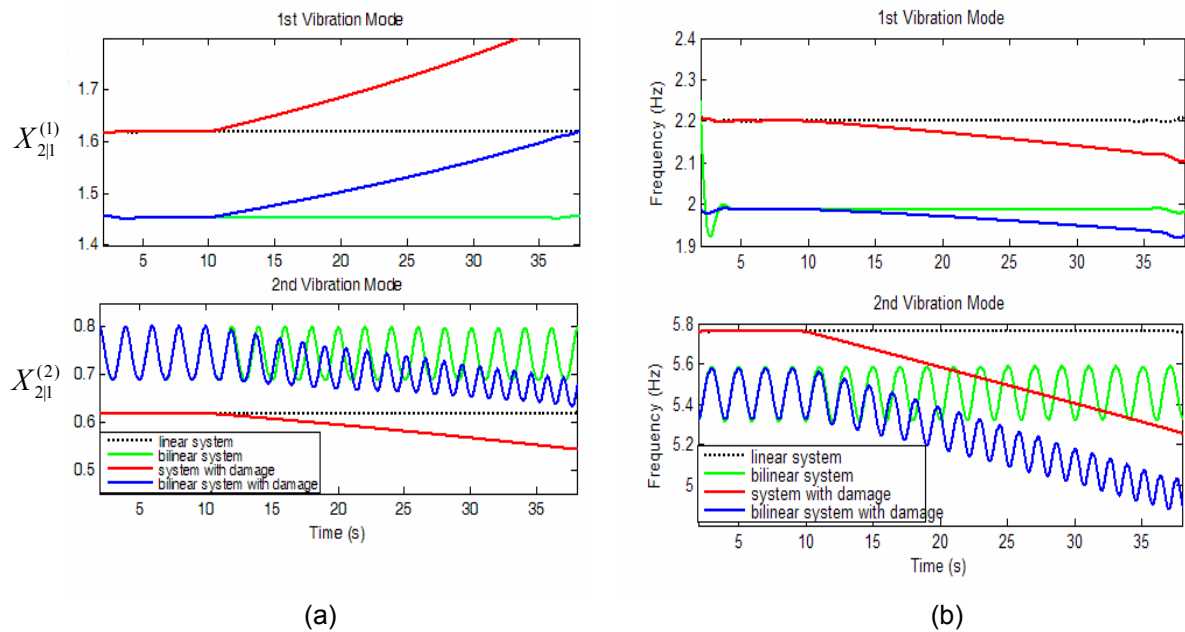


Figure 7.5. (a) Instantaneous mode shape and (b) instantaneous frequency, for systems of different nature in case of impulse excitation.

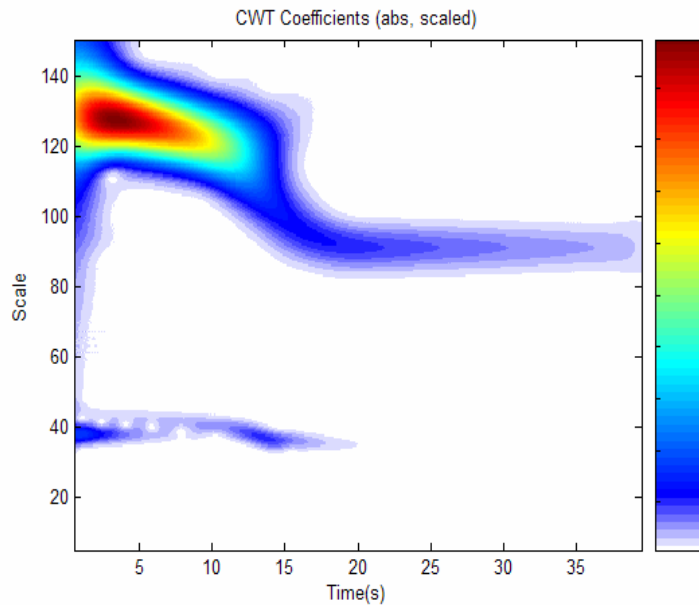


Figure 7.6. CWT map of the displacement response measured at M1, for a bilinear system with damping, subjected to impulse excitation

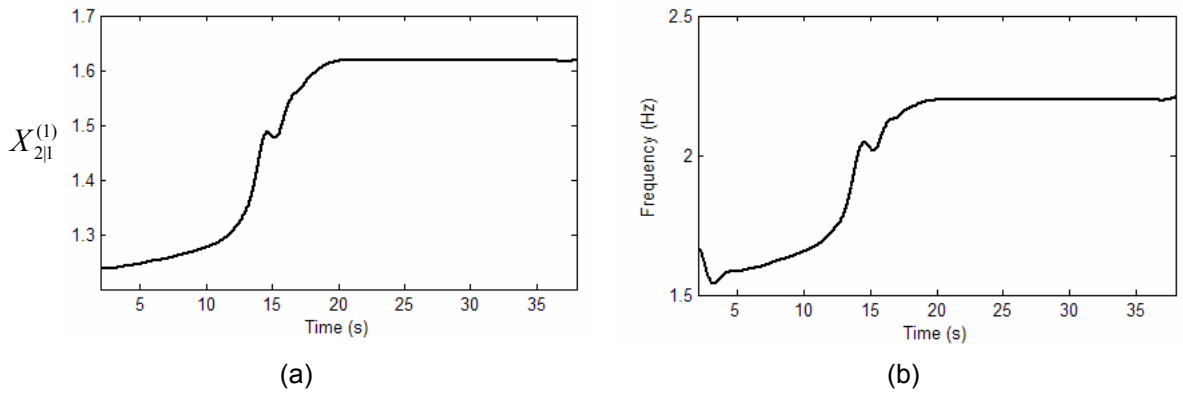


Figure 7.7. Normalized Instantaneous mode shape and instantaneous frequency for the first vibration mode in case of a bilinear system with damping, subjected to impulse excitation

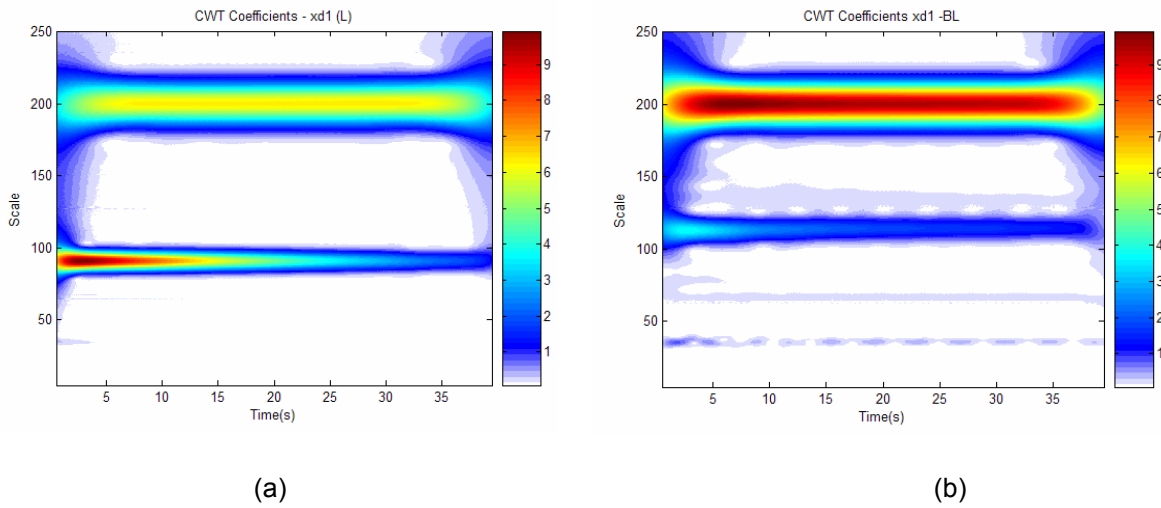


Figure 7.8. CWT map of the displacement response measured at M1, harmonic excitation (a) linear system (S1), (b) bilinear system (S3);

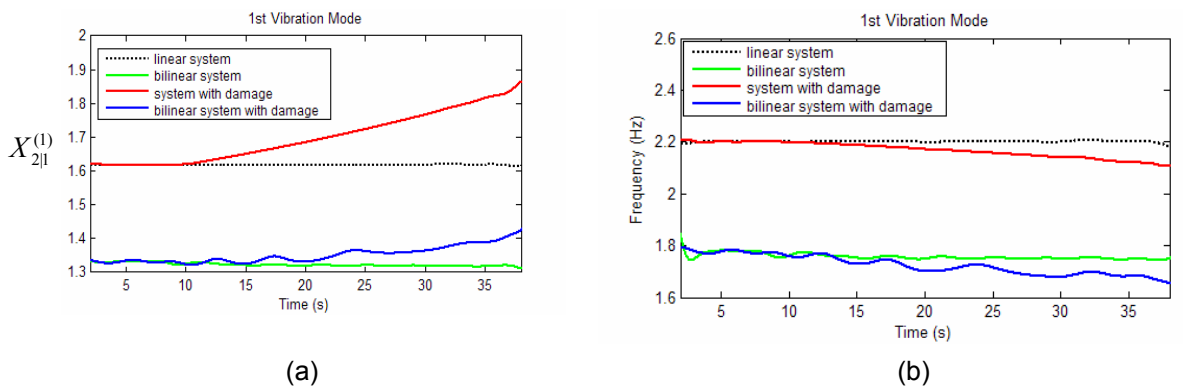


Figure 7.9. (a) Instantaneous mode shape and (b) instantaneous frequency for a system with damping subjected to a harmonic excitation

Chapter 8

APPLICATIONS TO EXPERIMENTAL DATA

8.1 Introduction

In Chapters 4, 5 and 6, instantaneous modal parameters, identified by wavelet approach, have been proposed to be used for SHM and damage detection. The methods have been tested on simulation data and good results were obtained. However, various factors such as modeling errors, signal contamination by noise, insufficient measurement data, structural nonlinearities, insensitivity to local damage etc. might have significant impact on practical applications of the approaches. The purpose of this study is to evaluate the performance of the proposed approaches using the experimental data from:

1. ASCE- SHM benchmark studies, Phase 2 of the experiments performed on August 4-7, 2002, at the University of British Columbia. Various loadings were applied to the prototype structure and data of two hammer tests, before and after damage, are analyzed in present study. Damage was introduced between tests by removing some braces between floors.

2. a shaking table test of a full-size two-story wooden building structure, conducted at the Disaster Prevention Research Institute, Kyoto University, Japan, on June 22, 2000. The structure was excited by the 1940 El Centro Earthquake ground motion (NS component) scaled at several target levels and the tests were run step by step from small scales up to large ones until the structure lost its load-carrying capacity. Damages to various extents were observed during the tests.

8.2 ASCE SHM Benchmark Study

To coordinate research activities in the area of system identification and damage detection a benchmark study was proposed by the ASCE Task Group on Health Monitoring (Johnson et al., 2004). The CWT ridge method, proposed in Chapter 4 to identify the instantaneous modal parameters, is applied for simulation and experimental data from this benchmark study. Change in the identified instantaneous modal parameters may indicate damage into the structure.

8.2.1 Description of the Structure

This section provides a brief description of the structure used in the benchmark study. For detailed information, the reader is referred to Johnson, et al (2004) and the SHM Group's web page (<http://wusceel.cive.wustl.edu/asce.shm/>).

The structure is a scaled model of a 4 story building, consisting of a two-bay by two-bay steel-frame with a total height of 3.6m and a plan of 2.5m x 2.5 m, as shown in Fig. 8.2.1. Each story is composed by 9 columns of 0.9 m in height, 12 beams of 1.25m in length, 8 lateral braces and 4 floor weights (one per bay). The weights of the first floor are 800 kg and those on the second and the third floors are 600 kg. On the fourth floor, there are either four identical weights of 400 kg for a symmetric model or three weights of 400 kg and the fourth one of 550 kg in order to create some asymmetry in the structure; the symmetric model is employed in this study. All members are hot rolled steel with nominal yield stress of 300 MPa.

8.2.2 Simulation Data Results

The methodology proposed in Chapter 4, for the case of impulse or free vibration responses, is validated, first, for simulation data. In the present study, the response of the structure during a hammer test is simulated. Damping was ignored. The hit was applied at the first floor in the x direction (Fig.8.2.1b). No damage occurred during the first 10 seconds. A gradual damage was introduced in the time interval from 10 to 30 seconds. Damage consists in a linear degradation of the material properties represented by

the Young's modulus of the braces of the fourth floor. During a time interval of 20 seconds, the Young's modulus is reduced linearly by 25%. Afterwards, for the next 10 seconds, no new damage occurred. The time increment used in simulation is $dt=0.005$ seconds. The response is obtained based on the FEM model for 12DOF system, provided by the Task Group for Phase II study. Since the model used in this simulation describes a symmetrical structure about both x and y directions, only the acceleration response in the x -direction, i.e. the direction of the excitation, is of interest. The CWT ridge method is then applied to find the instantaneous modal frequencies and the normalized instantaneous mode shapes. The results are in good agreement with the stiffness degradation assumed in the simulation of the response data.

Figure 8.2.1 presents a map of the modulus of CWT coefficients. The CWT is performed on the acceleration response of the fourth floor with a scale range from 1 to 150, which corresponds to a frequency range from 100Hz to 6.6Hz. The complex Morlet wavelet with $F_c=5/dt=1000$, and $F_b=dt^2 = 2.5 \cdot 10^{-5}$, is chosen as mother wavelet. The computational noise in CWT results is removed by a filtering technique applied, first, in scale domain and then in time domain. Three bands of high value coefficients can be identified, therefore in this scale range there are three dominant wavelet ridges. The first band corresponds to the scales from 100 to 130, the second band is from 35 to 50, and the last band is from 20 to 30.

In order to improve the accuracy of the results, and in the same time to reduce the computational effort, the CWT is performed separately for each of the observed bands with a smaller scale increment. After identifying the ridges, the relevant instantaneous modal frequencies are calculated by formula 4.14. The results are plotted in Fig.8.2.3 and Fig.8.2.4. It can be observed that the instantaneous modal frequencies are constant for the first 10s, then slowly decrease as a result of the stiffness degradation, and are again constant after time equals to 30s. This observed behavior describes exactly the damage scenario used in the data simulation. Since damage evolves slowly, the obtained results should be comparable to those calculated by modal analysis if the system parameters at the each specific time instant are frozen. More accurate results for comparison can be obtained by solving the dynamic eigen-value problem for this time-varying system. Due to the computational burden in solving the dynamic eigenvalue problem, the first approach was preferred.

Table(8.2.1) shows the comparison for the modal frequencies. Good agreement is obtained, the relative errors between the modal frequencies obtained by these two methods are between -0.5% and 0.5%.

The normalized instantaneous mode shapes are calculated for the first three identified vibration modes. The instantaneous mode shape is normalized by the mode shape component corresponding to the fourth floor, therefore the IN mode shape vector can be expressed as: $X_{n,1}^{(i)} = [1 \quad X_{2,1}^{(i)} \quad X_{3,1}^{(i)} \quad X_{4,1}^{(i)}]^T$, where $i=1,2,3$.

The results are plotted in Fig.8.2.5. A comparison of the results by CWT and modal analysis is presented in Table(8.2,2). The relative error between normalized mode shapes calculated by CWT ridge and those obtained by modal analyses is smaller than 5%.

It should be noted that in Fig.8.2.3(b) the component corresponding to the third floor of the modal shape vector of the second mode is broken between $t = 14$ and 23 seconds. An interpretation may be given based on Fig.8.2.5 that plots the wavelet coefficient map of the acceleration response of the third floor zoomed in the scale range corresponding to the second vibration mode. The low amplitude of the CWT coefficients in the time interval mentioned above indicates that participation of the second modal component in the third floor response is insignificant in this transition stage when its value changes from positive to negative. The contribution of the second vibration mode to the response is in fact of the order of computational noise, therefore the second mode shape component becomes very difficult to identify. Similarly, on the CWT coefficient map of the second floor response plotted in Fig.8.2.6, the ridge cannot be identified in the scale range of 22 to 30 and time interval from 25s to 40s.

Time (sec)	Vibration Mode / frequency (Hz)					
	1 st mode		2 nd mode		3 rd mode	
	CWT	Modal analysis	CWT	Modal analysis	CWT	Modal analysis
5	8.85	8.8655	25.12	25.1488	40.98	41.1072
20	8.77	8.7842	23.81	23.8330	38.53	38.5617
35	8.58	8.604	21.27	21.315	35.84	35.853

Table 8.2.1. Comparison of the modal frequency results obtained by CWT and modal analysis

Time (sec)		Vibration mode					
		1 st mode		2 nd mode		3 rd mode	
		CWT	Modal analysis	CWT	Modal analysis	CWT	Modal analysis
5	1 st floor	0.28	0.284	-0.79	-0.797	0.93	0.933
	2 nd floor	0.62	0.618	-0.79	-0.792	-0.48	-0.485
	3 rd floor	0.86	0.864	0.12	0.120	-0.84	-0.842
	4 th floor	1	1	1	1	1	1
20	1 st floor	0.27	0.270	-0.66	-0.662	1.07	1.072
	2 nd floor	0.59	0.588	-0.73	-0.739	-0.30	-0.300
	3 rd floor	0.83	0.829	N/A	0.018	-1.06	-1.064
	4 th floor	1	1	1	1	1	1
35	1 st floor	0.24	0.241	-0.51	-0.514	1.51	1.516
	2 nd floor	0.52	0.527	-0.69	-0.690	N/A	-3.544
	3 rd floor	0.75	0.759	-0.20	-0.206	-1.50	-1.502
	4 th floor	1	1	1	1	1	1

Table 8.2.2. Comparison of the normalized instantaneous mode shapes results obtained by CWT and modal analysis

8.2.3 Experimental Data Results

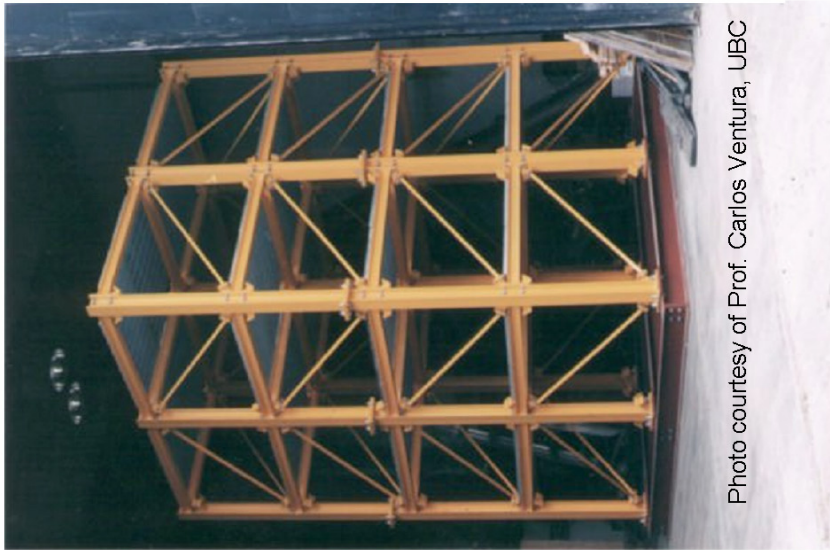
The validation in the previous subsection, was performed in conditions of zero measurement noise and undamped structure. In order to test the efficiency of the method for practical applications, the methodology presented in Chapter 4 is also applied for experimental data from the ASCE benchmark studies (<http://wusceel.cive.wustl.edu/asce.shm/benchmarks.htm>). The structure used in the experiment is shown in fig. 1(a). Damage was introduced by removing some braces between tests. Various loadings were applied to the prototype structure and the acceleration responses at all four floors were recorded during tests. In the present study only data of two hammer tests, before and after damage, are analyzed. Since damage was introduced between two runs, the structure is in fact piecewise invariant. To investigate the performance of the proposed methodology in experimental conditions, the approach is applied to these data by considering the time invariant structure as a special case of time varying systems.

Instantaneous modal frequencies and normalized instantaneous mode shapes are identified, by CWT ridge method. A change in their value is an indication that damage occurred.

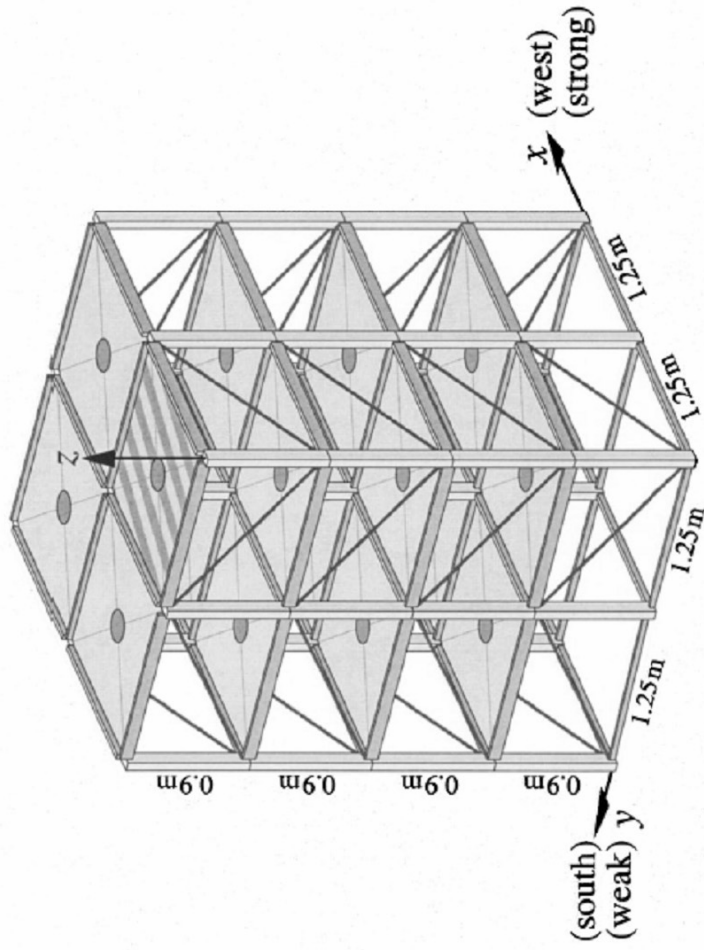
During the first test, the hammer hit was applied at the first floor on east face, south side column, inside flange, in north direction. First the undamaged structure, configuration no. 1 in the benchmark study, is subjected to the test. The sampling frequency is 1000Hz. In the paper are analyzed the responses measured in north direction on west side at each floor. CWT with Complex Morlet wavelet as mother wavelet is performed on the measured responses. The parameters of the mother wavelet are: $F_c = 5/dt = 5000$ and $F_b = dt^2 = 10^6$. Few high value coefficient bands are observed on the CWT coefficient map, as can be seen in Fig. 8.2.7, which plots the CWT of the acceleration response measured at the 1st floor. We concentrate the attention on the last ridge corresponding to the scale interval between 300 and 400, which represents a vibration mode with the lowest identified modal frequency.

The instantaneous frequency determined by analyzing the response measured at each floor is presented in Fig.8.2.8. As it can be seen, the results are in good agreement with each other. Small differences can be due to the measurement noise and wavelet transform end effects at the beginning and end of the time interval. The frequency is approximately constant, 14.44Hz, which is an indication that damage does not occur during test. Also, the normalized instantaneous mode shape is constant, as can be seen from Fig.8.2.9.

During the second test, a damaged structure is considered. Damage was simulated by removing all east side braces (configuration no. 2), immediately after the first test. A comparison between instantaneous frequency for damaged and undamaged structure is presented in Fig. 8.2.10. It can be observed that the modal frequency decreased to 12.69 Hz. The same comparison is performed for the normalized instantaneous mode shape, as shown in Fig.8.2.11. It can be observed a change in the second and the third component of the NI mode shape vector.



(a)



(b)

Figure 8.2.1. The prototype structure of ASCE health monitoring benchmark studies. (a) the picture of the test structure at the University of British Columbia test structure <http://cive.seas.wustl.edu/wusceel/asce.shm/structure.htm>; (b) schematic drawing (Johnson, et al., 2004)

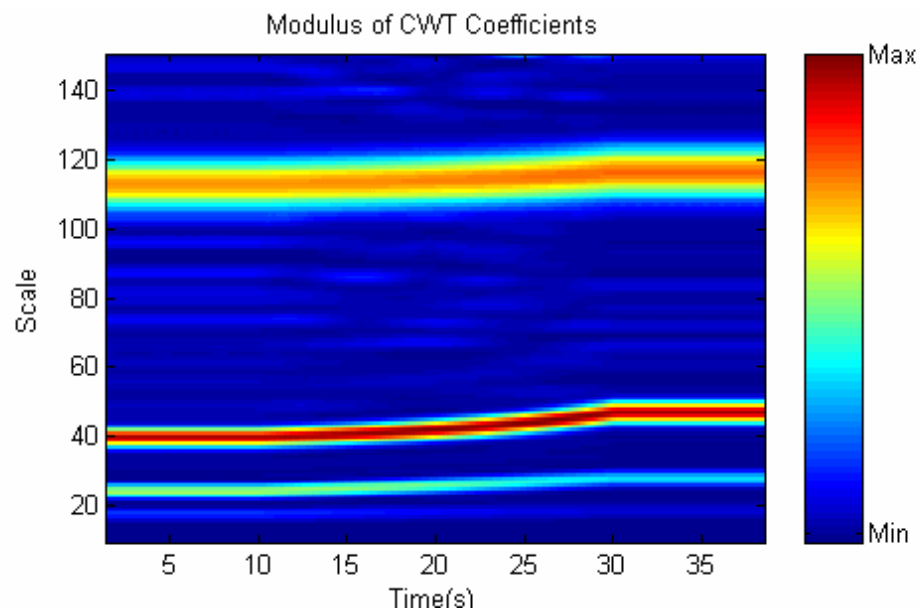


Figure 8.2.2. Map of CWT coefficient modulus of the acceleration response measured at the 4th floor

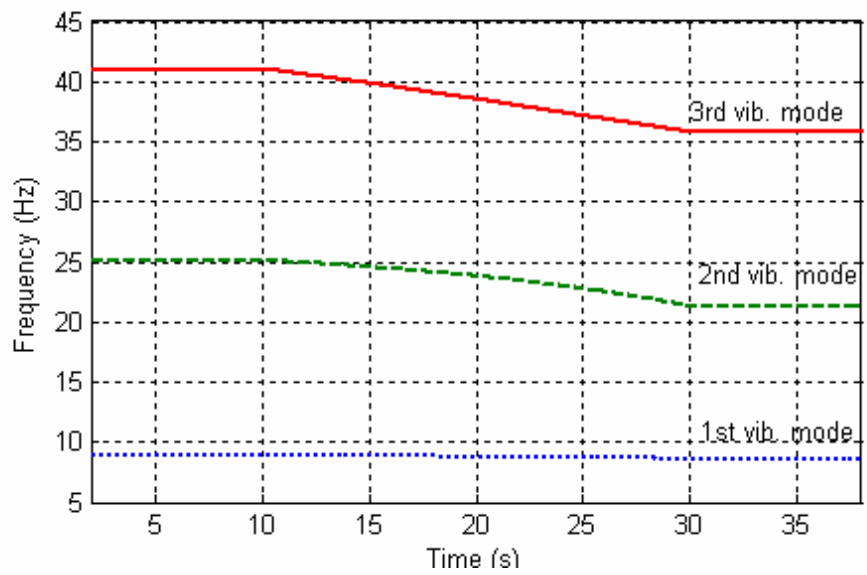


Figure 8.2.3. Instantaneous modal frequency for the first three vibration modes

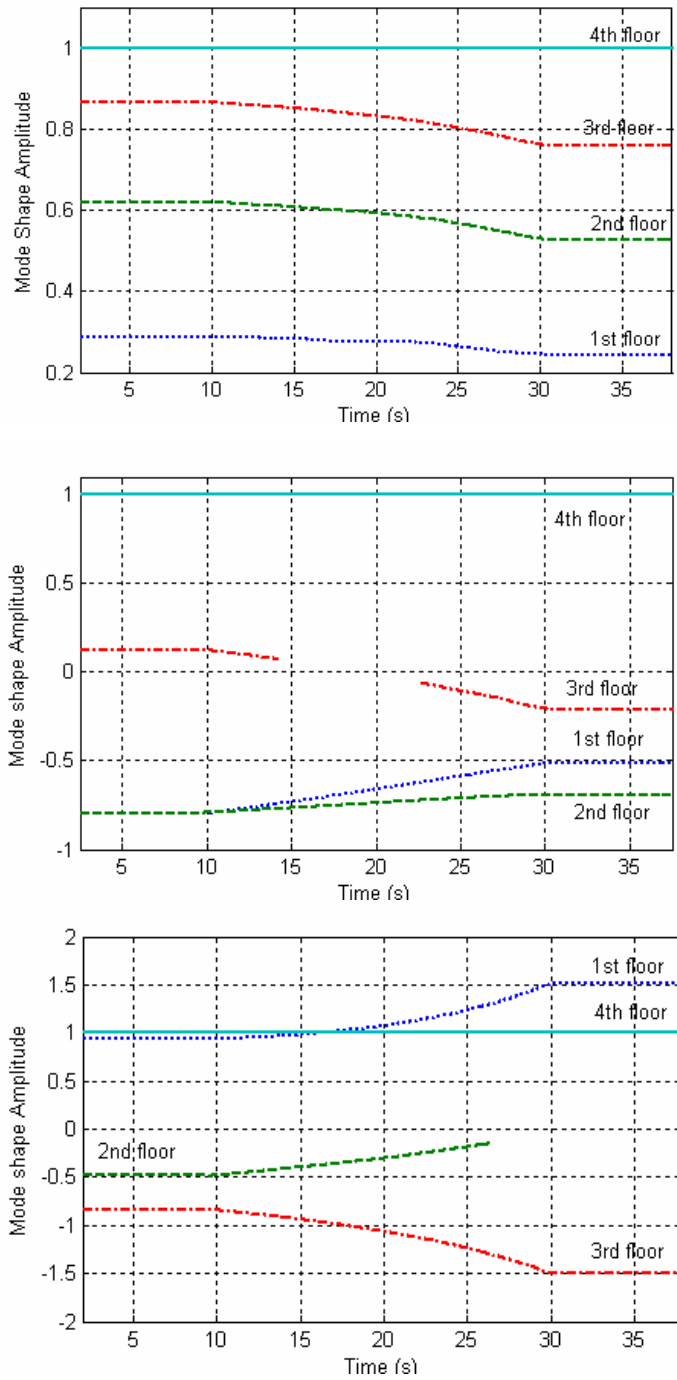


Figure 8.2.4. The normalized instantaneous mode shape; (a) the first vibration mode; (b) the second vibration mode; (c) the third vibration mode

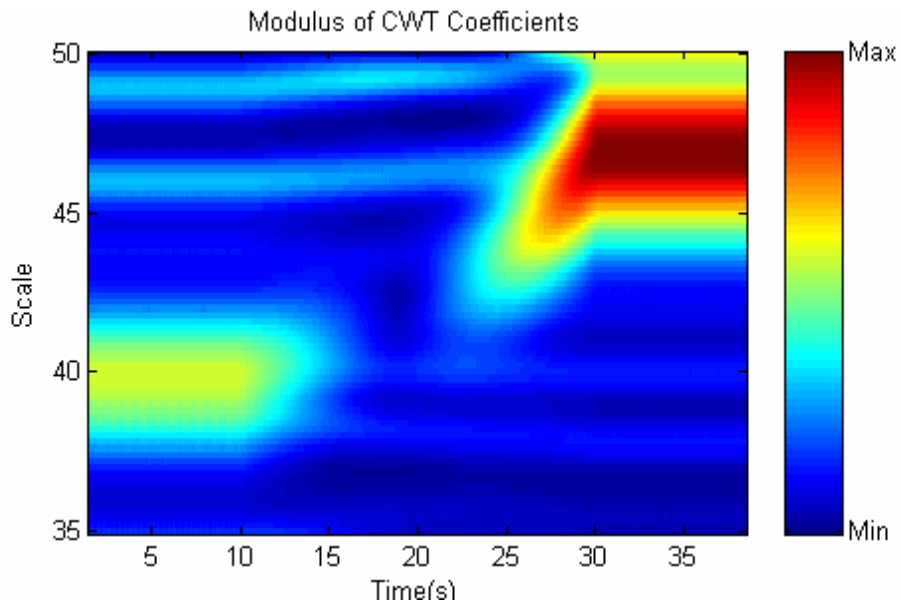


Figure 8.2.5. Map of the modulus of the CWT transform coefficients of the response measured at the 3rd floor.

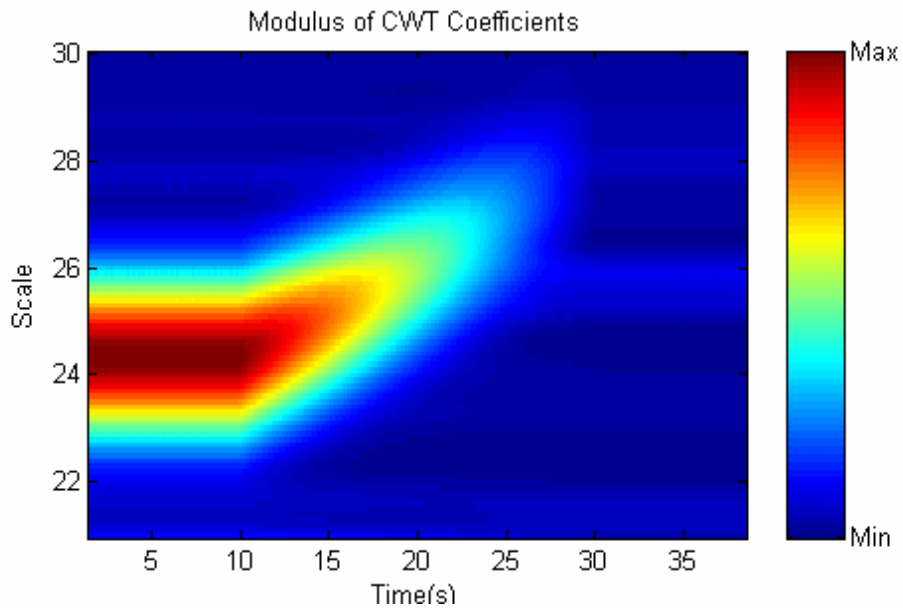


Figure 8.2.6. Map of the modulus of the CWT transform coefficients of the response measured at the 2nd floor.

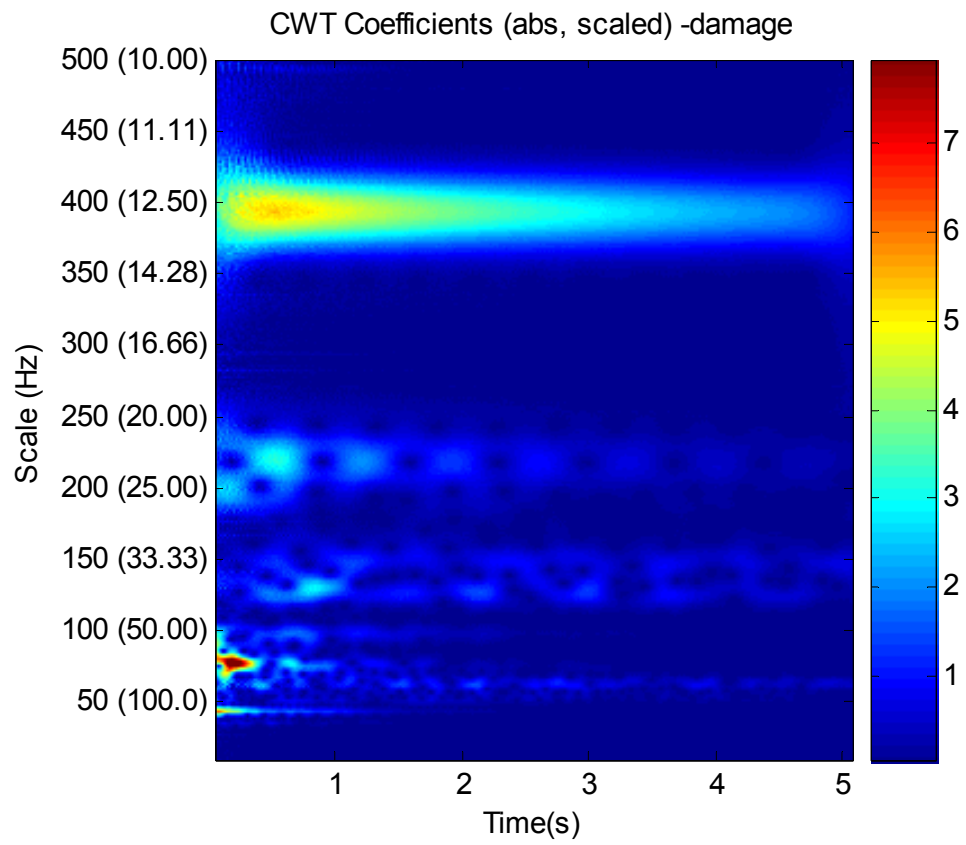


Figure 8.2.7. CWT of the response measured at the first story in North direction

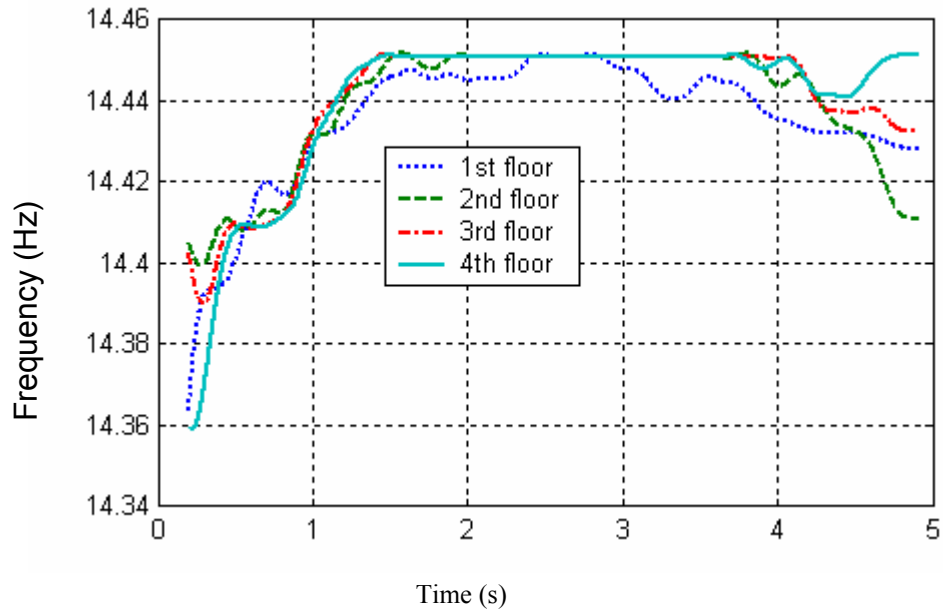


Figure 8.2.8. Instantaneous modal frequency by analyzing the response at each floor of undamaged structure

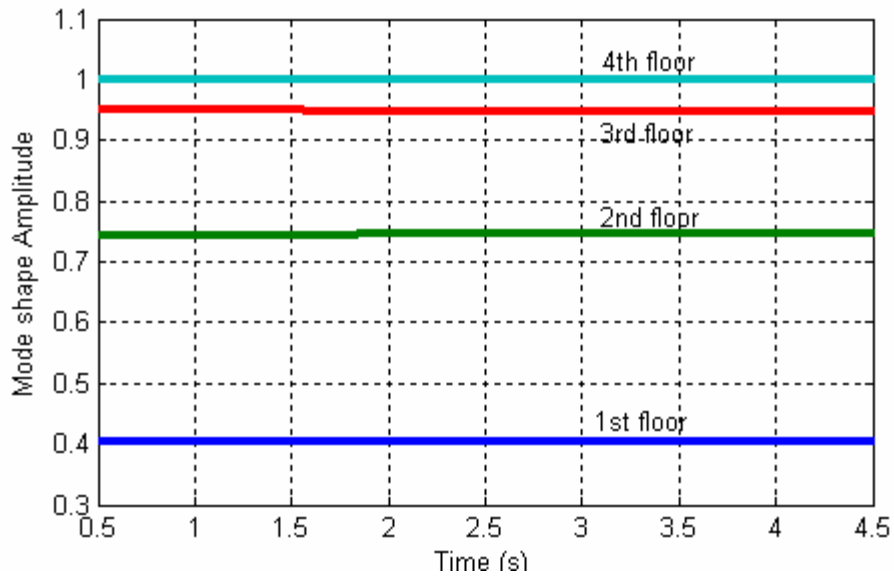


Figure 8.2.9. Normalized instantaneous mode shapes of undamaged structure.

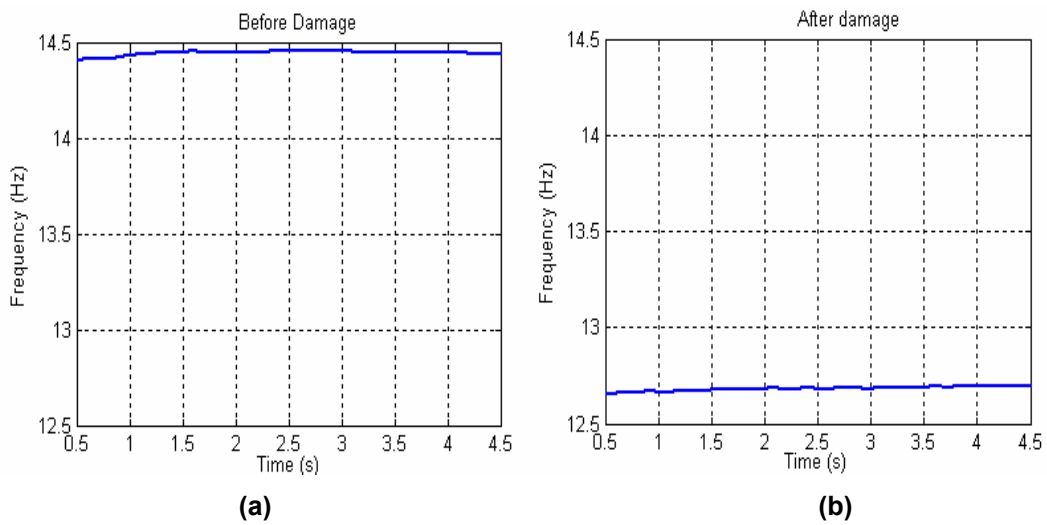


Figure 8.2.10 Instantaneous modal frequency (a) configuration no.1, undamaged structure; (b) configuration no.2 – damaged structure

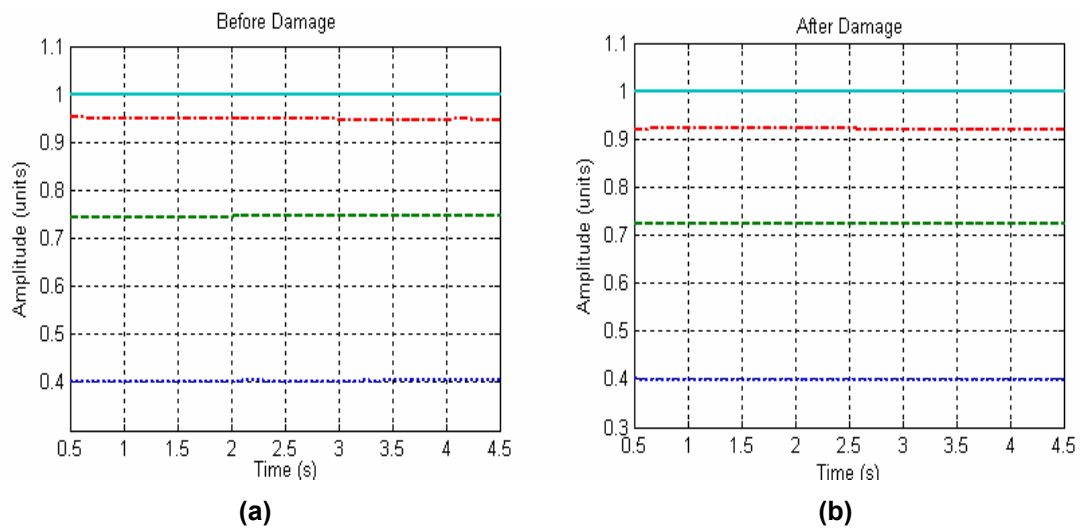


Figure 8.2.11. Normalized Instantaneous mode shape (a) configuration no1, undamaged structure; (b) configuration no.2 – damaged structure

8.3 Shaking Table Test of a Wooden Building Structure

The approaches presented in Chapter 5 and 6 are applied for data from a shaking table test of a full-size wooden building frame conducted at the Disaster Prevention Research Institute (DPRI), Kyoto University, on September 22, 2000.

The integrated Kalman filter and wavelet packet sifting process is used to estimate the instantaneous natural frequencies; wavelet packet decomposition in conjunction with the confidence index is employed to identify the normalized instantaneous mode shape. The results obtained from the evaluation of the instantaneous natural frequency agree quite well with the qualitative description of damage from the filed observation, however the normalized instantaneous mode shape presents high oscillation which makes it less reliable for SHM.

8.3.1. Experimental Setup

This section includes a brief description of the testing structure, facilities, test procedure, and some related results. For details of the shaking table test the reader is referred to Shimizu, et al (2004).

The specimen has the dimensions of a typical two-story small wooden house in the Kyoto area, that are: 5.46m long, 3.64m wide, and 5.88m high. The frame consists of four 120 mm x 120mm corner-columns erecting from the base through the first floor to the second floor; 105 mm x 105 mm inter-story columns; 105 mm x 240 mm beams; 45 mm x 105 mm wood braces of British-Columbia pine; and 27 mm x 105 mm studs. Steel bars of 2850 kg were added to the first floor to simulate to dead load and steel bars of 3000 kg were added to the second floor to simulate weight of a house above the second floor. Figure 8.3.1 provides an overview of the testing site and the wooden frame specimen on the shaking table.

The shaking table is provided with the ground acceleration signal recorded on NS direction during the 1940 El Centro Earthquake. To observe the seismic behavior of the wooden frame under seismic loading of various intensities, several runs of the test were

conducted. In each test run the frame was excited by the original ground motion record scaled at a *nominal* load level targeted at certain load intensity. The test was run step-by-step from the target level of 1 m/s^2 with 0.5m/s^2 increments until the frame lost its load-carrying capacity. The frame was mainly excited in its longitudinal direction. To study the dynamic behavior of the frame under damage, a few bi-directional loading cases were also conducted, but this uses only data from a single-direction loading cases. It should be pointed out that a target level, say, 1 m/s^2 was set to the input to the shaking table and the output of the shaking table to the frame may not necessarily as the target level due to the shaking table dynamics. The absolute displacement and acceleration responses are recorded during tests.

Before the seismic loading has been applied, several tests using sweeping harmonic and step loading and ambient vibration tests were performed to estimate dynamic characteristics of the wooden frame such as its natural frequencies and modal damping ratios. The results are listed in Table 8.3.1.

Direction	Natural frequencies (Hz)				decay constant
	1 st mode		2 nd mode		
	ambient	step	ambient	step	
Longitudinal	2.3	2.0	7.7	7.3	3.8
Lateral	2.3	2.0	6/8	6/2	3.6

Table 8.3.1 Estimates of the natural frequencies and the modal damping ratio of the wooden frame using ambient vibration and step-loading test (Shimizu et al., 2000)

Damage was developed within the wooden frame during different test runs. When the loading exceeded the target level of 1 m/s^2 , squeezing sound started near brace connections. Hair cracks occurred for braces at their junctions with studs and both ends when the loading exceeded the target level of 2m/s^2 . During the test run with the excitation level of 3.50 m/s^2 a first-story brace was damaged, as shown in Fig. 8.3.2. Then, one brace was damaged during each run of the test at levels of 4m/s^2 , 6m/s^2 , and 8m/s^2 , respectively. When the loading level achieved 10 m/s^2 , cracks occurred on all four corner-columns at

almost the same height, just below the first floor. The structure was viewed losing its loading-carrying capacity and the test stopped at this stage.

8.3.2. Simulation results

Dynamics of real structures subjected to transient loading, as seismic excitation, has complex nature, therefore many practical issues such as measurement noise, structural modeling errors, effects of damage severity and localization of damages, incomplete measurements and observability issues etc, must be properly addressed. A part of these issues has been addressed in Chapter 6, where a two-degree-of-freedom spring-mass-dashpot system has been used to study the applicability of integrated Kalman filter and wavelet packet sifting process for SHM. The excitation was the same as that applied to the wooden house, i.e. 1940 El Centro Earthquake ground motion (NS component) scaled at maximum value of 2m/s^2 . In order to describe the notations used in this chapter, the dynamics of this system is repeated here:

$$\begin{bmatrix} M1 & 0 \\ 0 & M2 \end{bmatrix} \begin{bmatrix} \ddot{u}_1 \\ \ddot{u}_2 \end{bmatrix} + \begin{bmatrix} C_{d1} + C_{d2} & -C_{d2} \\ -C_{d2} & C_{d2} \end{bmatrix} \begin{bmatrix} \dot{u}_1 \\ \dot{u}_2 \end{bmatrix} + \begin{bmatrix} K1 + K2 & -K2 \\ -K2 & K2 \end{bmatrix} \begin{bmatrix} u_1 \\ u_2 \end{bmatrix} = \begin{bmatrix} M1 & 0 \\ 0 & M2 \end{bmatrix} \begin{bmatrix} -1 \\ -1 \end{bmatrix} a_g \quad (8.3.1)$$

where:

u_1, u_2 are the relative displacements in respect to the ground, measured at the first floor and second floor, respectively.

a_g - is the ground excitation, i.e scaled acceleration signal from 1940 El Centro Earthquake ground motion (NS component)

Other notations in this section are x_1, x_2 for the absolute displacements measured at the first and second floor, respectively.

The parameters of this model have been chosen so that the system has a similar dynamic behavior with the wooden house after it has been subjected to the excitation of level 2m/s^2 . The mass M_1 is 2800kg and the mass M_2 is 3000kg. The initial value of the stiffness of each spring is 500 KN/m and the system damping is assumed to be a Rayleigh damping. The damping matrix was chosen proportional to the initial stiffness matrix with a factor of 0.005. The natural frequencies of this system are $f_1=1.278$ Hz and $f_2=3.387$ Hz. In

order to study the applicability of the method for SHM, a damage scenario, consisting of a gradual degradation of inter-story stiffness K_1 , was considered. In Chapter 6, it has been shown that the instantaneous frequency can be identified in condition of measurement noise and partial measurements. The instantaneous mode shape shows some oscillations which can make this quantity not reliable for SHM in case its change due to damage is not big enough in comparison to the oscillation due to measurement noise, non-stationarity of excitation or other existing conditions. It was also found that damping is difficult to identify. For a detailed discussion, the reader is referred to Chapter 6, and especially to those comments related to Fig. 6.5(b).

In addition to the studies presented in Chapter 6, one more study which analyzes the sensitivity of the natural frequency and normalized mode shape to the change of stiffness K_1 and K_2 is presented in Figs. 8.3.3-8.3.4. The stiffness is decreased linearly in steps by a certain percent and the system is considered time invariant for that step. The changes in the natural frequency and mode shape vector are reported to the initial values, as shown in eq. (8.3.2). The first mode shape component is used for normalization, therefore the i^{th} normalized mode shape vector is $[1 \ X_{2,1}^{(i)}]^T$. Notation (0) and (n) refers to the initial (reference) values and modified values.

$$\begin{aligned}
 K_1 \text{ change}(n) &= \frac{K_1(0) - K_1(n)}{K_1(0)} * 100, \quad K_2 \text{ change} = \frac{K_2(0) - K_2(n)}{K_2(0)} * 100 \\
 f_i \text{ change}(n) &= \frac{f_i(0) - f_i(n)}{f_i(0)} * 100, \\
 X_{2,1}^{(i)} \text{ change}(n) &= \frac{X_{2,1}^{(i)}(0) - X_{2,1}^{(i)}(n)}{X_{2,1}^{(i)}(0)} * 100, \quad i = 1, 2
 \end{aligned} \tag{8.3.2}$$

From Figs. 8.3.3-8.3.4 we can see that a decrease in the values of K_1 and/or K_2 has as effect reduction in the natural frequency, for both vibration modes. The change in the stiffness affects the mode shape in a more complex way. As example, for the first vibration mode a decrease of stiffness K_1 , at constant K_2 , has as effect an increase of $X_{2,1}^{(i)}$ (negative change), and a decrease of stiffness K_2 at constant K_1 has as effect a decrease of $X_{2,1}^{(i)}$

(positive change). Also, a reduction with the same percent of K_1 and K_2 will not significantly affects the mode shape.

8.3.3. Experimental Data Results

8.3.3.1 Identification of Normalized Instantaneous Mode Shape and Instantaneous Frequency

Practical aspects of identification of instantaneous modal parameters (natural frequency, modal damping ratio and normalized mode shape) are studied using data recorded while the wooden house structure was subjected to the excitation of level 3.5m/s². According to field observation a brace in the first story has been damaged, during this test run.

During the experiments absolute displacements and accelerations, i.e $x_1, x_2, \ddot{x}_1, \ddot{x}_2$, have been measured and they are shown in Fig 8.3.5(a),(c). Maximum ground acceleration is 4.75m/s² at t= 6.sec. The maximum acceleration at the first and second floor is 5.35m/s² at 6.9s and 6.74m/s² at t= 6.37, respectively. The inter-story drift, defined as the difference between the displacements at two consecutive floors, is plotted in Fig. 8.3.5(b). The structure experiences a maximum inter-story drift of 0.095 m at the level of the first story and 0.040 at the level of the second story, both localized in the first 10 seconds of the recording. The time resolution of the recording is dt=0.01s.

The frequency content of the responses is illustrated by the Fourier spectrum and CWT map in Figs. 8.3.6-8.3.7. The FFT of the response shows that the energy of the signals is distributed mainly in the range 0-10Hz. Multiple peaks localized around 1 Hz, in the structural response spectrum, may indicate a non-stationary signal. The nonstationary nature of the excitation and responses can be clearly observed on the CWT maps in Fig. 8.3.7. On the CWT map of the relative acceleration responses at the first and the second floors, two high energy bands can be observed: one in the scale range of 10- 75 and the other one in the scale range of 75-300. This indicates two vibration modes whose natural frequencies correspond to these regions. The complex Morlet function, with the central frequency and bandwidth parameters given by $F_c=2/dt=200$ and $F_b=2dt^2=2 \cdot 10^{-4}$, was chosen as mother wavelet for CWT.

In order to apply the Kalman filter, using the procedure explained in Chapter 6, the velocity signals should be, also, available. In this study, these signals are obtained by time integration of the acceleration responses. The first 5 seconds of the record are excluded from integration, because the signal magnitude is at the level of measurement noise. Velocity plots are shown in Fig. 8.3.8. To verify the integration procedure, the displacement results obtained by integration of the velocities are compared to the measured displacements. Results are shown in Fig. 8.3.9, and only minor differences are observed.

Wavelet packet decomposition is performed simultaneously on relative accelerations of the first and second floors, i.e. \ddot{u}_1 and \ddot{u}_2 , respectively. Discrete Meyer wavelet was chosen as mother wavelet. The decomposition process is illustrated in Fig. 8.3.10. The decomposition node number and the corresponding energy of each node are written on Fig. 8.3.10, by colors yellow and magenta, respectively. The confidence index (CI) is calculated for each pair of the reconstructed components whose energy is greater than 5% of total corresponding signal energy. If most of the CI values are in the validation range of 0.98 - 1.02 the decomposition stops for that branch and the reconstructed component is sifted out as a dominant vibration modal response.

Fig. 8.3.11, shows the confidence indices for nodes (5,0), (6, 1) and (7,3). The WP node (7,3) is chosen to give the sifted signal. It can be observed that the confidence index for decomposition level (7,3) is most of the time in the validation range (0.98-1.02) marked by dot lines on the plots. From time resolution point of view, as well as component energy, a lower decomposition level is preferred. For example, level (7,3) is preferred to the level (8, 6), which also has a good confidence index.

In the present study, only the first vibration mode can be identified, because the confidence index for the second vibration mode is out of the validation range for component energy greater than 5%. Once the decomposition level is selected, the normalized instantaneous mode shape and the instantaneous natural frequency can be identified using the procedures described in Chapters 5 and 6.

Figure 8.3.12 plots the confidence index, instantaneous frequency of the sifted signals and normalized mode shape component $X_{2,1}^{(1)}$. The instantaneous frequency of the

sifted signals, although is in the range of the first instantaneous natural frequency, is not necessary the first instantaneous natural frequency of the system. The regions where the confidence index is out of validation range are marked by semi-transparent rectangles in Figs. 8.3.12-8.3.13. It can be observed that a confidence index out of validation range is associated to big oscillations in the $X_{2,1}^{(1)}$. Note that $X_{2,1}^{(1)}$ is calculated as the ratio of the analytical amplitudes of the sifted signals, at node (7,3) i.e $X_{2,1}^{(1)} = A_{\ddot{u}_{2,(m,n)}} / A_{\ddot{u}_{1,(m,n)}}$, where (m,n)=(7,3). From analytic amplitude plots in Fig. 8.3.13.b, we can point out that when the signal intensity is very small, the analytic amplitude is more affected by factors as mode mixture and noise in the signal. A correction should be applied to the NI mode shape in these regions. The estimate of the NI mode shape can be improved by different techniques; Kalman smoother has been used in this study. The NI mode shape was simulated as a random walk process, as shown in eq. (8.3.3). The Kalman smoother measurement equations is described in (8.3.4) and it employs the calculated analytical amplitudes of sifted signals.

$$X_{2,1}^{(1)}[k+1] = X_{2,1}^{(1)}[k] + w[k] \quad (8.3.3)$$

$$A_{\ddot{u}_{2,(m,n)}}[k] = X_{2,1}^{(1)}[k] A_{\ddot{u}_{1,(m,n)}}[k] + v[k] \quad (8.3.4)$$

$w[k]$ and $v[k]$ represent the process and measurement noise, respectively, and they are assumed to be independent, zero mean Gaussian white processes, with the variances as $\mathbf{Q}[k]$ and $\mathbf{R}[k]$. In this study after multiple simulations with different values for $\mathbf{Q}[k]$ and $\mathbf{R}[k]$, we found that $\mathbf{R}[k]=1$; $\mathbf{Q}[k]=0.001$ gives a small measurement innovation values.

Figure 8.3.13(c) represents the estimate of NI mode shape component by Kalman smoother, plotted on top of that calculated directly as the ratio of the analytic amplitudes.

In order to estimate the instantaneous natural frequency and instantaneous modal damping ratio, a Kalman filter procedure as explained in the Chapter 6.1 is used. Performing a numerical sensitivity study consisting in measurement innovation vs. process noise and measurement noise covariances, the following values for $\mathbf{Q}[k]$ and $\mathbf{R}[k]$ have been chosen for simulation:

$$\mathbf{Q} = \begin{bmatrix} 1 & 0 & 0 & 0 \\ 0 & 0.01 & 0 & 0 \\ 0 & 0 & 0.01 & 0 \\ 0 & 0 & 0 & 0.01 \end{bmatrix}, \quad \mathbf{R} = \begin{bmatrix} 1 & 0 \\ 0 & 1 \end{bmatrix} \quad (3.3.5)$$

Figure 8.3.14(a),(b) shows the estimated results for instantaneous natural frequency and estimated modal damping ratio. The success of the Kalman filter estimation is quantified by the measurement innovation, which reflects the discrepancy between predicted measurement and actual measurement. Measurement innovation is plotted in Fig. 8.3.15(a). For a quantitative evaluation of the prediction errors, the measurements are plotted in Fig. 8.3.15(b). It can be observed that the measurement innovation is less than 10% from the relative accelerations obtained from actual measurements. Estimated values for the instantaneous damping ratio presents high oscillations and therefore it may not be reliable for SHM. The oscillations are due to factors as:

- the contribution of the damping term to the measured response is small
- the method used to estimate damping ratio. Because we wanted to take advantage of the optimality of the Kalman filter for linear systems, modal damping is not estimated directly. It is calculated by using the ratio between two estimated measures, and therefore the error in each term may highly affect the obtained result. For better results, filtering techniques for nonlinear systems, as particle filter, are recommended.

8.3.3.2 Damage Detection in the Structure

In the following, damage assessment is done by comparing the results from three consecutive runs of the test at excitation level of 3, 3.50 and 4m/s². According to the field observations, damage occurred as follows:

Excitation level (m/s ²)	Damage reported
3	no significant damage
3.5	a brace in the first story damaged
4	another brace damaged

Damage observed during the test run with the excitation of level 3.5m/s^2 is illustrated in Fig.8.3.2.

First, CWT of the relative acceleration responses at the first floor, \ddot{u}_1 , are performed. Maps of absolute values of the CWT coefficients are presented in Fig.8.3.16. By visual inspection, it can be observed that there is a shift in the distribution of the signal energy along scale axis from level 3 to level 4, which is equivalent to a reduction of system natural frequency. This may indicate damage into the system.

The instantaneous natural frequency, estimated by the integrated Kalman filtering technique and wavelet packet sifting process is presented in Fig. 8.3.17. Results obtained during the first 3 sec. of the estimation procedure are considered irrelevant, due to the wavelet end effects and the errors due to Kalman filter accommodation, and they are marked by a semitransparent rectangle. For the load level of 3m/s^2 , the instantaneous frequency is about constant, i.e. 1Hz. This observation corresponds to the field observation, when no significant damage has been reported. For load level of 3.5m/s^2 and 4m/s^2 there is a decrease of the instantaneous frequency, from 0.96 Hz at the end of run with excitation intensity of 3m/s^2 to 0.89Hz at the end of the run with excitation intensity of 3.5m/s^2 and then 0.79 Hz at the end of run with excitation intensity of 4m/s^2 . From figure 8.3.17(b), which presents the results for excitation level $=3.5\text{m/s}^2$, we can draw the conclusion that important damage occurred in the time interval 10-15 sec, around 12 seconds. The IN mode shape component is not plotted since its trend cannot be isolated from high oscillations due to different causes, as it was explained.

The results from all available test runs are summarized in Figs. 8.3.18 - 20. Figure 8.3.18 shows the estimated instantaneous natural frequencies, Fig. 8.3.19 shows the estimated instantaneous modal damping ratio and Fig. 8.3.20 illustrates the identified IN mode shape component $X_{2,1}^{(1)}$, as well as its estimated value by Kalman smoother. Starting with excitation level of 3m/s^2 there is a decreasing trend in the instantaneous natural frequency, which indicates structural damage into the structure and it corresponds to the field observations. However, the results for excitation level 1, 1.5, 2, 2.5 are somewhat confusing. For excitation of level 1m/s^2 , we found an increase in the first natural frequency.

This increase is also seen on CWT map of \ddot{u}_1 , in Fig. 8.3.21, where the high energy band which indicates the first mode has been marked by a orange lines. The increase in the natural frequency is also confirmed by Fourier spectra in Fig. 8.3.22. The relative acceleration response, \ddot{u}_1 , was divided in two signals. The first signal contains the record from 5s to 20s and the second signal consists of the record from 20s to 40s. Fourier transform of each signal has been performed and the spectra, normalized by the maxim value for convenience of the comparison, are plotted in Fig. 8.3.22. There is a clear shift of the peak from 1.73 Hz to 1.95 Hz. As an explanation: during the first run of the test, while the excitation has a low magnitude (max amplitude is 1.4m/s²), due to the nature of the wooden frame, the healthy structure increases its stiffness due to a process of strengthening of the joints. A normalized instantaneous mode-shape, which is about constant, points out a similar change in the stiffness of each floor. There is a discontinuity in the instantaneous natural frequency values, from excitation level 1m/s² to 3m/s². Since no significant damage was reported during these test runs, it is supposed that the structure was subjected to other experiments which damaged the structure between these test runs. This assumption is also supported by plot of FFT in Fig. 8.3.23. We can see a clear shift in the dominant peaks of the spectrum without any significant damage reported. The author is aware that this wooden house structure has been also subjected to the ground excitation recorded during the 1995 Kobe earthquake and, also, to few bi-directional excitations, but information regarding the time when these tests were performed was not available.

The trend in the normalized instantaneous mode shape is difficult to be identified during a test run. However, a decrease in the mode shape can be seen if the results from the runs are plotted together, from low to high excitation intensity, as shown in Fig. 8.3.20.

The instantaneous modal damping ratio, identified by methods presented in this dissertation, is not reliable for SHM due to the difficulties in identification, which have been mentioned before.



Figure 8.3.1. An overview of the test site and the wooden frame specimen on the shaking table (from Shimizu et al, 2000).



Figure 8.3.2. A damaged wooden brace occurred during the test run at the load level 3.50m/s². A secondary damage occurred in the stud connected to the damaged brace. (from Shimizu et al; 2000).

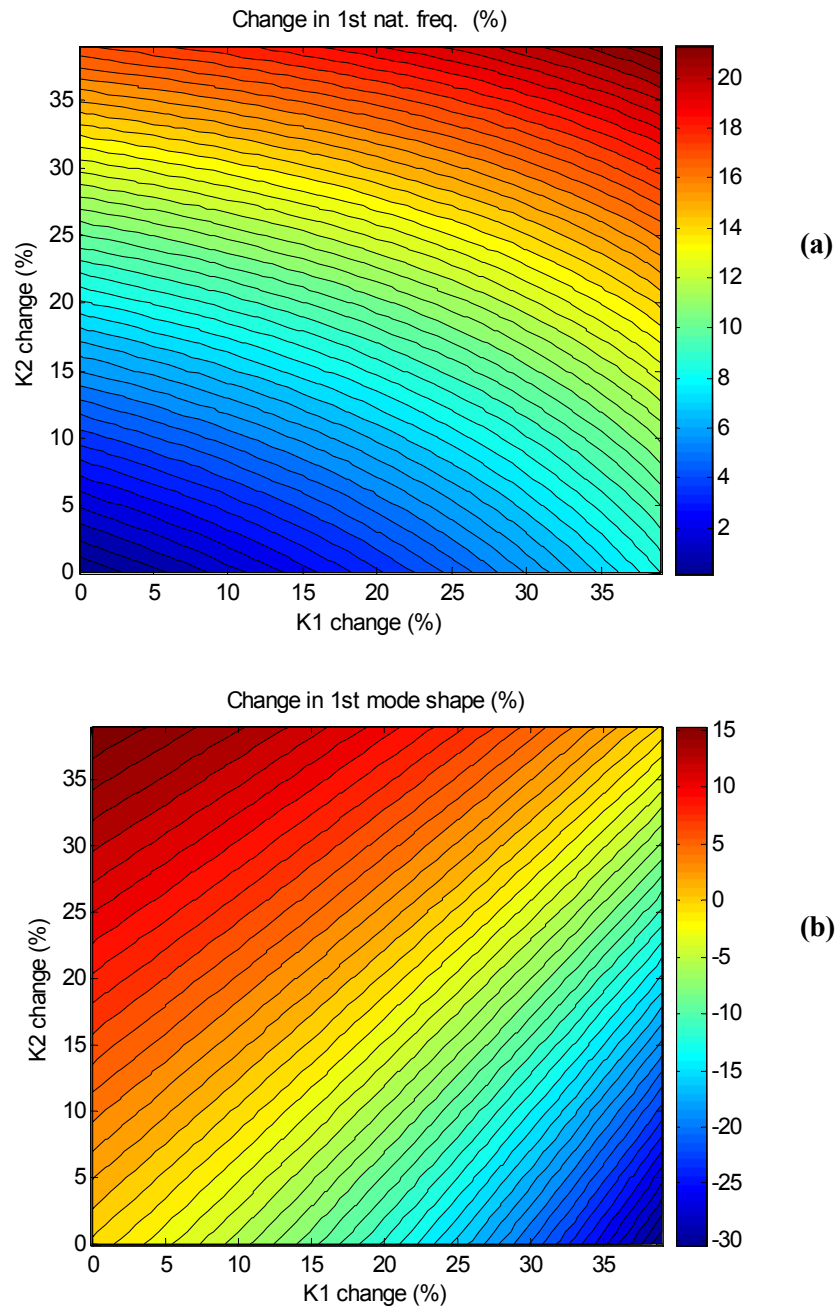


Figure 8.3.3 First vibration mode. (a) Change in the natural frequency and (b) mode shape component $X_{2,1}^{(1)}$ with the change in system stiffness (K1 and K2)

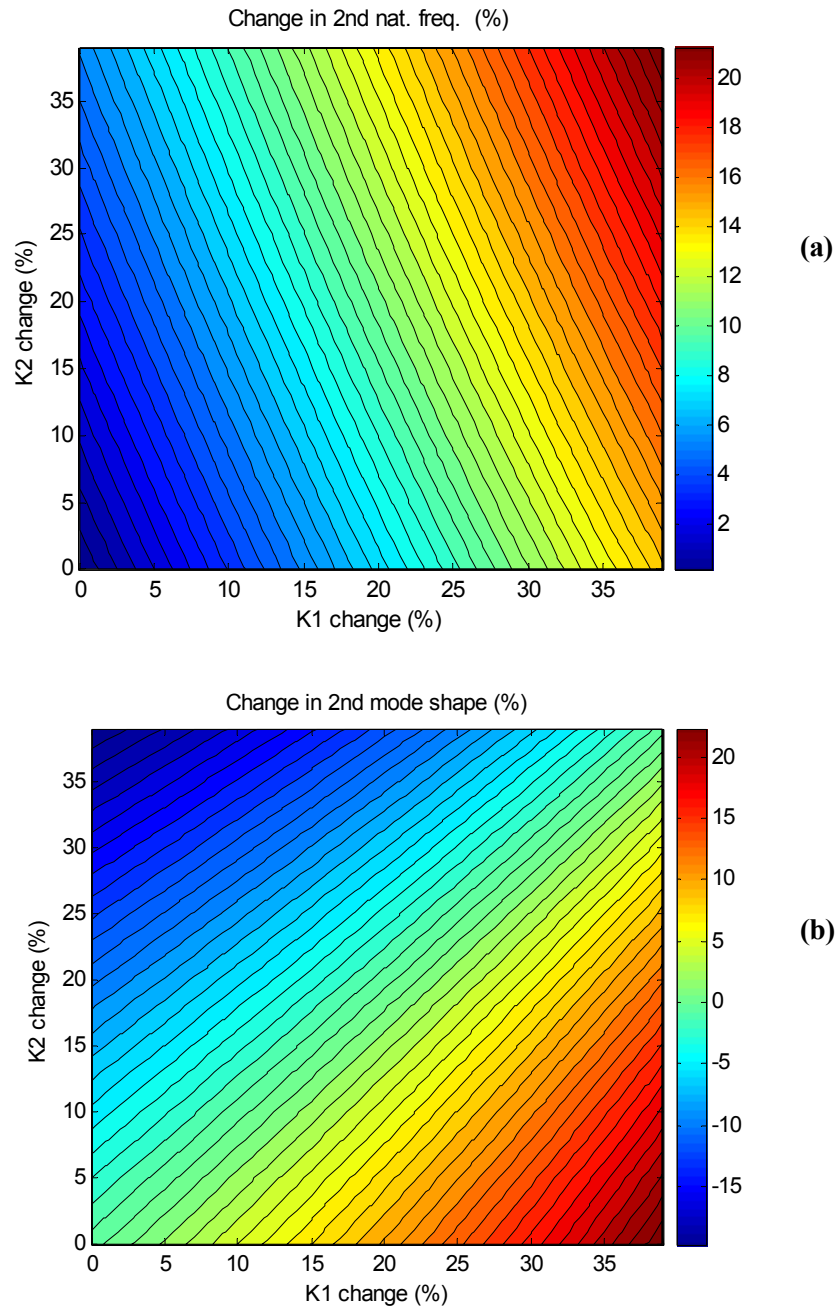


Figure 8.3.4 Second vibration mode. (a) Change in the natural frequency and (b) mode shape component $X_{2,1}^{(2)}$ with the change in system stiffness (K1 and K2)

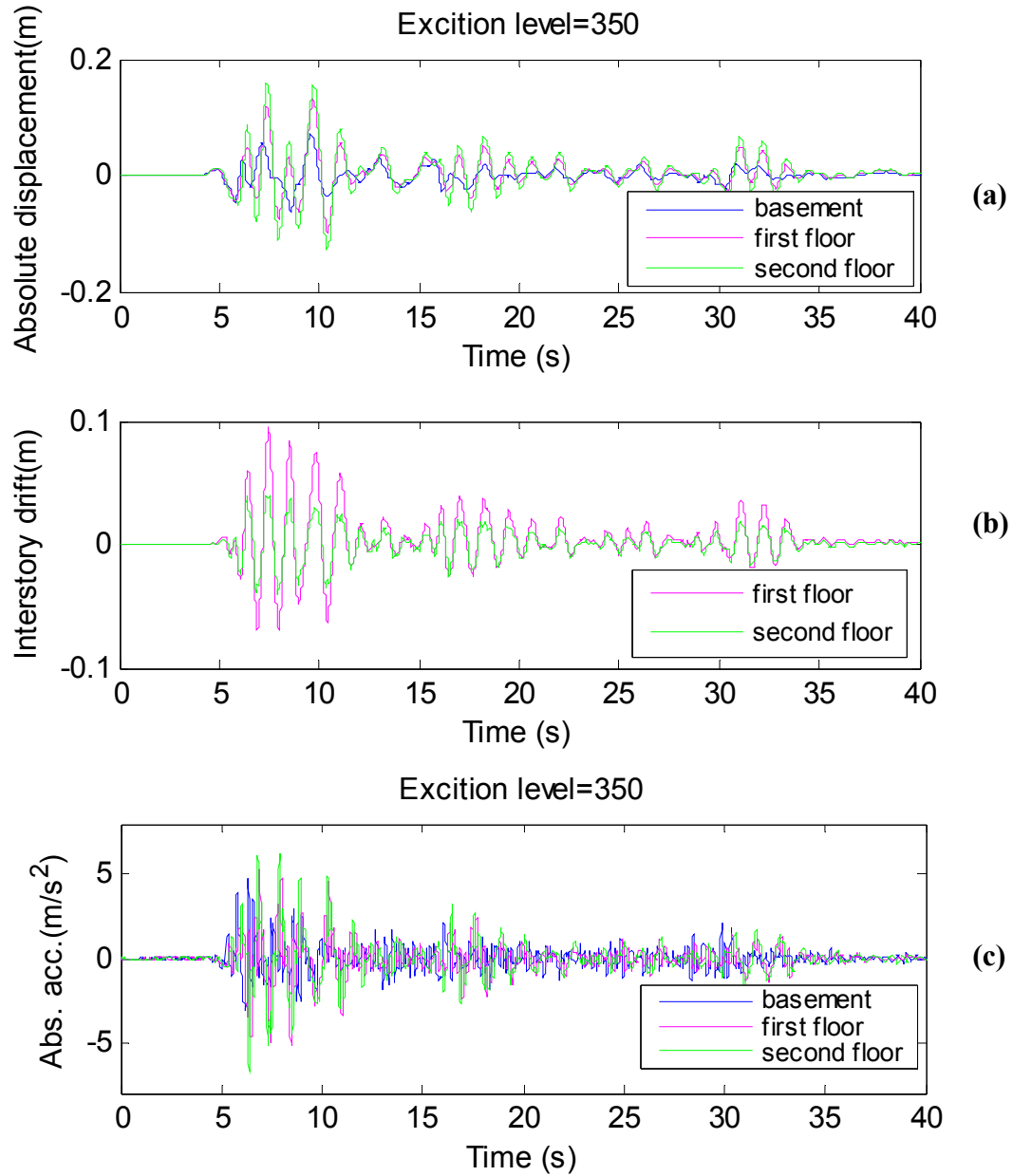
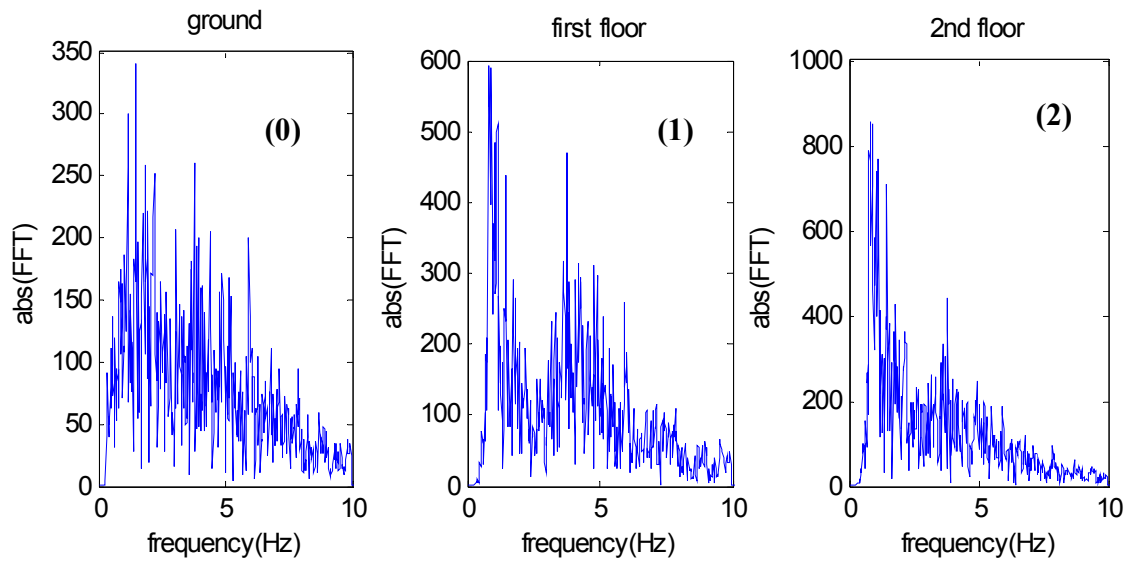
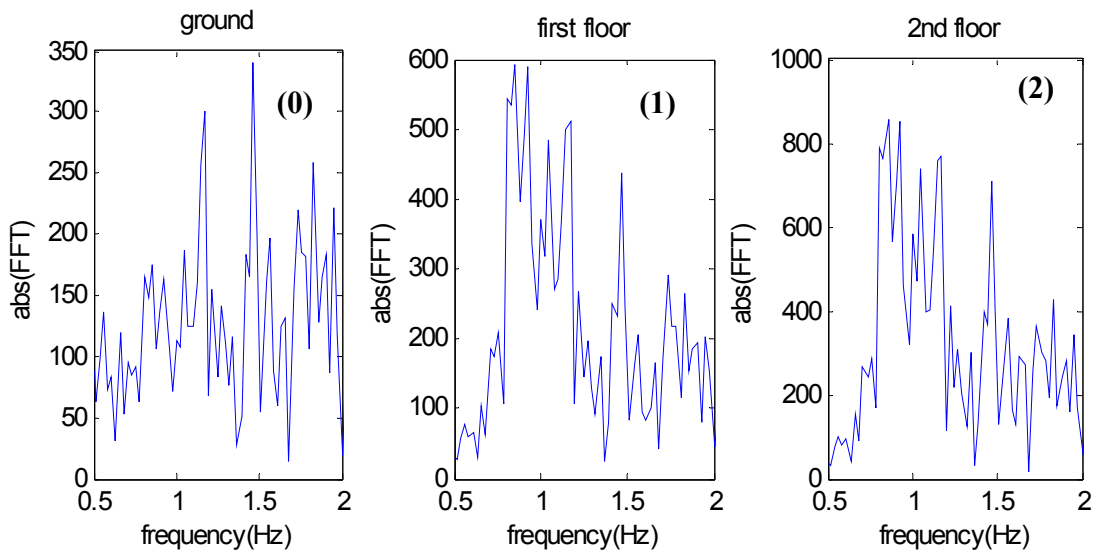


Figure 8.3.5 (a) Plots of absolute displacements: first floor: $x_1(t)$ (magenta) , second floor- $x_2(t)$ (green) , basement- $x_g(t)$ (blue); (b) plots of the inter-story drift $x_2(t)-x_1(t)$ (green), $x_1(t)-x_g(t)$ (magenta); (c) Plots of the absolute acceleration: first floor (magenta) , second floor (green) , basement (blue);



(a)



(b)

Figure 8.3.6. (a) Fourier spectrum of the relative of: (0) ground acceleration; (1) relative acceleration of the 1st floor (2) relative acceleration of the 2nd floor; (b) Zoom in plots for frequency range 0.5 – 2 Hz.

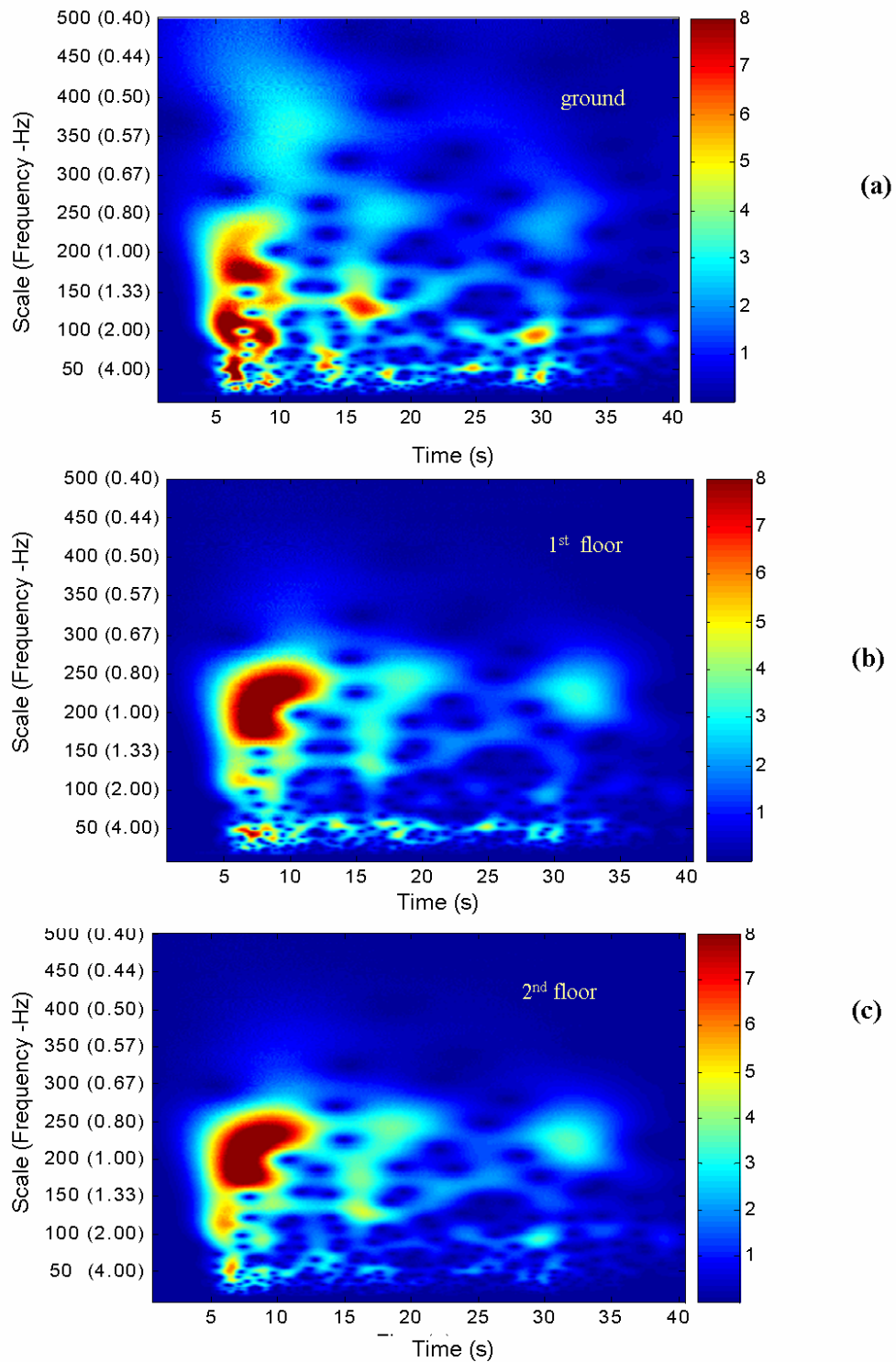


Figure 8.3.7. CWT maps of: (a) the ground acceleration, (b) the relative acceleration of the first floor and (c) the relative acceleration of the second floor. "Relative" – means in respect to the ground.

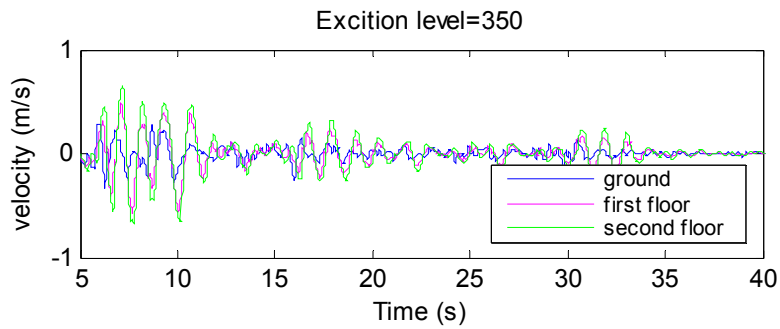


Figure 8.3.8 Plots of the absolute velocity obtained by integration: first floor (magenta) , second floor (green) , basement (blue);

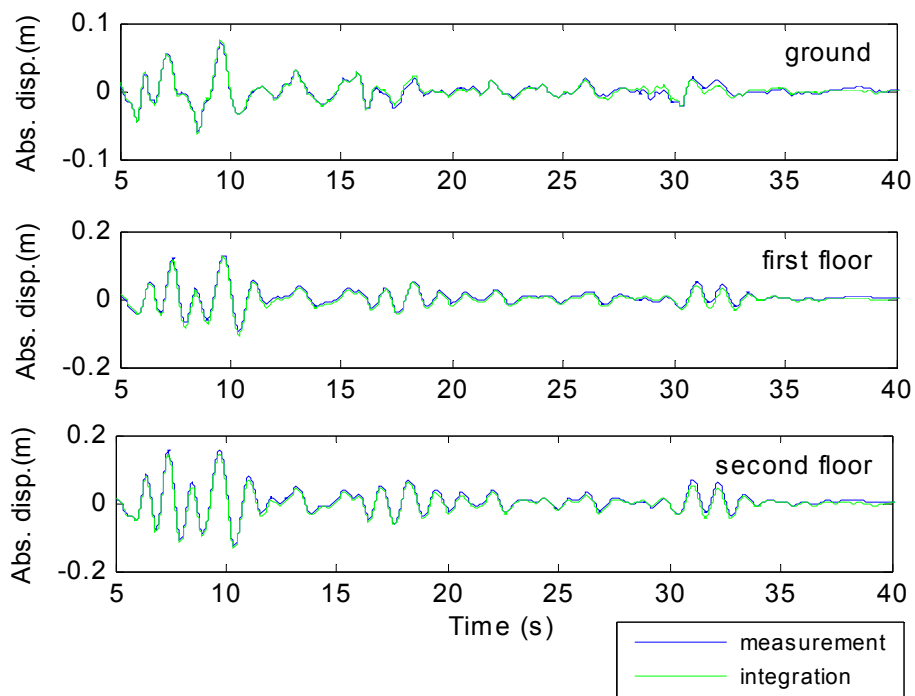


Figure 8.3.9. Comparison between the measured displacement signals and those obtained by time integration of the measured acceleration responses.

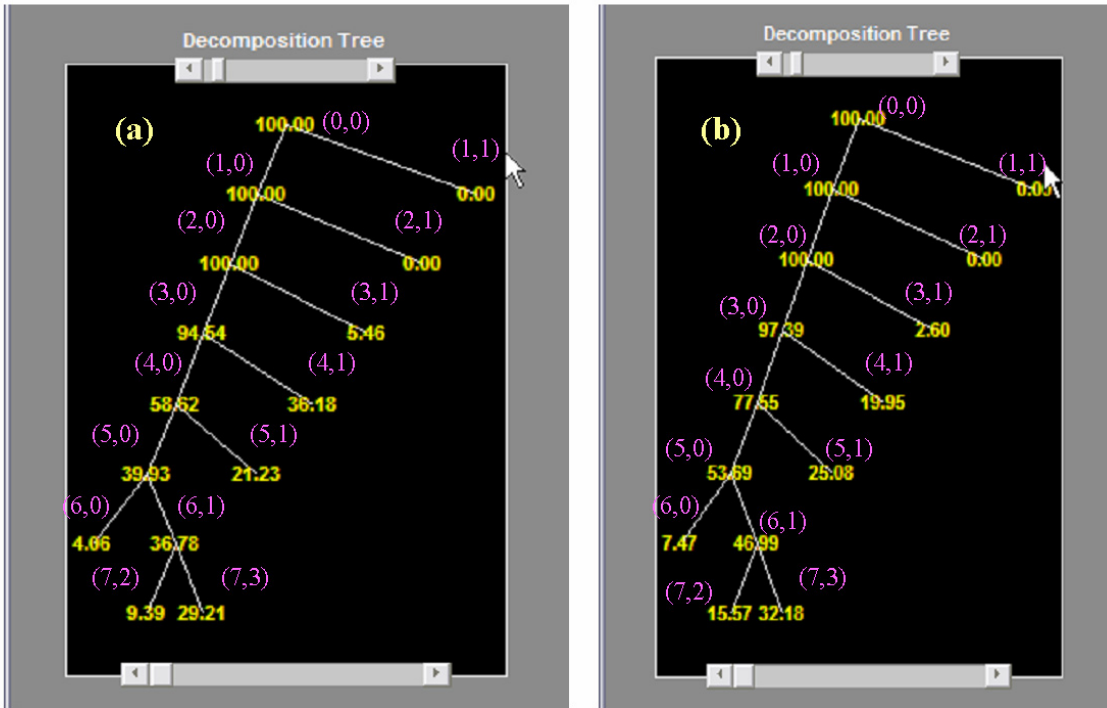


Figure 8.3.10. Decomposition tree for a) relative acceleration of the first floor ; b) relative acceleration measured at the second floor

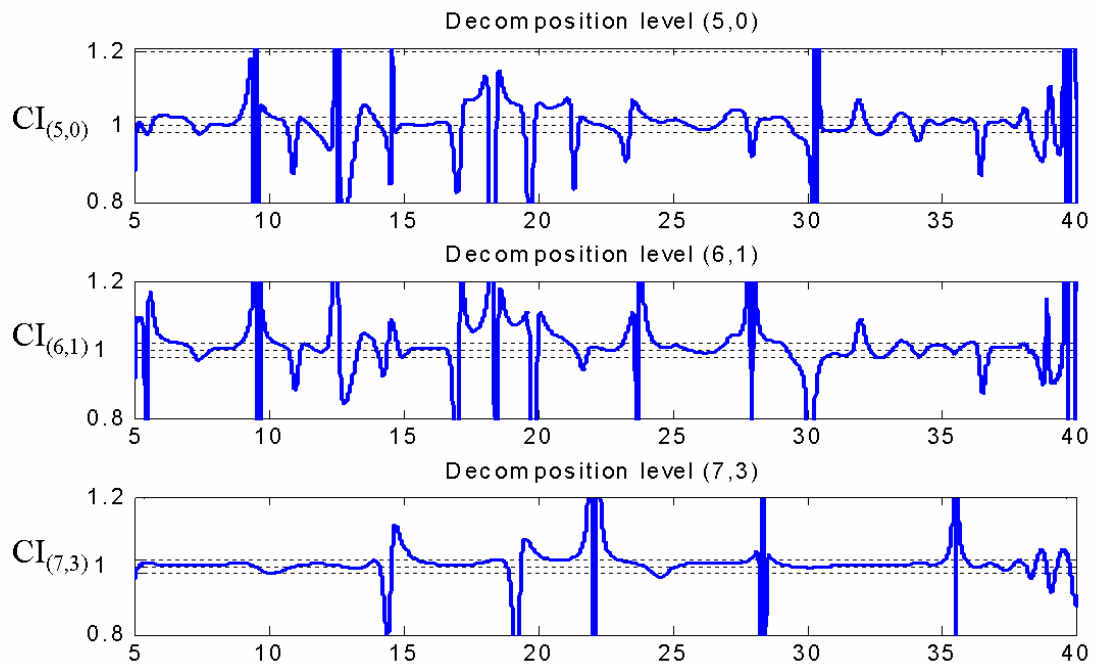


Figure 8.3.11. Confidence index (CI) for different decomposition levels

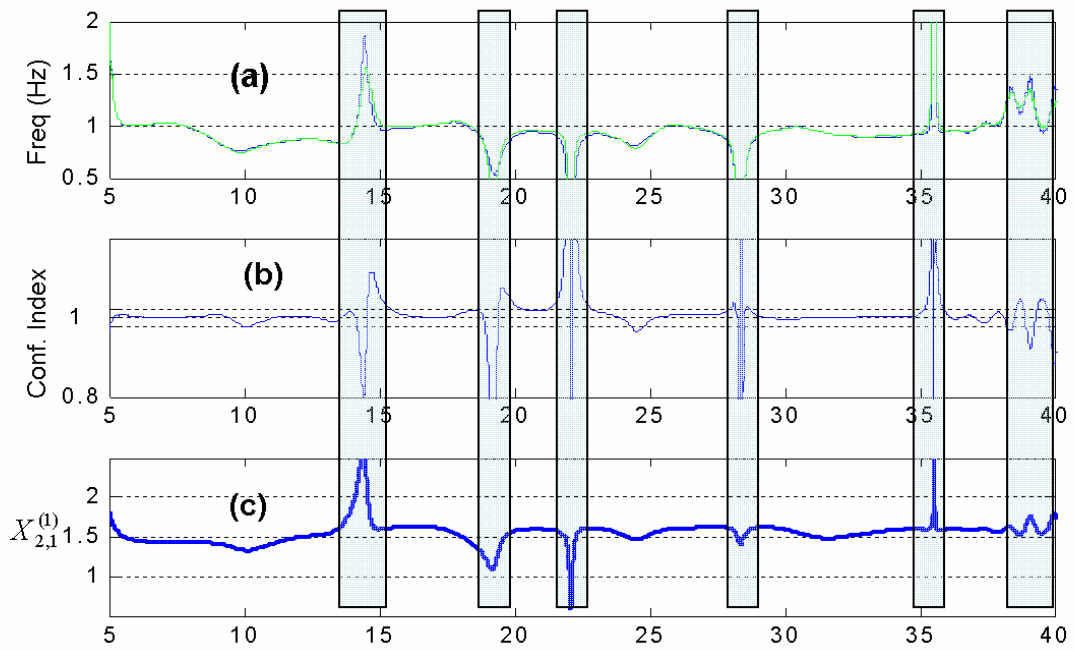


Figure: 8.3.12 (a) Instantaneous frequency of the reconstructed signals at node (7,3) (blue – 1st story, green – 2nd story); (b) Confidence index; (c) Normalized mode shape component

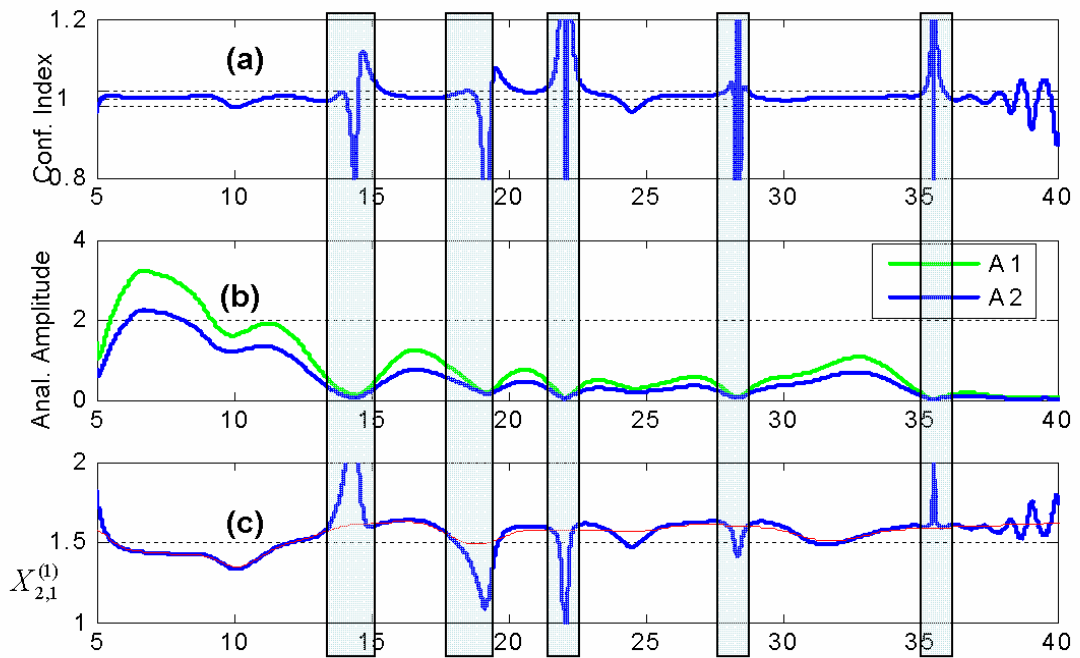


Figure 8.3.13 a) Confidence index; (b) Analytic amplitudes of $\ddot{u}_{1,(7,3)}$ (A1) and $\ddot{u}_{2,(7,3)}$ (A2); (c) calculated NI mode shape (blue); estimated NI mode shape by Kalman smoother (red)

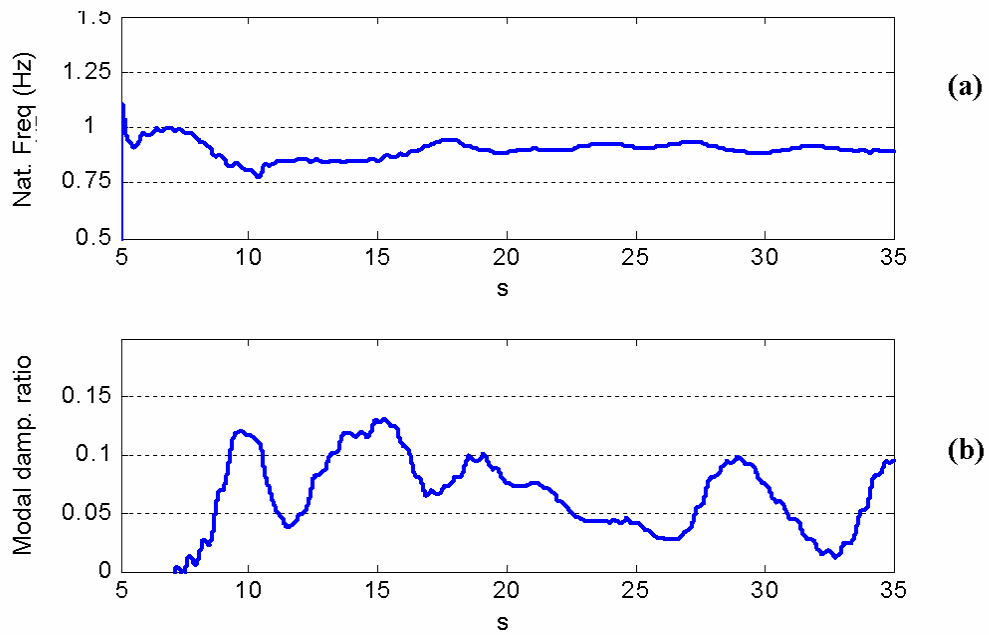


Figure 8.3.14 (a) Estimated instantaneous natural frequency; (b) Estimated instantaneous modal damping ratio

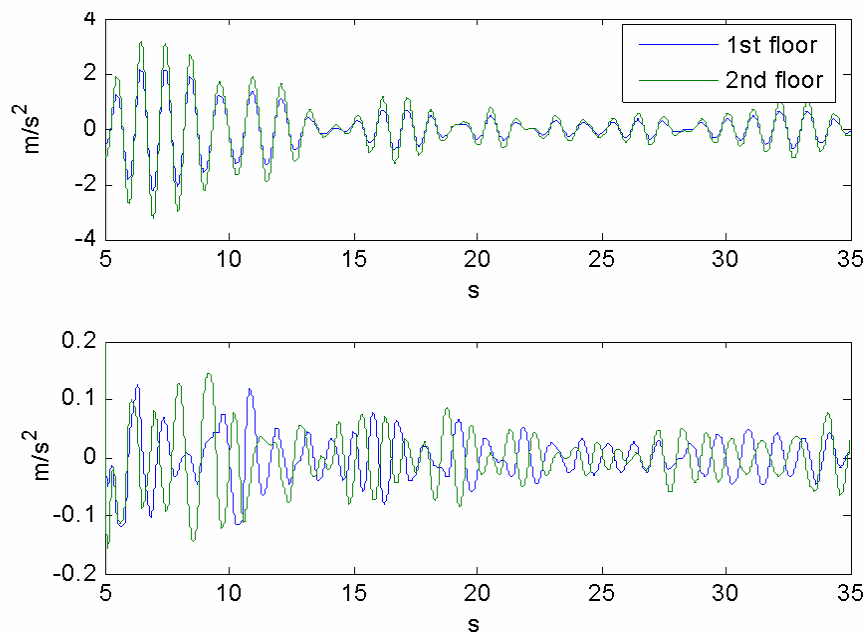


Figure 8.3.15 (a) Relative accelerations obtained from actual measurements; (b) innovation (blue data for the first story, green – data for the second story)

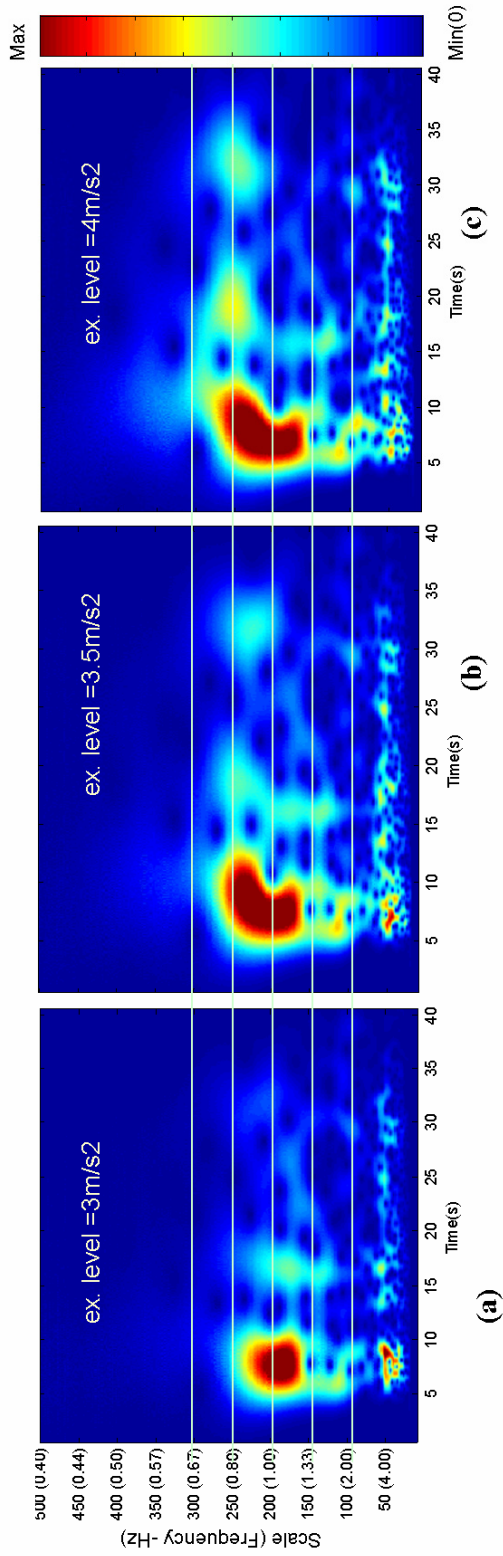


Figure 8.3.16. CWT of the relative acceleration response of the first floor while the structure was subjected to an excitation of level (a) 3m/s²; (b)3.5m/s²; (c) 4m/s².

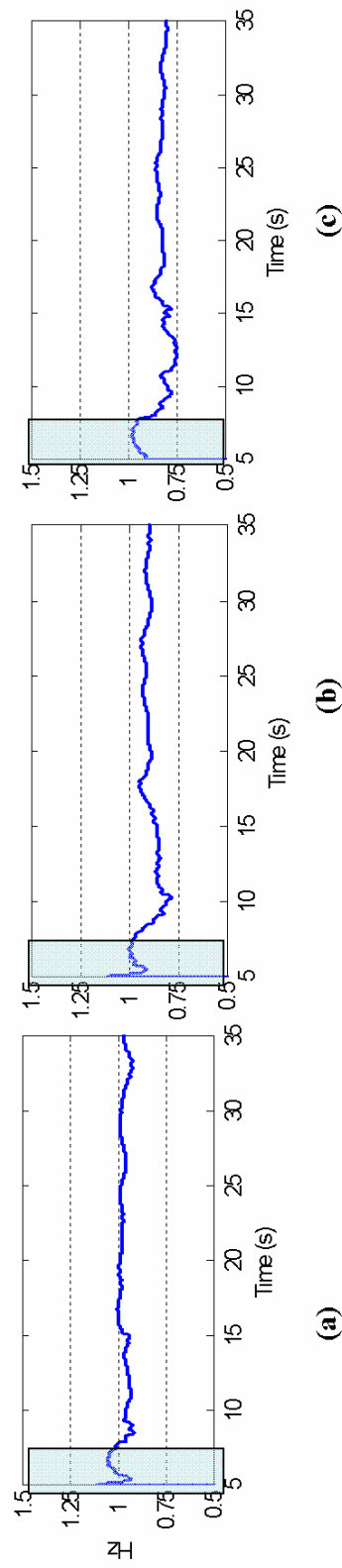


Figure 8.3.17. Identified instantaneous natural frequency of the wooden house while the structure was subjected to an excitation of level (a) 3m/s²; (b)3.5m/s²; (c)4m/s²

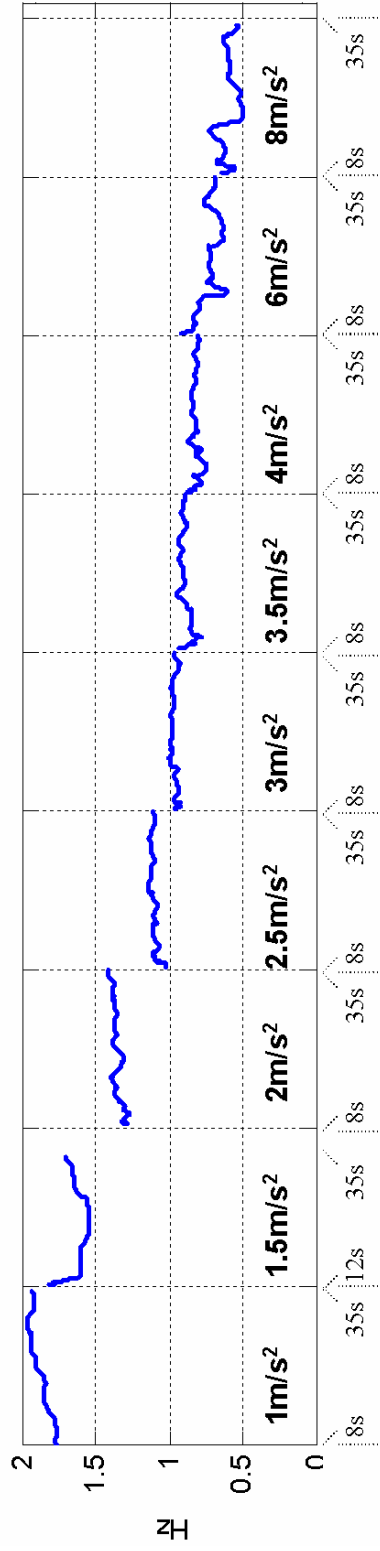


Figure 8.3.18. Identified instantaneous natural frequency for different excitation levels

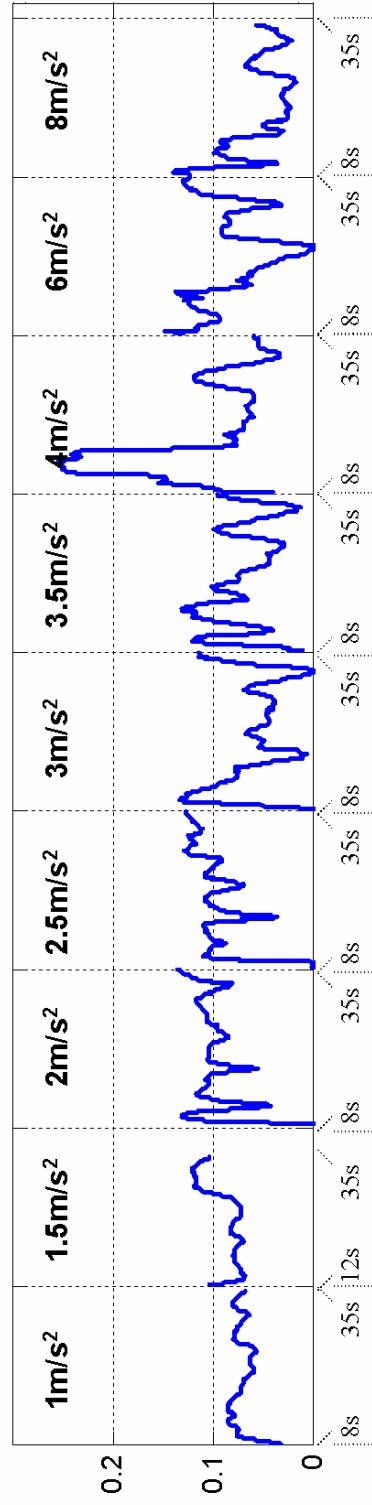


Figure 8.3.19. Identified instantaneous modal damping ratio for different excitation levels

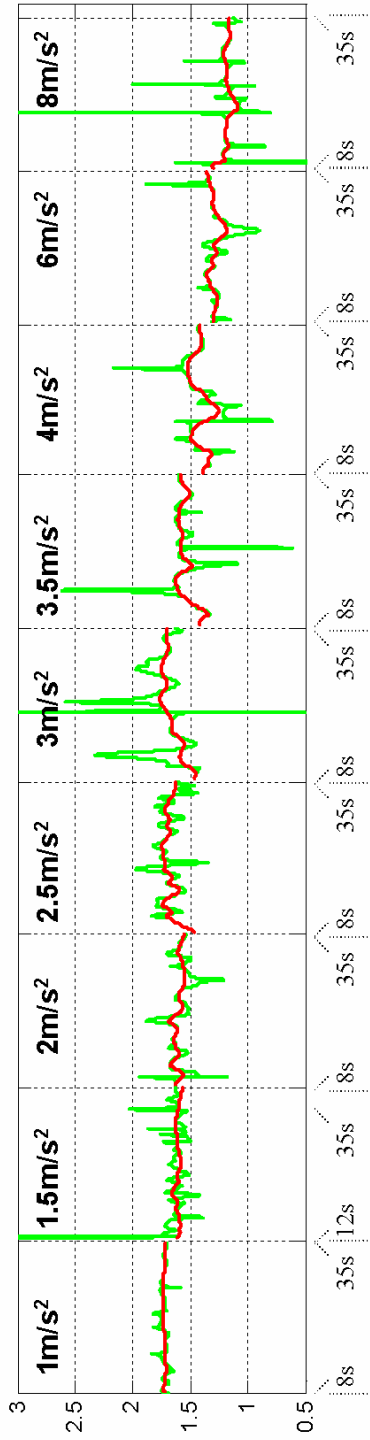


Figure 8.3.20 Identified normalized instantaneous mode shape for different excitation levels

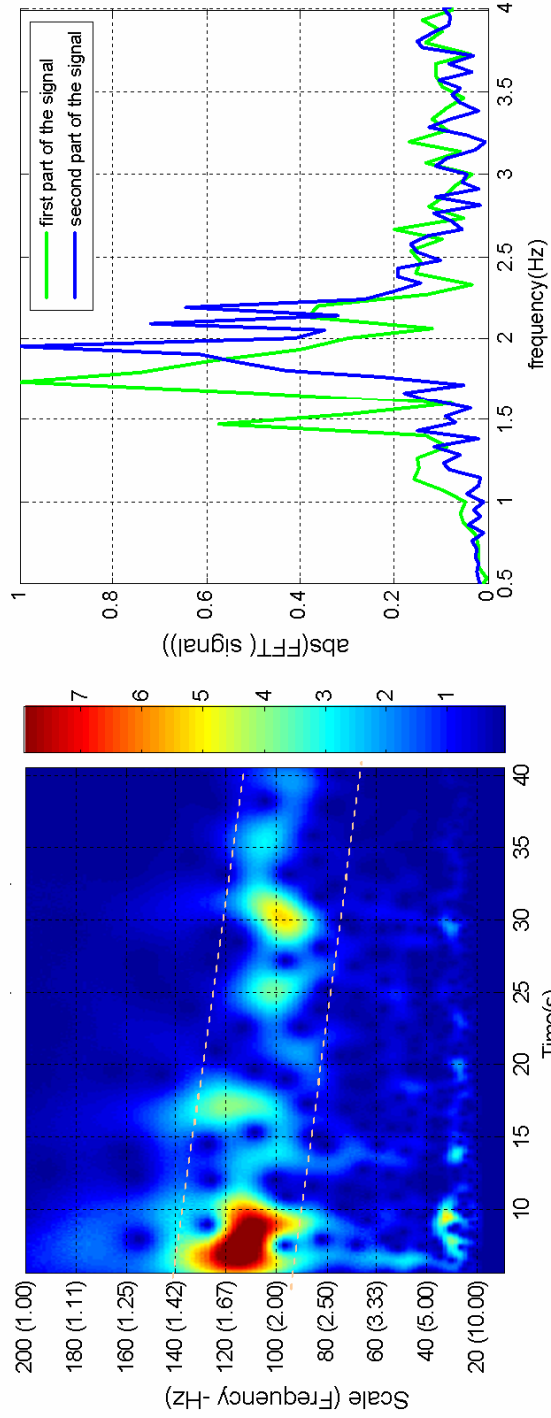


Figure 8.3.21. CWT of i_1 (excitation level =100)

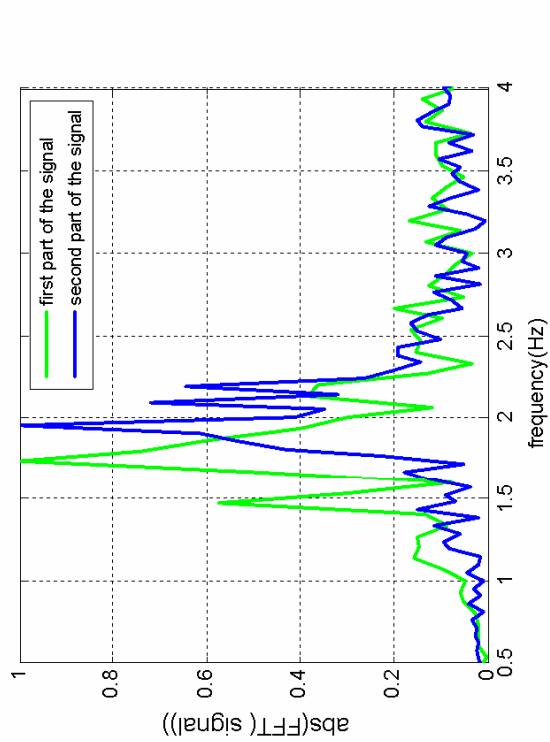


Figure 8.3.22. Fourier spectrum of i_1 , normalized by its maximum value; green signal recorded from 5s to 20s; blue – signal recorded from 20s to 40s (excitation level =100)

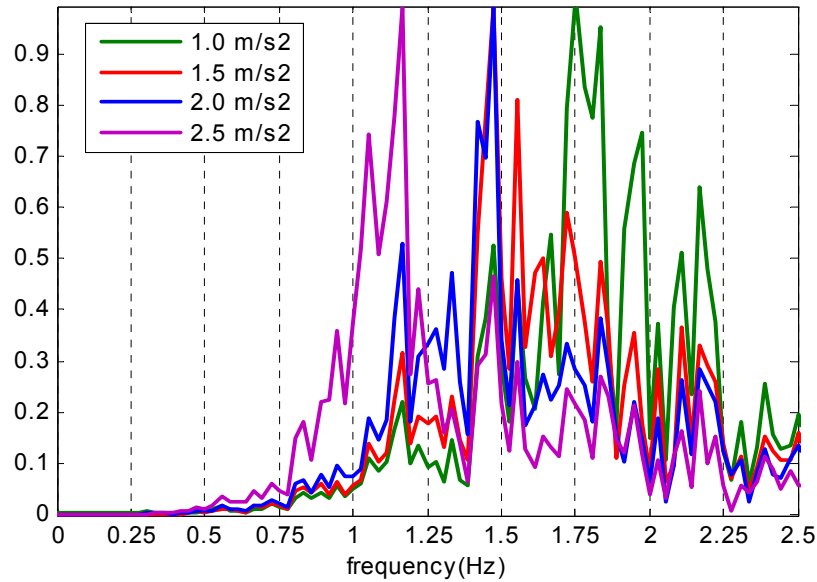


Figure 8.3.23. Fourier spectrum of \ddot{u}_1 normalized by its maximum value, for different excitation levels

8.4 Summary

This study presents applications to experimental data of the instantaneous modal parameters–based approach for SHM and damage detection. Any change in these quantities may well indicate occurrence and evolution of damage. The method was applied for two sets of experimental data: one from experimental Phase 2 of ASCE- SHM benchmark studies and the other one from shaking table test of a full-size two-story wooden building structure.

In the ASCE- SHM benchmark studies, the test structure was a scaled prototype of a 4 story steel-frame. Damage was introduced between two runs of the test. Data collected during few hammer tests before and after damage have been analyzed. Considering the invariant structure as a particular case of a time varying one, the instantaneous modal frequencies and normalized instantaneous mode shapes are identified by CWT – ridge method. Their values are constant during each test run (an indication of no-damage in each

individual run) and different from one run to the other (an indication that damage occurred between two runs), which is in agreement with the damage scenario specified in the testing procedure.

In the second set of experiments the nature of the loading is more complex. The shaking table was provided with the ground acceleration signal recorded on NS direction during the 1940 El Centro Earthquake, scaled at various intensities. Several runs of the test were conducted; in each test run the frame was excited by the original ground motion record scaled at a nominal load level targeted at certain load intensity.

The integrated approach consisting in Kalman filter and wavelet packet sifting process is used to estimate the instantaneous natural frequencies; wavelet packet decomposition in conjunction with the confidence index is employed to identify the normalized instantaneous mode shape.

The results obtained from the evaluation of the instantaneous natural frequency agree quite well with the qualitative description of damage from the field observation. Starting with excitation level of 3m/s^2 there is a decreasing trend in the instantaneous natural frequency, which indicates structural damage into the structure and it corresponds to the field observations. The trend in the normalized instantaneous mode shape is difficult to be identified during a test run, due to high oscillations. However, a decrease in the mode shape can be seen if the results from the test runs are plotted together, from low to high excitation intensity. The instantaneous modal damping ratio, identified by methods presented in this dissertation, is not reliable for SHM due to the difficulties in identification. Nonlinear estimation techniques, such as particle filter, are recommended to improve the results.

Chapter 9

CONCLUDING REMARKS

9.1 Summary and Main Contributions

Current global damage identification techniques based on vibration measurements have limitations such as the assumption of time invariance while data is collected, the availability of the impulse responses, or the requirement for a physical model of the structure. These limitations make many of the methods inapplicable for damage detection and SHM of a structure with evolving damage while the structure is in use and its physical model is not available.

This dissertation proposes a vibration-based approach to detect and monitor structural damage by tracking the instantaneous modal parameters. Any change in the instantaneous modal parameters may well indicate occurrence and evolution of damage. Abrupt and gradually developed damage can be thus identified. It is assumed that the structure with gradual deterioration can be treated as a linear slowly time-varying system and a structure with sudden damage is treated as a linear system before and after damage. It is, also, assumed that the structure is lightly damped and has well separated vibration modes.

1. A required step in achieving this objective was to develop the theoretical basis of time varying vibration modes and instantaneous modal parameters. It has been proved that using the dynamic eigenvalue problem the response of a linear time varying system can be decomposed in a sum of time varying vibration modes characterized by modal parameters which have physical significance, i.e. positive instantaneous modal frequency, real

instantaneous mode shapes and real modal damping. These instantaneous modal parameters are related to the system physical properties by the dynamic eigenvalues/eigenvectors of the associated first-order system in state space. For identification purpose, a normalized instantaneous mode shape vector has been defined as the instantaneous mode shape vector normalized by one of its components which is different of zero; therefore, the normalized instantaneous mode shape has a component which is equal to unity along time record, while all other components may show time dependence.

The instantaneous frequency of the modal responses is practically independent of the measurement location/DOF and is the same for displacement, velocity and acceleration vectors up to a term of the order of epsilon (much less than 1), if the assumption of slow varying system holds. A second order formulation for each modal response, where the instantaneous natural frequency and instantaneous modal damping ratio appear explicitly, has also been proposed. If the linear system is not slowly time-varying, one cannot guaranty that real vibration modes with the same instantaneous frequency for different DOFs can be identified in the responses. By a numerical simulation study it is shown that the assumption of slow varying is not so restrictive for damage detection and it could cover many real cases.

2. Methods of identification of instantaneous frequency of the free vibration responses previously proposed by other authors, such as CWT – ridge method and WPS technique in conjunction with Hilbert transform, are employed for identification of instantaneous modal frequency and normalized instantaneous mode shape vector. The approach is tested on simulation data from a 3DOF with progressive stiffness degradation and nonzero initial conditions. The identified results are in good agreement with those obtained by solving the dynamic eigenvalue problem.

3. Since free vibration responses of a time varying system are not available in the case of real applications, the identification techniques using forced vibration responses were proposed in Chapters 5 and 6. The normalized instantaneous mode shape is identified from the forced vibration response by using a wavelet packet sifting process in conjunction with Hilbert transform. A confidence index, calculated using the instantaneous frequency of the

sifted signals, is introduced to validate the identified results. This method may not require the measurement of the excitation.

The time-varying Kalman filter is integrated with the wavelet packet sifting technique and the second order formulation of the time-varying vibration modal responses to identify the instantaneous natural frequencies and the instantaneous modal damping ratios. The physical significance of the sifted components by wavelet packet sifting technique is ensured by introducing a new sifting criterion based on the confidence index.

The effectiveness of the proposed approaches is illustrated for simulation responses of a multi-degree-of-freedom system subjected to a base excitation. Two damage scenarios, sudden stiffness loss and progressive stiffness degradation, and different base excitations including real earthquake signals and stationary signals simulated as discrete Gaussian white noise processes are considered. The robustness of the methods in the presence of measurement noise and incomplete measurements is addressed.

5. To identify the instantaneous modal parameters from the measurement data it was assumed that the structure can be approximated by a linear slowly time varying system in the case of progressive damage or a linear system before and after damage in case of sudden damage. To address the nonlinear nature of the structure, a preliminary study on the meaning of instantaneous modal parameters and their use for SHM of systems with bylinear restoring forces has been performed. It was illustrated that change in the identified instantaneous modal parameters may have different patterns for the linear system, the system with slow stiffness degradation, and the system with bilinear restoring forces.

6. The performance of the proposed approach has been evaluated on two sets of experimental data: one from experimental Phase 2 of ASCE- SHM benchmark studies and the other one from a shaking table test of a full-size two-story wooden building structure. It was found that the instantaneous natural frequency agrees quite well with the qualitative description of damage from the field observation. The normalized instantaneous mode shape presents some oscillations in the case of forced vibration data, but its trend is clear as damage level increases. The instantaneous modal damping ratio, identified by methods

presented in this dissertation, is not reliable for SHM due to the difficulties in identification. Nonlinear estimation techniques are recommended for improving the results.

9.2 Future Work

The work in this dissertation can be extended in few directions:

1. In this dissertation we made the assumptions that the structure can be approximated by linear slowly time varying or piecewise linear time invariant system and that its vibration modes are well separated. The future work may address these two issues.

a) Considering that a structure with damage can have a nonlinear behavior, the preliminary study on the meaning of instantaneous modal parameters for bilinear systems should be extended for systems with other types of nonlinearities and plastic hysteretic behavior.

b) The separation of vibration modes is a common assumption in many of the existing time-frequency identification methods, even in the case of a time invariant system. In the present study, the idea was to use those response signal components with a minimum mode mixture and not to address the mode mixture. A confidence index out of validation range may indicate that the mode mixture is significant and in that case the results are not reliable for SHM. The approach can be improved in two ways:

- developing identification techniques for systems with closely spaced time varying vibration modes for the case of free vibration as well as forced vibration. The approaches from classical modal analysis may constitute a source of inspiration for further development.
- investigating the effect of mode mixture on the confidence index and its departure from unity value.

2. We found that very good results for modal instantaneous frequency and normalized instantaneous mode shape are obtained from free vibration data. Developing a deconvolution technique to obtain the free response of a time varying system subjected to stationary or nonstationary excitations may constitute a further research topic.

3. In the dissertation the instantaneous modal frequency and damping ratio have been calculated from modal stiffness and modal damping estimated by a linear Kalman filtering technique. The results can be improved if they are estimated directly by using a nonlinear filtering techniques; particle filter is a suggestion.

4. The instantaneous modal parameters have been defined based on the dynamic eigenvalue and eigenvectors. In developing the time varying vibration modes the only assumptions were that the eigenvectors satisfy certain slow varying criteria and the complex eigenvalues come in the conjugate pairs. No assumption on the algorithm required to solve this problem has been made. To give a physical interpretation of the results and to test the time varying vibration mode concept we propose the quasistatic algorithm. However, we consider that there is room to improve the algorithm of solving the dynamic eigenvalue problem.

4. In this dissertation the methodology is tested on numerical simulation and experimental data. More experiments are recommended, and we propose to alternate the high level excitations, which are most likely to damage the structure and reveal the nonlinear behavior, with low-level ambient excitation when the structure is in its linear regime. Also, it is recommended to perform the experiments on structures which have a physical model and to compare damage identification results obtained by instantaneous modal parameters with those results obtained by using tracking methods. Validation of the approach using real data should be also addressed.

APPENDIX

In this Appendix we justify the few approximations used in Chapter 3. If not mentioned, the notations are the same as those in Chapter 3.

Theorem

Consider the following equation as the state space representation of a linear time varying second order dynamic system whose solution is $\mathbf{x}(t)$.

$$\dot{\mathbf{y}}(t) = \mathbf{A}(t)\mathbf{y}(t), \quad \mathbf{y}(t) = \begin{bmatrix} \mathbf{x}(t) \\ \dot{\mathbf{x}}(t) \end{bmatrix}$$

Let $\mathbf{A}(t)$ be a $2N \times 2N$ matrix whose elements are continuous real functions of time on the time interval $T = [t_0, t_f]$.

Let $\mathbf{u}(t) = [u_1(t) \ u_2(t) \ \dots u_k(t) \ \dots u_{2N}(t)]^T$, and $\lambda(t) = \omega(t) + i\gamma(t)$ be the solution of the dynamic eigenvalue problem¹ associated to matrix $\mathbf{A}(t)$.

If:

$$\mathbf{A1} \quad , \quad k = 1 \dots 2N, \quad \forall t \in T$$

Then:

1. $\frac{|\dot{u}_k(t)|}{|u_k(t)|} \ll |\lambda(t)|, \quad k = 1 \dots 2N, \quad \forall t \in T$
2. $\frac{d(\arg(u_k(t)))}{dt} + \omega(t) \cong \omega(t) \quad , \quad k = 1 \dots 2N, \quad \forall t \in T$

¹ $\mathbf{A}(t)\mathbf{u}(t) = \lambda(t)\mathbf{u}(t) + \dot{\mathbf{u}}(t), \quad \forall t \in T$

3. $|u_{2k}| \cong |\lambda| |u_k|, \quad k = 1 \dots N, \quad \forall t \in T$
4. $|\dot{u}_{2k} + \lambda u_{2k}| \cong |\lambda|^2 |u_k|, \quad k = 1 \dots N, \quad \forall t \in T$

If, in addition,

$$\mathbf{A2} \quad \frac{|\dot{\lambda}(t)|}{|\lambda(t)|} \ll \omega(t), \quad \forall t \in T$$

$$\mathbf{A3} \quad \frac{|\ddot{u}_k(t)|}{|u_k(t)| |\lambda(t)|} \ll \omega(t), \quad k = 1 \dots 2N, \quad \forall t \in T$$

Then:

$$\mathbf{5.} \quad \frac{d(\arg(\dot{u}_{2k}(t) + \lambda(t)u_{2k}(t)))}{dt} + \omega(t) \cong \omega(t), \quad k = 1 \dots N, \quad \forall t \in T$$

Note:

1. For the easiness of the reading the following notations are introduced:

$$u_R(t) = \text{real}(u_k(t)), \quad u_I(t) = \text{imag}(u_k(t))$$

2. Expression in **A1**, **A2**, and **A3** can be reformulated as:

$$\mathbf{A1} \quad \text{There exists } \varepsilon_1 \ll 1 \text{ so that } \frac{|\dot{u}_k(t)|}{|u_k(t)| \omega(t)} \leq \varepsilon_1, \quad k = 1 \dots 2N, \quad \forall t \in T$$

$$\mathbf{A2} \quad \text{There exists } \varepsilon_2 \ll 1 \text{ so that } \frac{|\dot{\lambda}(t)|}{|\lambda(t)| \omega(t)} \ll \varepsilon_2, \quad \forall t \in T$$

$$\mathbf{A3} \quad \text{There exists } \varepsilon_3 \ll 1 \text{ so that } \frac{|\ddot{u}_k(t)|}{|u_k(t)| |\lambda(t)| \omega} \ll \varepsilon_3, \quad k = 1 \dots 2N, \quad \forall t \in T$$

$$\mathbf{Proof 1:} \quad \frac{|\dot{u}_k(t)|}{|u_k(t)|} \ll |\lambda(t)|, \quad k = 1 \dots 2N, \quad \forall t \in T$$

Using assumption (A1) and triangle inequality, it results that:

$$\frac{|\dot{u}_k|}{|u_k|} \leq \varepsilon_1 \omega \leq \varepsilon_1 |\lambda|, \quad \text{where } \varepsilon_1 \ll 1 \quad \rightarrow \quad \frac{|\dot{u}_k(t)|}{|u_k(t)|} \ll |\lambda(t)|$$

Proof 2: $\frac{d(\arg(u_k(t)))}{dt} + \omega(t) \cong \omega(t)$, $k = 1 \dots 2N$, $\forall t \in T$

$$\frac{d}{dt}(\arg(u_k(t))) = \frac{d}{dt} \left(\text{atan} \left(\frac{u_I}{u_R} \right) \right) = \frac{u_R \dot{u}_I - \dot{u}_R u_I}{u_I^2 + u_R^2} \quad (\text{A2.1})$$

Using the triangle inequality for complex numbers, it results:

$$\left| \frac{u_R \dot{u}_I - \dot{u}_R u_I}{u_I^2 + u_R^2} \right| \leq \left| \frac{u_R \dot{u}_I}{u_I^2 + u_R^2} \right| + \left| \frac{\dot{u}_R u_I}{u_I^2 + u_R^2} \right| = \frac{|u_R| |\dot{u}_I|}{|u|^2} + \frac{|\dot{u}_R| |u_I|}{|u|^2} \leq \frac{|\dot{u}_I|}{|u|} + \frac{|\dot{u}_R|}{|u|} \quad (\text{A2.2})$$

Employing assumption **A1** , eq. (A2.2) can be written as:

$$\frac{|\dot{u}_I|}{|u|} + \frac{|\dot{u}_R|}{|u|} \leq \varepsilon_1 \omega(t) + \varepsilon_1 \omega(t) = 2\varepsilon_1 \omega(t) \quad (\text{A2.3})$$

Combining A2.1, A2.2, and A2.3 it results that:

$$\left| \frac{d}{dt}(\arg(u_k)) \right| \leq 2\varepsilon_1 \omega \Rightarrow \omega - 2\varepsilon_1 \omega \leq \left| \frac{d(\arg(u))}{dt} + \omega \right| \leq \omega + 2\varepsilon_1 \omega \quad (\text{A2.4})$$

$$\rightarrow \frac{d(\arg(u(t)))}{dt} + \omega(t) = \omega(t) + O(\varepsilon)$$

Comment:

Equation (A2.4) gives a bound for the eigenvector contribution to the instantaneous frequency of the modal component.

Proof 3 $|u_{2k}| \cong |\lambda| |u_k|$, $k = 1 \dots N$, $\forall t \in T$

Since the state space vector component $y_{2k}(t) = \dot{y}_k(t)$, the eigenvector component $u_k(t)$ is related to $u_{2k}(t)$ as follows:

$$u_{2k} = \lambda u_k + \dot{u}_k, \quad \text{for } k = 1 \dots N \quad (\text{A3.1})$$

Using the triangle inequality and assumption **A1** , $|u_{2k}|$ is bounded as follows:

$$\left| \lambda u_k - \dot{u}_k \right| \leq |u_{2k}| \leq |\lambda u_k| + |\dot{u}_k| \quad (\text{A3.2})$$

$$\left| \lambda u_k - \dot{u}_k \right| \geq \left| \lambda u_k \right| - \varepsilon_1 |\lambda u_k| = |\lambda u_k| (1 - \varepsilon_1); \quad (\text{A3.3})$$

$$\left| \lambda u_k + \dot{u}_k \right| \leq |\lambda u_k| + \varepsilon_1 |\lambda u_k| = |\lambda u_k| (1 + \varepsilon_1); \quad (\text{A3.4})$$

Combining (A4.2), (A4.3) and (A4.4), it results:

$$|\lambda u_k|(1 - \varepsilon_1) \leq |u_{2k}| \leq |\lambda u_k|(1 + \varepsilon_1) \Rightarrow |u_{2k}| = |\lambda| |u_k| + O(\varepsilon_1) \quad (\text{A3.5})$$

$$\rightarrow |u_{2k}| \cong |\lambda u_k| \quad \text{for } (\varepsilon_1 \ll 1)$$

Proof 4. $|\dot{u}_{2k} + \lambda u_{2k}| \cong |\lambda|^2 |u_k|, \quad k = 1 \dots N, \quad \forall t \in T$

$$|\lambda u_{2k}| - |\dot{u}_{2k}| \leq |\lambda u_{2k} + \dot{u}_{2k}| \leq |\lambda u_{2k}| + |\dot{u}_{2k}| \quad (\text{A4.1})$$

Employing the assumption **A1**, the lower and upper bounds for $|\lambda u_{2k} + \dot{u}_{2k}|$ can be expressed as:

$$\|\lambda u_{2k} - \dot{u}_{2k}\| \geq \|\lambda u_{2k} - \varepsilon_1 \lambda u_{2k}\| = |\lambda u_{2k}|(1 - \varepsilon_1); \quad (\text{A4.2})$$

$$|\lambda u_{2k}| + |\dot{u}_{2k}| \leq |\lambda u_{2k}| + \varepsilon_1 |\lambda u_{2k}| = |\lambda u_{2k}|(1 + \varepsilon_1); \quad (\text{A4.3})$$

Combining (A4.2), (A4.3) and (A4.4), it results that:

$$|\lambda u_{2k}|(1 - \varepsilon_1) \leq |\lambda u_{2k} + \dot{u}_{2k}| \leq |\lambda u_{2k}|(1 + \varepsilon_1) \quad (\text{A4.4})$$

Using the expression (A4.4), the terms in the above inequality can be written as:

$$|\lambda u_{2k}|(1 - \varepsilon_1) \geq |\lambda|^2 |u_k| (1 - \varepsilon_1)^2 \quad (\text{A4.5})$$

$$|\lambda u_{2k}|(1 + \varepsilon_1) \leq |\lambda|^2 |u_k| (1 + \varepsilon_1)^2 \quad (\text{A4.6})$$

Therefore $|\lambda u_{2k} + \dot{u}_{2k}|$ is bounded as:

$$|\lambda|^2 |u_k| (1 - \varepsilon_1)^2 \leq |\lambda u_{2k} + \dot{u}_{2k}| \leq |\lambda|^2 |u_k| (1 + \varepsilon_1)^2 \quad (\text{A4.7})$$

$$|\lambda|^2 |u_k| (1 - 2\varepsilon_1) \leq |\lambda u_{2k} + \dot{u}_{2k}| \leq |\lambda|^2 |u_k| (1 + 2\varepsilon_1 + \varepsilon_1^2) \quad (\text{A4.8})$$

$$\rightarrow |\lambda u_{2k} + \dot{u}_{2k}| = |\lambda|^2 |u_k| + O(\varepsilon_1) \quad (\text{A4.9})$$

$$\rightarrow |\dot{u}_{2k} + \lambda u_{2k}| \cong |\lambda|^2 |u_k|, k = 1 \dots N$$

Proof 5 $\frac{d(\arg(\dot{u}_{2k}(t) + \lambda(t)u_{2k}(t)))}{dt} + \omega(t) \cong \omega(t), \quad k = 1 \dots N, \quad \forall t \in T$

For simplicity, let denote $u_a(t) = \dot{u}_{2k}(t) + \lambda(t)u_{2k}(t)$ and $u_{aR} = \text{real}(u_a(t))$,
 $u_{aI}(t) = \text{imag}(u_a(t))$. With these notation the first term of the above expression is written as:

$$\frac{d(\arg(\dot{u}_{2k}(t) + \lambda(t)u_{2k}(t)))}{dt} = \frac{d(\arg(u_a))}{dt} \quad (\text{A5.1})$$

$$\frac{d}{dt}(\arg(u_a(t))) = \frac{d}{dt} \left(\text{atan} \left(\frac{u_{aI}}{u_{aR}} \right) \right) = \frac{u_{aR}\dot{u}_{aI} - \dot{u}_{aR}u_{aI}}{u_{aI}^2 + u_{aR}^2} \quad (\text{A5.2})$$

Using the triangle inequality for complex numbers, it results:

$$\left| \frac{u_{aR}\dot{u}_{aI} - \dot{u}_{aR}u_{aI}}{u_{aI}^2 + u_{aR}^2} \right| \leq \left| \frac{u_{aR}\dot{u}_{aI}}{u_{aI}^2 + u_{aR}^2} \right| + \left| \frac{\dot{u}_{aR}u_{aI}}{u_{aI}^2 + u_{aR}^2} \right| = \frac{|u_{aR}||\dot{u}_{aI}|}{|u_a|^2} + \frac{|\dot{u}_{aR}||u_{aI}|}{|u_a|^2} \leq \frac{|\dot{u}_{aI}|}{|u_a|} + \frac{|\dot{u}_{aR}|}{|u_a|} \quad (\text{A5.3})$$

$$\frac{|\dot{u}_{aI}|}{|u_a|} \leq \frac{|\dot{u}_a|}{|\lambda u_{2k}|(1-\varepsilon_1)} = \frac{|\ddot{u}_{2k} + \dot{\lambda}u_{2k} + \lambda\dot{u}_{2k}|}{|\lambda u_{2k}|(1-\varepsilon_1)} \leq \frac{|\ddot{u}_{2k}|}{|\lambda u_{2k}|(1-\varepsilon_1)} + \frac{|\dot{\lambda}u_{2k}|}{|\lambda u_{2k}|(1-\varepsilon_1)} + \frac{|\lambda\dot{u}_{2k}|}{|\lambda u_{2k}|(1-\varepsilon_1)} \quad (\text{A5.4})$$

Using the assumption **A3**, the first term of eq. (A5.4) can be expressed as:

$$\frac{|\ddot{u}_{2k}|}{|\lambda u_{2k}|(1-\varepsilon_1)} \leq \frac{\varepsilon_3 \omega}{(1-\varepsilon_1)} \quad (\text{A5.5})$$

Using the assumption **A2**, the second term of eq. (A5.4) can be expressed as:

$$\frac{|\dot{\lambda}u_{2k}|}{|\lambda u_{2k}|(1-\varepsilon_1)} = \frac{|\dot{\lambda}|}{|\lambda|(1-\varepsilon_1)} \leq \frac{\varepsilon_2 \omega}{(1-\varepsilon_1)} \quad (\text{A5.6})$$

With the assumption **A1**, the last term of eq. (A5.4) is given as:

$$\frac{|\lambda\dot{u}_{2k}|}{|\lambda u_{2k}|(1-\varepsilon_1)} = \frac{|\dot{u}_{2k}|}{|u_{2k}|(1-\varepsilon_1)} \leq \frac{\varepsilon_1 \omega}{(1-\varepsilon_1)} \quad (\text{A5.7})$$

Combining eqs. (A5.1) and (A5.5-5.7), it results:

$$\left| \frac{d(\arg(\dot{u}_{2k}(t) + \lambda(t)u_{2k}(t)))}{dt} \right| \leq \frac{2(\varepsilon_1 + \varepsilon_2 + \varepsilon_3)}{(1-\varepsilon_1)} \omega \quad (\text{A5.8})$$

$$\rightarrow \frac{d(\arg(\dot{u}_{2k}(t) + \lambda(t)u_{2k}(t)))}{dt} + \omega = \omega + O(\varepsilon) \quad (\text{A5.8})$$

$$\rightarrow \frac{d(\arg(\dot{u}_{2k}(t) + \lambda(t)u_{2k}(t)))}{dt} + \omega \cong \omega$$

REFERENCES

- Allemang, R., Brown, D. (2002), Experimental modal analysis, in Harris' Shock and Vibration Handbook (5th Edition), Harris C.M., Piersol, A.G. 2002, McGraw-Hill.
- Bernal, D., Beck, J. (2004), J. Eng. Mech., special issue, vol. 130(1).
- Biemans C., Staszewski W. J., Boller C., Tomlinson G. R. (2001), Crack detection in metallic structures using broadband excitation of acousto-ultrasonics, Journal of Intelligent Material Systems and Structures, vol. 12(8), pp. 589-597.
- Boashash, B. (1992), Estimating and interpreting the instantaneous frequency of a signal. I. Fundamentals, Proceedings of the IEEE, vol. 80(4), pp:520-538.
- Brown, R.G. (1983), Introduction to random signal analysis and Kalman filtering, New York, Wiley.
- Carmona, R., Hwang, W.L., Torresani, B. (1997), Characterization of signals by the ridges of their wavelet transform, IEEE Transactions on Signal Processing, vol. 45(10), pp. 2586.
- Carmona, R., Hwang, W.L, Torresani, B. (1998), Practical Time-Frequency Analysis, Academic Press.
- Chang, C.C., Sun, Z. (2001), Continuous condition assessment for bridges based on wavelet packet decomposition, Proceedings of SPIE - The International Society for Optical Engineering, vol. 4337, pp. 357-367.
- Chang, F.K. ed. (1999), Structural Health Monitoring, Proc., 1st Int. Workshop on Structural Health Monitoring, Stanford University, CA, USA.
- Chang, F.K. ed. (2001), Structural Health Monitoring, Proc., 3rd Int. Workshop on Structural Health Monitoring, Stanford University, CA, USA.
- Chang, F.K. ed. (2003), Structural Health Monitoring, Proc., 4th Int. Workshop on Structural Health Monitoring, Stanford University, CA, USA.
- Chang, F.K. ed. (2005), Structural Health Monitoring, Proc., 5th Int. Workshop on Structural Health Monitoring, Stanford University, CA, USA.
- Chen, C.T. (1999), Linear system theory and design, 3rd ed., Oxford Univ. Press.
- Ching, J., Beck, K., Porter, A., Shaikhtudinov, R. (2004), Real-time Bayesian state

estimation of uncertain dynamical systems,” Report No. EERL 2004-01, California Institute of Technology, Pasadena, California.

Chui, C. K. (1992), *An Introduction to Wavelets*, Academic Press, San Diego, CA.

Chui, C.K. (1997), *Wavelets: A mathematical Tool for Signal Analysis*, SIAM, Philadelphia, 1997.

Corbin, M., Hera, A., Hou, Z. (2000), Locating damages using wavelet approach, Proceedings of The 14th Engineering Mechanics Conference (EM2000), Austin, Texas.

Daubechies, I. (1992), *Ten Lectures on Wavelets*. Philadelphia, PA: SIAM.

Delprat, N., Escudie, B., Guillemain, P., Kronland-Martinet, R., Tchamitchian, P., Torresani, B., (1992), Asymptotic wavelet and Gabor analysis: extraction of instantaneous frequencies, *IEEE Trans. Inform. Th.*, vol. 38(2), pp. 644-664.

Demetriou, M.A. (2000), On-line damage detection, assessment and accommodation in civil infrastructure systems, Proceedings of the Fourth IFAC Symposium on Fault Detection, Supervision and Safety for Technical Processes:SAFEPROCESS’00, Budapest, Hungary, 14–16 June, 2000.

Demetriou, M.A. (2005), Using unknown input observers for robust adaptive fault detection in vector second-order systems, *Mechanical Systems and Signal Processing*, vol.19, pp. 291–309.

Doebling, S. W., Farrar, C. R., Prime, M. B. (1998), A summary review of vibration-based damage identification methods, *The Shock and Vibration Digest*, vol. 30(2), pp. 91-105.

Doebling, S.W., Farrar, C.R., Prime, M.B., Shevitz, D. (1996), Damage identification and health monitoring of structural and mechanical systems from changes in their vibration characteristics. Los Alamos National Laboratory Report, LA-13070.

Farrar, C. R., Doebling, S. W., and Nix, D A. (2001), Vibration-Based Structural Damage Identification, *Philosophical Transactions of the Royal Society of London Series A: Mathematical, Physical and Engineering Sciences*, vol. 359, pp. 131-149.

Farrar, C., Sohn, H. (2005), *Structural Health Monitoring: A Statistical Pattern Recognition Approach* , John Wiley & Sons.

Friswell, M.I, Mottershead, J.E. (1995), *Finite Element Model Updating in Structural Dynamics*, Kluwer Academic Publishers Group.

Fugate, M.L., Sohn, H., Farrar, C. R. (2000), Unsupervised learning methods for vibration-based damage detection, 18th IMAC., San Antonio, TX.

Gabor, D. (1946), Theory of communications, *J. IEEE*, vol. 93(3), pp. 429-457.

Ghanem, R., Romeo, F. (2000), A wavelet-based approach for the identification of linear time-varying dynamical systems, *Journal of Sound and Vibration* , vol. 234(4), pp.555-

576.

Ginsberg, J.H. (2001), *Mechanical and Structural vibrations : Theory and Applications*, New York: John Wiley & Sons.

Giurgiutiu, V , Cuc, A. (2005), *Embedded Non-destructive Evaluation for Structural Health Monitoring, Damage Detection, and Failure Prevention*, *The Shock and Vibration Digest*, vol. 37(2), pp.83-105.

Govorukhin V.N. (2005), <http://www.math.rsu.ru/mexmat/kvm/matds/>

Hahn, S.L. (1996), *Hilbert Transforms in Signal Processing*, Artech House, Norwood, Maryland.

Hans, S., Ibraim, E., Pernot, S., Boutin, C., Lamarque C.-H. (2000), *Damping identification in multi-degree-of-freedom systems via a wavelet-logarithmic decrement – Part 2: Study of a Civil Engineering Building*, *Journal of Sound and Vibration*, vol. 235(3), pp. 375-403.

Hellier, C.J. (2001), *Handbook of Nondestructive Evaluation*, New York : McGraw-Hill.

Hera, A., Hou, Z. (2001), *Wavelet-based approach for ASCE structural health monitoring benchmark studies*, *Proceedings of the 3rd International Workshop on Structural Health Monitoring*, Stanford University, Stanford, CA.

Hera, A., Hou, Z. (2003), *Wavelet approach for damage detection using experimental data of ASCE Benchmark Study*, *The 16th ASCE Engineering Mechanics Conference*, University of Washington, Seattle, CD-ROM.

Hera, A., Hou, Z. (2004), *Application of wavelet approach for ASCE structural health monitoring benchmark studies*, *Journal of Engineering Mechanics*, vol.130(1), pp. 96-104.

Hera, A., Shinde, A., Hou, Z. (2004), *A comparative study of the empirical mode decomposition and wavelet analysis on their application for structural health monitoring*, *Proceedings of IMECE04, ASME International Mechanical Engineering Congress*, Anaheim, CA, USA, CD-ROM.

Hoshiya, M., Saito, E. (1984), *Structural identification by extended Kalman filter*, *J.Eng. Mech.*, vol.110(12), pp. 1757-1770.

Hou, Z., Hera, A., Liu, W., Hendrickson, D. (2003), *Identification of instantaneous modal parameters of time-varying systems using wavelet approach*, *The 4th International Workshop on Structural Health Monitoring*, Stanford University, CA, pp. 725-732.

Johnson, E. A., Lam, H. F., Katafygiotis, L. S., and Beck, J. L. (2004) , *Phase I IASC-ASCE structural health monitoring benchmark problem using simulated data*, *J. Engrg. Mech.*, vol. 130(1), pp. 3-15.

Kijewski, T., Kareem, A. (2003), *Wavelet transforms for system identification in civil engineering*, *Computer–Aided Civil and Infrastructure Engineering*, vol.18(5),pp.339-355.

- Kijewski, T., Kareem, A. (2002), On the presence of end effects and their melioration in wavelet-based analysis, *Journal of Sound and Vibration*, vol. 256(5), pp.980-988.
- Kloet P. van der, Neerhoff F.L. (2002), Dynamic eigenvalues for scalar linear time-varying systems, *International Symposium on Mathematical Theory of Networks and Systems*, Notre Dame, Indiana, U.S.A., pp. 8.
- Lamarque, C.-H., Pernot S., Cuer A. (2000), Damping identification in multi-degree-of-freedom systems via a wavelet-logarithmic decrement –Part 1: Theory, *Journal of Sound and Vibration*, vol. 235(3), pp. 361-374.
- Lynch, J.P. (2004), Linear classification of system poles for structural damage detection using piezoelectric active sensors, *SPIE 11th Annual International Symposium on Smart Structures and Materials*, San Diego, CA, USA.
- Mahmoud, M., Abu Kiefa, M.A. (1999), Neural network solution of the inverse vibration problem, *NDT & E International*, vol. 32(2), pp. 91-99.
- Mallat, S. G. (1989), A theory for multiresolution signal decomposition: the wavelet representation, *IEEE Trans. Pattern Analysis Machine Intel.* Vol.11, 674-693.
- Mallat, S. (1999) *A Wavelet Tour of Signal Processing*, San Diego: Academic Press, 1999.
- Maruyama, O., and Hoshiya, M. (2001), System identification of an experimental model by extended Kalman filter, *Proc. Structural Safety and reliability, ICOSSAR 2001*, CD-ROM.
- Masuda, ., Noori, M., Sone, A., Yamashita, Y. (2002), Time-varying modal identification by Monte Carlo filter, *15th ASCE Engineering Mechanics Conference*, Columbia University, New York, NY.
- Masri, S. F., Nakamura, M., Chassiakos, A. G., and Caughey, T. K., 1996, Neural network approach to detection of changes in structural parameters, *Journal of Engineering Mechanics*, vol. 122(4), pp. 350-360.
- Misiti, M., Misti, Y., Oppenheim, G., Poggi, JM, (1996), *Wavelet Toolbox User's Guide*, The MathWork, Inc., Natick, Ma.
- Mottershead JE and Friswell MI (1993) Model updating in structural dynamics: A survey, *Journal of Sound and Vibration*, vol. 167(2), pp 347-375.
- Mottershead JE and Friswell MI (1998) (Editors), *Mechanical Systems and Signal Processing Special Issue on Model Updating*, vol. 12(1).
- Paya, B. A. , Esat, I. I. , Badi, M. N. M. (1997), Artificial neural network based fault diagnostics of rotating machinery using wavelet transforms as a preprocessor, *Mechanical Systems and Signal Processing*, vol. 11, pp. 751–765.
- Piombo, B.A.D., Fasana, A., Marchesiello, S., Ruzzene, M. (2000), Modeling and identification of the dynamic response of a supported bridge, *Mechanical Systems and*

Signal Processing, vol. 14(1), pp. 75-89.

Prince, P.J., and Dorman J.R. (1981), High order embedded Runge-Kutta formulae, *J.Comp. Appl. Math.*, vol. 7, pp.67-75.

Qing,X., Kumar, A, Zhang, C., Gonzalez, I., , Guo, G., and Chang, F.K. (2005), A hybrid piezoelectric/fiber optic diagnostic system for structural health monitoring, *Smart Mater. Struct.* vol. 14, pp. 98–103.

Trendafilova, I. and Hetlen, W. (2003), Categorization and pattern recognition methods for damage localization from vibration measurements, *Mechanical Systems and Signal Processing*, Vol.17(4), pp. 825-836.

Robertson, A. N., Park, K. C. , Alvin, K. F. (1998), Identification of structural dynamics models using wavelet-generated impulse response data, *ASME Journal of Vibrations and Acoustics*, vol. 120(1), pp. 261-266.

Ruzzene, M., Fasana, A., Garibaldi, L., Piombo, B. (1997), Natural frequency and damping identification using wavelet transform: Application to real data, *Mechanical Systems and Signal Processing*, vol. 11(2), pp. 207-218.

Rytter, A. (1993), *Vibration Based Inspection of Civil Engineering Structures*, Ph. D. Dissertation, Department of Building Technology and Structural Engineering, Aalborg University, Denmark.

Shimizu, H., Suzuki, Y., Suda, T., Kitahara, A. (2004), Seismic Performance of Wood House by Full-Scale Shaking Tests of Two-stoied Post and Beam Wooden Frames, 13th World Conference on Earthquake Engineering, Vancouver, Canada.

Shinde, A., Hou, Z. (2004), A wavelet packet based sifting process and its application for structural health monitoring, *Proceedings of American Control Conference*, Boston, Massachusetts , USA, pp. 4219-4224.

Shinde, A. (2004), A wavelet packet based sifting process and its application for structural health monitoring, MS Thesis, WPI, Ma.

Shinde, A., Hou, Z (2005), A wavelet packet based sifting process and its application for structural health monitoring , *Structural Health Monitoring*, vol. 4(2), pp.153-170.

Shinozuka, M.,, Ghanem, R. (1995), Structural system identification.II., Experimental verification., *J. Eng. Mech.*, 121(2), pp. 1233-1240.

Sohn, G., H., Farrar, C., Inman, D. (2003), Overview of piezoelectric impedance-based health monitoring and path forward, *The Shock and Vibration Digest*, vol. 35(6), pp. 451–463.

Staszewski, W. J. (1997), Identification of damping in MDOF systems using time-scale decomposition, *Journal of Sound and Vibration*, vol. 203(2), pp. 283-305.

Staszewski, W.J., Tomlinson, G.R. (1994), Application of the wavelet transform to fault

- detection in a spur gear, *Mechanical Systems and Signal Processing*, vol.8(3), pp. 289-307.
- Staszewski, W.J., Worden, K. (1997), Classification of faults in gearboxes: Pre-processing Algorithms and Neural Networks, *Neural Computing and Applications*, vol.5, pp.160-183.
- Sun, Z., Chang, C. C. (2002), Structural damage assessment based on wavelet packet transform, *Journal of Structural Engineering*, vol.128(10), pp. 1354-1361.
- Sun, Q., Tang, Y., (2002), Singularity Analysis Using Continuous Wavelet Transform For Bearing Fault Diagnosis, *Mechanical Systems and Signal Processing*, vol.16(6), pp. 1025-1041.
- Van Der Kloet, P., Neerhoff, F. L. (2000), Diagonalization algorithms for linear time-varying dynamic systems, *International Journal of Systems Science*, vol. 31(8), pp. 1053-1057.
- Wang, W.J., McFadden, P.D. (1995), Application of orthogonal wavelets to early gear damage detection, *Mechanical Systems and Signal Processing*, vol. 9(5), pp. 497-507, 1995.
- Worden, K., Allen, D., Sohn,H., Stinemat, D.W., Farrar, C.R. (2002), Extreme value statistics for damage detection in mechanical structures, Los Alamos National Laboratory, Report LA-13903-MS.
- Worden, K. (1997), Structural fault detection using a novelty measure, *Journal of Sound and Vibration* , vol. 201(1), pp.85-101.
- Wu, M.Y. (1980), A new concept of eigenvalues and eigenvectors and its applications, *IEEE Transactions on Automatic Control*, vol.25(4), p. 824 – 826.
- Wu, M.Y. (1984), On stability of linear time-varying systems, *Int. J. Syst. Sci.*, Vol. 15(2), pp. 137–150.
- Wu, M.Y. (1974), A note on stability of linear time-varying systems, *IEEE Transactions on Automatic Control*, vol. 19(1), pp. 162.
- Yang, J., Lin, S. (2005), Identification of parametric variations of structural based on least Squares Estimation and adaptive tracking technique, *J. Eng. Mech.*, vol.131(3), pp.290-297.
- Yoshida, I., Sato, T. (2002), Health monitoring algorithm by Monte Carlo Filter based on non-gaussian noise, *Journal of Natural Disaster Science*, vol.24 (2), pp.101-107.
- Zadeh. L.A., Desoer, C.A. (1963), *Linear System Theory; The State Space Approach*, McGraw-Hill, (New York).
- Zhou, G. et al, (2002), Damage detection and assessment in fibre-reinforced composite structures with embedded fibre optic sensors-review, *Smart Mater. Struct.* vol.11, pp. 925-939.